The Dynamics and Control of a Three-Wheeled Tilting Vehicle

Van Poelgeest, Auguste

Award date:
2011

Awarding institution:
University of Bath

THE DYNAMICS AND CONTROL OF A THREE-WHEELED TILTING VEHICLE

Auguste van Poelgeest

A thesis submitted for the degree of Doctor of Philosophy

University of Bath

Department of Mechanical Engineering

January 2011

ABSTRACT

The objective of this study was to develop a new Steer Tilt Control (STC) algorithm inspired by real driver behaviour and to test it in simulation with an experimentally validated non-linear vehicle model.

In order to develop an exhaustive simulation model of the vehicle and to process experimental data correctly, a large number of modelling aspects were taken into consideration. The objective of the study was to identify the unique kinematics of a three-wheeled tilting vehicle and determine the importance of the kinematic effects on the vehicle system. In order to fully understand this unique class of vehicle, the effect of the driver's mass on the vehicle inertia's and the effect of the tilting on the vehicle's yaw inertia were considered. A wide-ranging expression for the driver's perceived acceleration was derived and the roll dynamics of the non-tilting part of the three-wheeled tilting vehicle assembly were modelled. The steering torque of the vehicle as fully analysed and, using the simulation model, methods to model the effect of a crosswind on the vehicle, to test the effect of driving up or downhill, and to determine the effect of road camber on the vehicle dynamics were considered.

To create a better understanding of the control task, road experiments were carried out using an instrumented tilting three-wheeler to investigate the driver steer inputs necessary to both balance the vehicle and follow a fixed trajectory. The experimental results demonstrated that the drivers' steering inputs varied even though they had to complete identical tasks. This result confirmed that there are multiple ways to control the roll of the vehicle. The results also showed that the tilt angle always led the steering angle and for a transient manoeuvre, the tilt angle was larger than the balanced tilt angle at the start of the manoeuvre and smaller than the balanced angle at the end of the manoeuvre. The next step in the investigation was the development of a comprehensive non-linear dynamics model of a tilting three-wheeler including a tyre model and a driver model. A new method was developed to estimate the parameters of a Magic Formula Tyre model using the road testing data. The vehicle and tyre model were validated using data from a range of test runs.

The importance of a driver in the loop was recognised and the elements of a driver trajectory-tracking model were studied. The aim was to develop a driver model that demonstrated good

tracking and some similarity to real driver behaviour. The final model used the yaw rate demand to determine an anticipatory control steer angle and the current heading error and the vehicle's lateral position error measured in the vehicle's local axis system to make small steering adjustments.

The STC method based on Proportional Integral Derivative (PID) control was tested with the vehicle model to determine its performance with the non-linear dynamics and the driver in the loop. It was shown that the driver model had the tendency to act against the STC and that the two could only act simultaneously for a very limited range of demand trajectory and velocity combinations. The crosswind, hill driving, and road camber models were combined with the vehicle simulation without a driver but with the PID based STC. The simulations showed that these environmental factors made the control task significantly more difficult. More importantly, it showed that these factors demanded an increased number of vehicle states to be fed back to the controller.

A new algorithm for STC was developed using the full vehicle and driver model. One of the criteria was that the control algorithm had to be realizable in practice. The resulting controller was a logic algorithm that would choose an action based on the steering angle and velocity and the vehicle speed with online gain adjustment based on direction and order of magnitude of the perceived acceleration. The basis of the control was adjustment of the driver's steering input and it was shown that the vehicle's deviation from the driver's intended path was minimal.

ACKNOWLEDGEMENTS

This thesis would not have been possible without the knowledge, guidance and above all patience of my supervisors Dr Jos Darling and Professor Kevin Edge.

I am also indebted to the technical staff of the 4E and 8E laboratories for their efforts to keep the test vehicle going and occasionally helping me to fix my bike.

Many thanks go out to my friends and colleagues at the University of Bath, especially Team BathStreet, for the teatime banter and listening to my (occasional) rants.

To my parents Jaap en Guus: I am ever grateful for your continuous encouragements and cheers from the side lines

My sincere apologies go to Anil, who has had to endure all my chagrins and frustrations, especially during the write-up.

Finally, I would like to dedicate this thesis to the memory of my brother Jan Jaap, who never got to finish his Magnum Opus.

CONTENTS

NOMENCLATURE

UPPERCASE

Symbol	Description	Unit
A	area	m
C_α	tyre slip stiffness	N rad^{-1}
C_γ	tyre camber stiffness	N rad^{-1}
F	force	N
I	inertia	kg m^2
L	wheelbase	m
M	moment	Nm
R	radius	m
R_f	front tyre radius	m
R_r	rear tyre radius	m
R_T	tyre cross sectional radius	
T	torque	Nm
X	global longitudinal position	m
Y	global lateral position	m

LOWERCASE

Symbol	Description	Unit
a	distance from the vehicle CG to the front contact patch	m
a_X	longitudinal acceleration	m s^{-2}
a_Y	total lateral acceleration including the centripetal acceleration	m s^{-2}
b	distance from the vehicle CG to the rear contact patch	m
d	perpendicular distance from acceleration sensor to roll axis	m
g	gravitational constant = 9.81	m s^{-2}
h	(centre of gravity) height	m
k	gain	-
k_p	proportional gain	
k_i	integral gain	
k_d	derivative gain	
m	mass	kg
s	Laplace operator	-
ds	distance travelled	m
t	time	s
t_t	normal trail	m
v	velocity	m s^{-1}
w	track width	m
x	longitudinal direction, position or displacement	(m)
y	lateral direction, position or displacement	(m)
z	vertical direction, position or displacement	(m)

GREEK LOWERCASE

Symbol	Description	Unit
α	wheel slip angle	radians
γ	camber angle	radians
δ	steering angle	radians
ε	castor angle	radians
ω_w	rotational velocity of the wheel	radians s^{-1}
ϕ	roll angle	radians
ψ	yaw angle	radians

SUBSCRIPTS

Symbol	Description
b	balanced
c	relating to the rolling cabin
cf	centrifugal
CG	relating to the centre of gravity
CGr	relating to the rear unit centre of gravity
d	demand
f	relating to the front (wheel/tyre/assembly)
ff	feed forward
joint	measured at the joint
per	perceived
r	relating to the rear (wheel/tyre/assembly)
s	relating to steer or the steer assembly
ss	steady state
w	relating to the wheel
world	measured in the world (global) coordinate system
X, x, or xx	relating to the longitudinal direction or the roll axis
Y, y, or yy	relation to the lateral direction or pitch axis
Yf	relating to the lateral direction on the front wheel
Yr	relating to the lateral direction on the rear wheel
Z, z or zz	relating to the vertical direction or yaw axis

CHAPTER 1. INTRODUCTION

The aim of this chapter is to place the study of three-wheeled vehicles into context. A brief history of three-wheeled vehicles demonstrates how this type of vehicle has evolved throughout the decades. Subsequently a summary of recent developments illustrates what the future may hold for the three-wheeler. Both overviews highlight the stability problems that are commonly associated with three-wheelers and the development of adding roll control to the vehicle. The next two sections give an overview of the status quo in theoretical and experimental work regarding roll control. The final two sections give an overview of the research objectives and the scope and order of the Thesis.

1.1 THREE-WHEELERS

1.1.1 Three-Wheeled Vehicles: A Brief History

Three-wheeled vehicles have traditionally been of two principal types: delivery vans and economical commuter vehicles and have been popular amongst manufacturers of small delivery vehicles, usually in a 2 rear wheel, 1 front wheel configuration. Many models of various sizes were produced during the last century, where the two wheels would generally support the load and the single wheel would often be steered. This allowed vans to be small enough for city centre deliveries, but robust enough for significant payloads. For small commuter vehicles, the three-wheeler was popular because it saved space and a two front wheel, one rear wheel configurations allowed the vehicle to be tear-drop or bullet shaped for improved aerodynamics. For this reason, it is common to find electric cars with three-wheels. One of the earliest instances of an electric three-wheeler (1920) was a design published in 'Wirtschafts-Motor – Nutz-Motor' [1]. However, by the 1930s the average automobile was configured with four wheels, yet companies such as the Birmingham Small Arms Company (BSA) Figure 1.1, Daihatsu, Morgan and Reliant continued to produce three-wheelers. Therefore, studies into the stability of this type of vehicle were on-going. In 1933, Wesnigk [2] discussed the design of three-wheeled vehicles and the importance of stability and riding characteristics in the dimensioning process and weight distribution. For stability, the centre of gravity should be as close to the ground as possible, and preferably be closer to the single wheel than the two wheels to reduce the occurrence of rollover. For handling, the centre of gravity should not be too close to the single wheel, because that would result in

extreme yaw accelerations. Overall, the design of a three-wheeler may require more work than a four-wheeler to find a compromise between good handling and an acceptable stability range. Though when an appropriate design has been decided on, the vehicle can offer as good handling and stability as a four-wheeler, plus a reduction in size and improved aerodynamics.

Figure 1.1 – Birmingham Small Arms Company (BSA) 1932 standard model (source: www.3wheelers.com)

Figure 1.2 – BMW Isetta (source: http://www.atomium.be/)

After the Second World War, small three-wheeled cars gained popularity such as the Messerschmitt and the Isetta Figure 1.2. So far, three-wheelers were generally designed as cars with one front or one rear wheel. Often they were compact vehicles with particularly efficient engines, such as the General Motors commuter car described by Rishavy [3]. He discusses the development of a commuting vehicle (three-wheeler) for two people with a top speed of 130 kph. Though the performance was as good as could be expected from a conventional car, he claimed that the emissions were 30-40% less due to weight as well as size reductions. General Motors did not stop there; they developed more concept cars that were small and efficient such as the Lean Machine and the Lifejet [4]. These two concepts dealt with one stability problem associated with three-wheelers: rollover. Both concept cars used a tilting mechanism to lean the vehicle into a turn like a motorcycle.

Since most three-wheelers were designed as cars, they were often compared to their four-wheeled counterparts. Chang and Ding [5] compared the steady state turning dynamics of the two types of vehicle under acceleration and braking. Effects such as the rollover dynamics, oversteer and understeer, and sliding and skidding were investigated to conclude that a three-wheeler could be as stable as a four-wheeled vehicle. Regardless of the number of wheels, when designing a vehicle great care has to be taken when outlining weight distribution, dimensioning and the geometry of the steering system.

From the history of the three-wheeled vehicle, it can be concluded that a three-wheeled arrangement can offer space, weight and aerodynamic benefits leading to reduced emissions. Although three-wheelers have been associated with instability, in particular rollover, they can be very stable. The stability is, as with any vehicle, dependent on the design of the wheel arrangement and the weight and load distribution.

1.1.2 Three-Wheeled Vehicles: A Future

Concerns over global warming and the depletion of oil reserves have led automobile manufacturers to develop alternatives to four-wheeled, 5-seater, oil dependent cars. According to the UK office for national statistics [6], since 1986 the average car occupancy has dropped to 1.56 occupants per car and 1.2 occupants for commuter journeys. One commercial alternative for the standard 5-seater car is the Smart car, which has space for the driver and one passenger. Although it is an improvement on the standard car in terms of size, the fuel efficiency [7] was not improved significantly in comparison with larger, 4/5-seater, compact cars [8].

Another category of alternative car is the tall and narrow vehicle. This type of car allows two people to sit upright, one in front of the other. In this configuration, the vehicle only takes up half the width of a car. Often, tall and narrow vehicles have two or three-wheels. A two-wheeled example is the Ecomobile by Peraves, who have since developed the MonoTracer [9]. These commercially available vehicles are enclosed with only two wheels; hence, they need stabilisers to park and stop at traffic lights. A three-wheeled vehicle eliminates this need for stabilisers.

Two novel prototype three-wheeled vehicles have been previously developed at the University of Bath in conjunction with a number of European partners: Zedis [10] and CLEVER [11-13]. The objective of CLEVER was to build a tall and narrow vehicle that could seat two people. Furthermore, it had to be energy efficient. Due to its tall and narrow geometry, it was more likely to roll in a corner than a conventional four-wheeled car. This problem was solved by tilting the vehicle into the corner using two hydraulic actuators; this control action is called Direct Tilt Control (DTC). There are two issues with DTC, namely: it requires a large quantity of power during rapid dynamic steer manoeuvres at high speed, and the motion from upright to the tilted position could be experienced as 'unnatural' by the driver.

The reason why this motion feels 'unnatural' can be explained by the forces on the driver: gravity, centripetal acceleration and tilting torque. The resultant force vector during the tilting motion will be tangential to the body axis. This will cause the driver's vestibular system to sense a lateral acceleration. Once the correct tilt angle has been achieved, this vector will be pointing in the

direction along the driver's body axis (the driver's yaw axis). When that occurs, the balancing organs will not sense any lateral acceleration. For this reason, aeroplane passengers cannot 'feel' the plane changing direction: the acceleration vector is always parallel to the yaw axis.

Bicycle and motorcycle riders try to achieve this when balancing their vehicle while turning: maintaining the vehicle axis parallel to the acceleration vector ensures that the vehicle does not fall into the bend nor straighten up. It would be advantageous to use a similar force balancing method to tilt the vehicle. First, the driver will not experience any unpleasant forces, but more importantly, this approach could significantly reduce the power requirements for tilting. This type of tilting system is known as Steer Tilt Control (STC), because it applies countersteer to tilt the vehicle into a bend, just like a motorcycle rider. These control methods and the balanced lean angle are discussed in more detail in chapter 2.

Three-wheeled vehicles have a future as a mode of personal transport as can also be deduced from the current development of electric three-wheelers [14-17]. The design can offer weight and size reductions resulting in lower emissions than conventional cars without compromising on driver comfort. The future vehicles will differ from their historic counterparts in their ability to control the vehicle roll and therefore improve stability. The roll control can be achieved by either applying a direct roll moment (DTC) or a more sophisticated steer system mimicking a bicycle rider applying countersteer (STC).

1.1.3 Three-Wheeler Dynamics

The subject of this research study is a tilting tricycle. Hence, the differences in the dynamics between a bicycle and a tricycle are presented here. Cossalter et al.[15, 18] developed and investigated a tilting three-wheeled vehicle with a four-bar-mechanism as the tilt joint. The former paper focussed on the importance of the location and inclination of the tilt axis and the instantaneous centre of rotation and the effect on the load transfer between the rear wheels and the handling characteristics. Simulations and experimental measurements were employed to evaluate the steering torque, the handling characteristics, and the load transfer between the rear wheels. The authors concluded that each individual configuration of tilt axis location and inclination had its advantages and disadvantages. With the axis below the ground plane, the vehicle was more stable, but the handling was less good in comparison to the vehicle configured with the axis above the ground. A positive inclination of the tilt axis was found to improve the steering torque effort; however, the propagation of reaction forces with this configuration was sometimes experienced as unpleasant.

The second paper presented results from slalom tests with the vehicle presented in the first paper. The inclination of the tilt axis was not included in the test program. The results from the slalom test were used to determine a handling index. Subjectively, the vehicle with a roll axis above the ground was found to handle better than the roll axis below the ground. The objective was to find an index that confirmed this result. The authors settled on the maximum velocity at which a slalom manoeuvre could be completed.

What was learnt from the work by Cossalter et al. was that the tilt axis location and its inclination affected the dynamics of a three-wheeled tilting vehicle to such a degree that the driver could perceive the difference. The research also showed the importance of the tilt axis location on the load transfer between the two rear wheels of a three-wheeled tilting vehicle. It was shown that the vehicle design could be adjusted in order to limit the chance of rear unit rollover.

The main reference to the dynamics of a non-tilting three-wheeled vehicle comes from a standard by the Society of Automotive Engineers (SAE) [19]. The publication evaluates a four-wheeled vehicle, a three-wheeler with two wheels at the front (2F1R), and a three-wheeler with two wheels at the rear (1F2R). The following characteristics were compared: lateral stability, rollover stability during lateral acceleration, rollover stability while braking in a turn, and rollover stability while accelerating in a turn. To make these comparisons, linearised and simplified equations of motion were developed for the three vehicle configurations. The lateral stability is determined by finding the roots of the equation of motion. The equation of motion is quadratic and if the real parts of the roots are negative, the vehicle is assumed to be stable. It was shown that the three-wheeled vehicles were more limited in their stability by the ratio between the track width and the vertical centre of gravity location than the four-wheeler. The difference in stable velocity range between a 1F2R and a 2R1F is largely dependent on the longitudinal location of the centre of gravity. For a 1F2R arrangement, a centre of gravity location towards the rear of the vehicle is preferable and vice versa for a 2F1R arrangement. The three-wheelers assessed in this standard did not tilt, because they were not tall and narrow. However, it would be possible to expand the equations of motion to include the dynamics of a tilting three-wheeler.

1.2 TILT CONTROL: THEORETICAL FINDINGS

Karnopp and Hibbard [20] and Karnopp and Fang [21] published, in 1992, the early papers on the topic of the tilting of a narrow road vehicle. Karnopp and Hibbard highlighted the difference between a road vehicle and a tracked vehicle and produced a simplified analysis. With this analysis, they determined the lean angle to balance the lateral forces and to reduce the perceived

lateral acceleration to zero. Karnopp and Fang developed a model of the tilt dynamics for a road vehicle. This model related the steer angle to the body tilt angle assuming negligible tyre slip. The authors presented a proportional control system that aimed to track a demand tilt angle. The control system regulated the front steer angle to generate a body roll moment and achieve the correct tilt angle, assuming steady state conditions. Simulations of the model and the control system showed that a small amount of steer in the opposite direction is required to deal with sudden changes in the required demand tilt angle. This is called countersteer, which is defined as steer against the direction of turn. In 1993, Hibbard and Karnopp [22] presented an active tilt control system. A model of a tilting vehicle with tilt actuators showed that the perceived acceleration could be greatly reduced during cornering when the vehicle is tilted into the bend. This also helped to reduce the overturning moment on the vehicle. Two methods of tilting had now been demonstrated: a vehicle can be leaned into a turn by countersteering (Steer Tilt Control) or it can be leaned into a turn by a roll actuator (Direct Tilt Control).

In 1997, So and Karnopp [23] combined the two methods of Direct Tilt Control (DTC) and Steer Tilt Control (STC). They showed that when the vehicle is tilted by an actuator, it is always stable, but the driver may experience elevated levels of lateral acceleration at higher speeds. However, when the vehicle is countersteered to lean into the bend, the acceleration experienced by the driver is close to zero. This system did appear to require large and frequent steer inputs at lower speeds. Thus, the authors proposed a speed dependent switching system and showed that it performed well when tilting the vehicle. The same authors produced an additional paper on the subject [24] where they introduced a system that could switch between the two tilt systems depending on the error between the demand and the output lateral acceleration.

Snell [25], who has published work on aircraft control [26-30] , presented a novel method to combine DTC and STC. The approach redefined the control problem. The original aim was to force the tilt angle to the demand tilt angle: the angle at which the perceived acceleration is zero. However, the modified control law aimed to minimise or eliminate the perceived acceleration. The result was a reduction in the overshoot of perceived lateral acceleration when the DTC system was in operation. To achieve this control, a number of steps had to be taken. First, the problem of the tilt angle lagging behind the lateral acceleration had to be solved. This was achieved by introducing a lag term (prefilter) between the command acceleration and the output lateral acceleration. It also required a feedforward path of the demand acceleration to the moment input via another prefilter. The transfer functions for the prefilters were designed so that the effect of the steering (lateral acceleration) on the perceived acceleration was cancelled by an

equal and opposite force (the direct tilting moment). The result of the control law was a system that responded with countersteer in transient situations and a tilt moment in steady state situations.

Chiou and Chen [31, 32] referred to their roll control system as a double loop PID STC where both the roll angle and the roll velocity were fed back. The input to the first PID block as the roll angle error. The output of the first PID block was the roll velocity demand. This demand was compared to the roll velocity feedback and the error was the input to the second PID block. This second PID block output a steer angle for the steer control. The simulation results and the experimental test results that were presented in the literature did not convincingly demonstrate the controller's success. It was also noted that the control architecture could be reduced to a single PID control block.

Two concepts to control the roll angle of a tilting vehicle have been widely published. The first method, DTC, applies a force to the rolling assembly to directly force it to the tilt angle the control system has demanded. The second method, STC, adjusts the steer angle of the vehicle to cause a lateral acceleration, which will result in a roll moment. When the tilt angle demand from the control system is reached, the steer angle is again adjusted to cause another lateral acceleration that will stop the roll. DTC is the more appropriate control system when travelling at low speeds. At low speeds, the torque required to roll the tilting assembly tends to be small and at low speeds, STC requires large steering adjustments to remain balanced. At high speeds however, DTC would require large torques to force the tilting assembly to the correct roll angle, whereas STC only has to make small adjustments to the steer. A speed dependent hybrid system is therefore the best method to control the roll angle of a tilting vehicle.

The control algorithms presented in the literature were similar: determine a roll angle demand value, compare it to the roll angle feedback signal, and apply P-D or PID control to calculate the control action. The methods of determining the demand value varied, but the most important factor was the steer input from the driver and, in many cases, the forward velocity of the vehicle.

The forward velocity played a key role in the framework to combine the two control systems. The control law could be as simple as a hysteresis loop, but could also be as complex as the minimisation of the perceived acceleration.

In conclusion, to design a new roll control system, the following elements should be carefully considered: the vehicle state to be controlled, the vehicle state to be actuated, the calculation of the demand value, and the combination of DTC and STC.

1.3 TILT CONTROL: EXPERIMENTAL WORK

Thus far, all the control strategies were theoretical and they were only tested through models and simulations, so there was a need to show that the strategies worked in practice. In 2000, Pauwelussen [33, 34] presented a dynamic analysis of the tilt control mechanism found in the Vandenbrink Carver, see website [35]. In this system, the driver has to apply a steering torque to balance the steering torque of the front wheel, the tilting torque, the feedback torque from a torsion bar and the countersteer torque at the front wheel. The torque balance is made up by the feedback torque that is proportional to the lean angle, the torque required to countersteer that is proportional to the tilting torque, and the tilting torque from the actuators that is proportional to the driver steering moment. In practice, this system showed acceptable results for tilting and stability. What should be noted is that the ratios between torques were not derived; in other words, they had to be found through system tuning. Gohl et al. [36, 37] took a different approach. They reproduced the STC system from Karnopp and Fang [21] and improved the control system with a feedforward loop, and applied it to a prototype three-wheeled vehicle. This showed that it was possible to balance a vehicle using steering inputs derived from a controller alone. This work was continued by Kidane et al. [38-40], who demonstrated experimentally that steer tilt control was an effective balancing method. Drew et al. [11, 12] demonstrated that DTC was an effective method. DTC was employed on the CLEVER vehicle and practical tests showed that it could roll the vehicle to an appropriate roll angle for the driving conditions. Pohl and Conrads [16] demonstrated a successful DTC system for a vehicle with a complex rolling chassis, although the literature lacked details of the algorithm.

DTC and STC have not been widely tested in practice. DTC has been shown to work on the Vandenbrink Carver, the CLEVER vehicle and the Pohl and Conrads prototype. The two different vehicles were driven by different control algorithms, but in both cases, the roll angle was successfully controlled. STC has only been tested in a balancing context, that is, straight-line driving.

1.4 CONCLUDING REMARKS

It has been established that three-wheels can offer a stable vehicle platform if the wheel configuration and load distribution are appropriately assigned. In addition, a three-wheeled

vehicle could offer more options for improved aerodynamics, smaller carbon and surface footprint, and ultimately more economical designs. The stability of this type of vehicle can be greatly helped by leaning into a turn. The literature on the two methods to lean a vehicle into a turn has been discussed from both a theoretical and experimental viewpoint namely: Direct Tilt Control and Steer Tilt Control. Two important downsides to Direct Tilt Control were identified: reduced driver comfort and potentially large power requirements. Steer Tilt Control had not been tested thoroughly in practice. This form of control intends to mimic the control actions of a motorcycle rider by countersteering. It was noted that a motorcycle rider would learn to countersteer through practice, although balancing was largely aided by the vehicle geometry and gyroscopic moments.

1.5 RESEARCH OBJECTIVES

The main objective was to develop a vehicle and driver model for a three-wheeled tilting vehicle and to design a novel roll control system that has been tested with the complete vehicle system simulation. The first aim was to review of the current developments in vehicle modelling, roll control, two-wheeler control, driver modelling and tyre modelling. The second aim was to develop and investigate models and methods to quantify uncertainties and non-linearities in the vehicle system such as the kinematics and environmental factors. The outcome of this investigation had a direct effect on the data processing of experimental results of road tests as well as the vehicle modelling and simulation. The next aim was to set up an experimental test program to further the understanding of the driver's actions as he controls a three-wheeled tilting vehicle and to obtain data for the validation of the vehicle model. The final aim was to develop the new controller using a dynamic non-linear vehicle model as well as a driver model to determine how a person would react to a controller changing the original steering input.

1.6 SCOPE AND ORDER OF THIS THESIS

This Thesis consists of eight chapters and the following section outlines the structure of the chapters. Chapter 2 reviews the literature relevant to all the aspects of this Thesis: vehicle and roll dynamics modelling, roll control methods, two-wheeler control, driver modelling and tyre modelling. The literature is critically discussed and a number of roll control methods, bicycle control strategies and rider models have been replicated. This chapter illustrates the status quo in the various research fields, highlights the gaps in the current knowledge.

Chapter 3 presents a range of modelling considerations that apply to a three-wheeled tilting vehicle. These include the unique kinematics of a three-wheeled tilting vehicle, a study of the

steering torque definition, and a qualitative description of three external disturbances that can cause problems with the roll stability and trajectory tracking of a three-wheeled tilting vehicle.

To improve the understanding of the dynamics of a three-wheeled tilting vehicle and the control actions from a human driver, a number of driving experiments were carried out. Chapter 4 describes the experimental set up and the results.

Chapter 5 discusses the development of the vehicle model and the method of deriving the tyre model parameters using the experimental results in its first two main sections. The third section concerns the development of a driver model that tracks a demand trajectory using feedback signals and control actions that are similar to those of a real driver.

Chapter 6 covers the simulation work that has been carried out to validate the vehicle and tyre models, analyse a PID based Steer Tilt Control system, and to study the difficulties of controlling the roll when there are unknown changes to the driving environment.

Chapter 7 discusses the development of a novel steer tilt control method using all that was learnt from the experimental and simulation results. Chapter 8 concludes the Thesis and presents a number of thoughts on future work.

CHAPTER 2. LITERATURE REVIEW

The aim of this chapter is to critically review the literature relevant to the study of tilting three-wheelers and their control. The first section examines the analogy between the control of an inverted pendulum on a cart and the roll angle control of a tilting vehicle. The second section of the chapter gives an overview of vehicle modelling methods. The third section analyses the roll control methods that have been presented in the literature. As a part of the analysis, the vehicle models and roll controller have been replicated in Matlab/Simulink to verify the results that were presented in the literature. It was established that STC was similar to the control actions of a bicycle or motorcycle rider. Hence, the fourth section of this chapter is a review of two-wheeler control. The first part of this section explains the theory of bicycle dynamics. The following part discusses the literature on autonomous bicycles and the balancing of unmanned bicycles. As part of the review of the unmanned bicycle control method, the system was replicated and tested. The next part reviews the particulars of motorcycle control namely: the rider physique and skill, rider control actions, hands free riding and developments in motorcycle steer-by-wire systems. The control algorithm of the motorcycle steer-by-wire system was replicated to test if it performed as well as the literature claimed. Following on from bicycle and motorcycle control is an overview of driver modelling methods. This includes both car driver and motorcycle rider models as well as optimal motorcycle manoeuvring methods and rider robots. The various components of this rider robot control algorithm were replicated and the simulation results compared to those presented in the literature. The final section of this chapter gives an overview of tyre modelling theory and the various methods that have been presented in the literature and discusses the advantages and disadvantages of each method.

The axis system that will be used throughout the following chapters is the SAE Coordinate system [41] as shown in Figure 2.1. Here the forward velocity is positive along the longitudinal axis and a right turn has a positive yaw angle, lateral acceleration, and roll angle.

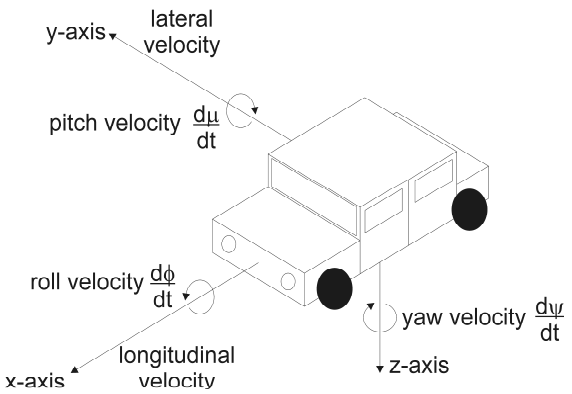

Figure 2.1 – SAE Coordinate System [41]

2.1 INVERTED PENDULUM ON A CART

A roll dynamics of a tilting vehicle are similar to those of an inverted pendulum on a cart. The lateral displacement of the vehicle becomes the left-to-right motion of the cart. A schematic of the pendulum on the cart is given in Figure 2.2. The pendulum has a mass m at height h from the pivot and inertia I. The pendulum's degrees of freedom are the roll angle φ and the lateral displacement y. The reaction forces and the pendulum pivot are R_Y horizontally and R_Z vertically. The cart has a mass M and can only displace laterally in the y direction. The cart is subject to an external force F, the pendulum pivot's reaction forces and the ground reaction forces N. The linearised equations of motion for this system are derived from the Free Body Diagrams: One equation for the sideways motion (2.1) and one for the pendulum roll (2.2).

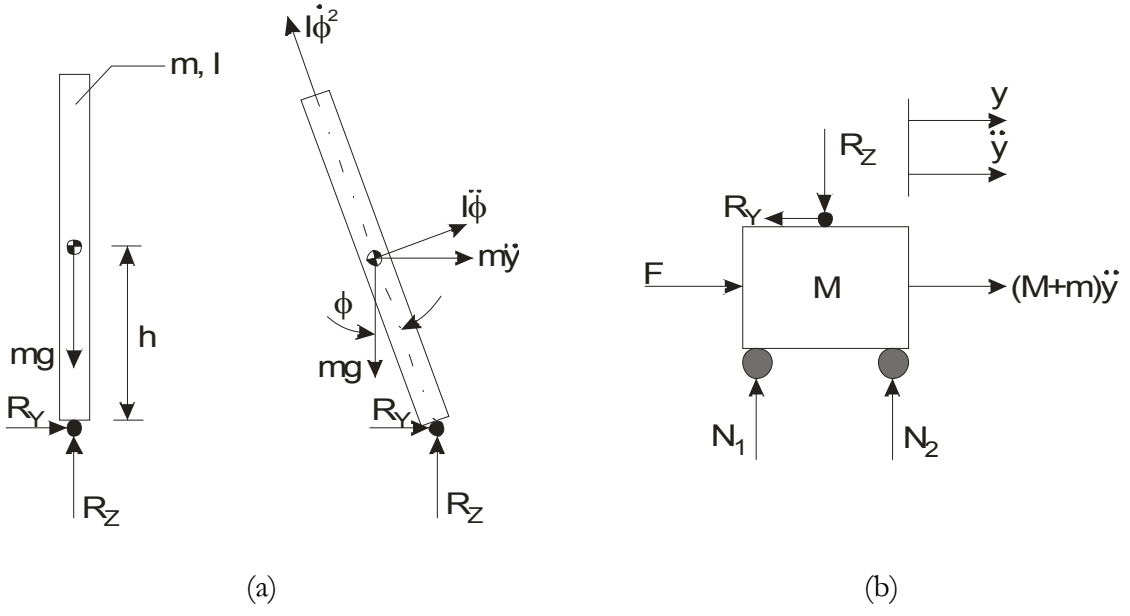

Figure 2.2 – Schematic Diagrams of an Inverted Pendulum on a Cart (a) Upright Pendulum (left) Tilted Pendulum (right) (b) Cart

$$(M+m)\,\ddot{y} - mh\ddot{\phi} = F \tag{2.1}$$

$$\left(I + mh^2\right)\ddot{\phi} - mgh\phi = -mh\ddot{y} \tag{2.2}$$

The equations of motion of a pendulum on a cart are typically simplified by excluding the roll velocity and by linearising the sine and cosine functions for a zero roll angle. For a pendulum on a cart, the control goal is often to maintain a zero tilt angle, so the linearisation is valid. However, a tilting vehicle could reach tilt angles up to 45 degrees, in which case the linearisation is no longer a close approximation. The pendulum roll can be controlled in various ways as shown by Dorf and Bishop [42]. The feasibility of these methods in a vehicle context will be discussed in Chapter 7.

2.2 VEHICLE MODELS

The following section describes two common vehicle models that are usually applied to simulate four-wheeled vehicles and how they can be adapted to simulate a tilting three-wheeler.

2.2.1 The Geometric 'Bicycle' Model

This basic vehicle model is generally referred to as the 'bicycle' model by Milliken and Milliken [43] since the front wheels are represented by single wheel and so are the rear wheels. Figure 2.3 shows a schematic of this 'bicycle' model and defines the basic geometry and degrees of freedom. The definition of this model includes the assumptions that there is no longitudinal or lateral load transfer, roll or pitch motion, a constant velocity, linear tyre cornering stiffnesses, position control, no aerodynamic effects, and no chassis or suspension compliance effects. These assumptions are justified since the purpose of this model is to study the basic vehicle motion.

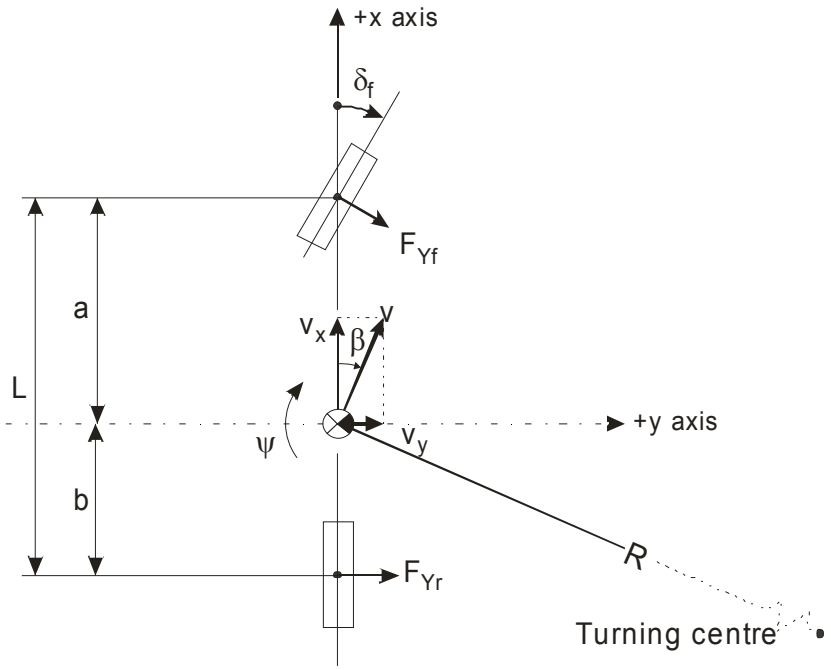

Figure 2.3 – Bicycle model schematic diagram based on Milliken and Milliken [43]

Low speed cornering with the 'bicycle' model can be described as a geometric problem. At low speed, the lateral acceleration is negligible, the tyre slip angles are zero, and the wheels roll in their own planes. The front and rear wheels roll along concentric circles, where the front wheels are located on a larger radius circle than the rear wheels. It can be shown that the steer angle is proportional to the turning radius and the wheelbase - assuming small angles. For an equal radius turn, a long wheelbase vehicle will require a larger steer angle than a short wheelbase vehicle. The geometric steer angle is commonly referred to as the Ackermann Steering Angle [44] and its definition is given in equation (2.3).

$$\delta_f = \frac{L}{R} \tag{2.3}$$

The bicycle model has three motion variables of interest: forward velocity v_x, lateral velocity v_Y and yaw velocity $d\psi/dt$. The vector sum of the forward and lateral velocities is the path velocity v, which is perpendicular to the corner radius R. The difference between the direction of the velocity vector sum and the attitude of the vehicle, its local x-axis, is the body slip angle β. To simplify the system, the forward velocity and the vector sum are assumed to be the same. This leaves the lateral velocity and the yaw rate as the two remaining degrees of freedom. The lateral acceleration consists of the rate of change in the lateral velocity and the centripetal acceleration as shown in equation (2.4).

$$a_{\mathrm{Y}} = v_{\mathrm{X}}\frac{\mathrm{d}\psi}{\mathrm{d}t} + \frac{\mathrm{d}v_{\mathrm{Y}}}{\mathrm{d}t} \tag{2.4}$$

The vehicle model does not include a roll as a degree of freedom. However, it can be used if it is assumed that the rolling cabin is mounted on top of a non-tilting platform as done by So and Karnopp [23, 24]. They assumed that the lateral velocity was proportional to the velocity vector of the front wheel(s) as shown in equation (2.5) and that the steering angle was defined by equation (2.3) so that the yaw rate could be defined by equation (2.6). Combining equations (2.5) and (2.6) into equation (2.4), the lateral acceleration was defined by equation (2.7).

$$v_{\mathrm{Y}} = \left(\frac{\mathrm{b}}{L}\right)\vec{v_{\mathrm{f}}} \cong \frac{v_{\mathrm{X}}}{L}\mathrm{b}\delta_{\mathrm{f}} \tag{2.5}$$

$$\frac{\mathrm{d}\psi}{\mathrm{d}t} = \frac{v_{\mathrm{X}}}{L}\tan\delta_{\mathrm{f}} \cong \frac{v_{\mathrm{X}}}{L}\delta_{\mathrm{f}} = \frac{v_{\mathrm{X}}}{R} \tag{2.6}$$

$$a_{\mathrm{Y}} = \dot{v_{\mathrm{Y}}} + \frac{\mathrm{d}\psi}{\mathrm{d}t}v_{\mathrm{X}} = \frac{\dot{v_{\mathrm{X}}}}{L}\mathrm{b}\delta_{\mathrm{f}} + \frac{v_{\mathrm{X}}}{L}\mathrm{b}\dot{\delta}_{\mathrm{f}} + \frac{v_{\mathrm{X}}^2}{L}\delta_{\mathrm{f}} \tag{2.7}$$

The roll equation So and Karnopp [23, 24] used to describe the roll dynamics of the vehicle was the roll equation for an inverted pendulum on a cart as shown in equation (2.2). This equation was combined with the definition of the lateral acceleration given by equation (2.7) resulting in equation (2.8). It was assumed that the mass of the platform was much smaller than the mass of the rolling cabin m and therefore negligible. The cabin roll inertia was given by I_{xx} and the height of the centre of gravity above the road was h.

$$\left(I_{\mathrm{xx}} + mh^2\right)\ddot{\phi} - mgh\phi = -mh\left(\frac{\dot{v_{\mathrm{X}}}}{L}\mathrm{b}\delta_{\mathrm{f}} + \frac{v_{\mathrm{X}}}{L}\mathrm{b}\dot{\delta}_{\mathrm{f}} + \frac{v_{\mathrm{X}}^2}{L}\delta_{\mathrm{f}}\right) \tag{2.8}$$

This vehicle model can be applied to both a four-wheeler and a three-wheeler since it assumes that the vehicle dynamics are dependent on the forward velocity and the steering angle only and not on road-tyre interaction. This vehicle model is very basic and relies on many assumptions. The question is whether a roll control system that is developed with this vehicle model could work in reality as there are such a great number of differences between a real vehicle's dynamics and the model.

2.2.2 *The Linear Dynamic 'Bicycle' Model*

This vehicle model also assumes that the road-tyre interaction of the two front wheels and the two rear wheels of a four-wheeler can be combined so that the vehicle is reduced to a single front and rear wheel. However, the dynamics of this vehicle are a result of force and moment generation through road-tyre interaction. A lateral force is generated because of the difference between the heading angle of the wheel and the wheel's velocity vector. This difference is called the slip angle and the slip angles of a front and rear wheel are illustrated in Figure 2.4. The definitions for the slip angles are linearised assuming they are small so that $\sin(\theta)\approx\theta$ and $\cos(\theta)\approx 1$. The model assumes that the tyre cornering stiffnesses are linear so the lateral forces are defined by equation (2.9). The factor two in equation (2.9) is for the two front and rear wheels of a four-wheeler. This can be adjusted appropriately for a three-wheeler configuration.

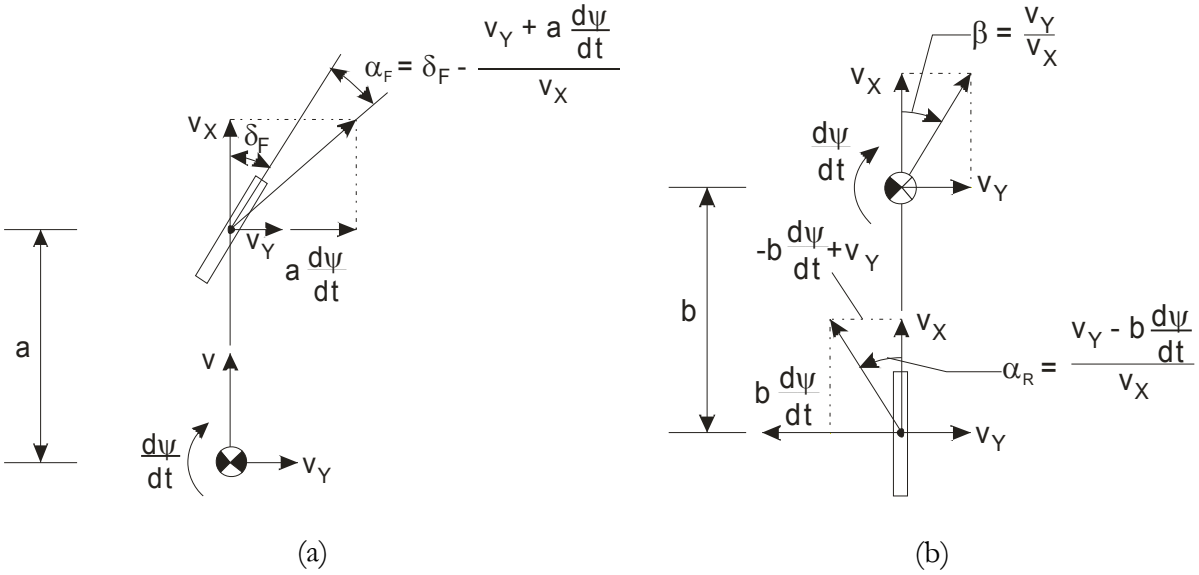

Figure 2.4 – Slip angle definition (a) Front wheel (b) Rear wheel as adapted from Milliken and Milliken [43]

$$F_{Yf} = 2C_{\alpha_f}\alpha_f \qquad F_{Yr} = 2C_{\alpha_r}\alpha_r \tag{2.9}$$

The dynamic vehicle model has four degrees of freedom namely: longitudinal translation X, lateral translation Y, yaw ψ, and roll φ. Hence there are four equations of motion as given by equations (2.10) to (2.13) based on section 1.3.1 of Pacejka [45]. Equation (2.10) defines the vehicle's longitudinal dynamics caused by the longitudinal tyre forces F_X. Equation (2.11) describes the vehicle's lateral dynamics. Equation (2.12) shows that the yaw dynamics are a result of the tyres forces as well as the aligning moments M_Z. The equation also includes the eventuality

that the degrees of freedom are not parallel to the inertia tensor by incorporating the I_{XZ} term and the roll acceleration. The roll dynamics are defined by equation (2.13). These equations assume that the roll angle is very small and therefore $\sin(\varphi)\approx\varphi$ and $\cos(\varphi)\approx 1$. It is also assumed that the gyroscopic moments from the wheels are small in comparison to the other moments acting on the vehicle. Also, the model does not include and steering dynamics. If the velocity is constant, equation (2.10) can be omitted.

$$m\left(\dot{v}_{\mathrm{X}} - v_{\mathrm{Y}}\dot{\psi} - h\phi\ddot{\psi} - 2h\dot{\psi}\dot{\phi}\right) = F_{\mathrm{Xf}} - \delta_{\mathrm{f}}F_{\mathrm{Yf}} + F_{\mathrm{Xr}} \tag{2.10}$$

$$m\left(\dot{v}_{\mathrm{Y}} + v_{\mathrm{X}}\dot{\psi} + h\ddot{\phi} - h\dot{\psi}^2\phi\right) = \delta_{\mathrm{f}}F_{\mathrm{Xf}} + F_{\mathrm{Yf}} + F_{\mathrm{Yr}} \tag{2.11}$$

$$\begin{aligned} I_{\mathrm{Z}}\ddot{\psi} - I_{\mathrm{XZ}}\ddot{\phi} - mh\left(\dot{v}_{\mathrm{X}} - v_{\mathrm{Y}}\dot{\psi}\right)\phi = a\delta_{\mathrm{f}}F_{\mathrm{Xf}} + aF_{\mathrm{Yf}} + M_{\mathrm{Zf}} \\ - bF_{\mathrm{Yr}} + M_{\mathrm{Zr}} \end{aligned} \tag{2.12}$$

$$\begin{aligned} &\left(I_{\mathrm{X}} + mh^2\right)\ddot{\phi} + mh\left(\dot{v}_{\mathrm{Y}} + v_{\mathrm{X}}\dot{\psi}\right) \\ &- I_{\mathrm{XZ}}\dot{\psi} - \left(mh^2 + I_{\mathrm{Y}} - I_{\mathrm{Z}}\right)\dot{\psi}^2\phi = 0 \end{aligned} \tag{2.13}$$

If the tilting vehicle is a rolling cabin on a platform, this vehicle model would be more suitable for control system development than the geometric model presented in section 2.2.1.

2.2.3 The (Non-Linear) Dynamic Motorcycle Model

The dynamics of a three-wheeled tilting vehicle are similar to the dynamics of a motorcycle since the vehicle roll and the steering assembly are similar. This non-linear model includes a non-linear definition of the slip angle as shown in equation (2.14).

$$\alpha_{\mathrm{f}} = \delta_{\mathrm{f}} - \tan^{-1}\left(\frac{v_{\mathrm{Y}} + a\dot{\psi}}{v_{\mathrm{X}}}\right) \qquad \alpha_{\mathrm{r}} = -\tan^{-1}\left(\frac{v_{\mathrm{Y}} - b\dot{\psi}}{v_{\mathrm{X}}}\right) \tag{2.14}$$

The tyre forces of this model are defined by equation (2.15) for a motorcycle and equation (2.16) for a three-wheeler with two rear wheels where γ is the camber angle. In equation (2.16) the

camber force from the rear wheels is placed in brackets as this is only a major force if the rear wheels tilt with the vehicle, otherwise it can be assumed that the rear roll is negligible.

$$F_{\mathrm{Yf}} = C_{\alpha_\mathrm{f}}\alpha_\mathrm{f} + C_{\gamma_\mathrm{f}}\gamma_\mathrm{f} \qquad F_{\mathrm{Yr}} = C_{\alpha_\mathrm{r}}\alpha_\mathrm{r} + C_{\gamma_\mathrm{r}}\gamma_\mathrm{r} \tag{2.15}$$

$$F_{\mathrm{Yf}} = C_{\alpha_\mathrm{f}}\alpha_\mathrm{f} + C_{\gamma_\mathrm{f}}\gamma_\mathrm{f} \qquad F_{\mathrm{Yr}} = 2C_{\alpha_\mathrm{r}}\alpha_\mathrm{r}\,(+2C_{\gamma_\mathrm{r}}\gamma_\mathrm{r}) \tag{2.16}$$

The equations of motion of the motorcycle model have been adapted from section 11.3 by Pacejka [45]. The lateral dynamics are defined by equation (2.17) where m_f is the mass of the steering assembly, k is the distance between the steering assembly's centre of gravity and the vehicle's main body centre of gravity, h is the vehicle's centre of gravity height above the road, e is the distance between the steering assembly centre of gravity and the steering axis, and ε is the angle between the steering axis and the road. Equation (2.18) shows that the yaw dynamics are also affected by the steering acceleration and the steering assembly's mass m_f and inertia I_{Zf}, the gyroscopic moments from the roll and steering velocity and the wheel speed ω_w and inertia I_{Yw}, the drag force F_d acting at the centre of pressure at h_d, and the front wheel load F_{Xf} and the steering geometry's trail t_t. The roll equation (2.19) shows that the roll is affected by tyre moments M_X and also the steering geometry t_t.

$$\begin{aligned} F_{\mathrm{Yf}} + F_{\mathrm{Yr}} = \quad & m\left(\dot{v_\mathrm{Y}} + v_\mathrm{X}\dot{\psi}\right) + \\ & + m_\mathrm{f}\,k\ddot{\psi} + mh\ddot{\phi}\cos(\phi) + m_\mathrm{f}\,e\ddot{\delta}_\mathrm{f} - \\ & - F_{\mathrm{Xf}}\cos(\varepsilon)\,\delta_\mathrm{f} \end{aligned} \tag{2.17}$$

$$\begin{aligned} a F_{\mathrm{Yf}} - b F_{\mathrm{Yr}} + M_{\mathrm{Zf}} + M_{\mathrm{Zr}} = \quad & m_\mathrm{f}\,k\left(\dot{v_\mathrm{Y}} + v_\mathrm{x}\dot{\psi}\right) + \\ & + I_\mathrm{Z}\ddot{\psi} + I_{\mathrm{XZ}}\ddot{\phi} + \\ & + \left(m_\mathrm{f}\,e\,k + I_{\mathrm{Zf}}\cos(\varepsilon)\right)\ddot{\delta}_\mathrm{f} - \\ & - I_{\mathrm{Yw}}\dot{\phi}\omega_\mathrm{w} - I_{\mathrm{Yw}}\sin(\varepsilon)\,\dot{\delta}_\mathrm{f}\omega_\mathrm{w} - \\ & - F_\mathrm{d}\,h_\mathrm{d}\,\phi - F_{\mathrm{Xf}}\left(t_\mathrm{t} + a\cos(\varepsilon)\right)\delta_\mathrm{f} \end{aligned} \tag{2.18}$$

$$M_{Xf} + M_{Xr} = mh\left(\dot{v}_Y + v_X\dot{\psi}\right)\cos(\phi) + \\ + I_{XZ}\ddot{\psi} + \left(mh^2 + I_X\right)\ddot{\phi} - \\ - \left(t_t F_{Zf} + m_f\, e\, g\right)\delta_f - mhg\sin(\phi) \tag{2.19}$$

A simplified and linearised motorcycle model was used by Gohl et al. [36, 37]. Equations (2.20) to (2.22) define the lateral, yaw, and roll dynamics respectively as specified by Gohl et al.. These equations show similarities with equations (2.17) to (2.19). In the definition of the lateral acceleration the yaw acceleration of the steering assembly, the steering acceleration and the steering geometry factors had been omitted, but the roll velocity had been added for completeness. The latter term was later omitted, since its magnitude was negligible in comparison to the other forces. The definition of the yaw dynamics excluded the aligning moment from the tyres, the lateral acceleration of the steering assembly, the inertia product I_{XZ} since it was assumed that the degrees of freedom were parallel to the principal axes of inertia, and the aerodynamic drag force F_d. The steering torque T_s represented the steering acceleration and the steering geometry terms of the equation. The definition of the roll dynamics assumed that the tyre moments were negligible. Furthermore, instead of the vehicle total lateral acceleration, the resultant lateral force F_Y was used represent the acceleration. For completeness, the roll velocity was included in the roll equation, but it was omitted later due to its negligible magnitude. Again, the steering torque T_s represented the steering dynamics as seen in equation (2.19).

$$F_{Yf} + F_{Yr} = m\left(\dot{v}_Y + v_X\dot{\psi}\right) + mh\ddot{\phi}\cos(\phi) - mh\dot{\phi}^2\sin(\phi) \tag{2.20}$$

$$aF_{Yf} - bF_{Yr} = I_Z\ddot{\psi} + T_s\cos(\varepsilon) + \\ + 2\left(I_{Xw} - I_{Yw}\right)\dot{\phi}\omega_w - 2\left(I_{Xw} - I_{Yw}\right)\sin(\varepsilon)\dot{\delta}_f\omega_w \tag{2.21}$$

$$0 = \left(F_{Yf} + F_{Yr}\right)\cos(\phi) + \\ + \left(I_X + mh^2\right)\ddot{\phi} + mh^2\dot{\phi}^2\cos(\phi)\sin(\phi) - \\ - 2\left(I_{Xw} - I_{Yw}\right)\dot{\phi}\omega_w + 2\left(I_{Xw} - I_{Yw}\right)\sin(\varepsilon)\dot{\delta}_f\omega_w - \\ - T_s \tag{2.22}$$

In order to simulate the vehicle, Gohl et al. linearised the equations assuming that the roll angle φ was close to zero. The slip angles were also linearised, the tyre stiffnesses were assumed linear and the camber angle was assumed equal to the roll angle. The test vehicle used by Gohl et al. had two front wheels so the definition of the lateral force from equation (2.16) was reversed.

It is debatable whether it can be assumed that the roll angle is small and can therefore be linearised since the roll angle could reach up to 45 degrees. Secondly, it was deemed unlikely that the degrees of freedom were parallel to the principal axes of inertia. Also, the camber and the roll angle are not the same where the difference increases with greater tyre widths. The kinematics of the steering assembly results in additional disparity between the roll angle and the camber angle as well as the steering angle at the handle bars and the steering angle on the road plane as described by Cossalter [46]. In conclusion, this model may be oversimplified in comparison to the motorcycle model presented at the beginning of this section.

2.3 DIRECT TILT CONTROL

The aim of this section is to demonstrate, in simulation, how Direct Tilt Control works by replicating the results presented in the literature. DTC refers to a roll control system that calculates a roll angle demand and outputs a roll moment using a roll actuator. The roll angle demand can be determined in various ways as demonstrated by Kidane et al. [38-40] and the roll actuator can be any type of actuator.

So and Karnopp [23, 24] modelled a vehicle with DTC as shown in Figure 2.5. They used the geometric vehicle model as discussed in section 2.2.1. The inputs to the system are the steer angle at the front wheel δ_f and the forward velocity v_x. The vehicle dynamics are modelled using equation (2.7). The controller can therefore estimate the lateral acceleration from the steer and speed inputs. This lateral acceleration is then used to calculate the desired tilt angle φ_d as shown in equation (2.23). This roll angle is based on the assumption that the perceived acceleration a_{per} defined in equation (2.24) is zero when the vehicle is balanced. The perceived acceleration is measured at a height d from the roll axis usually located behind the driver's head. The perceived acceleration is zero when the vehicle is balanced because the resultant force and therefore the acceleration vector is parallel to the rolled vehicle's vertical axis as shown in Figure 2.6.

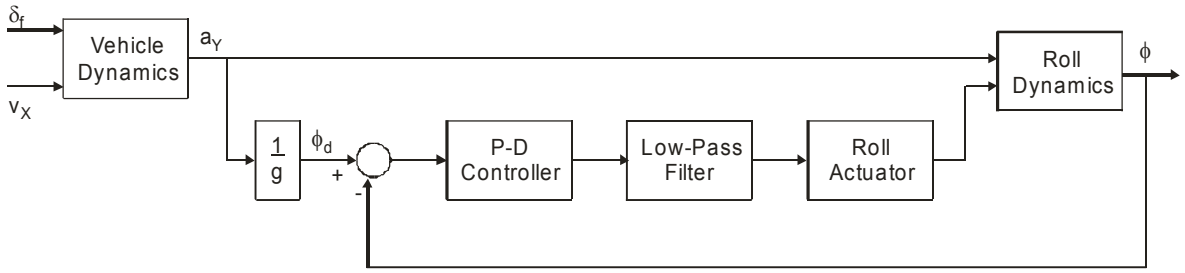

Figure 2.5 – DTC block diagram based on So and Karnopp [23, 24]

$$\phi_{\mathrm{d}} = \tan^{-1}\left(\frac{a_{\mathrm{y}}}{g}\right) \approx \frac{a_{\mathrm{y}}}{g} \tag{2.23}$$

$$a_{\mathrm{per}} = a_{\mathrm{y}}\cos(\phi) + d\ddot{\phi} - g\sin(\phi) \tag{2.24}$$

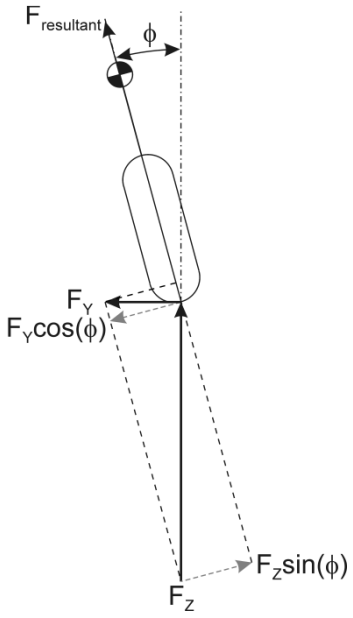

Figure 2.6 – Schematic illustrating the forces when the vehicle is rolled to the balanced roll angle based adapted from [20]

This demand tilt angle is compared to the measured tilt angle and the error is the input to the control system that consists of a Proportional-with-Approximate Derivative (P-D) controller and a roll actuator. The latter is presented as a spring-damper system. The output of the control scheme is a moment that is applied to the tilting body. An external roll moment M_{roll} was added to the roll dynamics from equation (2.8) as shown in equation (2.25). This equation was linearised to give the transfer function relating the roll angle to the lateral acceleration and the external roll moment as shown in equation (2.26).

$$\begin{aligned}\left(I_{\mathrm{X}}+mh^{2}\right)\ddot{\phi} = \quad & mgh\sin\left(\phi\right) - \\ & -mh\left(\frac{\dot{v_{\mathrm{X}}}}{L}\mathrm{b}\delta_{\mathrm{f}}+\frac{v_{\mathrm{X}}}{L}\mathrm{b}\dot{\delta}_{\mathrm{f}}+\frac{v_{\mathrm{X}}^{2}}{L}\delta_{\mathrm{f}}\right)\cos\left(\phi\right) + \\ & + M_{\mathrm{roll}}\end{aligned} \tag{2.25}$$

$$\phi = \frac{-mh\left(\frac{\dot{v_{\mathrm{X}}}}{L}\mathrm{b}\delta_{\mathrm{f}}+\frac{v_{\mathrm{X}}}{L}\mathrm{b}\dot{\delta}_{\mathrm{f}}+\frac{v_{\mathrm{X}}^{2}}{L}\delta_{\mathrm{f}}\right)+M_{\mathrm{roll}}}{\left(I_{\mathrm{X}}+mh^{2}\right)s^{2}-mgh} \tag{2.26}$$

First, the controller was tested with the input data given by So and Karnopp [23, 24] seen in Table 2.1. The goal was to replicate the results. For the individual DTC block, this exercise was successful. As was shown in the original paper, the system could not match the demand roll angle: this was caused by delays from the tilt dynamics. The difference in tilt angle can be seen in Figure 2.7 and is largely influenced by the actuator system response. In the second test, data from the CLEVER vehicle were used to model the vehicle and roll dynamics. With the CLEVER parameters, the roll angle and other states were analogous to those achieved with the original parameters.

Variable	So and Karnopp	CLEVER
mass m [kg]	200	434
roll inertia I_X [kg m^2]	50	14.5
wheelbase L [m]	2.2	2.4
distance from CG to front axle a [m]	1.1	1.53
distance from CG to rear axle b [m]	1.1	0.87
CG height above the road h [m]	1	0.51
distance from road to sensor d [m]	1	-
time constant DTC τ [s]	0.01	-
time constant STC τ [s]	0.01	-
DTC proportional gain k_p	15	-
DTC k_d	10	-
STC k_p	20	-
STC k_d	0.5	-
DTC actuator Spring stiffness [N/m]	11000	-
DTC actuator Damper coefficient [Ns/m]	900	-

Table 2.1 – Comparison of the input data from So and Karnopp [23, 24] and CLEVER

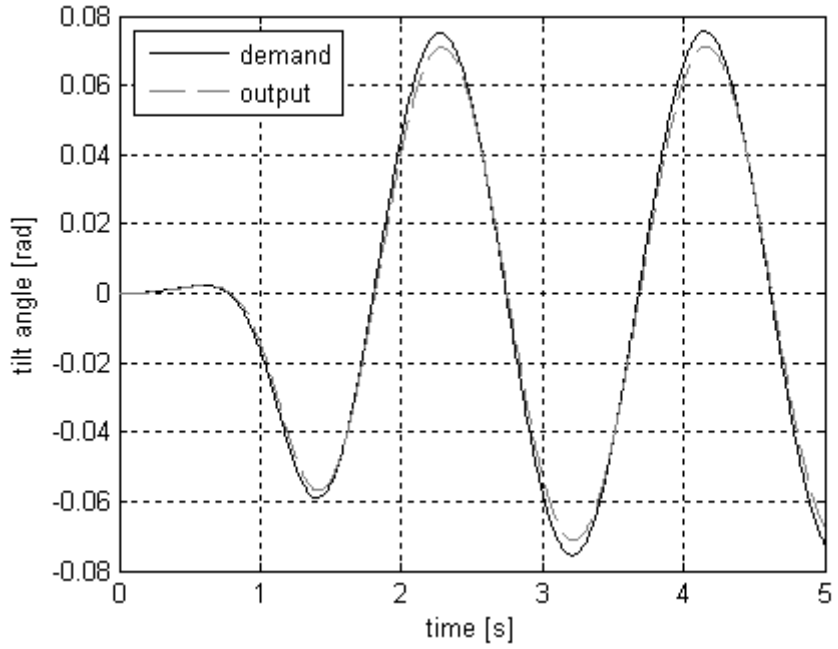

Figure 2.7 – DTC tilt angle demand and output comparison: image created from Matlab simulation results illustrating identical results to So and Karnopp [23, 24]

Kidane et al. [38-40] have recently presented a simulation and experimental study combining DTC and STC. For DTC, two definitions for the desired tilt angle were investigated. The first definition determined the desired lean angle according to the yaw rate as shown in equation (2.27) and the second determined the desired lean according to the total lateral acceleration as shown in

(2.28). The first definition assumes steady state turning where the lateral acceleration consists of the centripetal component only. The second definition includes transient effects as well as the acceleration caused by the gyroscopic moment as a result of the wheels spinning and the vehicle yawing. Both definitions aim to achieve a zero net moment acting at the centre of gravity of the vehicle.

$$\phi_{\mathrm{d}} = \frac{\mathrm{d}\psi}{\mathrm{d}t}\frac{v_{\mathrm{x}}}{g} = \frac{v_{\mathrm{x}}^2}{gR} = \frac{v_{\mathrm{x}}^2\delta_{\mathrm{f}}}{gL} \tag{2.27}$$

$$\phi_{\mathrm{d}} = \frac{\dot{v}_{\mathrm{Y}}}{g} + \frac{v_{\mathrm{X}}}{g}\dot{\psi} - \frac{2\left(I_{\mathrm{Xw}} - I_{\mathrm{Yw}}\right)\omega_{\mathrm{w}}}{mgh}\dot{\psi} \tag{2.28}$$

Kidane et al. [38-40] had tested the controller in simulation and in an experiment with an inverted pendulum on the back of a truck. Both tilt angle definitions ensured the controller stabilised the system, but the controller torque as calculated from equation (2.30) was significantly different. The torque estimated when using equation (2.27) to calculate the desired tilt angle was at least ten times larger than the torque estimated when the desired tilt angle was calculated with equation (2.28). A lower torque requirement is preferable in terms of the power needs of the control system and in this vehicle, the gyroscopic moments were significant enough to affect a notable difference in the demand roll angle calculation. It was noted that definition (2.28) was limited in its operational success by the fact that it required an accurate lateral acceleration measure devoid of noise. A third definition for the desired tilt angle was specified as being proportional to the driver's steer input as shown in equation (2.29). The advantage of this final definition was that during transient manoeuvres, the DTC system would not act against the STC system. As the driver intends to turn right, the STC system would turn the steering left first, which a regular DTC system would interpret as a signal to lean left. With both STC and DTC acting on the driver input, both controllers will be trying to achieve the same goals.

$$\phi_{\mathrm{d}} = k\left(\mathrm{driver\_input}\right) \tag{2.29}$$

$$M_{\mathrm{roll}} = -k_{\mathrm{p}}\left(\phi - \phi_{\mathrm{d}}\right) - k_{\mathrm{d}}\dot{\phi} \tag{2.30}$$

The DTC systems described above have only been validated in simulation or by minimal experimentation. However, the CLEVER vehicle has a working DTC system, see [11]. It uses the

driver steer angle and the forward velocity measurement to determine an open loop balanced lean angle as shown in equation (2.27).

This lean angle is achieved by opening the hydraulic circuit valve to let flow into one of the actuators, as shown in Figure 2.8. The actuator position is then fed back to verify the control action. This tilt control system required a number of adjustments in terms of signal processing, but overall it successfully leaned the vehicle whilst driving such that low levels of perceived acceleration were achieved and the driver felt that the vehicle was 'balanced' both statically and dynamically.

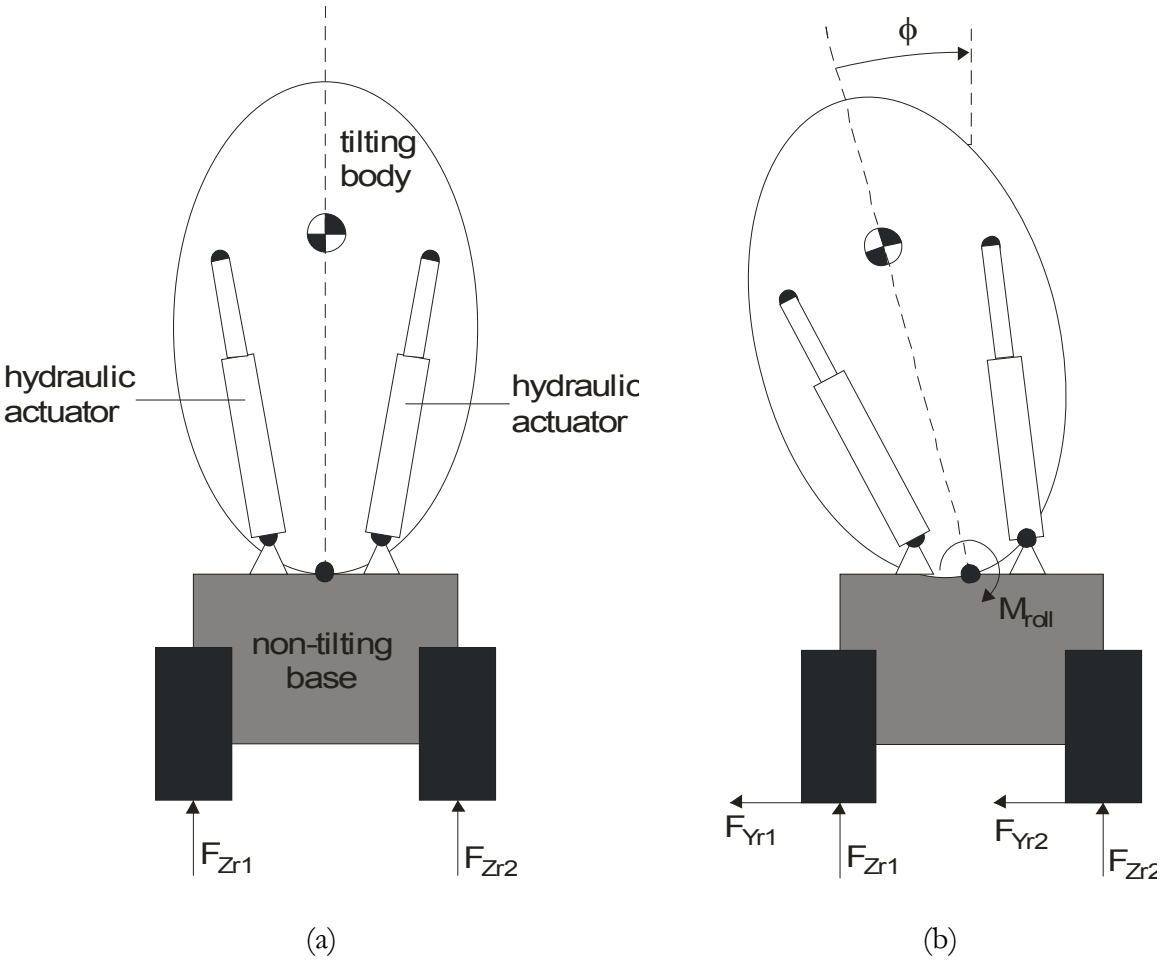

Figure 2.8 – CLEVER tilt system (a) schematic of the upright vehicle illustrating the vehicle components (b) schematic of the tilting vehicle illustrating the roll angle φ and the roll moment at the joint M_{roll} caused by the actuator extension

Although the dynamic tilt control was satisfactory, the DTC system had a few shortcomings. It required transient powers of up to 1 kW to lean the vehicle in a worst-case scenario, see Drew at al. [11]. Yet the major problem was the rear non-tilting unit rolling out of the bend. During testing, there were several occasions where the inner wheel of the rear unit lifted off the ground,

and in most cases resulted in the rear unit rolling over [47]. This occurred under a combination of circumstances: a heavier driver, a rapid steer input, and high levels of lateral accelerations. These conditions led to large tilting torque demands. Although the hydraulic actuators were acting on the rolling cabin, the reactions forces were applied through the rear unit. These reaction forces generated a roll moment on the rear unit that together with the roll moment caused by the side forces from the rear tyres led to load transfer from the inner wheel to the outer wheel and subsequent rollover.

The rear unit on its own could be regarded dynamically as a three-wheeled unit where the tilt joint is the single front wheel support. In this analogy, the rear unit is a tall and narrow vehicle. The load transfer between the two rear wheels could be determined from the three-wheeler dynamics equations from Huston et al. [19] using the geometric variables shown in Figure 2.9.

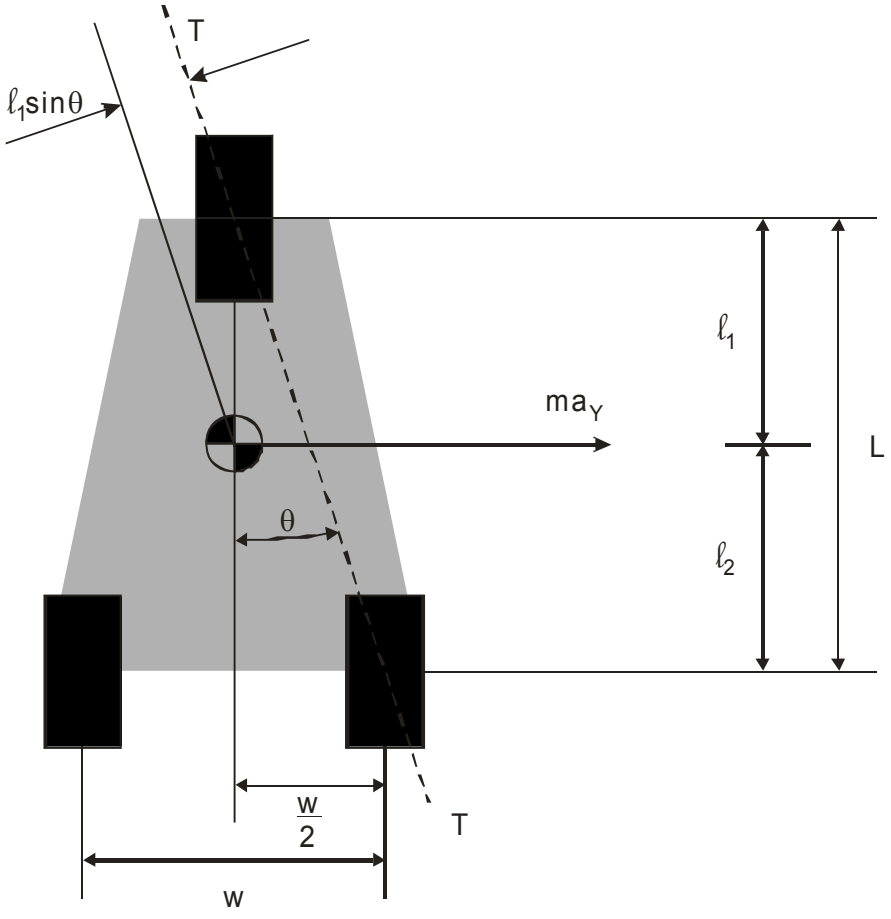

Figure 2.9 – Rollover diagram of three-wheeler

Equation (2.31) defines the moment about the TT-axis show in Figure 2.9. This axis is the line of support from the front wheel or the tilt joint to one of the rear wheels. The moment about this axis is caused by the lateral acceleration and gravity acting on the centre of gravity. The normal

load on the rear wheel that does not lie on the TT-axis is defined by equation (2.32). When this normal load is zero, the rear unit could roll over. The critical rollover velocity at which this occurs is given by equation (2.33). It was noted that this method of determining the normal load was somewhat unconventional, using lateral acceleration rather that individual lateral tyre forces, yet it simplified the derivation.

$$M_{\mathrm{TT}} = m_{\mathrm{r}} g \ell_1 \sin(\theta) - m_{\mathrm{r}} \frac{v_{\mathrm{x}}^2}{R} \cos(\theta)\, h_{\mathrm{CGr}} \tag{2.31}$$

$$F_{\mathrm{Zr1}} = \frac{M_{\mathrm{TT}}}{\cos(\theta)} = m_{\mathrm{r}} g \ell_1 \tan(\theta) - m_{\mathrm{r}} \frac{v_{\mathrm{x}}^2}{R} h_{\mathrm{CGr}} \tag{2.32}$$

$$F_{\mathrm{Zr1}} = 0$$

$$v_{\mathrm{roll}} = \sqrt{\frac{g \ell_1 R w}{2 h_{\mathrm{CGr}} (\ell_1 + \ell_2)}} \tag{2.33}$$

Figure 2.10 shows how the rear unit rollover velocity for the CLEVER vehicle varies with the radius of the trajectory. In this steady state condition, the CLEVER rear unit does not roll over until the cornering acceleration is greater than 1g. However, in combination with an actuator induced roll moment and additional transient lateral accelerations, the unit could roll before reaching such cornering conditions.

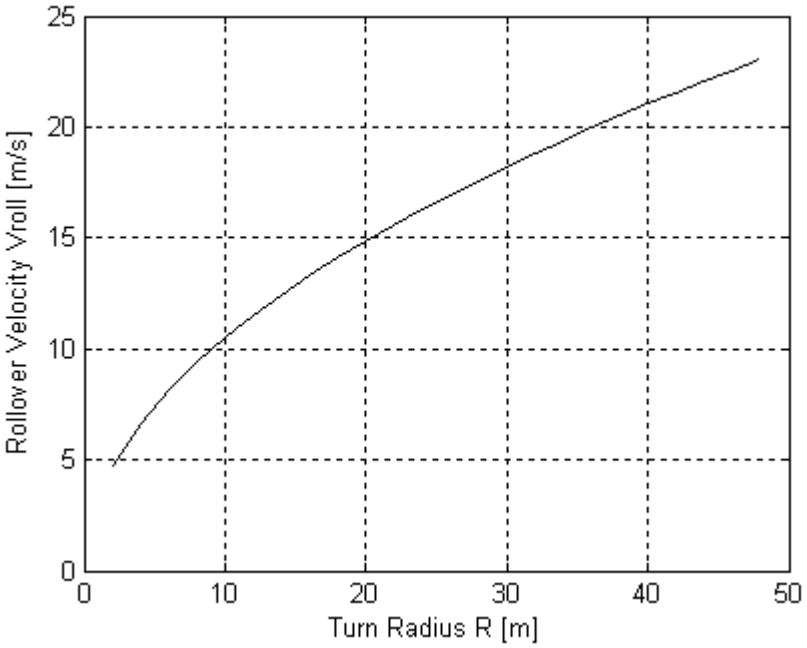

Figure 2.10 – Steady State rollover velocity for various turning circle radii

In the above equations, it was assumed that the roll axis of the rear unit lay on the road plane. However, the tilting pivot on the vehicle lies above the road plane, meaning that the rear unit would roll about this tilting axis also. This effect was described by Cossalter et al. [18] who noted the risk of the rear unit rolling out of the bend. In the development of the three-wheeled tilting moped, the load transfer ΔF_{Yr} of the rear wheels was thoroughly studied and characterised by equation (2.34). In this equation, the lateral displacement of the roll axis centre $y_{R.C.}$ is the lateral position of the instantaneous rotation centre, h_{CGr} is the height of the rear unit centre of gravity, $h_{R.C.}$ is the height of the rotation centre above or below the road plane. These parameters are illustrated in Figure 2.11 and Figure 2.12. This equation is similar to (2.31), but accommodates a tilt axis that does not lie on the road plane. It shows that when the tilt axis lies above the road plane, and $h_{R.C.}$ is positive, the load transfer gains an extra term in $F_{Yr}\, h_{R.C.}$. Assuming a similar steady state constant radius trajectory, the critical velocity for a vehicle with a fixed inclined tilt axis, such as CLEVER, above the ground is given by equation (2.35). This equation defines a different rollover velocity from equation (2.33), because it includes the roll axis location. It was noted that this equation included the centripetal force acting on the rear unit as well as the tyre side force in the load transfer equation. By adding this term, the equation predicts a lower critical velocity than without it.

The roll axis location above the ground results in a shorter the height of the centre of gravity above the roll axis, and a smaller rollover moment. The effect of the roll axis on the tilting part of the vehicle will be discussed in more detail later in chapter 3.

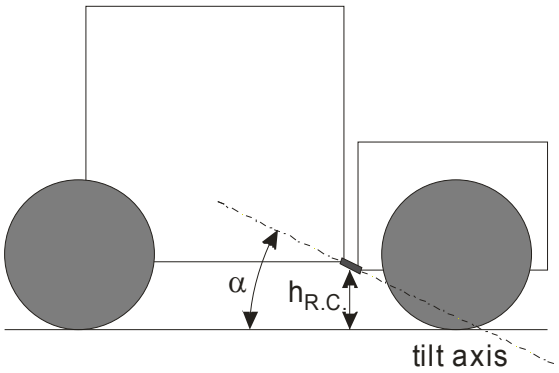

Figure 2.11 – Side-on view of the tilt axis definition

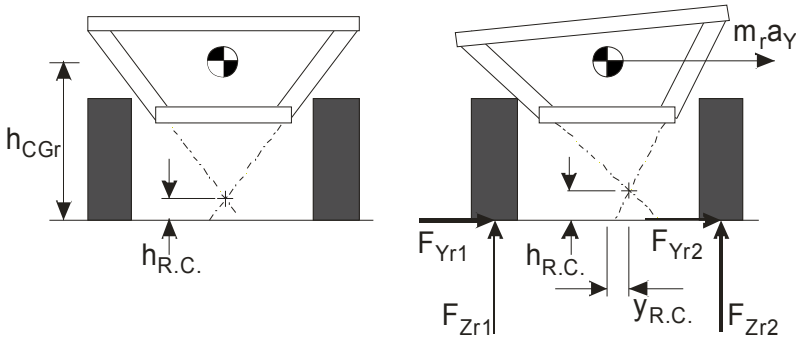

Figure 2.12 – Rear view of the tilt axis and the forces on the rear unit

$$\Delta F_{\mathrm{Zr}} = \frac{\left(m_{\mathrm{r}} g - \left(F_{\mathrm{Zr1}} + F_{\mathrm{Zr2}}\right)\right) y_{\mathrm{R.C.}} + m_{\mathrm{r}} \frac{v_{\mathrm{x}}^2}{R} \left(h_{\mathrm{CGr}} - h_{\mathrm{R.C.}}\right) + \left(F_{\mathrm{Yr1}} + F_{\mathrm{Yr2}}\right) h_{\mathrm{R.C.}}}{w} \tag{2.34}$$

$$\text{assuming } F_{\mathrm{Yr1}} + F_{\mathrm{Yr2}} = \frac{a}{L} m \frac{v_{\mathrm{x}}^2}{R}$$

$$v_{\mathrm{roll}} = \sqrt{\frac{mg\, awR}{L\left(m_{\mathrm{r}}\left(h_{\mathrm{CGr}} - h_{\mathrm{R.C.}}\right) + h_{\mathrm{R.C.}} \frac{a}{L} m\right)}} \tag{2.35}$$

2.4 STEER TILT CONTROL

The aim of this section is to demonstrate the workings of Steer Tilt Control as it has been presented in literature and to illustrate where its shortcomings lie. Steer Tilt Control refers to a roll controller that modifies the steering angle input from the driver to ensure roll stability. This roll control is based on what is called countersteer, which is a small amount of steer that is applied in the opposite direction of the turn and causes a small change in the lateral acceleration. This change in lateral acceleration may be small, but it can cause a small roll moment and once the vehicle is rolling, the gravitational acceleration ensures the roll continues.

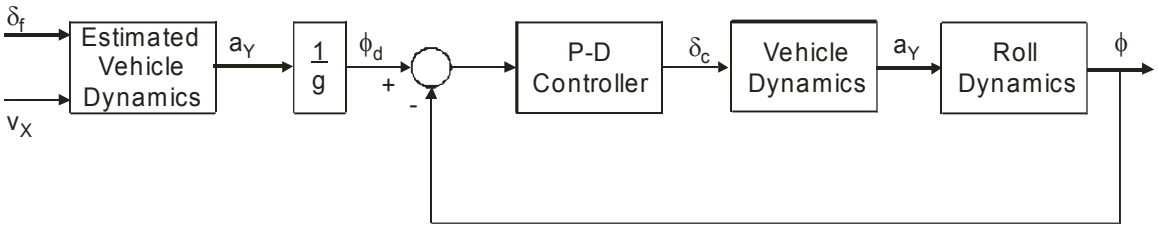

Figure 2.13 – STC block diagram as adapted from So and Karnopp [23, 24]

A schematic representation of the STC system is shown in Figure 2.13. The inputs are the steer angle δ_f and forward velocity v_x. These are used to estimate the lateral acceleration a_Y using equation (2.7). The roll angle demand is then determined using equation (2.23). This demand value is compared to the measured tilt angle and the error is used as the input to the controller. This is a P-D controller with negative gain. The negative gain is necessary to deal with the non-minimum phase nature of the system: to roll to the right, a lateral force to the left is required and vice versa. The output of the controller is a steer angle δ_c. This steer angle is the angle at which the vehicle will be steered instead of the driver steering input. This steer angle will cause the vehicle's lateral acceleration in combination with the forward velocity assuming the vehicle's lateral dynamics can be modelled with equation (2.7). If the roll dynamics are modelled according to equation (2.8) the only input to the roll equation is the lateral acceleration and the output is the roll angle φ, which is fed back. It should be noted that no actuator dynamics are included in this model. In other words, the control steer is applied instantaneously and the steer angle immediately generates a lateral acceleration. The controller was executed in Matlab/Simulink and tested with the input data and vehicle parameters used by So and Karnopp [23, 24] shown in Table 2.1.

The original simulation results produced by So and Karnopp [23, 24] were successfully replicated. In the second test, data from the CLEVER vehicle were used as the parameters. Once more,

results were analogous to those with the original data. The DTC system does not change the driver's steer input δ_f, so the DTC data in Figure 2.14 are equal to the simulation's the steer input. The STC system does change the steer angle in its control action and this output δ_c was shown to be significantly larger the input shown in Figure 2.14. This increased steer angle δ_c resulted in an equally increased lateral acceleration as illustrated by Figure 2.15. However, the model showed that the demand tilt angle was accurately tracked as seen in Figure 2.16.

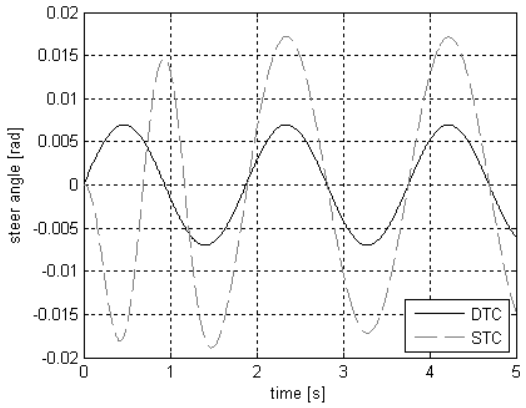

Figure 2.14 – Replicated result of So and Karnopp [23, 24] STC system: Variation in front wheel steer angle where the DTC signal is equal to the driver steer input δ_f

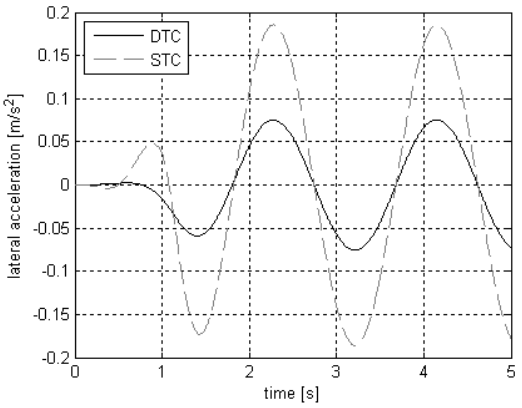

Figure 2.15 – Replicated result of So and Karnopp [23, 24] STC system: Variation in lateral acceleration where the DTC signal is equal to the lateral acceleration the driver would expect given the input steer δ_f and speed v_x

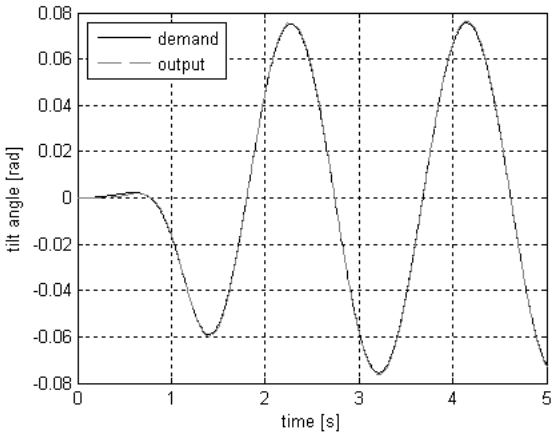

Figure 2.16 – Replicated result of So and Karnopp [23, 24] STC system: STC tilt angle demand and output comparison

Gohl et al. [36, 37] presented an STC computer model with promising results. The vehicle was modelled by equations (2.20) to (2.22). The simulation results showed that both the lean and the steer angle could be controlled to follow an input demand. Moreover, the experimental results

confirmed that the vehicle could be balanced with the proposed control scheme. A block diagram of this system is presented in Figure 2.17. The system input is the desired tilt angle. This tilt angle is compared to the compensated feedback. Proportional control is then applied to the error. The result is steer angle compensation. The compensation steer angle is added to the steer angle for the desired tilt, calculated from feedforward block G_{ff}. This sum is the angle at which the vehicle is steered. The forward speed is kept constant. The steer angle is applied to the vehicle dynamics, which consists of the steering dynamics and the tilt dynamics, and the output is the tilt angle. This model was translated to a Simulink block model with the same dynamic equations as the previous models and vehicle parameters as shown in Table 2.2. The same dynamic equations were used in order to compare the control strategies appropriately. However, it was found that the results were different from the results in the literature [36, 37]. In the literature, the system appeared to be performing well: the tilt angle tracked the demand with minimum error and the intended path was followed.

Variable	Gohl et al.	CLEVER
mass m [kg]	96	434
rolling mass m_t [kg]	[96]	283
yaw inertia I_Z[kg m^2]	60	235.5
pitch inertia I_Y[kg m^2]	60	[235.5]
roll inertia I_X [kg m^2]	18	14.5
wheelbase L [m]	1.53	2.4
front contact patch to CG a [m]	0.69	1.53
rear contact patch to CG b [m]	0.84	0.87
CG height above the ground h [m]	0.25	0.51
sideslip stiffness front $C_{\alpha f}$ [N/rad]	3500	11880
sideslip stiffness rear $C_{\alpha r}$[N/rad]	5480	32650
camber stiffness front $C_{\gamma f}$ [N/rad]	1000	2330
camber stiffness rear $C_{\gamma r}$[N/rad]	2000	-

Table 2.2 – Vehicle parameters used by Gohl et al. [36, 37] in comparison to the CLEVER vehicle

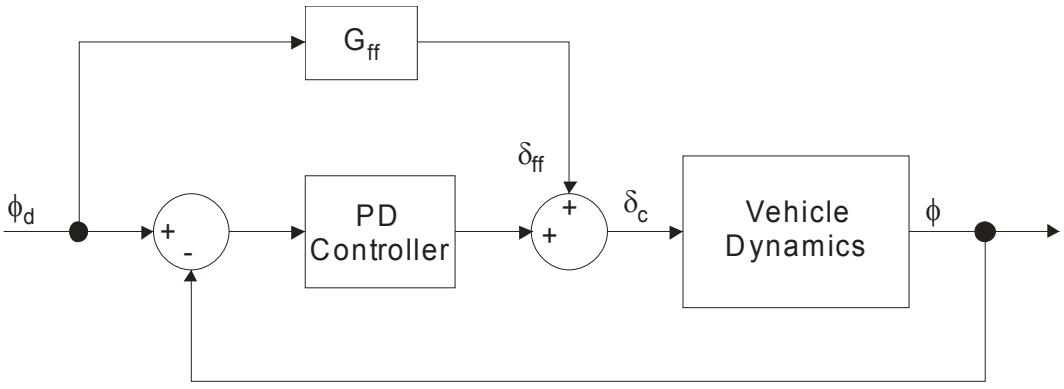

Figure 2.17 – Block diagram of STC method presented by Gohl et al. [36, 37]

Figure 2.18 shows a very different result from the literature. The rise time to achieve the correct tilt angle was unacceptably long and the overshoot was equally unacceptable. The steer angle used to calculate the demand tilt angle is plotted against the steer angle the controller required to force the vehicle to this demand in Figure 2.19. This result showed that the controller applied very large steering adjustments to track the tilt angle. Consequently, the lateral acceleration and perceived acceleration that result from this output steer angle are equally large, see Figure 2.20. Most importantly, the path response contains a significant error, shown in Figure 2.21. The Proportional Directional controller allowed the gains to be adjusted to improve the system response in terms of tilt angle. However, increasing the gains would increase the control steer angle and therefore the lateral acceleration. This would not be acceptable, since the control steer angle was already large, that is greater than 45 degrees or 0.78 radians.

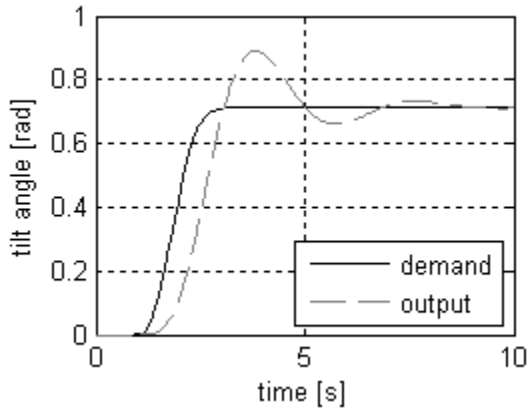

Figure 2.18 – Simulation result using STC system by Gohl et al. [36, 37]: Comparison of tilt angle demand φ_d and output φ

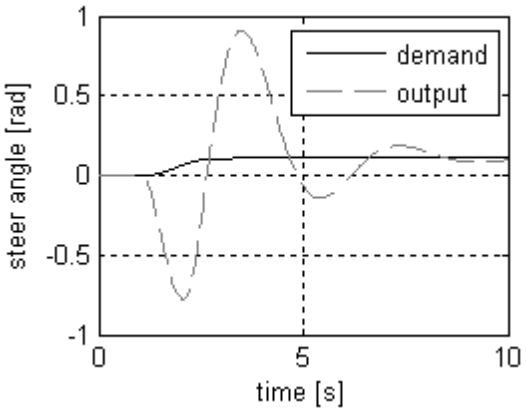

Figure 2.19 – Simulation result using STC system by Gohl et al. [36, 37]: Comparison of steer angle demand δ_f and output δ_c

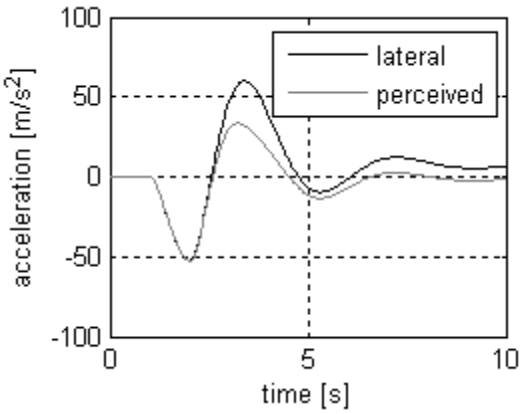

Figure 2.20 – Simulation result using STC system by Gohl et al. [36, 37]: The lateral acceleration

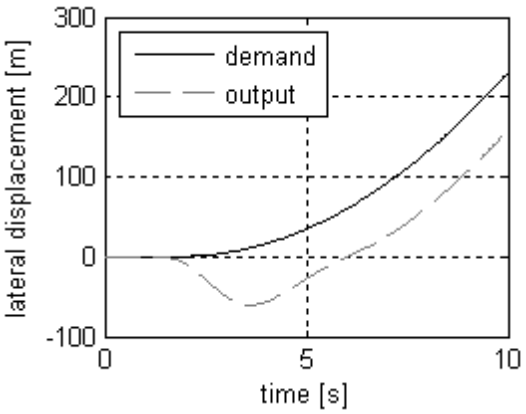

Figure 2.21 – Simulation result using STC system by Gohl et al. [36, 37]: Variation in lateral displacement

The STC system developed by Kidane et al. [38-40] assumed that the desired tilt angle was proportional to the driver input. The driver model set the driver actions proportional to the lateral error defined by equation (2.36), the heading error defined by equation (2.37), both shown in Figure 2.22, and the feedforward steer angle to follow the trajectory given by equation (2.38). The vehicle model was defined by equations (2.20) to (2.22).

$$\ddot{e_1} = \left(\dot{v_Y} + v_X\dot{\psi}\right) - \left(v_X\dot{\psi}_d\right) \tag{2.36}$$

$$e_2 = \psi - \psi_d \tag{2.37}$$

$$\text{driver\_input} = -k(e_1 + e_2 ds) + \delta_{ff} \tag{2.38}$$

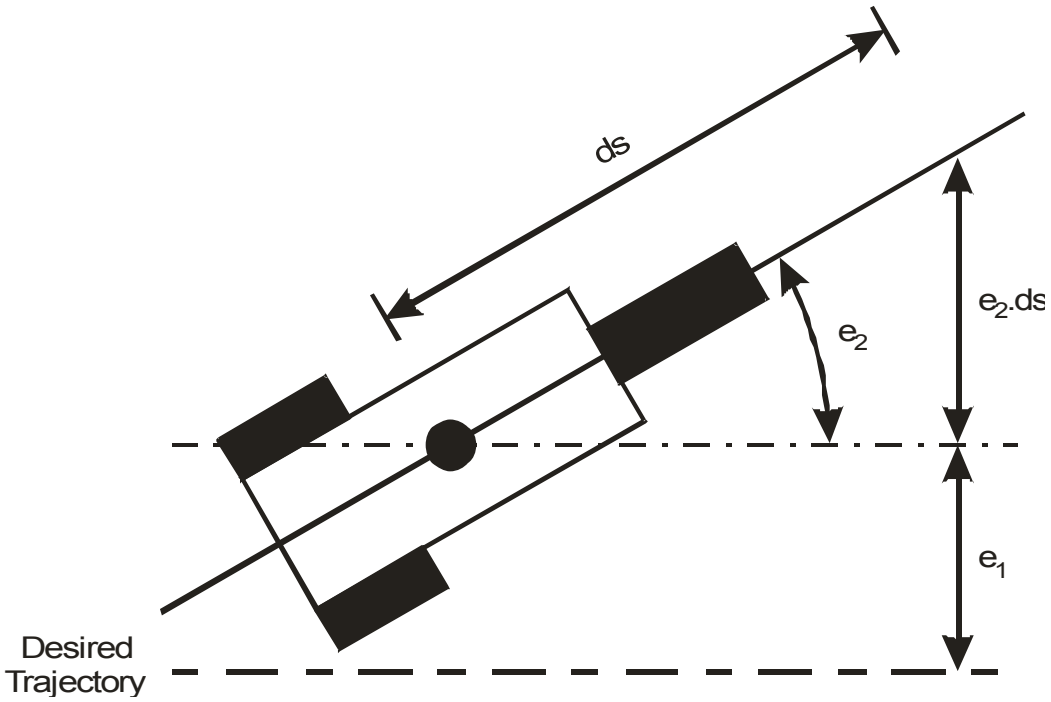

Figure 2.22 –Trajectory error as interpreted by Kidane et al. [38-40]

Combining equation (2.29) and (2.38), the desired tilt angle becomes proportional to the lateral position error, the heading error and the steer angle required for the desired path as shown in equation (2.39). The scaling factors and gains could be adjusted to suit the driver's handling preferences. With the demand lean angle defined, the STC steer angle output could be determined from the error in lean angle plus the steady state steer angle as shown in equation (2.40).

$$\phi_d = k_s(-k(e_1 + e_2 ds) + \delta_{ff}) \tag{2.39}$$

$$\delta_c = k_p(\phi - \phi_d) + k_d\left(\dot{\phi} - \dot{\phi}_d\right) + \delta_{ss} \tag{2.40}$$

With definition (2.40), the steady state steer angle needed to be defined. The definition in (2.41) is derived from assuming that at steady state, the steer angle is equal to equation (2.42) and substituting for linearised slip angle definitions. This definition, whether rewritten in terms of just the yaw rate or just the lean error, would require online system adaptation or learning since mass, velocity, and tyre properties are not fixed.

$$\delta_{\mathrm{ss}} = \frac{L}{v_{\mathrm{X}}} + \alpha_{\mathrm{f}} - \alpha_{\mathrm{r}} \tag{2.41}$$

$$\delta_{\mathrm{ss}} = \dot{\psi}_{\mathrm{d}} \left[\frac{L}{v_{\mathrm{X}}} + \frac{v_{\mathrm{X}} m}{L} \left(\frac{b}{2C_{\alpha_f}} - \frac{a}{2C_{\alpha_r}} \right) \right] + \phi_{\mathrm{ss}} \left(\frac{C_{\gamma_r}}{C_{\alpha_r}} - \frac{C_{\gamma_f}}{C_{\alpha_f}} \right) \tag{2.42}$$

Rather than relying on accurate system information or controller adaptation, the steady state steer angle could be replaced by an integral control term. This integral term would also act on the error in the lean angle as shown in equation (2.43).

$$\delta_{\mathrm{c}} = k_{\mathrm{p}} (\phi - \phi_{\mathrm{d}}) + k_{\mathrm{d}} \left(\dot{\phi} - \dot{\phi}_{\mathrm{d}} \right) + k_{\mathrm{i}} \int (\phi - \phi_{\mathrm{d}}) \mathrm{d}t \tag{2.43}$$

This STC system is essentially PID control. Where it differs from the other systems is the definition of the desired lean angle. This lean angle is based purely on the driver command and in practice would only require measurement of the driver steer angle input and vehicle speed. The order of the control actions is given in Table 2.3. The value of the scaling factor, which sets the proportion between the desired lean angle, and the driver steer angle is very important for the driver experience since it will determine how quickly the vehicle will respond and therefore how the vehicle will turn: a tight turn or a wide turn.

1.	Driver wants to change direction
2.	Driver steers and changes the steer angle
3.	The desired lean angle is set to be proportional to the driver input (2.38)
4.	The difference between the measured lean angle and the desired lean angle is detected
5.	The controller outputs a steer angle
6.	The change in steer angle results in a slip angle between the tyre and the road
7.	The slip angle causes a lateral tyre force
8.	The side force causes the vehicle to yaw and lean

Table 2.3 – Steer Tilt Control flow chart

This system was integrated with the DTC system and was tested in simulation and to a very limited degree validated by experimentation. In simulation, the desired trajectory was set to the following: go straight ahead for 50m, and then turn at a constant yaw rate. The simulations were run with constant velocity as well as a changing velocity. The simulation results showed that the vehicle was balanced and that the desired trajectory was followed within 0.125m of lateral error. However, the steering adjustments from the controller were applied at a very high frequency. In reality, an actuator would have to apply these adjustments and tyre forces would have to build up for the control to have an effect. The actuator and the tyres will introduce a significant lag term in the control system, and it is questionable whether high frequency control steering demands could be effectuated. The experimental results showed that the desired tilt angle was reasonably well tracked by the controller. However, this did not show how well the trajectory was followed. Also, the experimental results were presented for the combined DTC and STC system and the manoeuvre velocity was below the velocity threshold after which STC was applied.

2.5 TWO-WHEELER CONTROL

The controller output to manage the trajectory and/or the leaning of a tilting three-wheeler was expected to be similar to the outputs of a bicycle or motorcycle driver model or the outputs of the controller of an autonomous bicycle or motorcycle. In the following section autonomous two-wheeler control models and driver models for both bicycles and motorcycles were reviewed.

2.5.1 Bicycle Dynamics

Since STC is based on a motorcycle/bicycle rider, it is important to appreciate how a bicycle is steered. In [48], Fajans gives a detailed description of the physical steering system based on the scientific analysis of the bicycle by Whitt [49]: A right turn is initiated by applying a torque to the handlebars to turn the front wheel left. The tyre forces generated by this action leans the rider and the bike to the right. It also attempts to lean the front wheel to the right. The gyroscopic reaction of the front wheel is to turn right, counteracting the steering torque. At this point, the

steering angle has stopped increasing. Subsequently the leaning torque overcomes the steering torque and the front wheel starts steering towards the right. As the bicycle is still turning left, the lean angle continues to increase until the steering angle passes through zero and the front wheel is steering right. Consequently, the tyre forces change direction and the vehicle reaches an equilibrium state in which the resultant moment on the leaning body is zero. Since no more leaning torque is applied to the wheel, the steering angle stabilises and the bicycle continues to execute a right turn. Table 2.4 to Table 2.7 and Figure 2.23 describe the sequences of events associated with balancing and turning at either low or high speed (these were adapted from Cossalter [46]).

1.	Motorcycle leans right
2.	Rider steers right and motorcycle yaws/turns right
3.	Slip angle at the tyre generates tyre force and tilt moment to counteract the lean
4.	Motorcycle is vertical again

Table 2.4 – Low speed balancing

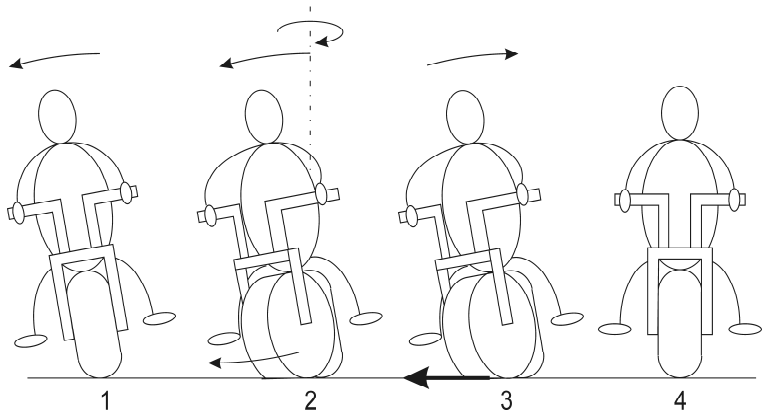

Figure 2.23 – Low Speed Balancing

1.	Motorcycle leans right
2.	Gyroscopic moment from roll and wheel rotation causes a steering moment to the right
3.	The motorcycle yaws/turns right
4.	The tyre force caused by the steering action results in a roll moment to the left
5.	Because of the roll velocity towards the left, the gyroscopic moment causes steer to the left
6.	The motorcycle leans left and the process starts again

Table 2.5 – High Speed Balancing

1.	Rider steers left, causes yaw to the left and rolls to the right

2.	Motorcycle moves to the left
3.	Because of the tyre camber thrust, the lateral force changes direction from the left to the right
4.	The yaw rate changes direction from the left to the right
5.	The rider turns the steering to the right

Table 2.6 – Low Speed Right Turn

1.	Rider steers left, causes yaw to the left and rolls to the right
2.	The lateral force and the gyroscopic moment from the fast steering rate and wheel rotation cause a large roll rate to the right.
3.	The large roll rate allows the rider to turn the steering to the right shortly after the countersteer.

Table 2.7 – High Speed Right Turn

The speed effects are largely caused by gyroscopic moments. The wheels of the cycle rotate about the lateral y-axis. The vehicle will roll, rotate about the x-axis, and yaw i.e. rotate about the z-axis. Where there are two rotations, there will be a resulting gyroscopic moment. The faster the wheels spin, the more important the resulting moment. When cornering, the vehicle yaws and the resulting gyroscopic moment is about the roll axis. This moment does not significantly affect the vehicle roll, but it does cause a moment about the steer axis, which tends to realign the front wheel to its straight-ahead position. When the vehicle rolls, the resulting gyroscopic moment is about the yaw axis. Again, it does not affect the vehicle yaw significantly, but it does help the driver steer into a turn and steer out of a turn. In other words, when leaning into the turn the resultant yaw moment steers into the turn, and when rolling out of the turn the resultant yaw moment steers the front wheel back to its straight-ahead position. In conclusion, gyroscopic effects can aid the driver in steering the vehicle through a manoeuvre without having to apply large steering torques. Finally, when steering the front wheel, the resultant gyroscopic moment is a roll moment. When steering from right to left, the resultant roll will be from left to right, so this gyroscopic moment helps to lean the cycle into the turn when countersteering. It could be said that this last gyroscopic moment is the reason a rider countersteers. Bicycle control is a combination of the driver making steering adjustments because he wants to change direction and the geometry of the two-wheeler resulting in torques which aid the driver when balancing and changing direction. When designing a roll control system that actuates the steering angle, the nature of the aforementioned torques should be included in the design.

2.5.2 Bicycle Control

2.5.2.1 The Autonomous Bicycle

Getz and Marsden [50] presented a system for an autonomous bicycle. First, a method for roll angle tracking was presented. The demands for roll angle and forward speed were predefined as functions of time. The system had to track these demands. Then the bicycle roll angle and forward speed were made to converge exponentially to the demand values. The second goal was to prove that the bicycle could follow a path. Now demands for x and y coordinates were predefined as functions of time. The bicycle model had to track these demands ignoring roll angle and mass. The x and y coordinates were related to the forward speed and the steer angle: the controlled states. In other words, the demands for forward speed and steer angle could be tracked. The final goal was to combine these two tracking demands to produce an autonomous bicycle that could follow a path without falling over. The approach was to determine a roll angle trajectory that would be compatible with the error dynamics of the ground plane tracking. The roll angle would then be forced to track this trajectory. It was assumed that the roll angle would have to be controlled on a much faster time scale than the x and y coordinates. This assumption allowed for the demand steer and speed to be fixed in the roll angle time scale. The implementation of this method was as follows. A roll angle equilibrium equation depending on gravity, steering, forward speed, and geometry was defined. Through mathematical manipulation and optimisation, the roll angle was forced to follow the trajectory defined by the path following demand while converging to the ideal values from the equilibrium equation.

This work was further developed by Getz [51] who presented an improved method to achieve both path following and balancing. Although relevant in terms of a method to track a path as well as balance, this control strategy assumed a known forward path. In the case of a driver steering and controlling the throttle, there is no prior knowledge of the path the driver intends to take.

2.5.2.2 Balancing an unmanned bicycle

Lee and Ham [52] presented a control algorithm which could balance an unmanned bicycle by lateral displacement of the centre of mass as shown by simulation results. It was recognised though that there was still a need to incorporate the balancing function with path tracking. Tanaka and Murakami [53] also presented a method to balance an unmanned bicycle, but this bicycle included a steering controller. The linearised bicycle model showed that the steer angle and the roll angle were related. Therefore, as the demand value was defined for the roll angle, it was translated to a demand value for the steer angle using proportional derivative control.

Additionally, a proportional derivative control system with a disturbance observer was put into place to control the steer actuation. This system was tested first in simulation and later by experimentation. It was found that the disturbance rejection was good. However, similarly to the work of Lee and Ham [52], it was noted that there was no directional control present. To check the effectiveness of this control strategy, the controller was built in Matlab/Simulink by the author as shown in Figure 2.24. The results presented in Figure 2.25 - Figure 2.27 were generated using the Matlab/Simulink model. Figure 2.25 shows that after a steering torque disturbance at the start of the simulation, the controller returns to zero lean. Figure 2.26 shows that the steering response is significant. Finally, as Tanaka and Murakami noted, the resulting path of the cycle was uncontrolled as shown in Figure 2.27.

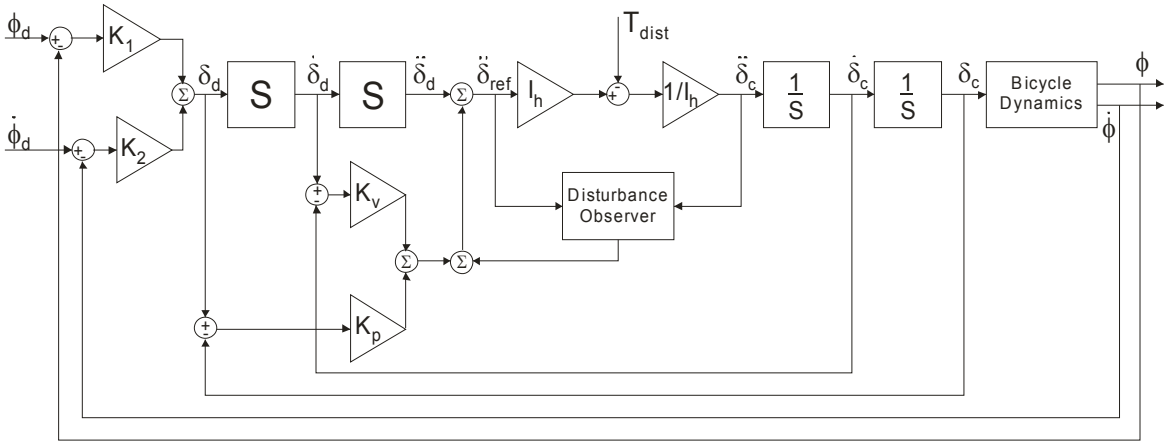

Figure 2.24 – Block diagram of lean control system adapted from Lee and Ham [52]

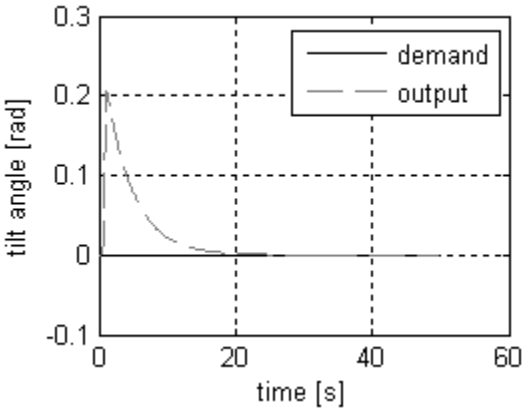

Figure 2.25 – Replicated simulation results: Lean angle disturbance response with control system by Lee and Ham [52]

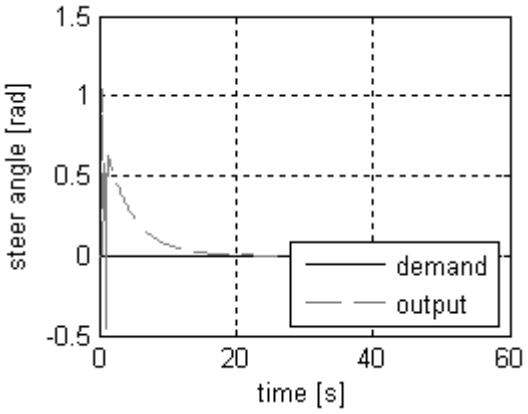

Figure 2.26 – Replicated simulation results: Steer angle disturbance response with control system presented by Lee and Ham [52]

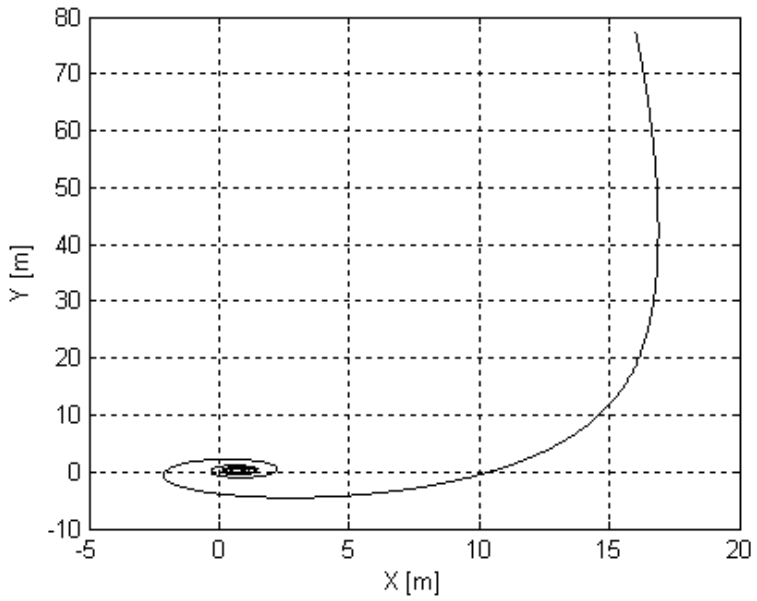

Figure 2.27 – Replicated simulation results: Trajectory result after a disturbance with control system by Lee and Ham [52]

The need for path control led Tanaka and Murakami to improve the bicycle control method as presented in [53]. Two types of controller were proposed which included a path following function and a lean control function: a lateral velocity controller and a steering function controller. Both the types of controller determined a lean angle demand that was then used with the previously described tilt controller. The lateral velocity controller is shown in Figure 2.28. The derivative of the lateral position demand is compared to the bicycle lateral velocity. The error is then used to determine the demand lean angle. The steering function controller is presented in Figure 2.29. It required feedback of the lateral position, the direction angle and the path curvature

to determine the demand lean angle. It was noted that although these signals are readily available in simulation, in reality a signal such as path curvature would be very difficult to determine. In simulation, the lateral velocity controller was capable of forcing the lean angle to zero after an external disturbance. However, in terms of trajectory it achieved the correct direction angle after the disturbance, but not the correct lateral position. The steering function controller forced the lean angle to zero and achieved the correct trajectory. In simulation the steering function controller was also found to be more effective. These results were interesting, but it was noted that the future trajectory needed to be known to determine the control action. This, as was mentioned in relation to the work by Getz [51], is not the case when managing steering and throttle inputs from a driver.

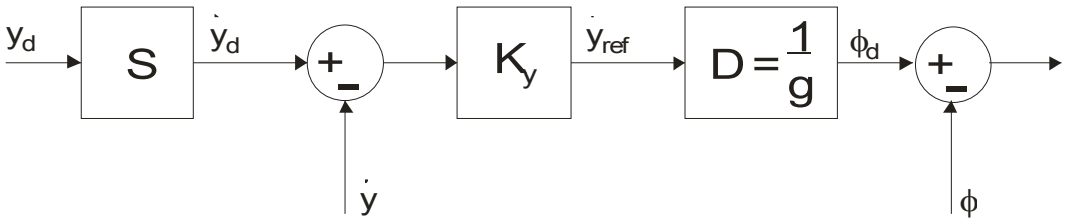

Figure 2.28 – Block diagram of lateral velocity controller presented by Tanaka and Murakami [53]

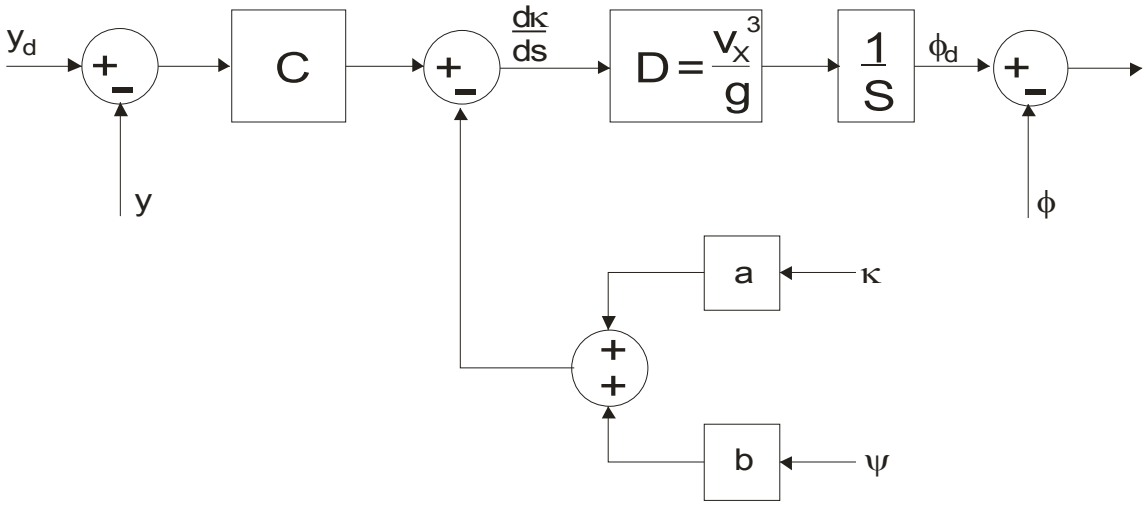

Figure 2.29 – Block diagram of steer function controller presented by Tanaka and Murakami [53]

2.5.3 Motorcycle Control

2.5.3.1 Rider Component

The Society of Automotive Engineers compiled a number of investigations concerning motorcycle dynamics and rider behaviour in 1978. Two of these investigations were of particular interest namely the study by Weir and Zellner [54] and the experiments by Rice [55].

The former noted the importance of the rider as the controller of the two-wheeled vehicle, as well as the contribution of the rider to the mass and inertial properties of the system and therefore the tyre load. It was also noted that the rider's body motions could add to the disturbances acting on the system. The rider was identified as an important factor in the open loop and closed loop stability of the motorcycle, because he applied open loop control through learned manoeuvres, compensatory control in response to perceived errors, and feedforward control through system knowledge and familiarity. The investigation showed that the rider model had a significant effect on the stability of the cycle in terms of its three modes: capsize, weave and wobble. The implications of this are that the driver model architecture should be carefully chosen and could be the source of instabilities in the vehicle system.

The experimental work by Rice [55] showed how the driver experience affected the efficiency of the steering input and the top speed at which a manoeuvre could be successfully achieved. The study showed that motorcycle performance needed to be considered in terms of the vehicle dynamics and the rider. The results also showed that one single manoeuvre could be accomplished in various ways: there was great variation in the magnitude and direction of the applied steer torque and the roll angle of the driver with respect to the vehicle. The paths of the different drivers would have been different, but in all cases, the lane change had been achieved. This implied that there are various solutions to modelling the rider, though some solutions will be more efficient than others. In these experiments, the roll angle of the rider in relation to the vehicle was measured, but the effect of this roll angle was not considered.

2.5.3.2 Rider Control Actions

The rider roll, its effect, and other rider control actions were investigated by Katayama et al. [56]. The aim of the study was to develop a rider model and validate it with experimental data. The model assumed that the rider output consisted of three torques: upper body roll, lower body roll and steering torque. Subsequently, the upper body dynamics would result in a reaction torque on the lower body, the lower body dynamics would result in a reaction torque on the motorcycle, and finally the motorcycle dynamics would result in a reaction torque on the upper body. The control actions were determined to depend on the roll angle and the weighted heading error distribution. Initial model studies showed that the effect of the steering torque was 12 times larger than that of the lower body torque and 80 times larger than that of the upper body torque. Subsequent studies showed that the steering torque was the most important control action, and the lower body torque played an assisting role. It was also shown that the rider's upper body roll opposed the roll of the vehicle; in other words, the rider would try to remain upright and not roll

with the vehicle. Finally, it was shown that with appropriate gains, the model and the experimental results followed the same trends. Overall, the most important finding was that the steering torque was the most important control action from the driver and it depended on vehicle roll and the heading error. Although the rider's posture was not the most important control action, Chi [57] demonstrated that the posture could improve the motorcycle's stability.

2.5.3.3 Hands Free Riding

The previous research did not include the condition where the rider lets go of the handlebars and balances the bike by shifting his weight laterally and roll his upper body. This was investigated by Yokomori et al. [58] for straight-line running of motorcycles. It was found that the change in lateral centre of gravity position controlled the rolling motion when following a straight trajectory. The driver's reaction time was a limiting factor on the stability of the cycle, as was the forward velocity: a slow driver reaction time and low forward velocities reduced the stable operating region of the motorcycle. Another factor in the overall stability of the cycle was the difference between the location of the motorcycle centre of gravity and the rider centre of gravity: the smaller the difference, the closer the overall system dynamics were to those of a single pendulum system rather than a double pendulum, and better overall stability of the system. From this study, it was concluded that for a straight-line trajectory, the rider control inputs are minimal. In addition, it could be deduced that a small lateral shift on the rider's part could have a significant effect on the roll moment depending on the forward velocity. Therefore, to avoid the rider interfering with an automated controller, his lateral motion should ideally be restricted.

2.5.3.4 Motorcycle Steer-by-Wire System

The driver was not constrained in the steer-by-wire system for motorcycles developed by Marumo and Nagai [59]. The controller was developed to simplify motorcycle steering so that the driver input could be via a steering wheel or joystick. The first stage in the development was a controller similar to STC with a feedforward $G_{\varphi}^{-1}(0)$ and feedback loop as shown in Figure 2.30. Simulation showed that more states had to be fed back to the controller to properly manage the vehicle path. A set point regulator for optimal control was proposed for the task. This method compared the vehicle states $\mathbf{x}$ with the steady state values $\mathbf{x_0}$ for a specific point in time and executed an optimisation algorithm. The controller was shown to perform well in simulation, but was not experimentally tested. The limitations of this type of control were the amount of information required about all the vehicle states $\mathbf{x}$ plus the assumption that all the manoeuvres are steady state.

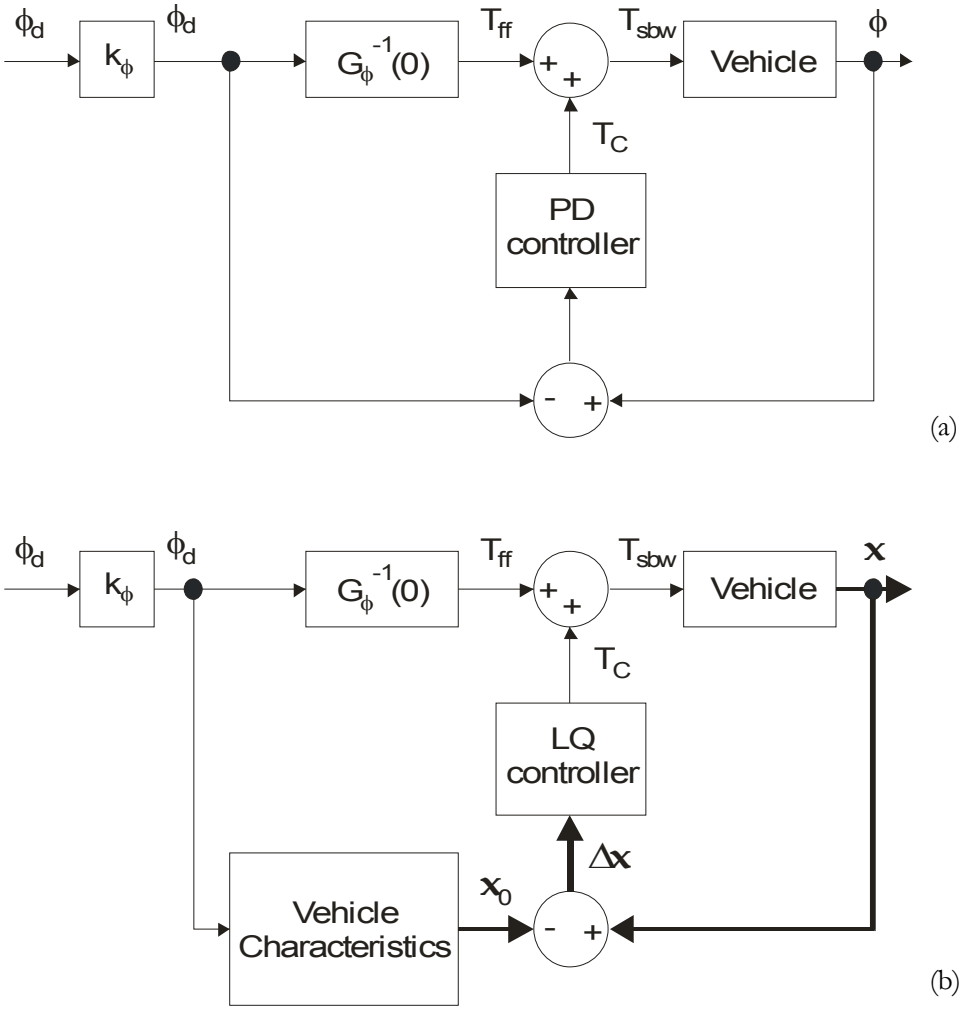

Figure 2.30 – Block diagram of motorcycle controller presented by Marumo and Nagai [59] (a) with PD Controller (b) with LQ controller

2.6 DRIVER MODEL CONSIDERATIONS

The objective of the research reported in this Thesis is to develop a controller that ensures leaning stability of a tilting three-wheeled vehicle whilst conforming to the path the driver intended to take similar to the fusion model by Iuchi [60]. To fully test the control strategy in simulation, a model of the human driver was also required. This section reviews a number of models from literature as well as human driver characteristics to be taken into account. Models of the human driver are of great importance in vehicle dynamics modelling and simulation as can be seen from the list of references.

2.6.1 Multiple Loop Driver Model

These elements were also found in the driver model hierarchy and implementation by Plöchl and Lugner [61] based on previous work by McRuer [62]. The road trajectory was mathematically formulated in an inertial frame, Figure 2.31. The 3-level model consisted of anticipatory control,

compensatory control, which is based on the prediction of the position ahead, and local deviation control, i.e. deviation from the desired path. The first two levels formed classic 2-level control, which could be overridden by the third level of control: anticipatory or feedforward control assumes that the driver will steer according to the estimated curvature. The compensatory control or feedback control tries to reduce or compensate the previewed deviation from the trajectory with a steering response. Plöchl and Lugner had tested this control architecture with a vehicle model in simulation and successfully manoeuvred around obstacles and negotiated turns. Improvements to this model were presented later by Plöchl [63].

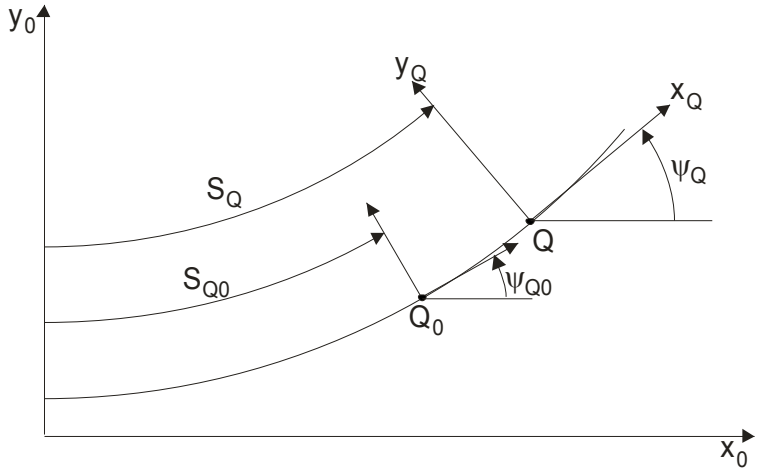

Figure 2.31 – Vehicle trajectory in the reference frame

2.6.2 Motorcycle Rider Model

Car driver models illustrate the driver behaviour for path following very well. However, motorcycle driving is a more challenging task. The difficulty of riding a motorcycle is the combination of the balancing control and the path following control task. This was demonstrated by Frezza et al. [64] and Frezza and Beghi [65]. The driver is required to control engine torque, and tyre forces to follow a path while preventing the vehicle from falling. These goals often result in conflict. For example, to lean the motorcycle into a turn, the rider must first steer in the opposite direction to generate a tyre force that will tilt the cycle into the turn. From a control point of view, this is non-minimum phase behaviour. Motorcycles and bicycles share the same dynamic properties: both vehicles can be represented by an inverted pendulum on a cart. In spite of this, their control shows one significant difference. Whereas a bicycle rider can shift his weight to balance, a motorcycle rider is much more reliant on applying steer and controlling the throttle. Nevertheless, both vehicles bear the same difficulty of following a desired path whilst preventing the vehicle from falling over. This is a complex task well illustrated by trying to teach someone to

ride a bike: first, the novice has to get used to the roll dynamics and then he can start trying to balance at the same time. The ease of this control task is often related to the handling characteristics of the vehicle or the manoeuvrability of the vehicle. Manoeuvrability is the less subjective feature, because it is usually defined as the minimum time to complete a manoeuvre optimally. This can be done by a controller in the form of a virtual rider that performs closed-loop manoeuvres.

2.6.3 The Optimal Motorcycle Manoeuvre

The optimal manoeuvre concept defines the outline for the design of the virtual driver. In cars, the optimal manoeuvre is defined in terms of open-loop inputs. If this were applied to an unstable vehicle such as a motorcycle, the vehicle would fall over. Instead, the optimal manoeuvre should be defined as a trajectory that the closed-loop driver model must follow. When the minimum-time restriction is added to the constraints, the vehicle has to be worked to its performance limits. In this case, any disturbances that cause deviation from the trajectory would not be rejected by the closed-loop driver model. As a result, the vehicle would lag behind the desired trajectory and not be able to catch up. The trajectory tracking control can be made more robust when the goal is optimising the future result rather than making up for past errors. This can be achieved by specifying a velocity limit for the manoeuvre. This would be similar to a real driving situation where the driver has to obey speed limits. Thus, although trajectory tracking and path following with a specified velocity are similar tasks, the control actions required are different. For example, a vehicle going downhill controlled by a trajectory tracker will slow down and even reverse to remove the error whereas a path following controller will slow sufficiently to adjust the velocity to the reference value. The dynamic equations are similar to those used by Getz and Marsden [50]. However, they had to be transformed to exhibit a path following rather than trajectory tracking problem. To do this, the time variable was removed. This was achieved using the expression where a look-ahead distance or arc-length is defined in terms of the velocity and time. The dynamic equations then become dependent on the arc-length. When a velocity profile and a path profile are assigned, the optimal control problem becomes a quadratic cost function of the path error, the velocity error, and the roll angle, all with respect to the arc length rather than time. Optimisation of the roll angle and optimisation of the velocity and path are conflicting demands. Nonetheless, when the weighting of the roll angle is large, the controller can become more like a human rider: it will delay braking at the start of a turn to increase the yaw rate, it will slow down in the turn to reduce the roll angle, and it will accelerate coming out of a turn to pull the motorcycle up. With this model, the rider or controller is assumed to be rigidly attached to the motorcycle frame i.e. the rider is not leaning into a turn. By modelling the rider

with motorcycle as a two-degree-of-freedom inverted pendulum, the controller might lean the rider into the turn. The leaning into the turn should only serve to reduce the lean angle and not to control the balancing or the steer line. In order to achieve the minimum-time goal of the optimal control task, the width of the lane was constrained. The cost function for this task was expressed by Getz and Marsden as the time taken to achieve a certain length of a course. In the cost function, the velocity was expressed as the velocity on the tangent of the lane central line. In conclusion, a solution was found which relied on Model Predictive Control (MPC [sic]). This control method made it possible to work on trajectories. Normally, one would say that the roll angle is caused by the longitudinal and steering inputs. However, the MPC approach inverts this cause-effect structure. In other words, the roll angle becomes the input. The optimal trajectory of the roll angle is determined and, by inverting the dynamics, the longitudinal and steering actions are computed. This driver model could be used in simulation to compare the behaviour of a rider with the designed STC system. It would also be useful to compare the optimal rider behaviour with the measured rider control data.

2.6.4 Rider Robot

A simpler version bordering on a Steer-by-Wire approach to driver modelling was presented by Miyagishi et al. [66]. A control algorithm to mimic a bicycle rider was developed to evaluate two-wheeled vehicle dynamics. This rider robot had two control aims: maintain standing stability and follow a target course. To control the balance or standing stability, a proportional derivative control algorithm was applied to maintain the roll angle at a target value of zero. The block diagram of this system can be found in Figure 2.32. This system was successful at rejecting disturbances and maintaining an upright position. Now the path following was achieved by predicting the future position, k time steps ahead and comparing it to the target position k time steps ahead. The error between the target position and the predicted position determines the adjustment of the steer angle. This is illustrated in Figure 2.33. In isolation this path following algorithm performed well. The two systems were then put together to form the control algorithm for the two-wheeled vehicle. This combination control system is illustrated in Figure 2.34. The next step was to try the algorithm experimentally. This did not give any satisfactory results, so the controller was adjusted. The alterations can be seen in Figure 2.35. It was shown how this new controller stabilised the two-wheeled vehicle experimentally. In spite of this, when this control system was built in Matlab/Simulink according to the block diagram given by Miyagishi et al., the individual elements performed well, but the combined system was unstable. This would be expected since the controllers had exact opposite goals.

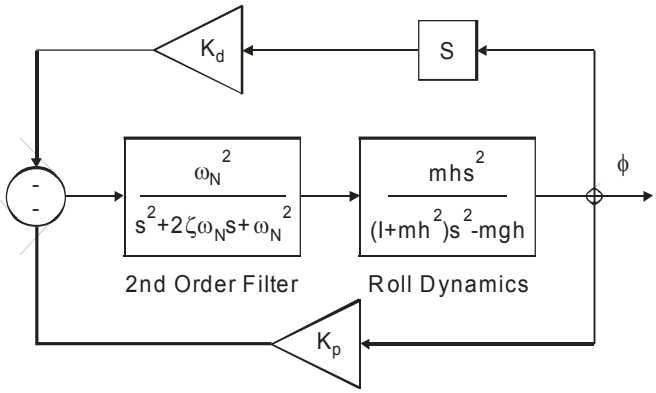

Figure 2.32 – Roll angle control block diagram adapted from Miyagishi et al [66]

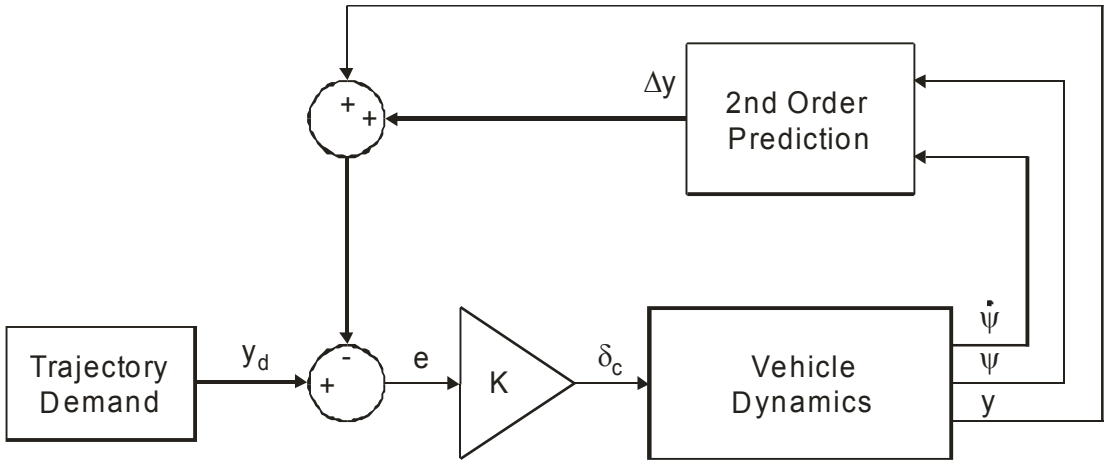

Figure 2.33 – Path following control block diagram adapted from Miyagishi et al [66]

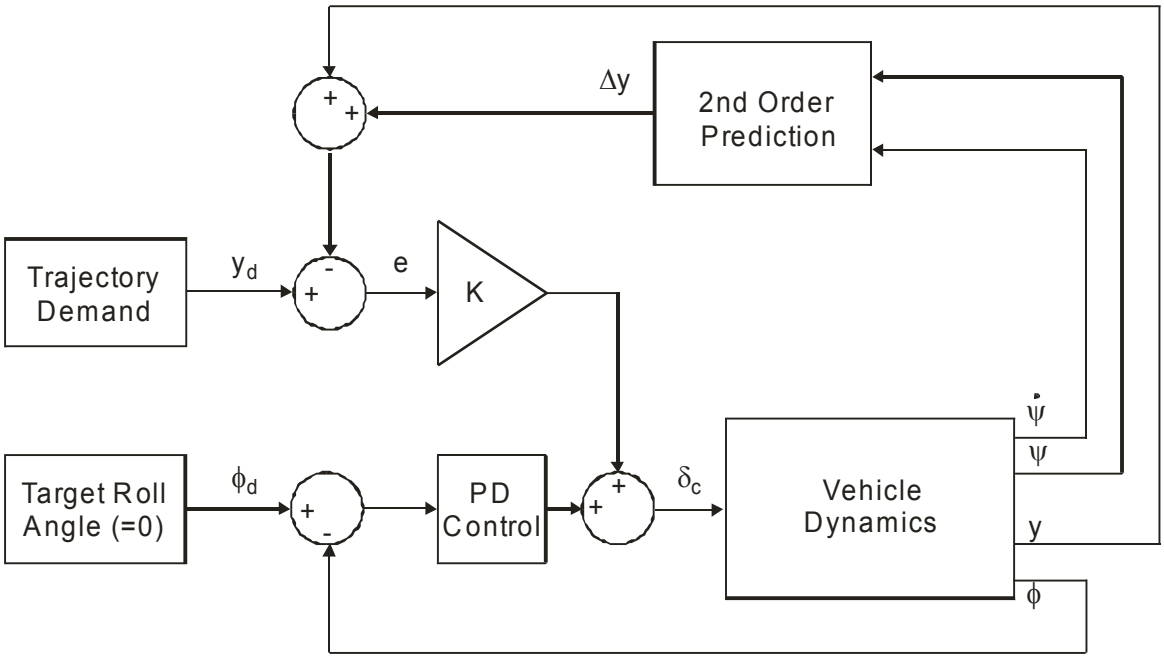

Figure 2.34 – Path following and roll angle control block diagram adapted from Miyagishi et al [66]

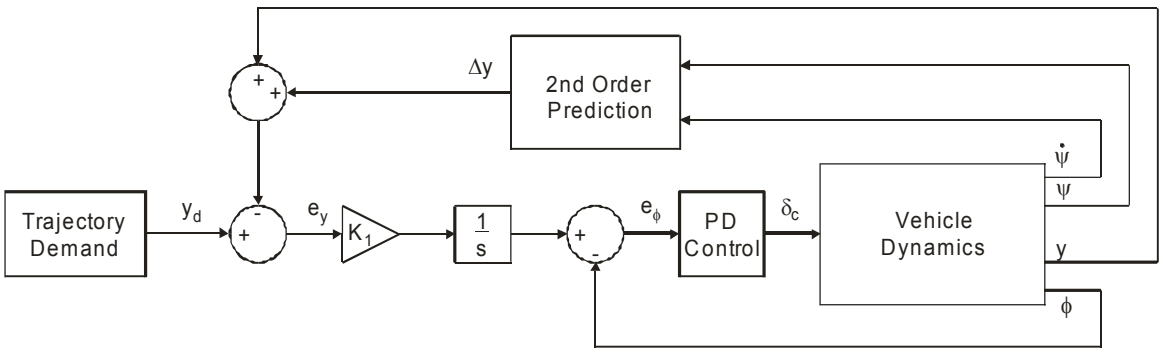

Figure 2.35 – Altered block diagram for the path following and roll angle control adapted from Miyagishi et al [66]

A more advanced steering system was proposed by Yuhara and Tajima [67]. In this model the driving method was defined as a navigation loop, a guidance loop, and a control loop; one nested in the other. The outer loop was the navigation loop; it determined the location, the orientation, the velocity, and other conditions to reach the destination. The middle loop was the guidance loop; it used the navigation loop's output and traffic or road information to determine a desired trajectory and a desired speed. The inner loop was the control loop; it activated the steering, the throttle, and the brake to execute the guidance loop output trajectory and speed. Current steering systems have a steering command mode that is rate dependent: the yaw rate is proportional to the steering angle. An alternative command mode would be a derivative steering concept where the steering command becomes an attitude command. Empirical data proved that this method required less driver skill and allowed for smaller minimum distances between the vehicle and an obstacle. Until now, the practical implementation of such a system had been an issue, but now it was deemed possible. The proposed steering system had three parts: a reference model of the vehicle yaw rate to steering wheel input, a yaw rate control system, and a recognition system for driving moods (relaxed or aggressive) and lateral control tasks (lane keeping or lane changing). This was implemented as follows: The driver has a desired path in his mind based on visual information. This path has a target angle of Ψ_d and the trajectory is related to the desired vehicle position in 1-2 seconds time. The driver implements a steering angle to achieve the path angle, where the relationship between the path and steering angle is assumed to be linear. The aim of the control model was to design a steering system gain, which would hold true for this linear relationship regardless of the vehicle speed or lateral acceleration. In addition, the steering gain had to be regulated with respect to the driver's mood: an aggressive mood increased the gain, and a relaxed mood decreased the gain. Finally, the lateral control task was defined as a multi-feedback control loop. The steering wheel angle was defined as a function of the vehicle lateral position relative to the centreline of the lane and of the heading angle relative to the tangent line

of the lane. This resulted in inner-loop yaw angle feedback and outer-loop lateral position feedback, see Figure 2.36.

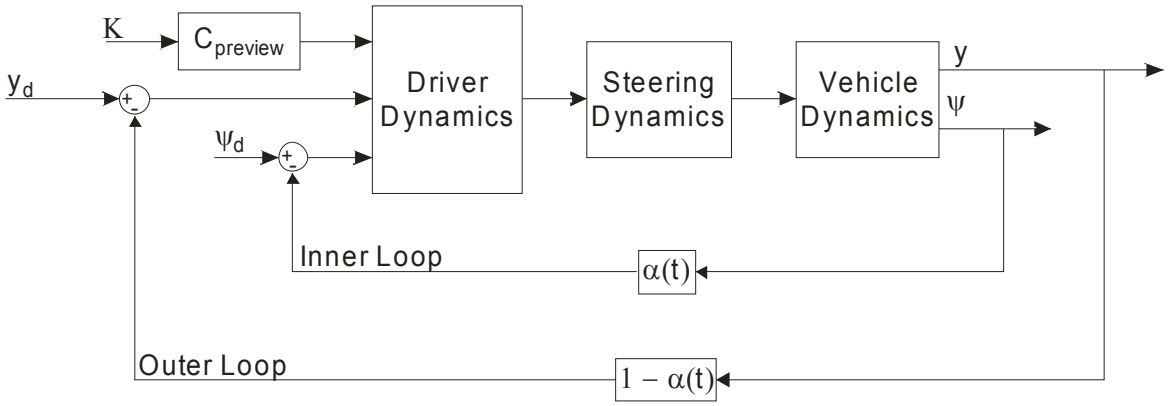

Figure 2.36 – Lateral control loop as presented by Yuhara and Tajima [67]

Depending on the control task, these loops could be weighted. By determining relationships between dynamic variables or setting these relationships, a multi-loop control scheme can be developed. This concept of multiple control loops could be of use for the development of a novel STC system. For example, the steering input from the driver determines a demand roll angle. This demand roll angle is compared to the actual roll angle and the roll angle controller outputs a demand value for a side force. Again, the demand is compared to the measured value and the controller outputs a steer angle. This steer angle results in a side force, which is fed back, and the side force results in a roll motion, which is also fed back.

2.7 TYRE MODELLING THEORY

The aim of this section is to give an outline of the role of tyres in the vehicle dynamic system with a view to selecting a suitable simulation model for a tilting three-wheeler. First, the forces and moments that are transferred to the vehicle are described based on the tyre theory by Blundell [68]. It is important to understand the role of each individual force and moment and how it should be included in a vehicle model. What follows is a brief overview of tyre testing methods. The final section examines the merits and limitations of various tyre modelling methods.

Tyres are the link between a vehicle and its environment; the vehicle dynamics are largely dependent on the properties of the tyres. The slip stiffness of the tyres determines the magnitudes of the longitudinal and lateral forces generated because of the slip angles. The tyre relaxation affects the tyre response time. The following section discusses the variety of theoretical tyre models that have been developed including their advantages and limitations. Subsequently,

the choice of the Pacejka Magic Formula [69] as the model for the vehicle simulation is discussed. The application of the Magic Formula algorithm is explained as well as a novel method of determining its parameters.

2.7.1 Tyre Forces and Moments

There are three forces and three moments acting on the tyre, each associated with one of the axes of the coordinate system, and some more significant than others. The first force to consider is the normal loading force along the z-axis (vertical), because it affects the magnitude of the other forces and moments. The other two forces are the lateral force along the y-axis, which allows the vehicle to turn, and the traction force along the x-axis, which makes the vehicle move forwards. The most important moment from a handling point of view is the self-aligning moment about the z-axis, which causes the tyre to return to its straight-line position. In addition, there is the rolling resistance moment about the y-axis and the overturning moment about the x-axis.

2.7.1.1 Normal (vertical) Force

Under most circumstances, the tyre can be treated as a linear spring damper system when calculating the vertical force. The tyre penetration or reduction in radius due to the loading is the displacement and the rate at which this occurs is the velocity. This model is very simple and may require some changes to cater for heavy vehicles or rough terrain. In general, the normal force will be close to the ground reaction force based on the load distribution of the vehicle and the number of wheels.

2.7.1.2 Longitudinal Force

Even without longitudinal acceleration or braking forces there will be tyre slip: The forward velocity of the tyre is its angular velocity multiplied by the effective radius. However, the tread material in approach to the contact patch has a tangential velocity of the angular velocity multiplied by the unloaded radius, so it is moving faster. The material will have to slow down when it reaches the contact patch, and it will slip. It will continue to slip as the radius becomes smaller towards the centre of the contact patch. Subsequently, the material will have to speed up again as the radius starts to increase towards the end of the contact patch. In addition, the sidewalls deform near the contact patch, resulting in a narrower contact area in the centre than at the ends. Due to hysteresis in rubber loading and unloading, the forces required to compress the tyre material at the front of the contact patch are higher than the forces required when unloading the rubber at the rear. This force imbalance means that the centre of pressure lies at a certain distance in front of the wheel centre. Therefore, the normal force acts on a point in front of the wheel centre, causing a moment, which opposes the rolling of the tyre: the rolling resistance

moment. Note that this moment is very small and tends to vary significantly, so accurate measurement is difficult.

The braking force is in essence a torque applied to oppose the rolling of the wheel. It slows the wheel down, causing a certain degree of slip of the tyre material. The braking increases the distance between the wheel centre and the centre of pressure of the contact patch because it forces the pressure distribution along the contact patch forward. The driving force has the exact opposite effect to the braking force.

2.7.1.3 Lateral Force

The generation of a lateral force and an aligning moment is a result of a slip angle and a normal force. The slip angle is the difference in the direction the wheel is travelling and the direction the wheel is pointing. The slip results in a lateral force, perpendicular to the longitudinal axis of the wheel. Because of the pressure distribution in the contact patch, the lateral force is not applied in the centre, but somewhat behind the wheel centre. This causes a moment that tends to return the wheel to its straight ahead position.

Camber also plays a role in lateral force generation. The camber angle is the angle between the wheel and the vertical z-axis. The camber also causes lateral slip and therefore a lateral force. However, under these conditions, the pressure distribution in the contact patch is such that the lateral force acts in front of the wheel centre. The resulting moment tends to disalign the wheel and steer it away from the straight-ahead position. Another effect of camber is deformation of the sidewall, although this can also be a result of cornering in general. The deformation can cause the contact patch to shift in the lateral plane. The result is that the normal force is not applied at the point where the wheel plane intersects the road plane but a small distance to the left or right. The moment originating from the normal force has the tendency to roll the wheel into the bend when the shift is due to slip, and it will straighten the wheel up when the shift is due to camber.

2.7.1.4 Lateral and Longitudinal Force Combined

When going straight ahead, either braking or accelerating, the maximum braking/driving force that can be generated by the tyre is the coefficient of tyre/road friction multiplied by the tyre normal load μF_Z. Under the pure cornering condition, which is cornering at a constant velocity, the maximum cornering force that can be generated is approximately μF_Z.

In reality, when cornering, the driver is likely to brake at the start of a turn [70], and accelerate once coming out of a turn. In other words, during a normal cornering manoeuvre, there will be both longitudinal and lateral slip. In this case, μF_Z is the maximum resultant force that can be

generated. This relationship between the maximum driving/braking force and the maximum cornering force is referred to as the friction circle defined by equation (2.44). For a given driving/braking force, the maximum lateral force that can be achieved is limited by this relationship.

$$F_R = \sqrt{F_x^2 + F_y^2} = \mu F_z \tag{2.44}$$

2.7.1.5 Force Generation

The generation of tyre lateral force is not instantaneous, but takes a small amount of time referred to as 'tyre lag'. It was found that the tyre had to roll a certain distance to sufficiently deflect and generate a force. This can be tested in various ways on a tyre test bench. An estimate of the relaxation length lies between 0.5 and 1.0 revolution of the tyre. A qualitative and quantitative description of the relaxation length was given by Loeb et al. [71]. They showed that kinematic tyre properties occurred when the tyre is rolling on a surface. The properties were the lateral force and aligning moment as a reaction to steer, camber, and braking. The most important property being the relationship between the steer and the lateral force because the lateral force was largely a result of the lateral deformation of the tyre carcass. There was a time delay between a steer input and a lateral force response, which was regarded as an important transient tyre property. This time delay was characterised by a measurement called the relaxation length. It would typically be measured by loading the tyre in its steered position on a stationary test surface. Subsequently the test machine would be started and the rolled distance measured until the tyre forces and moments reached an equilibrium state. This was found to be an inaccurate representation of reality: Normally the tyre would already be rolling when it is steered and the steer would not be applied as a step change.

An experimental method to determine the relaxation length and a mathematical model to match the test results was developed by Maurice and Pacejka [72]. The experimental method was called a pendulum experiment. A tyre was placed on a drum and as the drum rotated, the tyre rolled. The wheel axle was connected to a horizontal pendulum arm that allowed the wheel to translate left and right. Through this pendulum arm the vertical load on the tyre were varied. Finally, an actuator was connected to the wheel axle to be able to steer the wheel. The actuator could steer the wheel at small amplitudes up to a 30Hz frequency to determine the frequency response of the lateral force, the aligning moment and the overturning moment. A first order system was chosen to represent the transfer function between the input steer and the force output. The transfer function depended on the relaxation length, the rolling velocity and the cornering stiffness. These

variables could be derived from the test results. A rigid ring tyre model was developed with spring and damper "spokes" and a brush model to simulate tyre road interaction. The frequency response of this model was found and the resulting relaxation length was compared with the relaxation length of the experimental results. The comparison showed that the model predicted relaxation lengths in a similar range to the experimental results.

It was concluded that the cornering and lateral stiffnesses of the tyre were indicative of the relaxation length of a tyre. Additionally, it was found that a first order model would give a reasonably good indication of the time lag between the peak steer angle and the peak force.

2.7.2 Tyre Testing

Tyre characteristics can be measured on test benches that allow the tyre to roll on a belt at a range of speeds, slip angles, camber angles and loads. The test program should go through all possible combinations of speeds, slip angles, camber angles and vertical loads to get the best and most accurate results [73]. A typical test bench will measure the reaction forces and moments in the joints to determine the relationships such as the slip angle versus the lateral force [74].

Although tyre testing is normally done under controlled conditions, Sakai et al. [75] showed that tyre variables such as pressure, load, and manufacture affected the dynamic properties of the tyre. The work of Sakai et al. was carried out under laboratory conditions with a tyre-testing machine and one individual variable was changed at a time. They concluded that the tyre properties varied significantly with the internal tyre pressure, loading condition and manufacture. What this means in terms of dynamic motorcycle testing, is that even if the same tyre is used, the experimental results can vary depending on the mass of the driver and the inflation pressure of the tyres. When validating the test results against a computer model with a fixed tyre model, there will be errors because the tyre model does not account for the variation in inflation pressure and changes in the tyre pressure because of a relatively heavy or lightweight driver.

Cossalter et al. [76] presented an extensive summary of the results of motorcycle and scooter tyre testing. Results showed the effects of various working conditions. First, it was shown that different tyres could have very different characteristics due to the differences in manufacture, width, diameter, and loading. A rotating disk test rig was used to determine the tyre characteristics. This machine consists of a 3m diameter disk that rotates to mimic the road surface and vary the driving/braking force. The test wheel is held in position by an articulated arm that sets the wheel at a fixed sideslip and/or camber angle relative to the disk. The positioning arm contains a set of load cells to measure the moments and forces required to keep

the wheel in place and therefore measuring the forces generated by the tyre/road interaction. The arm was also equipped with a loading mechanism to vary the normal load on the tyre. Every tyre was tested for its lateral force generating capability for a range of camber angles, slip angles, and normal loads. The aim was to determine the tyre characteristics of a range of motorcycle and scooter tyres and determine the effect of a number of external factors: inflation pressure, road temperature and type of tyre testing machine. The internal tyre pressure was varied to up to 20% above the regular pressure. In general, the increased tyre pressure reduced the maximum normalized force the tyre could generate, i.e. the camber and sideslip stiffnesses were reduced. A similar tendency was measured in respect to the road surface temperature: higher temperatures reduced the camber and sideslip stiffnesses. The normal load did not greatly affect the camber stiffness, but the normalised sideslip stiffness was reduced by an increase in load. When the results were compared to those obtained from a rotating drum test machine and a flat bed machine, it was found that they were not identical. This demonstrated that the type of test machine could affect the tyre data and subsequently the model that is based on those data.

It is clear that tyre properties change significantly depending on their operating conditions. In addition, the test method could make a large difference when determining the tyre properties. This would mean that in practice there are very few certainties in modelling the tyres and taking the measurements. A method that would verify the tyre properties during an on-road vehicle test would therefore be desirable.

2.7.3 Tyre Models

In tyre modelling there is a trade-off between accuracy and complexity. In addition, the purpose of the model has to be taken into account. Tyre models are used in ride and vibration studies and in this case, the radial spring stiffness and damping characteristics of the tyre are important. This type of model could be a simple spring damper block, or a radial spring model where the tyre is modelled as a flexible ring with springs as spokes [77, 78]. For handling and dynamics studies, the lateral and longitudinal forces generated at the tyre contact patch have to be modelled. This type of tyre model will calculate the three orthogonal forces and moments at the contact patch and apply them at the wheel centre to predict the vehicle motion. Although all forces and moments are modelled, the rolling resistance moment and the overturning moment are often omitted as they are small and not of great importance in the overall dynamics.

A review of the methods of modelling shear force generation in pneumatic tyres under steady state conditions was published by Pacejka and Sharp [79]. The models were divided into three

main categories: physical models requiring computation to find the solution, simplified physical models that allow for analytical solutions and empirical models that use a formula to give a solution. The tyre relaxation was considered to be of small significance. It was argued that the relaxation length could be appropriately modelled by a first order lag.

At steady state, a physical model may assume that the tyre is made up of a number of identical elements. The model can be reduced to track one of the elements as it passes through the contact patch instead of tracking multiple elements simultaneously. Similarly, steady state conditions assume an upright tyre, so the properties across the width of the tyre can be assumed to be constant. Therefore, an uncambered wheel can be reduced to a single plane unit. Complex physical models can be very accurate in describing the tyre/road interaction, but can be costly in terms of computation time and effort. On the other side of the tyre model spectrum are formulae based on empirical models. These are useful when the tyre is considered as part of a larger vehicle system. Tyre models can be characterised by a number of features: accuracy, range, number of parameters, physical representation of the parameters, means of determining parameters, accuracy outside the range when extrapolating, and computational load. The ideal model is accurate within an extensive range, requires few parameters, which are directly linked to easily obtainable physical properties, and requires minimum computation time. In reality, different models cover different aspects of the ideal model and are suitable for certain applications only.

2.7.3.1 Analytical Methods

As discussed in the review by Pacejka and Sharp [79], there are various physical models [80-84]. One form of physical characterisation is the multi-spoke model. It models carcass flexibility through independently acting radial spokes aligned in a single plane. Every spoke is given characteristics that are known properties of the carcass. For example, the non-linear radial flexibility representing the approximate vertical equilibrium between the inflation pressure and normal stress when at the centre of the contact patch. A single spoke can be followed from an unstressed and unstrained condition through the contact patch in increments related to the distance between spokes. This requires a number of iterations to fully characterise the tyre. The advantage of the model is that it only requires a limited number of physical parameters. It performs well under steady state conditions, but lacks accuracy in transient conditions.

A second form of physical model is the brush model. This model simulates the tyre as a circular brush where the bristles are elastic and can deflect parallel to the road to represent slip (Pacejka [45]). The elasticity of the bristles represents all the components of the tyre: carcass, belt and tread elements. Although this is classed as a theoretical or physical model, it still requires a basic

level of knowledge of the tyre properties to model the elasticity of the tread elements. Other theoretical models include rigid ring models, and string models. These also require a level of knowledge of the tyre properties to model the elastic and damping properties of the tyre. The string model is similar to the brush model in the way that a string under stress models the tyre components (Pacejka [45]). The rigid ring model is somewhat more elaborate. It consists of a rigid ring with six degrees of freedom. This ring is in contact with the road through a residual stiffness and damping model as well as a slip model. The rigid ring is also in contact with the wheel rim via the sidewall stiffness and damping model. It is clear that this type of model is very useful in modelling and simulation, however it requires a substantial amount of knowledge of the tyre properties to work and extensive parametric data for the tyre in question. The disadvantage of the brush and string models is the difficulty involved with incorporating them within a full vehicle simulation. It also requires a number of tyre tests to establish various properties.

2.7.3.2 Interpolation Methods

This approach requires a look-up table generated from experimental results. The linear interpolation method assumes a linear progression between data points. However, the relationship between the tyre slip angle and the tyre force tends to be non-linear for larger slip angles. This method also requires the user to have a large database of measurements up to the extremes of the operating conditions. Several semi-empirical models have been developed that interpolate data, but also include more complex mathematical analysis [85-89].

2.7.3.3 The Magic Formula Tyre Model

A different approach to tyre modelling is to take a substantial amount of measurements and subsequently match the experimental data to a mathematical model. This is the principle of the Magic Tyre Formula. By recognising a number of features in experimental data plots, coefficients can be derived to form a formula that matches the data. Bakker et al. [90] presented the first stage of development of the Magic Tyre Formula. It was developed because the popular representations of measured tyre data were found to be inadequate. These representations included tables, graphs and formulae containing series such as Fourier and polynomials. The first two methods were not practical for application in theoretical studies. Presenting the data as a series made theoretical analysis possible, but it had many shortcomings: the large number of necessary coefficients for an accurate fit, the lack of good representation of rates of change, poor results when extrapolating outside the fitted range, coefficients having no meaning in the physical world. A good representation of measured tyre data should have a limited number of coefficients, these coefficients should have some meaning in physical terms, and it should perform well

outside the fitted range as well as in between data points. The Magic Tyre Formula that was presented had all these properties. The proposed method covered pure cornering or pure braking conditions only, but was a foundation for an improved model that included tyre characteristics during combined braking and cornering (Bakker et al. [91]). This model also included the non-isotropic properties of the tyre and accounted for influences from plysteer and conicity [92], rolling resistance and camber.

The definitive form of the Magic Formula tyre model was presented by Pacejka and Bakker [69]. It was shown how the formula was used to fit experimental data and how the parameters were related to the tyre characteristics. Figure 2.37 illustrates the D parameter, or peak force parameter of the formula, the slope of the linear tyre region BCD, and the horizontal and vertical shifts, S_H and S_V respectively, which are used to compensate for the camber angle and ensure that the curve passes through the origin. The equation given for the lateral force by Pacejka and Bakker is equation (2.45). The physical meaning of the equation parameters is given in table Table 2.8.

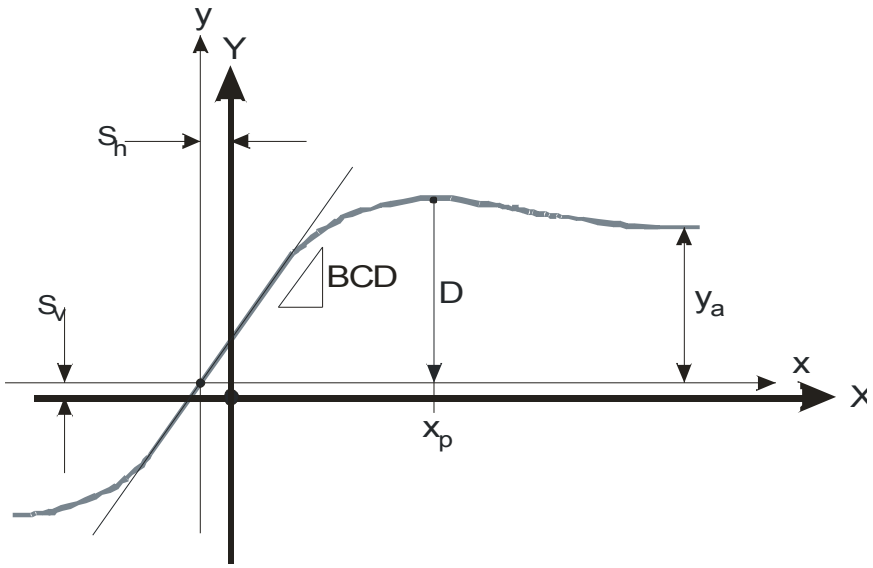

Figure 2.37 – Schematic diagram of Magic Formula fitting process where the x-axis represents the tyre slip angle and the y-axis represents the tyre force

$$
\begin{aligned}
y(x) &= D\sin\left[C\tan^{-1}\left(Bx - E\left(Bx - \tan^{-1}(Bx)\right)\right)\right] \\
Y(X) &= y(x) + S_{\mathrm{v}} \\
x &= X + S_{\mathrm{h}} \\
D &= \mu F_{\mathrm{z}} \\
\mu &= \left(a_1 F_{\mathrm{z}} + a_2\right)\left(1 - a_{15}\gamma^2\right) \\
BCD &= a_3 \sin\left(2\tan^{-1}\left(\frac{F_{\mathrm{z}}}{a_4}\right)\right)\left(1 - a_5\left|\gamma\right|\right) \\
C &= a_0 \\
E &= \left(a_6 F_{\mathrm{z}} + a_7\right)\left(1 - \left(a_{16}\gamma + a_{17}\right)\operatorname{sign}\left(\alpha + S_{\mathrm{h}}\right)\right) \\
B &= \frac{BCD}{CD} \\
S_{\mathrm{h}} &= a_8 F_{\mathrm{z}} + a_9 + a_{10}\gamma \\
S_{\mathrm{v}} &= a_{11} F_{\mathrm{z}} + a_{12} + \left(a_{13} F_{\mathrm{z}}^2 + a_{14} F_{\mathrm{z}}\right)\gamma
\end{aligned}
\tag{2.45}
$$

Y	=	corrected tyre force
y	=	uncorrected tyre force
x	=	effective slip angle
C	=	shape factor
D	=	peak force value
E	=	curvature factor
BCD	=	slope at small slip angles: linear tyre stiffness
B	=	stiffness factor at low slip values
S_h	=	horizontal shift
S_v	=	vertical shift due to camber
y_a	=	asymptote at high slip values
x_p	=	slip angle at which the peak force occurs

Table 2.8 – Qualitative description of the Magic Formula parameters

The Magic Formula version by Pacejka and Bakker [69] was the third version of the model and incorporated forces on the tyre resulting from longitudinal and lateral slip and camber all occurring simultaneously. The model focussed on providing an accurate representation of measured steady state tyre behaviour. The formula for pure slip was given as well as the modifications for combined slip model. The basis of combined slip was that a tyre/road interaction could produce a fixed maximum force whether reached under pure slip conditions or combined slip. Therefore, in a combined-slip case, the maximum lateral force would be smaller than in a pure lateral slip case.

Although Pacejka and Bakker [69] described the various parameters of the formula, a method for the exact determination was presented by Van Oosten and Bakker [93]. First, the forces acting between the road and the tyre were measured on a trailer pulled along a regular road. The advantage of this method was that the test conditions were as close to real life as possible. The disadvantage was that factors such as temperature, humidity and road surface were not constant and uncontrollable. The rig allowed the test tyre to be steered to a large range of lateral slip angles, braked to a large range of longitudinal slip angles, leaned to a reasonable range of camber angles, and loaded with a large variety of normal forces. A minimum test program was determined as follows: every test was done with 3 different vertical loads, where for each load the maximum stiffness was reached. The peak of the side force was reached and pure slip measurements were carried out with at least 2 camber angles excluding zero camber. For each camber angle, at least 6 measurements were taken under combined slip conditions. The data fitting procedure first determined the parameters for pure slip conditions and these were then fitted to the combined slip results. To optimise the fitting procedure, a least mean squares algorithm was used.

The Magic Formula tyre model was developed to suit car tyres only, so it only covered small camber angles. This was changed by De Vries and Pacejka [94] who set out with the objective to develop dynamic measurement methods as well as a tyre model for motorcycle simulations. It was recognised that the tyre model for cars focussed on the slip angles producing the tyre forces and moments leaving the effect of the camber angle underexposed. In order to use a Magic Formula tyre model for a motorcycle, the method would have to include the forces resulting from the lean angle. The proposed changes resulted in a model that treated the sideslip angle and the camber angle as equally important variables.

The Magic Tyre Formula appears to be a desirable method to model the tyre behaviour. It is a curve-fitting tool that allows the user to optimise the fit of a set of non-linear data. The development of the formula has shown that additional terms had to be included to improve the fit [95-98]. It was also shown how these terms were related to the measured data. The parameters that were tuned were not in any way related to the tyre or the road itself. What that meant was that if tyre A with width 120mm was tested and the results fitted, a completely new set of tests had to be done for tyre B, identical to A apart from its width. Nevertheless, the basic formula could be used as a trend curve in the development of a method to determine the tyre characteristics during on-road testing.

2.8 CONCLUDING REMARKS

The control problem of an inverted pendulum on a cart has been introduced as an analogy for a tilting vehicle. Vehicle models a varying complexity have been discussed. The geometric model was considered too simple. The various simplifications of the more complete models were not always appropriate: linearisation of the roll angle, the assumption that the principal axes of inertia were parallel to the vehicle degrees of freedom and the linear tyre stiffness.

The DTC and STC methods have been reviewed and vehicle systems that were presented in the literature were simulated in Matlab/Simulink. It was found that the DTC method was feasible in practice, but that it had its limitations. The most important problem was the rollover dynamics of the rear non-tilting unit. STC was a better control method for higher velocities, as it would eliminate the need for actuators reacting on the rear unit. The STC method was found to be an effective tilt control method in simulation studies. However, the studies presented in the literature did not always include full vehicle models or tyre models. Furthermore, no previous STC study included a steer actuation model.

Finally, tyre modelling theory has been reviewed to select a tyre modelling method that can be used in a simulation model. The 'Magic Formula' model was found to be best suited to the modelling requirements of a tilting three-wheeler in which both camber steer and slip steer are of importance.

CHAPTER 3. UNCERTAINTIES IN EXPERIMENTAL DATA PROCESSING AND VEHICLE MODELLING

The objective of this study is to develop and validate a model of a three-wheeled tilting vehicle and test a novel roll control algorithm with this model. The development process includes vehicle experiments for model validation and improved understanding of driver behaviour and computer simulations to verify the controller's performance. This chapter investigates a number of factors that cause perceived errors in experimental data and modelling methods to simulate environmental disturbances. First, the kinematics of the steering assembly are presented: the effect of the trail and the effect of the roll on the steer and vice versa. Next, kinematic equations to quantify the effect of the tilt axis inclination are derived. The importance of the mass and inertia of the driver on the vehicle dynamics is demonstrated. The calculation of the perceived acceleration is reviewed. The effect of the rear unit roll on the roll measurement is examined. The definition of the steering torque is assessed with a numerical example. Finally, modelling methods for three environmental disturbances, side wind, hill driving and road camber, are proposed.

3.1 KINEMATICS

A bicycle or motorcycle steering arrangement has a castor angle ε as shown in Figure 3.1. This means that the steering axis is at an angle with respect to the vertical. As a result, the wheel contact point and the point where the steering axis crosses the road plane are a certain distance apart. This distance is called the trail t. The trail is a very important geometric component that determines the handling properties of a motorcycle. The following section demonstrates the precise effects the trail has on the handling. The equations and descriptions are based on those by Cossalter [46].

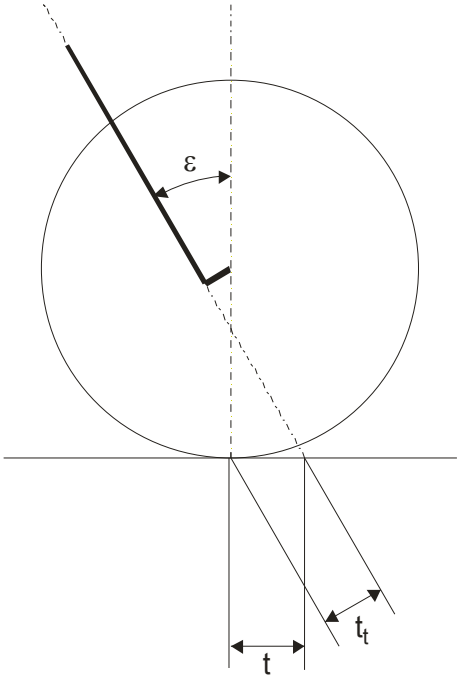

Figure 3.1 – Illustration of the castor angle ε, trail t and normal trail t_t

3.1.1 Steering head kinematics

As the handlebars turn, the steering head will have to lower for the contact patch to remain in contact with the road. This also means that the wheel centre lowers by a small amount. Cossalter [46] showed the extent of this displacement in relation to the steer angle. It was shown that even in extreme conditions, a 45° steering angle for instance, the wheel centre was lowered by less than 2mm. The suspension offset, this is when the steering axis does not pass through the wheel centre, was shown to play an important role in the determination of the wheel centre displacement: a non-zero offset reduced the displacement significantly. Although an important kinematic effect, this lowering of the wheel centre was not considered to be of great importance to the overall steering dynamics.

3.1.2 Pitch

The pitch of a motorcycle changes with the steering angle because of the castor angle. For small steering angles, the pitch is largely dependent on the normal trail t_t, and the wheelbase L, as shown in equation (3.1) where R is the wheel radius. It should be noted that the pitch angle caused by the steering angle and the roll angle is less than 1° for extreme values of steer and roll. The pitch dynamics are therefore mainly caused by accelerating and braking. Thus, the pitch dynamics can be assumed negligible when there is no harsh acceleration or braking.

$$\mu = -\frac{t_t - R_f \sin(\varepsilon)}{L}\delta_f \tan(\phi) - \frac{R_r - R_f}{L}\left(\frac{1}{\cos(\phi)} - 1\right) \tag{3.1}$$

3.1.3 Camber Angle

The camber angle is the effective roll angle of the front wheel and it is used when calculating the lateral force generated by the front tyre. The front wheel camber angle will not be equal to the roll angle of the motorcycle because of the steering angle. The camber angle can be determined from the steering angle, the roll angle, and the castor angle, and assuming a negligible pitch angle with equation (3.2).

$$\gamma = \sin^{-1}\left(\cos(\delta_f)\sin(\phi) + \cos(\phi)\sin(\delta_f)\sin(\varepsilon)\right) \tag{3.2}$$

Figure 3.2 illustrates how the camber angle and roll angle can differ significantly when the wheel is steered. It shows that the camber angle tends to be larger than the tilt angle as soon as the wheel is steered. The difference between the camber angle and the roll angle should be taken into account in the data processing and vehicle modelling. This is especially important when estimating lateral forces.

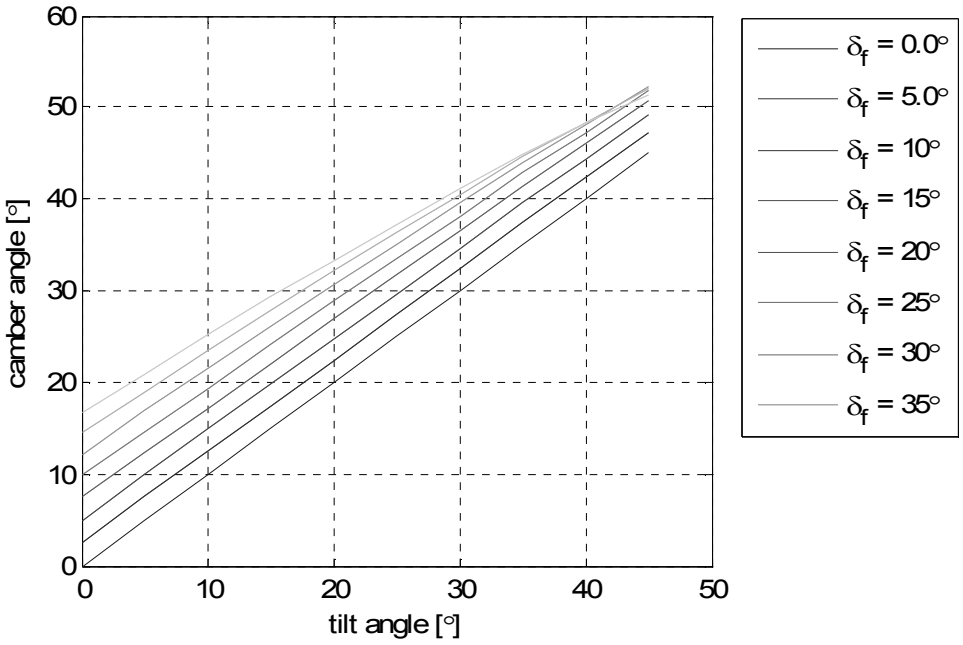

Figure 3.2 – Camber angle vs. Tilt angle as calculated with equation (3.2)

3.1.4 Kinematic Steer Angle

In the previous section it was shown how the camber angle and the roll angle differed because of the steering angle. The steering angle δ_f is defined as the angle between the steering assembly plane and the main vehicle body plane. However, as soon as the vehicle rolls, the angle on the road plane is no longer equal to this steering angle, but is the kinematic steering angle Δ as defined by Cossalter [46] in equation (3.3). Assuming the pitch angle is negligible and the term $\sin(\varphi)\sin(\delta_f)\sin(\varepsilon)$ is significantly smaller than $\cos(\varphi)\cos(\delta_f)$, the equation can be simplified to equation (3.4).

$$\Delta = \tan^{-1}\left(\frac{\sin(\delta_f)\cos(\varepsilon+\mu)}{\cos(\phi)\cos(\delta_f)-\sin(\phi)\sin(\delta_f)\sin(\varepsilon+\mu)}\right) \tag{3.3}$$

$$\Delta = \tan^{-1}\left(\frac{\cos(\varepsilon)}{\cos(\phi)}\tan(\delta_f)\right) \tag{3.4}$$

When equation (3.4) is plotted, as shown in Figure 3.3, it can be seen that the kinematic steer angle is largely affected by the castor angle when the roll angle is small: the kinematic steering angle tends to be smaller than the steering angle. Although the difference between the steering angle and its kinematic equivalent appears significant at extreme values of steer and roll, in the working area, up to 0.35 radians of steer and 0.60 radians of roll, the difference lies within 5%.

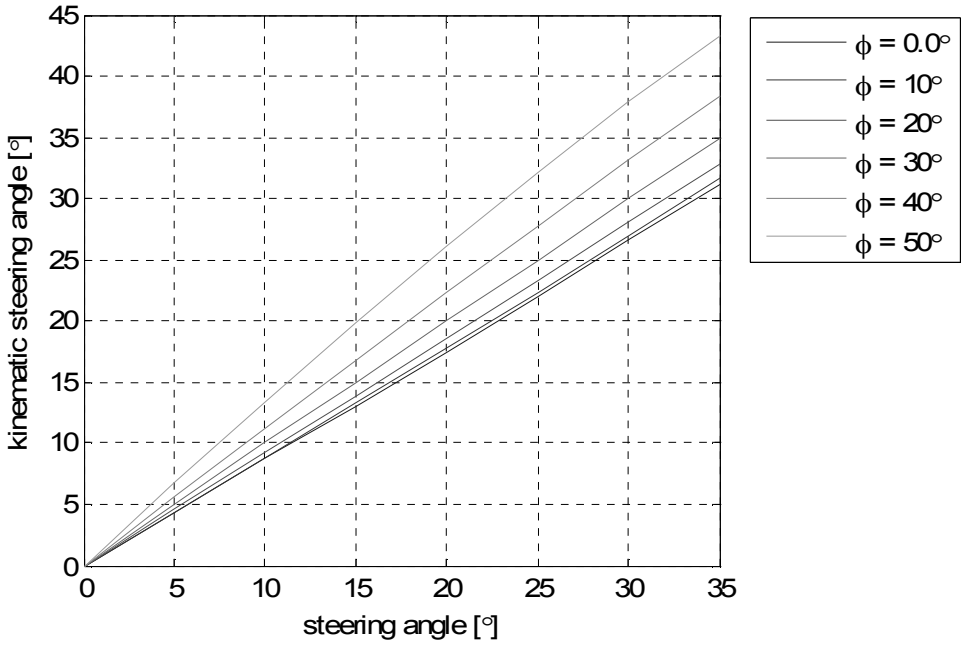

Figure 3.3 – Kinematic steer angle vs. Steer angle calculated with equation (3.4)

3.1.5 Tilt Axis Inclination

In the previous sections it as shown how the geometry of the steering assembly had an important effect on the kinematics of the steer and roll measurements. In the case of a tilting three-wheeled vehicle, the inclination of the roll axis and the point where it crosses the road plane also have an important kinematic effect. Figure 3.4 shows the tilt axis location on a vehicle such as CLEVER. As the cabin assembly rolls, it also pitches about the rear contact point and the tilt axis inclination angle α becomes smaller. Not only will the vehicle pitch but the cabin assembly will also yaw by a small amount with respect to the rear. The reduction in pitch angle is expected to be small, but the yaw could become large enough to have an effect on the vehicle dynamics: the yaw can be compared to the rear unit steering relative to the cabin assembly resulting in additional tyre forces [99]. The figure also shows that the point where the tilt axis crosses the road and the point from which the vehicle will pitch, the rear axle, are not in the same location.

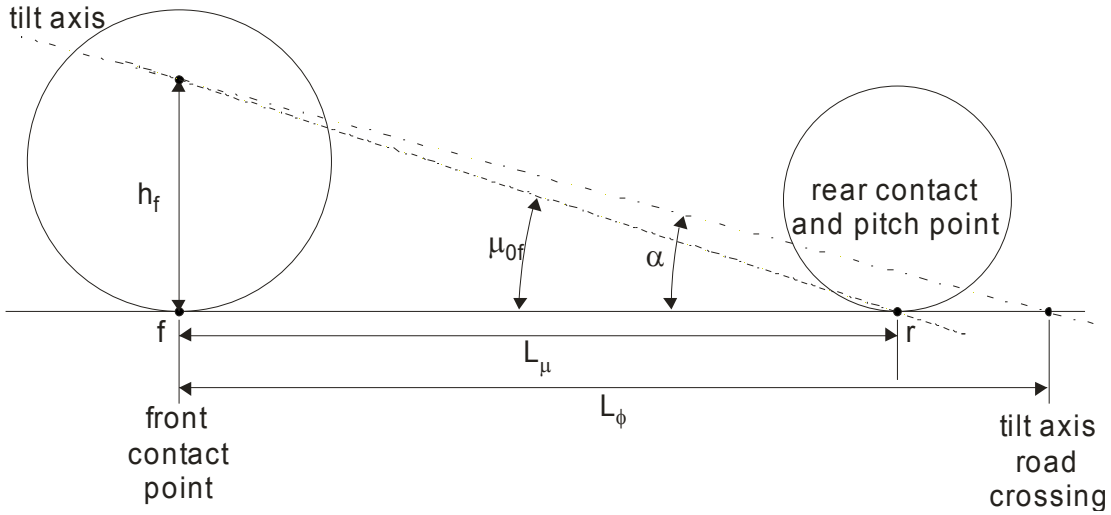

Figure 3.4 – Schematic illustrating the geometry of the tilt axis

To calculate the relative yaw, ψ_f, between the front and the rear, equation (3.5) was derived. This equation illustrates that this relative yaw between the front and the rear unit is dependent on the inclination angle of the tilt axis α and the roll angle measured on the joint φ_{joint}. This equation demonstrates that the rear steer changes dynamically as the vehicle rolls in and out of a turn. It also shows that the vehicle design, i.e. the inclination of the tilt axis, will affect the maximum amount of relative yaw or rear steer a vehicle can produce. This relative yaw results in the cabin assembly having a slightly small heading angle than the rear unit heading angle, so the rear unit can be said to steer into a turn. As a result, the slip angle at the rear will be larger and the tyres will generate larger side forces.

$$\psi_{\mathrm{f}} = \sin^{-1}\left(\sin(\alpha)\sin(\phi_{\mathrm{joint}})\right) \tag{3.5}$$

The roll angle at the joint was used to calculate the relative yaw. It is important to differentiate between the roll angle at the joint and the roll angle in the global axis system. The roll angle in the global axis system can be calculated using equation (3.6). The difference between the roll angle at the joint and the roll angle in the global axis will be small for most tilt axis geometries. Nonetheless, it is important to bear this difference in mind. The change in the inclination angle as a function of the real world roll angle can be verified using equation (3.7). This equation demonstrates that the change in the angle will be small.

$$\phi_{\mathrm{world}} = \sin^{-1}\left(\frac{\tan(\psi_{\mathrm{f}})}{\tan(\alpha)}\right) \tag{3.6}$$

$$\mathrm{d}\mu = \mu_{0_{\mathrm{f}}} - \mu_{\mathrm{f}}$$

where

$$\mu_{0_{\mathrm{f}}} = \tan^{-1}\left(\frac{h_{\mathrm{f}}}{L_{\mu}}\right)$$

$$\mu_{\mathrm{f}} = \sin^{-1}\left(\frac{h_{\mathrm{f}}\cos(\phi_{\mathrm{world}})}{\sqrt{L_{\mu}^2 + h_{\mathrm{f}}^2}}\right) \tag{3.7}$$

The cabin assembly of the vehicle is a large mass and inertia component of the vehicle system. As this assembly rolls and subsequently pitches, the centres of mass of the cabin also move. The result is an overall change in location of the vehicle centre of mass and most importantly its yaw axis. To track the displacement of a point P, shown in Figure 3.5, on the cabin assembly the equations below can be used.

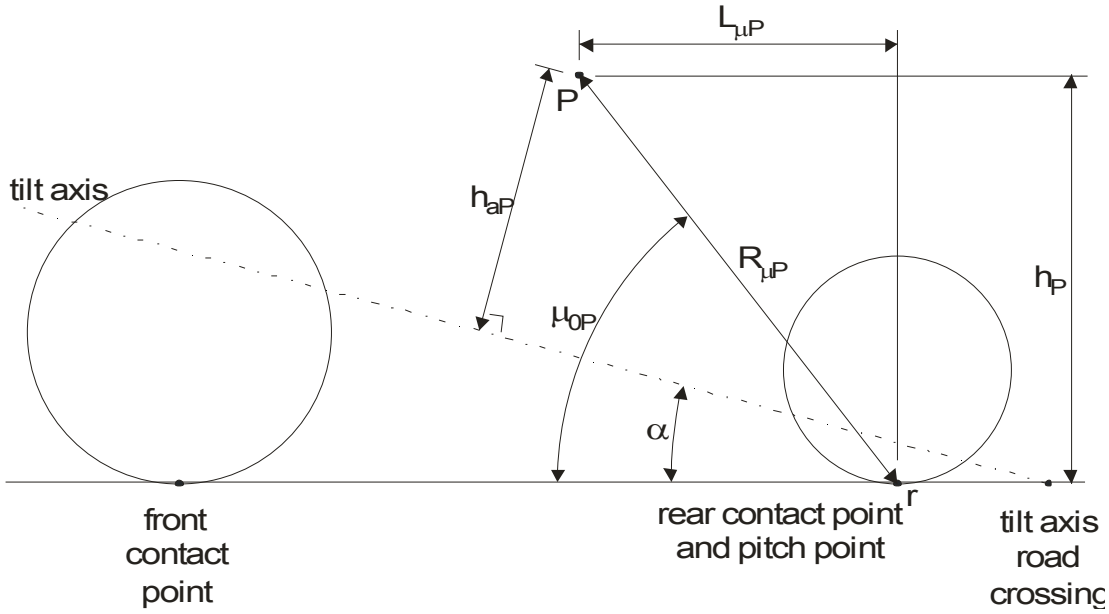

Figure 3.5 – Schematic illustrating a point P on the vehicle assembly

The calculations require the determination of the distance between the tilt axis and the point P using (3.8). This distance is necessary to determine the lateral displacement of the point P as defined in equation (3.9). This lateral displacement is particularly important as it will help determine the lateral displacement of the yaw axis as a result of the roll. The longitudinal and vertical displacements of the point P depend on the change in inclination. First the distance between the pitch point and the point P has to be calculated. This distance is not constant and changes with the roll as can be seen from equation (3.10). Next the original angle between the pitch point and the point P needs to be determined using equation (3.11).

$$h_{a_P} = \sqrt{\left(L_{\phi_P}^2 + h_P^2\right)} \sin\left(\tan^{-1}\left(\frac{h_P}{L_{\phi_P}}\right) - \alpha\right) \tag{3.8}$$

$$dy_P = -h_{a_P} \sin\left(\phi_{joint}\right) \tag{3.9}$$

$$R_{\mu_P} = \sqrt{\left(L_{\mu_P} + h_{a_P}\left(1 - \cos\left(\phi_{joint}\right)\right)\sin\left(\alpha\right)\right)^2 + \left(h_P - h_{a_P}\left(1 - \cos\left(\phi_{joint}\right)\right)\cos\left(\alpha\right)\right)^2} \tag{3.10}$$

$$\mu_{0_P} = \tan^{-1}\left(\frac{h_P - h_{a_P}\left(1 - \cos\left(\phi_{joint}\right)\right)\cos\left(\alpha\right)}{L_{\mu_P} + h_{a_P}\left(1 - \cos\left(\phi_{joint}\right)\right)\sin\left(\alpha\right)}\right) \tag{3.11}$$

Using the distance and the angle between the pitch point and the point P, and the change in inclination dμ from equation (3.7), the new longitudinal and vertical coordinate of the point P can be found using equations (3.12) and (3.13).

$$\mathrm{d}x_{\mathrm{P}} = R_{\mu\mathrm{P}} \cos\left(\mu_{0\mathrm{P}} - \mathrm{d}\mu_{\mathrm{f}}\right) - L_{\mu\mathrm{P}}$$

$$x_{\mathrm{P}} = \mathrm{d}x_{\mathrm{P}} + L_{\mu\mathrm{P}} \tag{3.12}$$

$$\mathrm{d}z_{\mathrm{P}} = -h_{\mathrm{P}} + R_{\mu\mathrm{P}} \sin\left(\mu_{0\mathrm{P}} - \mathrm{d}\mu_{\mathrm{f}}\right)$$

$$z_{\mathrm{P}} = h_{\mathrm{P}} + \mathrm{d}z_{\mathrm{P}} \tag{3.13}$$

3.2 MASS AND INERTIA

For a vehicle where the driver mass is a significant portion of the overall system mass, its effect on the system inertias can be important. The following section investigates how the vehicle inertias vary with the driver's mass. Equally important is the change of the vehicle inertias as the vehicle rolls: the roll causes the centres of mass of the rolling parts to displace laterally. The extent of the changes in inertia caused by the roll is also discussed in this section.

3.2.1 Driver Physical Model

A physical driver model was created in CAD software Solid Edge using anthropometric and density data from Clauser et al. [100]. Individual body parts with their variable densities were modelled to represent a driver seated with their hands on the handlebars. This type of model allowed for changes in driver size in terms of height as well as build. The driver model could then be added to a vehicle model to determine the vehicle's inertia properties with drivers of various sizes.

3.2.2 Vehicle Model with Driver

A 3D CAD model of the Honda Gyro was created to estimate the tilt and yaw inertias. The driver model was then added to the vehicle assembly to study the effect of the driver's size and weight on these inertias.

It was expected that a larger driver would cause the centre of mass location to move forward. This was investigated with using the CAD model and Figure 3.6 shows this displacement of the centre of mass with an increasing driver mass. This shows that there is a significant shift in the

location from a lightweight driver to a heavy driver: significant enough to affect the yaw dynamics which depend on the ratio of the centre of mass locations along the wheelbase.

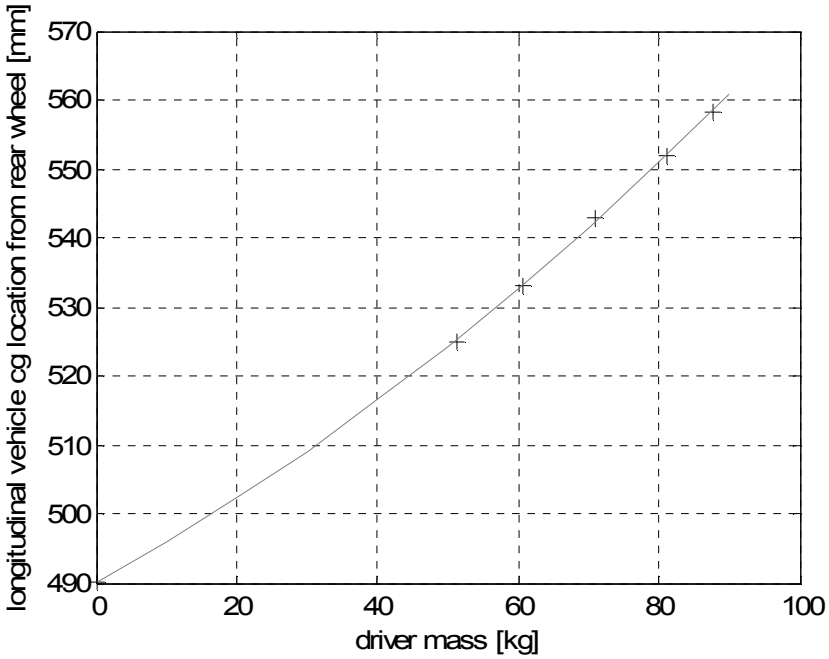

Figure 3.6 – Variation of longitudinal location of the centre of mass along the wheelbase because of a change in driver mass

The driver's mass will not only affect the yaw dynamics through this displacement, but it will also result in a change in yaw inertia as shown in Figure 3.7. It is expected that the displacement of the centre of mass will have a more significant effect on the yaw dynamics than the change in yaw inertia. Nevertheless, this investigation has shown that if the driver's mass is large in comparison to the overall vehicle mass, the possible variation in drivers should be taken into account in a mathematical model.

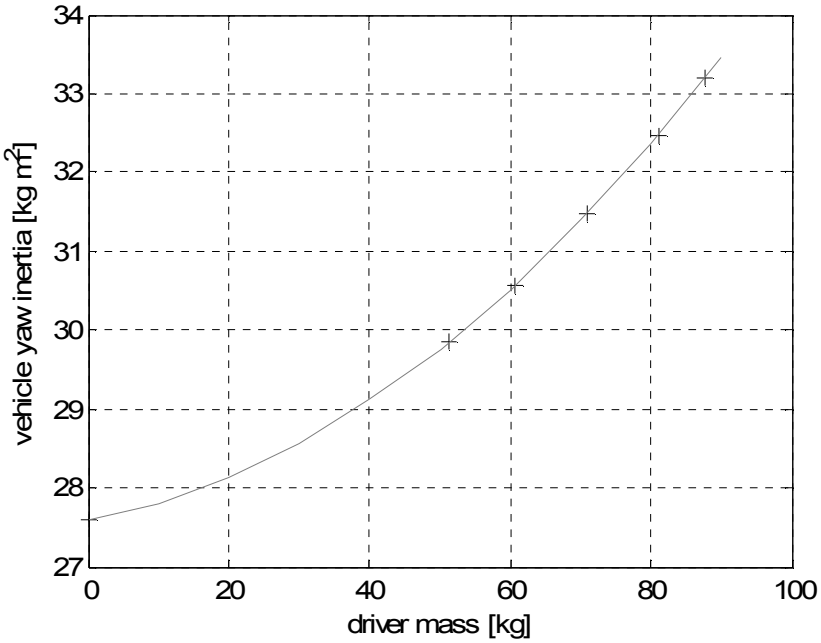

Figure 3.7 – Effect of the driver's mass on the overall yaw inertia of the vehicle

It was predicted that a change in the driver's mass would also shift the centre of mass vertically. This vertical shift has a significant effect on the roll dynamics. That is, the height of the centre of mass perpendicular to the roll axis changes the overall roll inertia of the tilting assembly. Figure 3.8 shows the variation in this centre of mass location with the driver's mass. It is important to note that the change in total roll inertia is the mass multiplied by the square of the height above the axis as shown in Table 3.1.

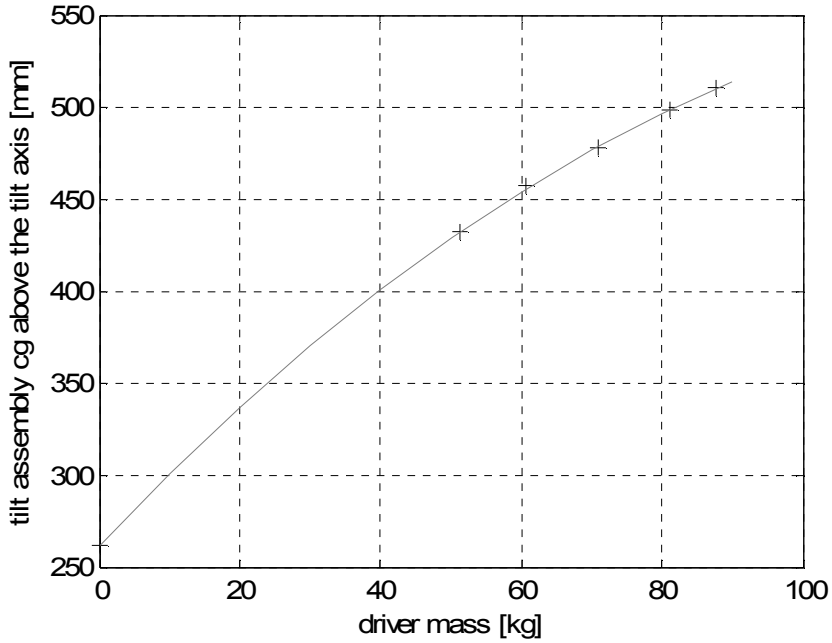

Figure 3.8 – Variation of location of the centre of mass of the tilting assembly perpendicular to the tilt axis

driver's mass [kg]	50	60	70	80	90
additional roll inertia $m_t*h_t^2$ [kg m^2]	9.31	12.4	15.8	19.7	23.9

Table 3.1 – Effect of the driver's mass on the additional roll inertia

It has been shown that the driver's mass increases the roll inertia by its increase as well as vertical shift, but is also increases as a result of the change in mass distribution in relation to the assembly as shown in Figure 3.9. The cumulative increase in roll inertia with the driver's mass is substantial and an important factor in the roll dynamics as well as roll control.

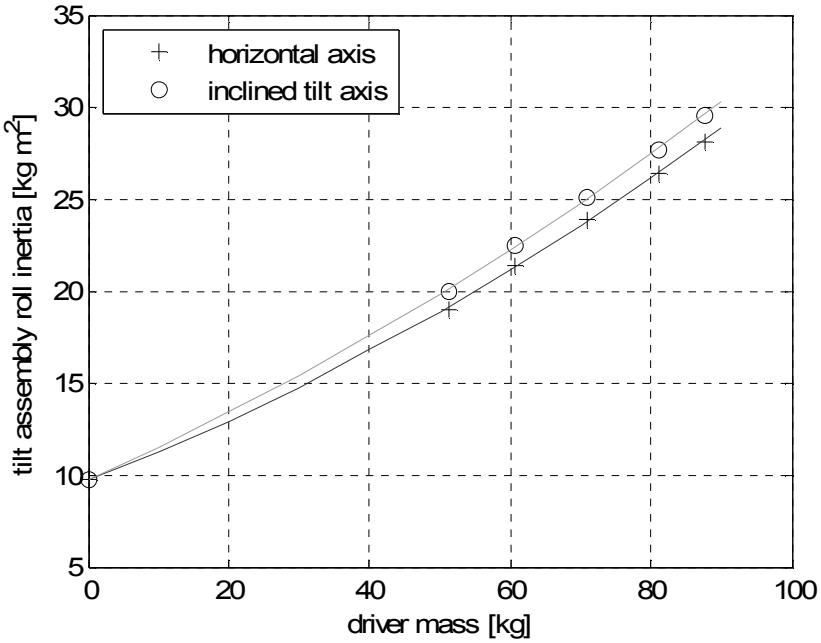

Figure 3.9 – Change in tilt assembly roll inertia with respect to the driver's mass where the tilt inertia is a) about the horizontal axis through the centre of mass parallel with the road b) about the inclined axis going through the centre of mass and parallel to the rotated tilt axis

3.2.3 Inertia Variations with Roll angle

A tilting three-wheeler with a non-tilting engine and rear wheel assembly is unique in many ways including the dynamic changes of the overall vehicle inertia during tilting. As the vehicle rolls, the mass distribution of the vehicle changes with respect to the reference axes. The centre of mass of the tilting assembly shifts laterally in comparison to the centre of mass of the non-tilting rear wheel assembly. As a result, the vehicle's centre of mass is displaced as the vehicle rolls and so is the vehicle's yaw axis and therefore yaw inertia. Figure 3.10 demonstrates how the yaw inertia varies with the roll angle as well as the driver's mass: the inertia becomes increasingly larger as the vehicle rolls. This is a unique characteristic that should be taken into account in the creation of any simulation models.

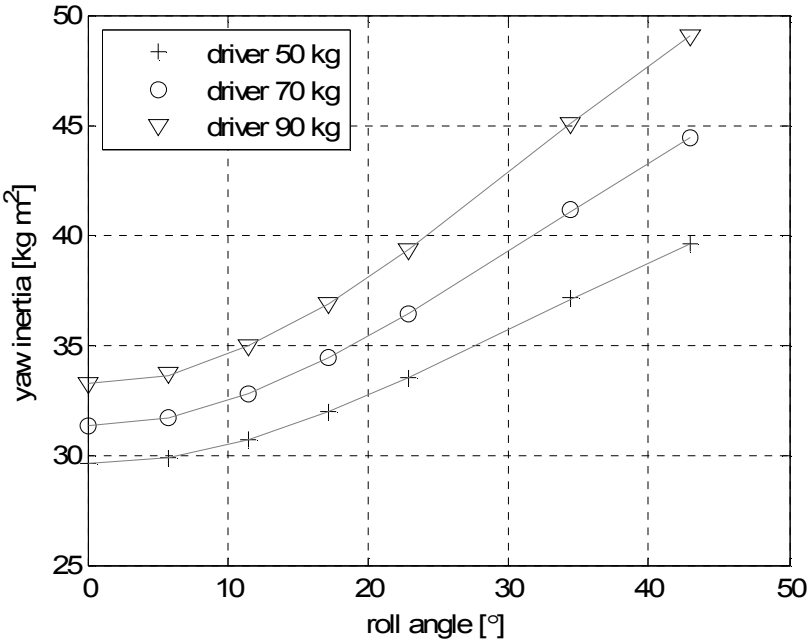

Figure 3.10 – Variation of the yaw inertia with the roll angle measured at the axis for various driver masses

3.3 PERCEIVED ACCELERATION DEFINITION

The driver's perceived acceleration has been used to determine whether the vehicle is balanced and to establish the driver's tilting experience. One of the aims of the experimental work is to verify that the driver aims to reduce this acceleration to zero. Thus the equation for the calculation of this state has been reviewed.

The perceived acceleration is defined as the acceleration perpendicular to the driver's yaw axis. In chapter 2 the perceived acceleration was defined as a component of the lateral acceleration, a component of the gravitational acceleration, and the tilt acceleration at the sensor location, see equation (2.23). This definition assumes that the sensor lies on the vehicle yaw axis, and that the roll axis lies on the ground and is parallel to the ground. These assumptions disregard too many dynamic effects when considering a three-wheeled tilting vehicle with an inclined tilt axis during transient manoeuvres.

Firstly, the vehicle yaw axis and the sensor are a certain distance dx apart in the longitudinal sense, so the effect of the yaw acceleration on the perceived acceleration should be included. Then the components of the gravitational acceleration and the lateral acceleration are measured in terms of the 'world' roll φ_{world} measured in the ISO coordinate system and not the rotational angle at the tilt joint φ_{joint}. The sensed lateral acceleration due to the roll acceleration is the roll measured at the joint and is multiplied by the perpendicular distance d from the roll axis. The

final component is the centripetal acceleration because of the roll velocity. Again, this is the roll velocity measured at the roll joint. The new definition for the perceived acceleration is given by equation (3.14).

$$a_{\mathrm{per}} = \left(a_{\mathrm{y}} + v_{\mathrm{x}}\frac{\mathrm{d}\psi}{\mathrm{d}t}\right)\cos\left(\phi_{\mathrm{world}}\right) - \mathrm{d}x\frac{\mathrm{d}^2\psi}{\mathrm{d}t^2} - g\sin\left(\phi_{\mathrm{world}}\right) + \\ + d\frac{\mathrm{d}^2\phi_{\mathrm{joint}}}{\mathrm{d}t^2} + d\left(\frac{\mathrm{d}\phi_{\mathrm{joint}}}{\mathrm{d}t}\right)^2\sin\left(2\phi_{\mathrm{joint}}\right) \tag{3.14}$$

3.4 REAR UNIT ROLL

As was established in chapter 2, the dynamics of the rear unit cannot be ignored. The roll angle of the cabin is measured on the joint between the cabin and the rear unit, so if the rear unit rolled out of the turn, this measured roll would be larger than the actual cabin roll. The original design experimental vehicle had a single suspension strut mounted between the front and the rear unit, however this had been replaced with a rigid link to allow the tilt axis inclination to be altered. As a result, there was no additional roll associated with the rear unit because of the suspension. In a different vehicle, such as CLEVER, the rear wheels are each mounted with an individual suspension strut allowing for the rear unit to roll relative to the rolling cabin assembly. Thus, when modelling and testing this type of vehicle, the effect of the rear wheel suspension should be taken into account.

The vertical stiffness of the tyre was approximated using data from Williams [101]. Here the total radial spring stiffness of the wheel and tyre was estimated at 250 kN/m. As an alternative, the modelling data from Captain et al. [77] suggested a radial spring stiffness of 569 kN/m and a damping coefficient of 462 Ns/m. Nevertheless, it could be assumed that the tyre would act as a very stiff component. As long as the cornering conditions would not result in one of the wheels lifting off as was discussed in chapter 2, the rear roll will be very small. In other words, the rear roll will be limited to less than one degree.

3.5 STEERING TORQUE

The objective of the research is to develop an active steering system. In order to select the components for the system, the order of magnitude of the torque the system has to produce should be estimated from the experimental data. The following section discusses which definition of the steering torque should be used for this purpose.

To change the steer angle, the driver has to apply a torque to the steering wheel or handle bars. This torque accelerates the steering assembly and changes the position of the steered wheel(s). It also has to balance moments known as aligning and disaligning tyre moments associated with camber, trail, and lateral and vertical tyre forces. When driving a car, it can be noticed that after steering into a turn, the steering wheel has the tendency to straighten up by itself. Therefore, if the driver intends to drive on a constant circular path, he will have to continue to apply a torque to the steering wheel in order to keep turning. The cause of the wheels returning to their straight-ahead position is a combination of tyre contact patch asymmetry and steering assembly geometry. These effects are also present in motorcycles and there are various equations [45, 48, 68, 102, 103] that estimate the torque the rider has to apply to enter a turn and to corner at steady state.

On a motorcycle the steering torque does not only consist of the product of the inertia of the steering assembly and the acceleration of the assembly. There are various forces, generated at the tyre contact patch, that act on the steering assembly at various points that do not lie on the steering axis. As a result, there are additional moments about the steering axis which have to be balanced by the driver. Some of these tend to straighten up the front wheel to its neutral straight-ahead position; they are called aligning moments and are considered to be negative. The moments that tend to steer the front wheel into the turn are positive and they are called disaligning moments.

The tyre contact patch trail is one of the major causes of the moment about the steer axis. The trail is the distance between the centre of pressure of the tyre contact patch and the point where the steer axis crosses the road plane. The normal (vertical) force and the side force act on the centre of the tyre contact patch and as soon as the wheel is steered or leans, these forces cause a moment about the steer axis. The normal force results in a disaligning moment and the side force tends to align the wheel. To keep the steer angle constant, the driver has to apply a force at the handlebars to compensate. In addition to the torques resulting from the trail, there are gyroscopic moments from the rotating front wheel.

A basic definition for the steering torque was given by Robinson [102]. The steady state steering torque was defined as a balance between the moments caused by the normal (vertical) force F_{Zf}, the brake or drag force F_{Xf}, and the lateral force F_{Yf}. Assuming that these forces act on the tyre contact patch directly below the wheel axle, these normal and lateral forces will cause a moment about the steer axis because of the trail. Figure 3.11 illustrates the definition of this moment arm as a component of the castor angle ε and the trail length t measured on the road. Figure 3.12 shows the magnitude of the components of the normal and lateral forces causing a torque about

the steer axis related to the roll angle. The moment caused by the longitudinal braking force is an effect illustrated by Figure 3.13: the lateral displacement d*y* of the tyre contact patch as the motorcycle wheel rolls. This displacement is defined by equation (3.15). The resulting steady state steering torque T_s is given by equation (3.16). This definition of the steering torque shows that during a steady state manoeuvre where the velocity and the lateral force are constant and where the lean angle is at the balanced lean angle, the torque is zero. Under any other circumstances, the driver has to apply some force to the handlebars to maintain the steer angle at the desired position. Although the axle load and the lateral force are the most significant influences on the steering torque in steady state, as soon as the driver changes the steer or the lean, other effects become important too.

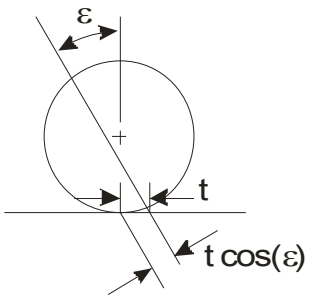

Figure 3.11 – Schematic diagram illustrating the trail and the moment arm for a moment about the steer axis caused by a force applied at the centre of the contact patch assumed to be directly below the wheel axle

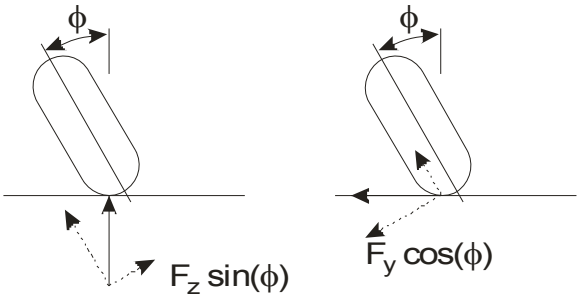

Figure 3.12 – Schematic diagrams illustrating the component of the normal (vertical) force and the component of the lateral tyre force which will cause a moment about the steer axis

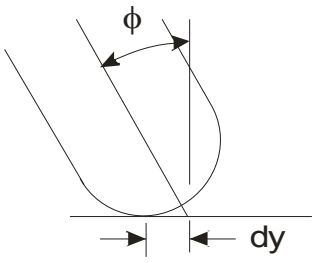

Figure 3.13 – Schematic diagram showing the lateral displacement of the contact patch from the tyre symmetry line as the tire rolls

$$\mathrm{d}y = t\sin(\Delta_\mathrm{f}) - R_\mathrm{f}\tan(\phi) \tag{3.15}$$

$$\begin{aligned} T_\mathrm{s} = \quad & m\,g\,t\cos(\varepsilon)\sin(\phi) + \\ & \pm F_\mathrm{X}\,\mathrm{d}y\cos(\varepsilon) + \\ & - m\left(\dot{v}_\mathrm{Y} + v_\mathrm{X}\dot{\psi}\right) t\cos(\varepsilon)\cos(\phi) \end{aligned} \tag{3.16}$$

Fajans [48] presented a definition for the steering torque similar to Robinson, but included one of the gyroscopic moments as well as the torque required to change the steer angle as shown in equation (3.17). The definition included the resultant moment from the front wheel with inertia I_{Yw} spinning at velocity ω_w and the roll rate. Although this definition included two transient terms, it did not include the gyroscopic moment from the rotating wheel and the yaw rate, and it assumed that the side force was proportional to the centripetal force.

$$T_\mathrm{s} = I_\mathrm{s}\ddot{\delta}_\mathrm{f} - \omega_\mathrm{w}\,I_\mathrm{Yw}\dot{\phi} + \frac{m\,g\,bt}{L}\phi - \frac{m\,v_\mathrm{X}^2\,b\,t}{L^2}\delta_\mathrm{f} \tag{3.17}$$

A more complete definition of the torque that the driver has to apply to steer was derived from Sharp's motorcycle model [103]. It included the lateral and normal force moments, the gyroscopic moments from the roll and the yaw velocities, the weight of the front assembly, and the accelerations as shown in equation (3.18). The various geometric variables used in this equation are shown in Figure 3.14.

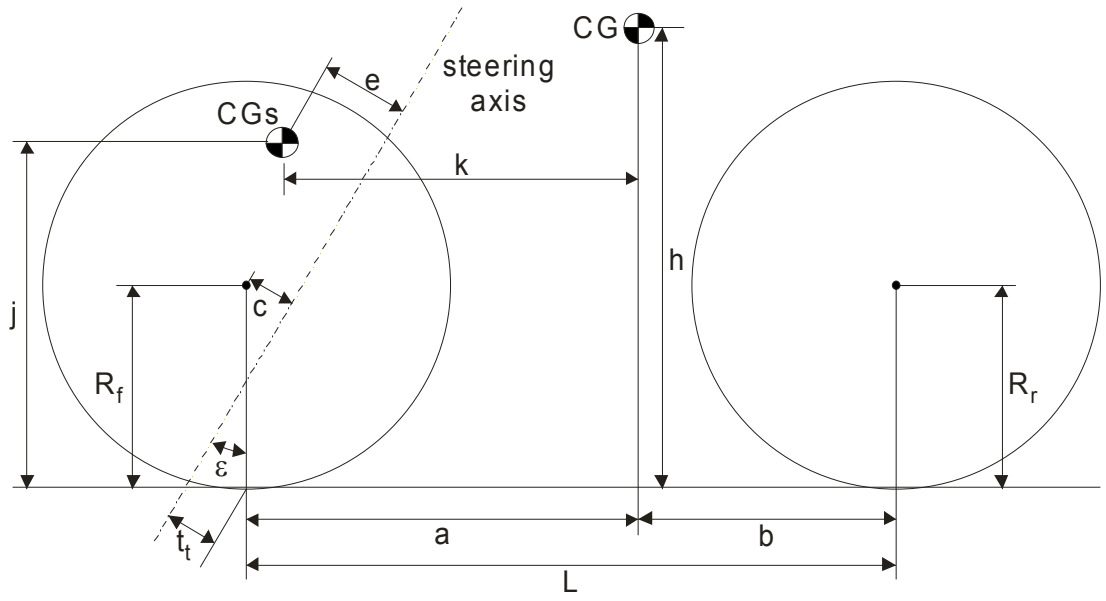

Figure 3.14 – Illustration of the geometric variables used in the steering torque equation by Sharp

$$
\begin{aligned}
T_s = \quad & t_t\, F_{Zf}\left(\sin(\varepsilon)\delta_f + \phi\right) + \\
& - t_t\, F_{Yf} + \\
& + \frac{v_X}{R_f}\, I_{Yw}\left(\dot{\phi}\cos(\varepsilon) - \dot{\psi}\sin(\varepsilon)\right) + \\
& + g\, m_f\, e\left(\sin(\varepsilon)\delta_f + \phi\right) + \\
& - m_f\, e\left(\left(\dot{v_Y} + v_X\dot{\psi}\right) + e\ddot{\delta}_f + j\ddot{\phi} + k\ddot{\psi}\right) + \\
& - I_{Zf}\left(\ddot{\delta}_f + \ddot{\phi}\sin(\varepsilon) + \ddot{\psi}\cos(\varepsilon)\right)
\end{aligned}
\tag{3.18}
$$

To illustrate how the definitions of steering torque compared and to appreciate the magnitude of the various factors that influence the steering moment, a simple manoeuvre was defined in terms of the steering angle and its derivatives. This calculation example assumed that the forward velocity was constant, there was no load transfer between the front and the rear wheels, the lateral acceleration was equal to the centripetal acceleration, and that the vehicle dynamics could be modelled with the geometric model described in chapter 2. Hence, the lateral velocity was defined by equation (2.5). The yaw rate was defined by equation (2.6). The lateral forces described by equation (3.19) were balanced so that the yaw acceleration was zero. Steering was defined so that the trajectory shown in Figure 3.15 was achieved. The steering angle to achieve this trajectory and the roll for this trajectory are given in Figure 3.16. The roll led the steer, because there would be a small amount of countersteer before the steer turned to the direction

the driver wanted to go. This leading roll angle was calculated with equation (3.20) where t was the current time and Δt the lead time. In this calculation example, the countersteer was omitted since it would be significantly smaller than the manoeuvre steer angle.

$$F_{\mathrm{Yf}} = \frac{b}{L} m \frac{\delta_{\mathrm{f}} v_{\mathrm{X}}^2}{L} \qquad F_{\mathrm{Yr}} = \frac{a}{L} m \frac{\delta_{\mathrm{f}} v_{\mathrm{X}}^2}{L} \tag{3.19}$$

$$\phi(\mathrm{t}) = \tan^{-1}\left(\frac{\delta_{\mathrm{f}}(\mathrm{t}+\Delta\mathrm{t})\, v_{\mathrm{X}}^2(\mathrm{t}+\Delta\mathrm{t})}{Lg}\right) \tag{3.20}$$

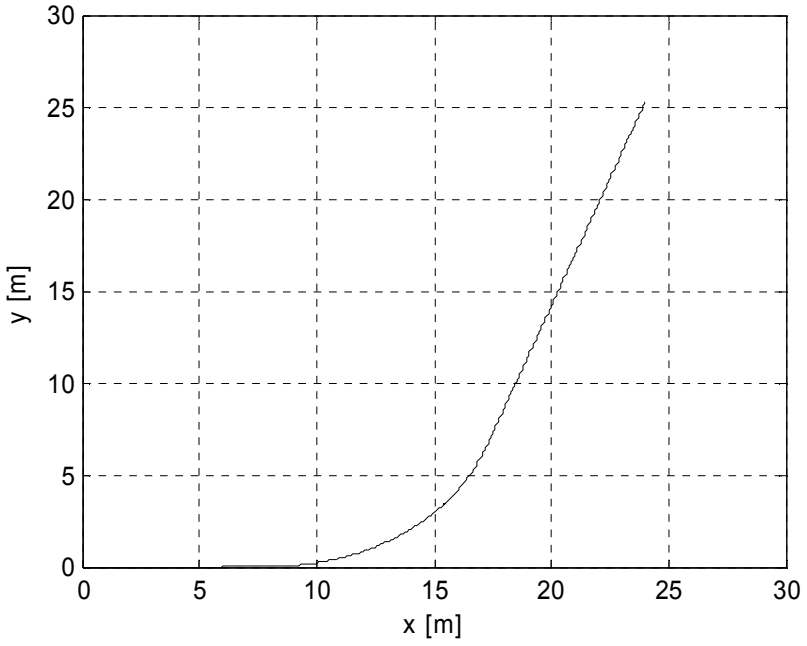

Figure 3.15 – Vehicle trajectory of the steer torque calculation example

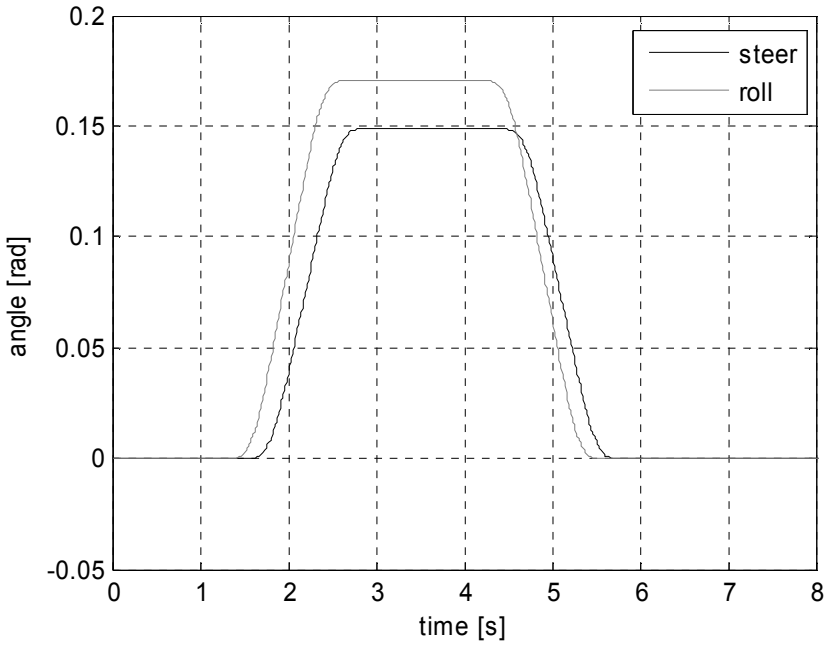

Figure 3.16 – Steer and roll angles of the steer torque calculation example

With these dynamic variables known, the steering torque for the manoeuvre was estimated. The estimations from equations (3.15) and (3.17) by Robinson and Fajans respectively were different from the estimation from equation (3.18) by Sharp, which was more thorough. In reality, the driver would expect to apply a disaligning torque at the start of the manoeuvre. During the steady state portion of the turn, the driver would still apply a disaligning moment due to the self-righting nature of the steering assembly. It may appear surprising that the driver would continue to apply a disaligning moment when exiting the turn. However, this is could be the case when the driver intends to limit the speed at which the wheel straightens. For this reason, the definition of steer torque by Sharp [103] was thought be the most appropriate for estimating the order of magnitude of this driver input.

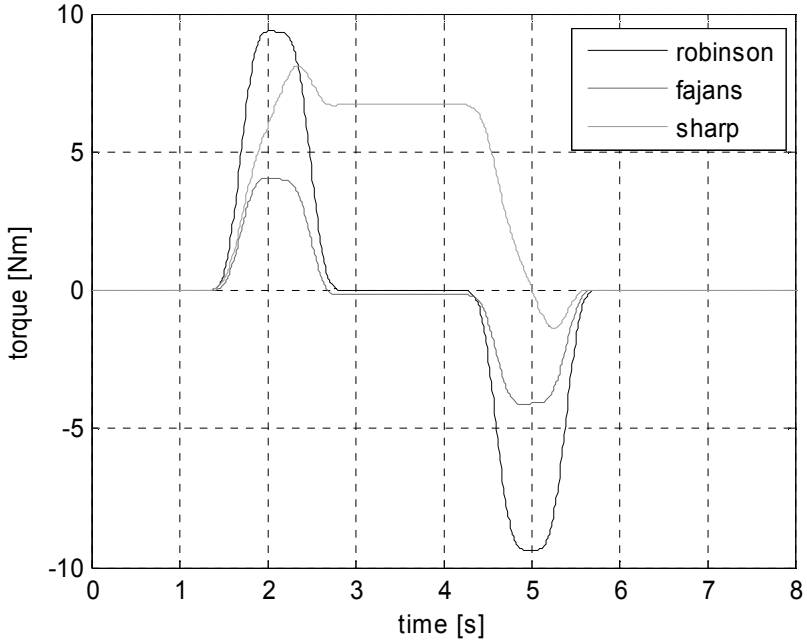

Figure 3.17 – Steer torque calculation example: driver steer torque according to Robinson [50], Fajans [27], and Sharp [51]

3.6 SIDE WIND

Crosswinds can have significant effects on the roll and directional stability of a vehicle [104-106], in particular a tilting vehicle. Whether the crosswind is a constant force, or whether there are gusts at unpredictable time intervals, the driver will have to make adjustments to the steering to ensure the vehicle does not roll over and stays on course. This is discussed in the following section.

3.6.1 Centre of Pressure

The centre of gravity of an object is the point where the mass is evenly distributed from that particular point. In other words, for any axis going through this point, the mass is equally distributed on either side of the axis. Similarly, the centre of pressure represents the point where the pressure acting on the object is equally distributed. The location of the centre of pressure is more difficult to determine than the centre of gravity, because it not only depends on the object's geometry, but also on the direction of the flow.

In case of a stationary vehicle experiencing crosswinds, it can be assumed that the wind pressure is equally distributed across the side of the vehicle and that the cross-sectional area of the vehicle is more or less a block in the path of the flow. The centre of pressure under these conditions is the point where the area of the vehicle is equally distributed. To find this point, an equation

similar to the equation to determine the centre of gravity can be used as shown in see equation (3.21). In this equation A_i is the area of an element i and x_i is the distance of the centre of that element from the reference frame.

$$\frac{\sum A_i x_i^2}{\sum A_i x_i} \tag{3.21}$$

The above equation assumes that the vehicle is stationary. Whilst stationary, crosswinds can roll a parked vehicle, but they are the most dangerous when travelling at speed. In this case, the aerodynamic drag is dependent on the vehicle velocity and the wind velocity as suggested by Iniguez-de-la-Torre and Iniguez [107, 108]. Now the vector angle of the two air speeds is the angle at which the drag force acts on the vehicle as shown in Figure 3.18.

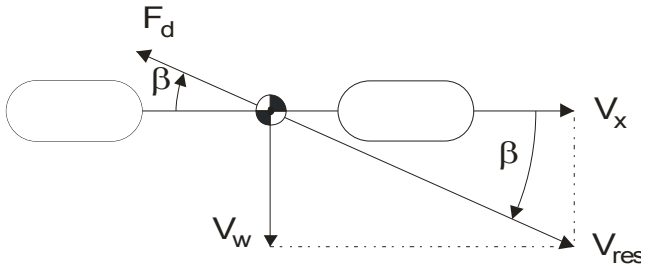

Figure 3.18 – Schematic showing how the forward velocity and the wind velocity cause an aerodynamic drag force at an incidence angle equal to the vector angle between the two velocities

Now the aerodynamic drag force acts at an angle in comparison to the longitudinal axis, the area exposed to the air flow has changed, and with it the centre of pressure location. As an example, the exposed area according to the incidence angle for four geometric objects is given in Table 3.2. For all four objects, the exposed area with the angle of incidence increases to a maximum area at around 45 degrees of angle of incidence, except for the rectangular prism, which peaks at around 25.

β [o]	0	10	20	30	40	50	60	70	80	90
Cube [m^2]	0.25	0.29	0.32	0.34	0.35	0.35	0.34	0.32	0.29	0.25
Rectangular Prism [m^2]	0.75	0.80	0.83	0.84	0.82	0.77	0.70	0.61	0.50	0.38
Cylinder [m]	0.20	0.24	0.27	0.30	0.31	0.32	0.31	0.30	0.28	0.25
Triangular Prism [m^2]	0.38	0.48	0.56	0.61	0.63	0.62	0.58	0.52	0.44	0.38

Table 3.2 – Exposed area of various geometric shapes (bxhxd): 0.5x0.5x0.5 cube, 1.0x0.75x0.5 rectangular prism, 0.5x0.5x1.0 cylinder, and 1.0x0.75x0.5 triangular prism

A Matlab program was written to estimate the location of this centre of area to emulate the centre of pressure. The program calculated the sum from equation (3.21) for the elements making up the side view of the Honda Gyro with driver as shown in Figure 3.19 and Figure 3.20.

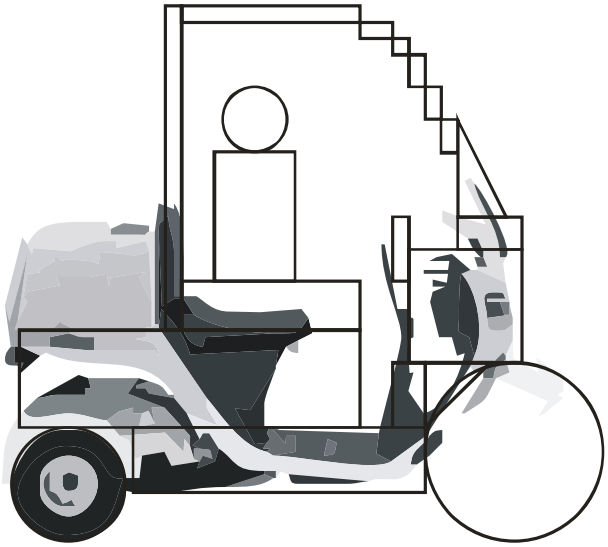

Figure 3.19 – Sketch of the simple geometric elements making up the side view of the Honda Gyro with driver

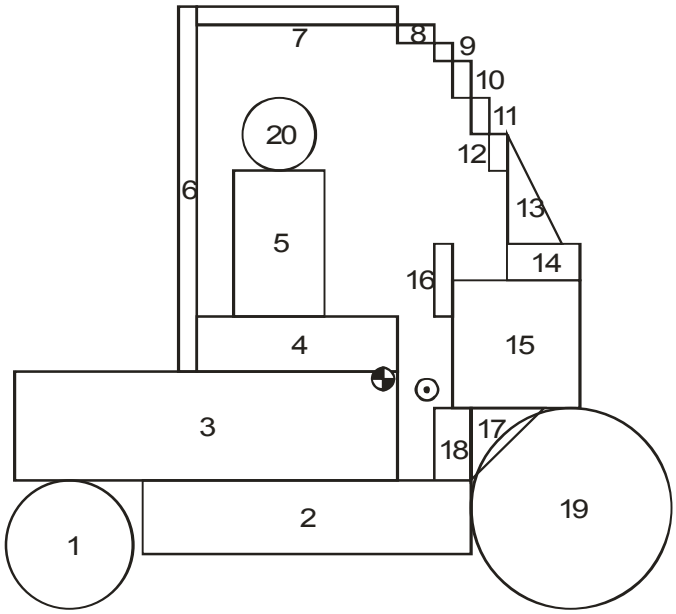

Figure 3.20 – Sketch of the elements making up the side view of the Honda Gyro with driver showing the locations of the centre of mass and the centre of pressure

For this side view, the location of the centre of area is estimated just above the top left corner of element 18 as shown in Figure 3.20. It can also be seen that this centre of area lies in front of and

below the centre of gravity. Overall, a gust of crosswind can have a significant disturbance effect on the vehicle dynamics. In chapter 7, a crosswind will be added to a vehicle simulation with roll controller to determine how the controller reacts to this external disturbance.

3.6.2 Forces and Moments

3.6.2.1 Roll

Whether the crosswind is constant or in the form of gusts, the force from the wind velocity will cause a roll moment. If the wind comes from the right, the vehicle will roll away from the wind direction, to the left. The magnitude of the roll moment is proportional to the height of the centre of pressure, which is where the wind force will act on the vehicle body.

If the crosswind is constant, the best way to balance the vehicle is to lean into the wind direction so that the roll moment from the wind force and the roll moment of the centre of gravity balance one another out. Figure 3.21 illustrates how the location of the centre of pressure h_{CoP} affects the roll angle necessary to balance the wind force. When the centres of pressure h_{CoP} and gravity h_{CoG} are in the same location, the forces perpendicular to the vehicle from the weight mg and the wind force F_W are equal and opposite. The balanced roll angle φ can be described by equation (3.22). From this equation, it can be deduced that for a constant wind force, the balanced roll angle increases when the centre of pressure lies above the centre of gravity. Similarly, when the centre of pressure lies below the centre of gravity, the balanced roll angle is smaller compared to the case where the centres are in the same location.

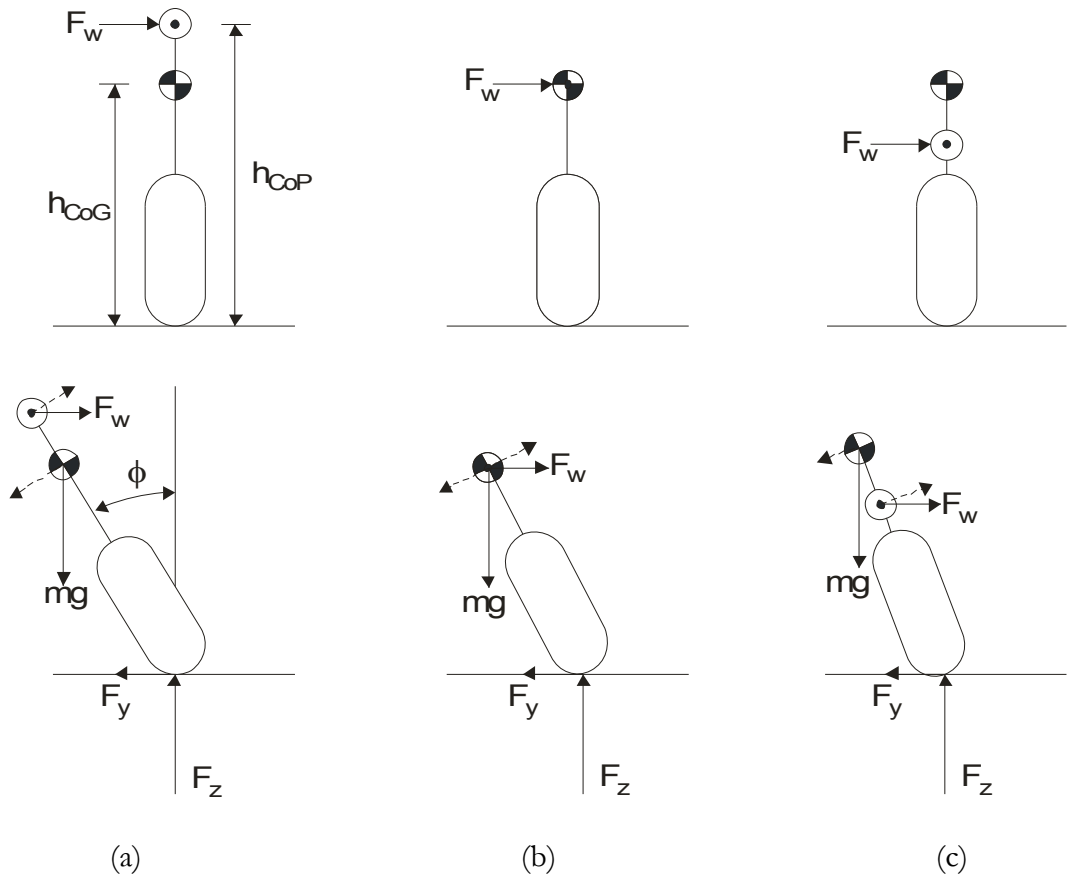

Figure 3.21 – Schematic showing the balance between the wind force and the centre of gravity offset for three cases: (a) the centre of pressure lies above the centre of gravity (b) the centre of pressure and the centre of gravity are at the same height (c) the centre of pressure lies below the centre of gravity

$$\tan(\phi) = \frac{h_{\mathrm{CoP}} F_{\mathrm{w}}}{h_{\mathrm{CoG}} m g} \tag{3.22}$$

For the case where there is a constant wind force, and assuming the driver manages to roll the vehicle to the balanced angle, the vehicle is not yet at steady state. When the vehicle is rolled, the camber angle between the front wheel and the road will result in a side force causing the vehicle to straighten up. Also, for a three-wheeled tilting vehicle, the rear wheels will steer as the vehicle rolls, adding to the total side force attempting to straighten the vehicle. The driver will have to compensate for the camber and rear steer side force by steering away from the wind direction. Overall, this situation will be difficult to control for a driver. To be able to handle a constant side wind, a steer tilt control system will have to include a sensor system that can detect the roll moment and a control algorithm which can adjust the steering to counteract the roll moment without veering off course.

In case the wind is not constant and comes in gusts, the driver cannot anticipate and cannot roll into the wind direction. However, as the gust causes a roll moment, the resulting camber will tend to straighten the vehicle back up. Nevertheless, steering adjustment from the driver may be necessary to ensure that the vehicle indeed straightens up and to get back onto the intended trajectory. If the roll is controlled by a steer controller, it will sense the roll caused by the wind force and steer the vehicle to straighten back up. It will not adjust for any path deviations and it will rely on the driver to make steering adjustments to return to the trajectory.

3.6.2.2 Yaw

Figure 3.22 shows how the wind force can cause a yaw moment depending on the longitudinal location of the centre of pressure in relation to the location of the centre of gravity. As the crosswind applies a force causing a lateral acceleration away from the wind direction, it appears that it would be preferable to have the centre of pressure located behind the centre of gravity so that the yaw moment from the wind force causes the vehicle to move back onto its trajectory. In the case of a tilting vehicle, this may not necessarily be preferable: a yaw moment away from the wind direction result in a roll moment causing the vehicle to straighten up again. Regardless of the location of the centres of pressure and gravity, the driver will have to make the steering adjustments to compensate for trajectory errors.

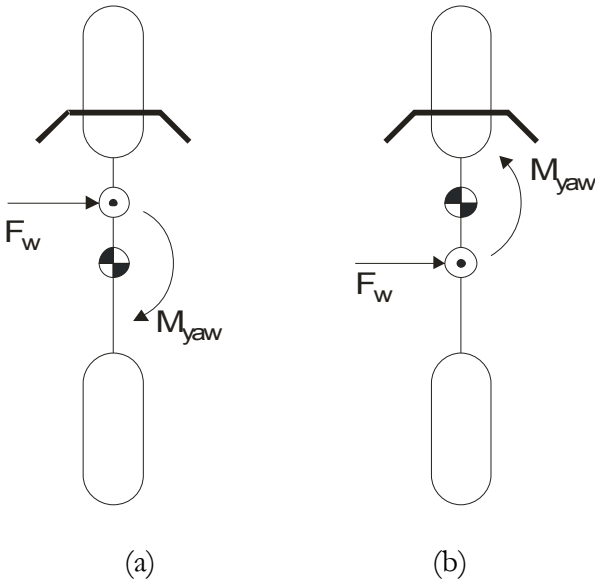

Figure 3.22 – Schematic illustrating the potential yaw effect from a wind force depending on the longitudinal distance between the centre of pressure and the centre of gravity: (a) the centre of pressure lies in front of the centre of gravity (b) the centre of pressure lies behind the centre of gravity

3.6.2.3 Steer

In the previous sections it was shown how the centre of pressure location affected the vehicle roll and yaw moments. This section will show that the location of the centre of pressure of the steer assembly and the wind force also have an effect on the steering. Figure 3.23 presents a schematic top and a side view of the steering assembly with the centre of pressure either in front of or behind the steering axis. If the centre of pressure lies in front of the steering axis, the wind force will result in a steering moment away from the wind direction. This steer will cause a roll moment opposing the roll from the wind force and negate the amount of steering adjustment necessary. In the unlikely event that the centre of pressure lies exactly on the steering axis, the wind force will not cause a steering moment. If the centre of pressure lies behind the steering axis, the wind force will steer the front wheel into the direction of the wind, which will increase the roll moment already cause by the wind force. The latter situation will make it more difficult for the driver to recover from a gust of wind.

In reality, the area of the wheel will be the largest area on which the wind pressure acts so the centre of pressure is likely to lie near the wheel axle. Also, the steering axis is likely to lie behind the wheel axis, so on most vehicles, the centre of pressure of the steering assembly is likely to lie in front of the steering axis, in the preferable location in terms of side wind resistance. The next section will discuss the centre of pressure location in further detail.

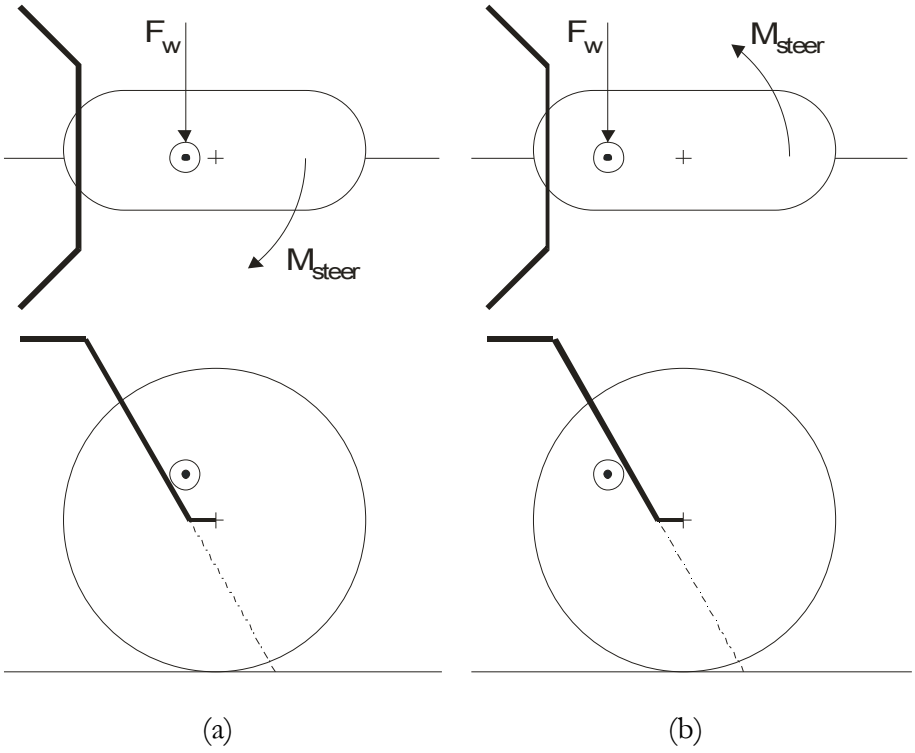

Figure 3.23 – Schematic illustrating the potential steering moment from a wind force depending on the longitudinal distance between the centre of pressure and the steering axis: (a) the centre of pressure lies in front of the steering axis (b) the centre of pressure lies behind the steering axis

3.7 HILL DRIVING

When driving uphill or downhill it would be expected that the dynamics of a vehicle would change. The cause of this change would be the difference in the direction of the normal or reaction forces on the wheels. To determine the overall change, first the equilibrium forces for rectilinear motion when driving on a flat surface were investigated as shown in Figure 3.24 (source: Cossalter [46]).

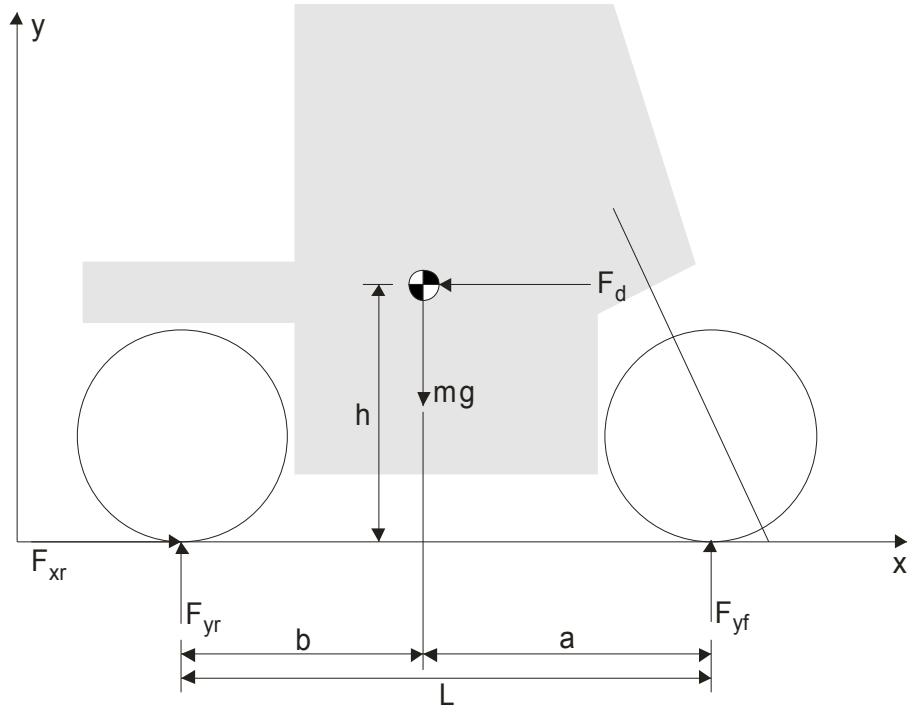

Figure 3.24 – Schematic diagram illustrating the horizontal and vertical forces on a straight running vehicle

Horizontally the driving force and the drag force were equated to zero: equation (3.23). Vertically, the weight was equated to the normal reaction on the front and the rear: equation (3.24). Then the moments about the centre of gravity were the equated to zero: equation (3.25). These moments came from the driving force, the rear normal reaction, and the front normal reaction. From these equilibrium equations, the static vertical loads can be determined: equation (3.26).

$$F_{x_r} - F_d = 0 \tag{3.23}$$

$$F_{z_r} + F_{z_f} - mg = 0 \tag{3.24}$$

$$hF_{x_r} - bF_{z_r} + aF_{z_f} = 0 \tag{3.25}$$

$$F_{z_r} = \frac{amg}{L}$$
$$F_{z_f} = \frac{bmg}{L} \tag{3.26}$$

The dynamic normal loads were also derived from these equilibrium equations. The loads consisted of one term related to the weight distribution and one term related to the load transfer due to accelerating and braking: equation (3.27). When accelerating, load is transferred from the front wheel to the rear, and when braking, load is transferred from the rear to the front. The rear wheel is the driving wheel, so when accelerating, the longitudinal force mainly originates from the rear. However, when braking, both the front and rear wheels are braked, so the longitudinal forces originates from both, hence the brackets in equation (3.27). The tyre side forces are dependent on the normal forces on the wheels. If there is an increased normal force on the rear due to load transfer, the side force from the rear increases. Similarly, if there is a load transfer to the front, the side force from the front wheel increases. To put this into context, when braking, there is a load transfer to the front, so the steering has greater effect.

$$\begin{aligned} F_{z_r} &= \frac{amg}{L} + \frac{hF_{x_r}(+hF_{x_f})}{L} \\ F_{z_f} &= \frac{bmg}{L} - \frac{hF_{x_r}(+hF_{x_f})}{L} \end{aligned} \tag{3.27}$$

When driving up or downhill, there will also be a load transfer between the front and rear wheels and a consequent change in steering effect. The equilibrium equation (3.24) now becomes (3.28). The dynamic loads have also been adjusted as seen in equation (3.29).

$$F_{z_r} + F_{z_f} - mg\cos(slope) = 0 \tag{3.28}$$

$$\begin{aligned} F_{z_r} &= \frac{amg}{L}\cos(slope) + \frac{hF_{x_r}(+hF_{x_f})}{L} \\ F_{z_f} &= \frac{bmg}{L}\cos(slope) - \frac{hF_{x_r}(+hF_{x_f})}{L} \end{aligned} \tag{3.29}$$

$$F_{x_r} = mg\sin(slope) + F_D + F_{friction} \tag{3.30}$$

Figure 3.25 shows how the normal load on the wheels changes with the gradient of the hill. The load transfer is for a Honda Gyro equivalent vehicle going uphill with a large enough driving force so that the vehicle does not roll back down the hill. Equation (3.28) illustrates that the static normal force will decrease with the hill gradient. There will be a sinusoidal increase in the driving force F_{Xr} shown in equation (3.30). As the decrease in the static normal force and the increase in

the moment from the driving force are non linear, the sum of the dynamic normal forces is not constant. The normal force on the front tyre decreases more than the normal force on the rear tyre increases. These differences will be greater if the vehicle is accelerating up the hill. In terms of the effects on the vehicle dynamics, the front wheel will have to be steered more to produce the same lateral force as it would on a flat road. The rear wheels will produce greater lateral forces for the same slip angle compared to a flat road.

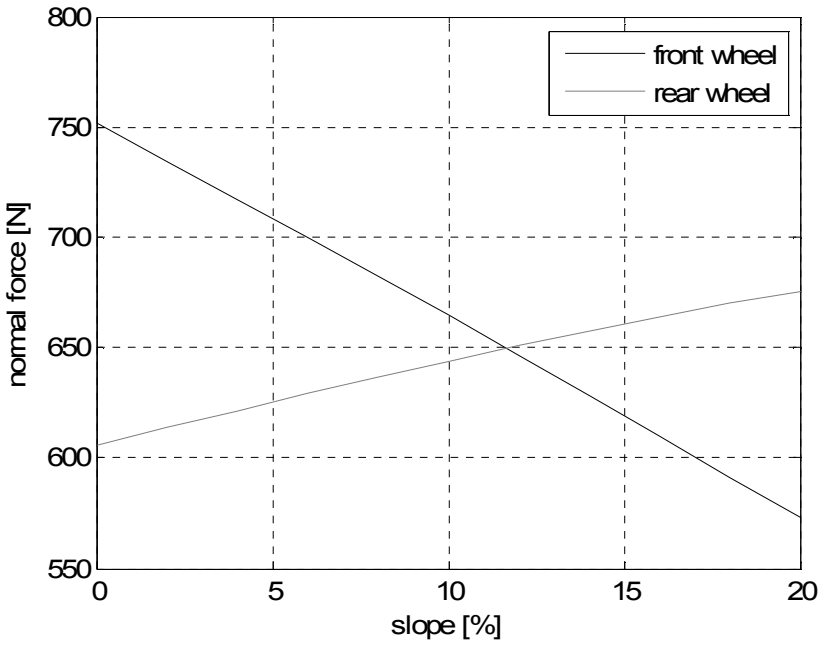

Figure 3.25 – Change in normal force on the front wheel and one of the rear wheels for a Honda Gyro equivalent vehicle on an uphill slope, acceleration just enough so that the vehicle does not roll back down the hill.

When going downhill, a vehicle would generally be allowed to roll down a hill with only a small amount of braking force to limit the velocity. Figure 3.26 shows the change in normal load on the front and the rear wheels when the vehicle is free to roll down the hill. In this case, the load of both wheels decreases as the gradient of the hill increases. The change is directly related to the cosine terms seen in equation (3.29). Under normal driving circumstances, it would be expected that the load transfer between front and rear wheels is smaller for a vehicle going down a hill than a vehicle going driving uphill. As a result, the lateral forces that can be generated at the tyres do not change as much with the gradient of the hill.

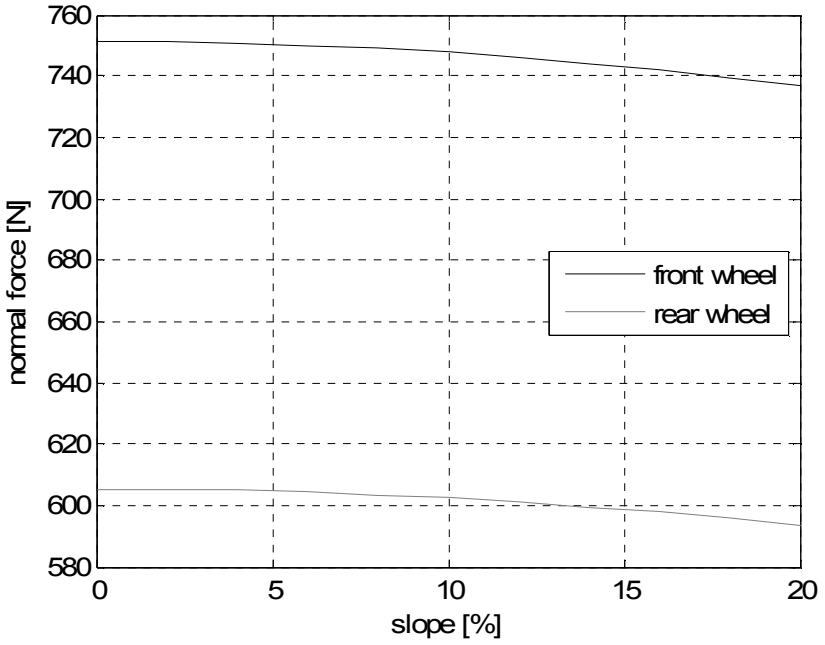

Figure 3.26 – Change in normal force on the front wheel and one of the rear wheels for a Honda Gyro equivalent vehicle on a downhill slope where the vehicle is free to roll down the hill, i.e. no braking

3.8 ROAD CAMBER

Roads are often constructed with a certain degree of curvature to aid drainage. Four-wheeled vehicles such as cars are not greatly affected by this lateral gradient on the road, but the dynamics of tilting three-wheelers and cycles can be affected by this road feature [109, 110]. Figure 3.27 shows a car, a four-wheeler, and a narrow tilting vehicle on a cambered road. Note that this is not a banked corner, such as motorway entry or exit slip road, but a straight road built so that rainwater drains easily to either side. A car driver will notice some change in the steering torque feedback, but the road profile will not cause a stability problem. Driving in a straight line along this type of road is somewhat more difficult for a tilting three-wheeler or cycle rider: to remain upright, as would be desired when driving in a straight line, requires the tilting part of the vehicle to be at a cambered position in relation to the road as shown in Figure 3.28. The relative camber angle will generate a side force, and the relative roll between the tilting unit and the rear unit will cause a slip angle at the rear wheels, which will also generate a side force. Without any intervention from the driver, the vehicle will accelerate towards the centre of the road and the rolling part will tend to rollover towards the gutter.

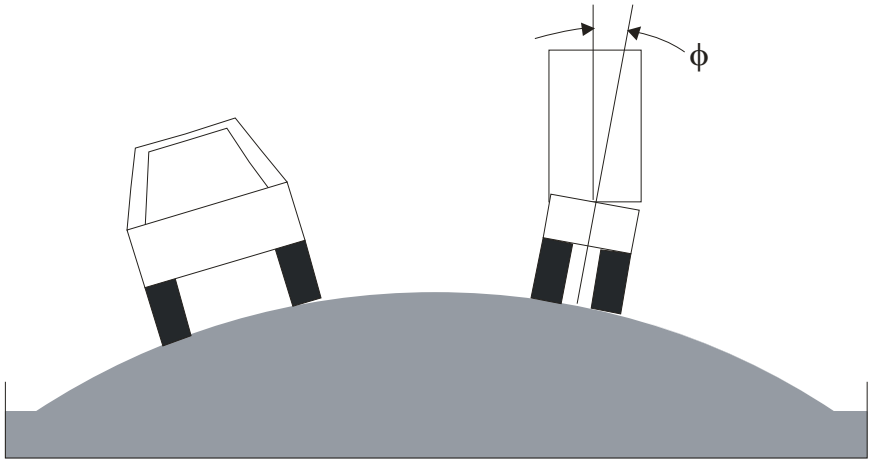

Figure 3.27 – Illustration of a car, a four-wheeler, and a tilting three-wheeler on a cambered road

Figure 3.28 illustrates how the front wheel of a tilting vehicle is rolled in relation to the road surface. To compensate for the lateral forces from the camber as well as the rear slip, the driver will have to steer towards the gutter in order to remain upright. The lateral force generated by the front steer slip angle will balance the lateral force generated by the camber angle and the rear wheel slip. Table 3.3 shows estimated values of the steer angle necessary to ensure a rectilinear path for a range of road camber gradients assuming that the lateral road-tyre friction coefficient is large enough to prevent the vehicle sliding [111].

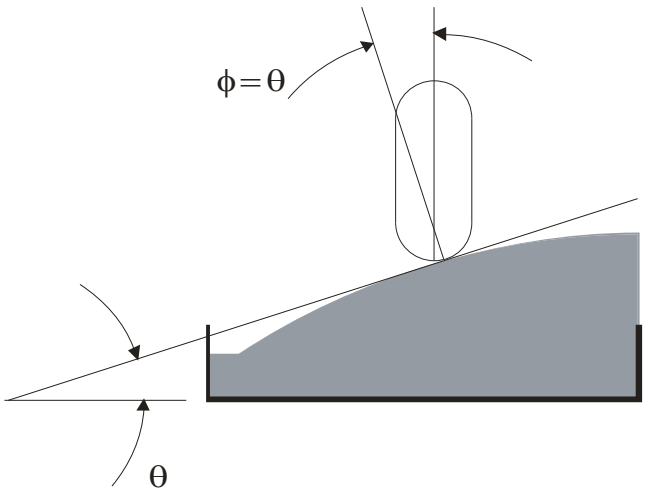

Figure 3.28 – Illustration of the front wheel of a tilting vehicle relative to the cambered road surface

camber θ [o]	0.0	5.0	10	15	20	25	30	35	40	45
corrective steer angle δ_f [o]	0.00	-2.10	-4.20	-6.30	-8.30	-10.3	-12.2	-14.1	-15.9	-17.6

Table 3.3 – Estimation of steady state corrective steer for various road camber gradients assuming a simple vehicle model as given by equations (2.5) and (2.6)

Although the lateral forces are balanced by steering towards the gutter, the yaw moment is doubled. In reality, a driver will have to constantly adjust the steering to balance the lateral forces and the yaw and roll moments. This could pose a problem for an automatic roll controller.

3.9 CONCLUDING REMARKS

The kinematics of a tilting three-wheeled vehicle were investigated. Calculation examples of known kinematic equations showed notable steering angle, roll angle, and camber angle. New equations describing the unique kinematics of a three-wheeled vehicle with an inclined tilt axis were presented. The most important finding was the relative yaw between the tilting assembly and the rear unit.

Differences in mass between drivers were shown to have an important effect on the vehicle's inertia's since the driver's mass is a significant portion of the total mass. The mass and inertia study also demonstrated that as the vehicle rolled, the overall yaw inertia changed.

It was shown that the previously published definition of the perceived acceleration omitted various dynamics. Therefore a new, more inclusive, equation to calculate the this acceleration has been presented.

A study of the roll dynamics of the rear unit concluded that the radial stiffness of the tyre ensured that the roll of the rear unit is negligible unless the conditions for its rollover are reached.

Various equations to determine this torque were found in the literature. The states of an example manoeuvre were calculated and applied to these equations to find the definition that would represent the driver's actions most accurately. It was shown that the simplified equations removed too much transient information.

It was shown that a gust of caused a disturbance to the lateral, yaw, and roll dynamics of a tilting vehicle. The magnitude of the disturbances was dependent on the location of the centre of

pressure in relation to the centre of gravity and in relation to the roll axis. The location of the centre of pressure for the side profile of the Honda Gyro was estimated using the average area distribution. It was found to lie a small distance above and behind the front wheel. This location placed it in front of and below the estimated location of the centre of gravity.

Driving up or down a hill was shown to affect the vehicle's normal force distribution. The gradient of the hill played a minor role in the load transfer between the front and the rear. The longitudinal force to drive up a hill was found to be the major factor in the load transfer between the front and the rear.

A model was presented to simulate the effect of road camber on a tilting three-wheeled vehicle. As simple calculation example demonstrated that this type of road could make it difficult for an automatic roll controller to maintain the vehicle's stability without driving off the road.

CHAPTER 4. THE EXPERIMENTAL DYNAMICS OF A PASSIVE TILTING THREE-WHEELER

Chapter 3 has shown that the kinematics of a tilting three-wheeler are unique; particularly so when the vehicle is comprised of a tilting and a non-tilting part. The tilting section can be considered to be similar to a motorcycle, the non-tilting section is more similar to a narrow car. An experimental test program was developed to expand the understanding of the vehicle dynamics as well as the driver's actions to successfully complete manoeuvres. The following chapter starts with a description of the test vehicle and the measurement methods. Subsequently, the objectives, procedure and results of a number of different manoeuvres are discussed.

4.1 EXPERIMENTAL SET UP

4.1.1 Test Vehicle

The vehicle that was used for the tests was a Honda Gyro Canopy, see Figure 4.1. It is a 49cc moped with a tilting front assembly and a non-tilting rear part. The two rear wheels and the engine mounted just above the rear wheels form the non-tilting part, the rest of the vehicle rolls like a conventional moped. This vehicle is thought to typify a tilting three-wheeler with tilting and non tilting parts. The joint between the front and the rear parts of the vehicle is never locked whilst driving, so that the driver must constantly adjust the steering to ensure that the vehicle is balanced. The moped engine limited the maximum vehicle velocity to approximately 50 kph (or 13.89 m/s). Naturally, the manoeuvre velocity was less than 50 kph, as the driver slowed to a safe velocity to complete the task.

Figure 4.1 – Illustrations of the Honda Gyro test vehicle

4.1.2 Measurements

4.1.2.1 Handlebar Steer Angle

The Honda Gyro was equipped with a linear position transducer to measure the steer angle. This was the simplest method to determine the steer angle assuming that under normal driving conditions the steer angle would be small enough to linearize: $\cos(\theta) \approx 1$ and $\sin(\theta) \approx \theta$. A schematic of this system is shown in Figure 4.2. The equations relating the steer angle θ_1 to the extension of the transducer x are given in (4.1) and (4.2). For small steer angles and L twice as large as c, the angle θ_2 remains very small and the relationship between x and θ_1 is approximately proportional.

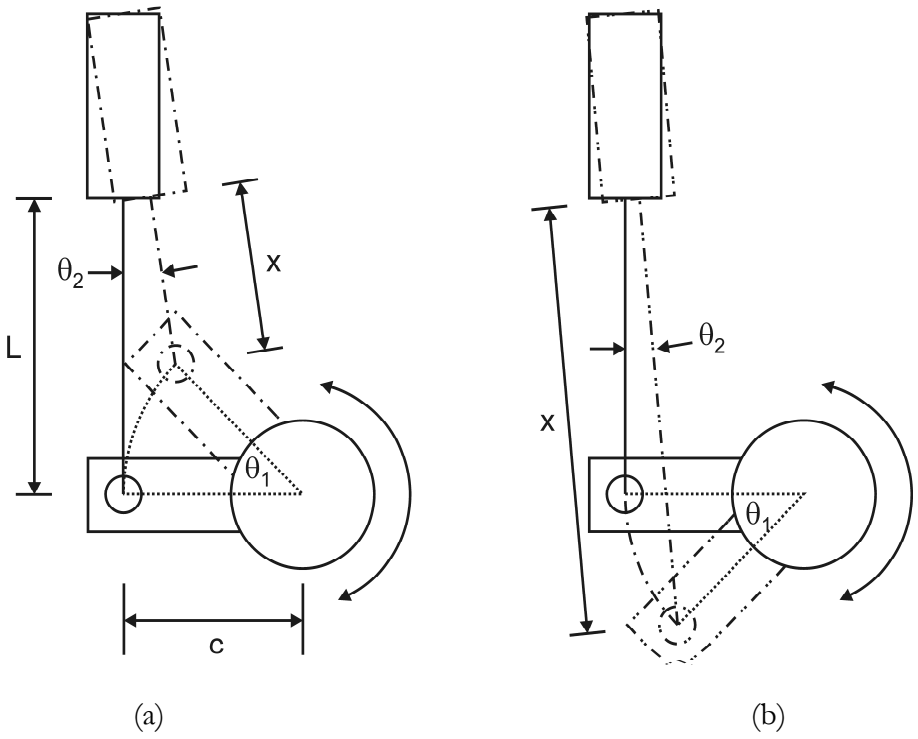

Figure 4.2 – Schematic of the linear steer angle measurement where the solid drawing represents the transducer and the steering column when not steered and the dotted line drawing represents the transducer and steering column when (a) steering right (b) steering left

$$\theta_2 = \tan^{-1}\left(\frac{c(1-\cos\theta_1)}{c\sin\theta_1 + L}\right) \tag{4.1}$$

$$x = \sqrt{(c\sin\theta_1 + L)^2 + (c - c\cos\theta_1)^2} \tag{4.2}$$

4.1.2.2 Tilt Angle

The tilt angle was measured using a rotary potentiometer mounted on the rear unit and connected to the tilting unit with a small belt drive. The rear unit was relatively light in comparison to the front and the wheels did not have individual suspension struts, therefore it was assumed that the roll of the rear was negligible and associated with the tyre compliance alone. The remaining measurements were derived from the data logger's in-built accelerometers and GPS system. The accelerometers were sampled at 100Hz and the GPS at 5Hz. From these measurements, the following variables could be derived: perceived acceleration, forward velocity, yaw angle and rate, and radius of turn.

4.1.3 Calibration

4.1.3.1 Steer Angle

The steer angle was calibrated by measuring the voltage for a range of extensions of the linear potentiometer. The relationship between the voltage and the potentiometer extension was assumed to be linear, so the slope and the offset from zero could be used as the calibration factors.

Steer Angle θ_1 [°]	-43.8	-35.5	-27.3	-19.0	-10.8	-2.51	0.00	14.0	22.2	38.7	47.0
Extension x [mm]	10	15	20	25	30	35	"0"	45	50	60	65
Voltage [V]	0.804	1.140	1.456	1.772	2.075	2.418	2.656	3.047	3.325	3.688	4.340

Table 4.1 – Calibration table for the linear potentiometer

4.1.3.2 Tilt Angle

To calibrate the rotary potentiometer that was used to measure the tilt angle, two different methods were tested. Using a compass, the stationary vehicle was tilted to a range of angles and the voltage from the potentiometer was noted. This method was too inaccurate, because it was too difficult to tilt to a precise tilt angle. The second method made use of an accelerometer mounted on the tilting part of the vehicle to determine the tilt angle. The stationary vehicle was

tilted in stages from upright to approximately 45 degrees. The measured acceleration corresponded to the tilt angle in proportion to $a_{measured} = g \sin(\varphi)$. The results of this calibration method are shown in Figure 4.3. The correlation between the voltage and the roll angle was shown to be approximately linear. The equation for a linear fit to the data of Figure 4.3 gives the calibration factors to determine the roll angle from a voltage.

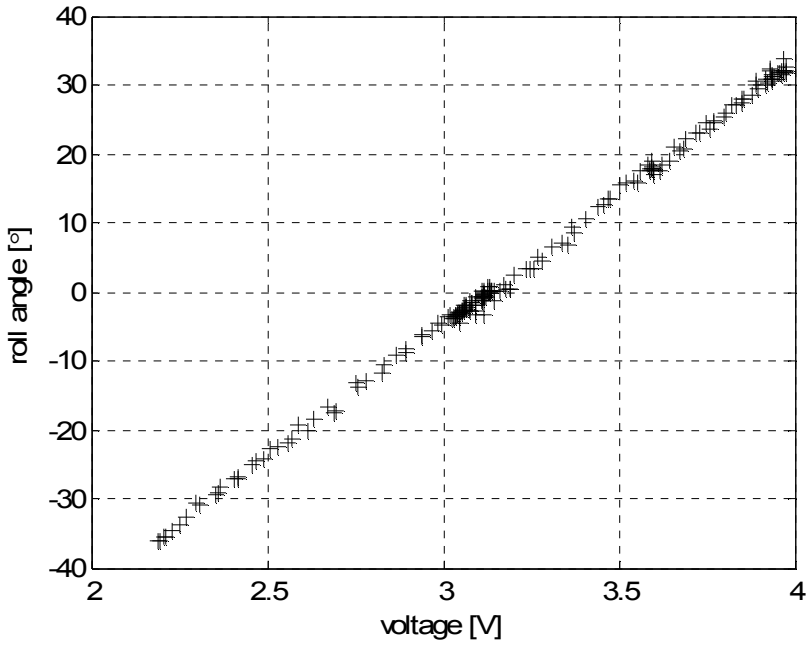

Figure 4.3 – Result of roll angle measurement calibration method using an accelerometer

4.1.4 Measurement and Estimation Errors

4.1.4.1 Heading Angle, Yaw Rate and Velocity

The data logger was equipped with a GPS receiver, and longitudinal and lateral accelerometers. The logger combined the GPS data with the acceleration signals to produce an X,Y-coordinate map, an estimate of the forward velocity, and an estimate of the heading angle and the yaw rate. The GPS positioning accuracy was known to be within 15 meters for the starting coordinate. However, once the initial position had been determined, the tracking accuracy was improved to approximately 3 meters. The GPS velocity measurement accuracy was estimated between 0.36 and 0.76 m/s. The heading angle accuracy was around 0.04 degrees during the manoeuvre. When comparing the GPS map of the track with a scaled satellite picture, the resemblance was excellent, see Figure 4.4. As a result, the variables derived from the GPS position coordinates were considered to be acceptable, these included the heading angle and the yaw rate, the longitudinal acceleration and velocity, and the lateral acceleration.

Accelerometer signals tend to suffer from electrical and vibration noise. Also, the GPS update frequency was fixed at 5Hz, which was not always fast enough to record acceleration changes. So to obtain the best possible result in acceleration measurement, the data logger combined the two measures.

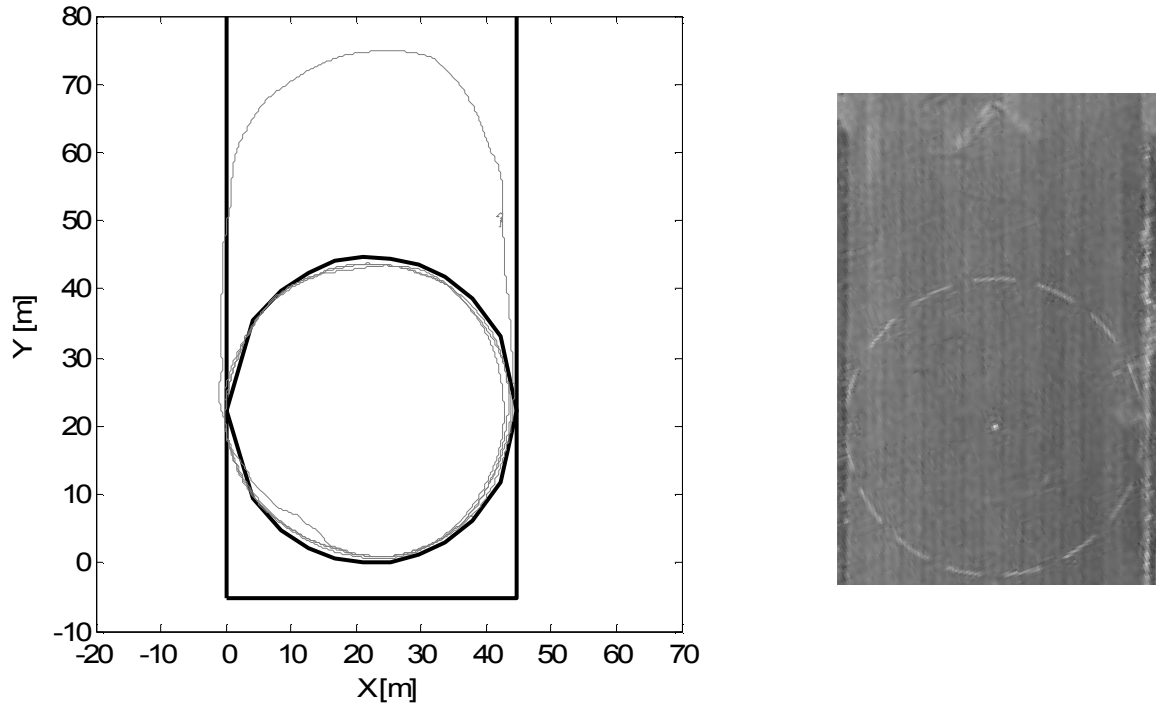

Figure 4.4 – (a) Plot of the x and y coordinates as measured by the GPS in light grey with thick black lines illustrating the tarmac region of the test track and the circle painted on the track (b) Aerial shot of the test area with the circle painted on the tarmac

4.1.5 Filtering

The engine of the vehicle and the road surface introduced noise into the measured signals. All the experimental data were therefore passed through a digital filter as part of the data processing. The ideal filter removes only what can be classified as noise and returns a perfect signal with every subtlety and detail of the measurement intact. In the context of a vehicle, it would be expected that the driver inputs and the subsequent dynamics occur at low frequencies, smaller than 5 Hertz. The engine was expected to add high frequency noise: electrical noise from the spark plug and small vibrations, both a result of the engine turning over at 5000+ rpm. Road noise was also expected to be of a much higher frequency than the driver inputs: greater than 100Hz (Kuijpers and Van Blokland [112]). Thus a low-pass filter was used for the transducer signals.

There are two main methods to realize a digital low-pass filter: Infinite Impulse Response (IIR) and Finite Impulse Response (FIR). The Matlab/Simulink Signal Processing Toolbox includes a Graphical User Interface (GUI) where a filter can be designed and analysed using a user-specified method. The Butterworth IIR filter was chosen on account of its properties (from Winder [113]): smooth frequency response, attenuation rises by n x -20 dB per decade) outside the pass band, depending on the filter order. The attenuation of a Butterworth filter is not as good as a Chebyshev filter of the same order, however the smooth response was found to be the more important filter feature.

The most important filter design decision was the cut-off frequency. This is defined as the frequency where the magnitude response of the filter is -3dB since this is the limit of the filter's bandwidth [42]. This frequency lies approximately halfway between the end of the pass band, the range of frequencies that are passed by the filter, and the start of the stop band, the range of frequencies the filter tries to remove from the signal. Figure 4.5 shows the unfiltered roll angle signal with the filter output signal for four 4th order filters with cut-off frequencies ranging from 2Hz to 16Hz. As would be expected, the lower the cut-off frequency, the smoother the filtered signal, with a loss of data as a result. It was thought that the 16Hz cut-off frequency filter, Figure 4.5 (d), did not remove enough noise and that the 4Hz cut-off frequency filter, Figure 4.5 (c), removed too much information. A cut-off frequency of 8Hz was thought to be acceptable, because frequency of the end of the pass band would lie at approximately 5.75Hz: greater than the driver input frequency.

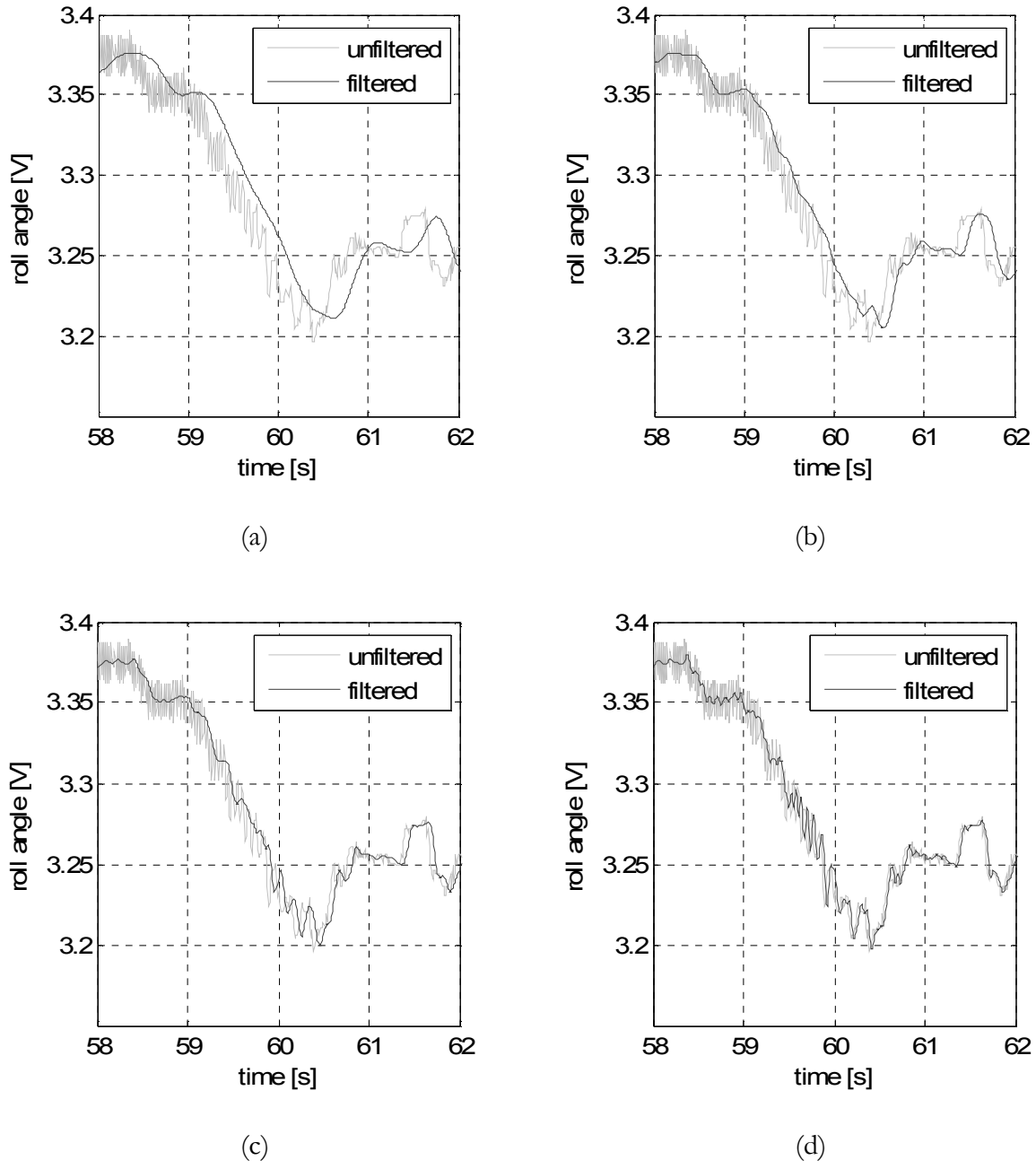

Figure 4.5 – Comparison of filtered roll angle signal of four 4th order with a range of cut-off frequencies (a) 2Hz (b) 4Hz (c) 8Hz (d) 16 Hz

The next important filter design decision is the filter order. The filter order will have an effect on the magnitude and phase response of the filtered signal. The phase shift of filters of different orders can be seen in Figure 4.6. This figure illustrates that a higher order filter introduces a larger phase shift in the filtered signal. This is not a major problem if all the data are filtered and therefore have more or less the same phase shift. More important are the variations in magnitude response. The differences between magnitude responses seen in Figure 4.6 are minimal. From an analysis point of view, the 2nd order filter had the smallest stop band magnitude, the magnitude

of the frequencies that the filter tries to remove, and the smallest step response overshoot settling time. Although these properties resulted in a smooth signal when the vehicle was in steady state, the 2nd order filter resulted in a less smooth signal under transient conditions and there was concern over data loss: some steering adjustments and resulting accelerations could be lost when using this filter. For these reasons, the 4th order filter was found to offer the best compromise in steady state and transient response.

As has been shown in the calculation examples, the filtering introduces a small phase lag; therefore, all the measurements should be passed through the same filter so that all the signals contain this lag.

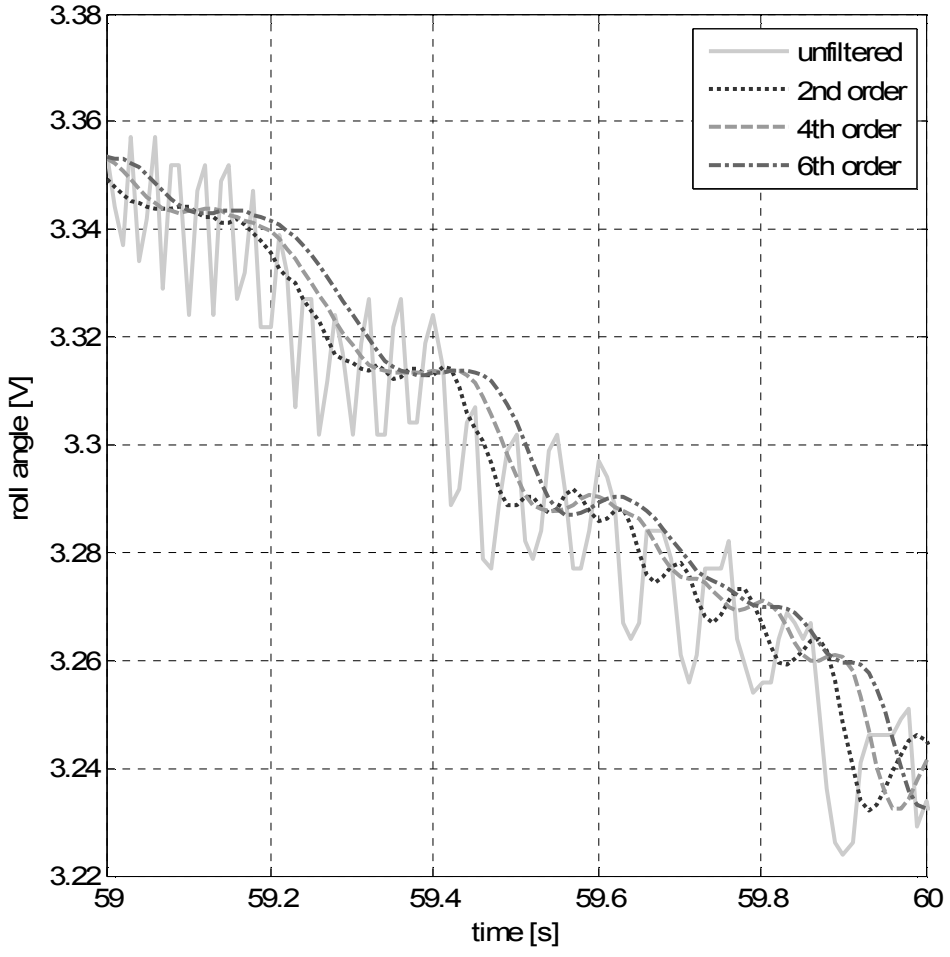

Figure 4.6 – Comparison of filtered roll angle signal of three 8Hz cut-off frequency filters or increasing orders

4.2 STEADY STATE MANOEUVRE

4.2.1 Objectives

The main aims of the steady state tests are set out in the section below. First, the relationship between the steer angle and the lateral acceleration was to be established. This relationship could be one of neutral steer, understeer or oversteer. As the vehicle leans when cornering, the relationship of the tilt angle with the lateral acceleration was also of interest. The objective was to determine whether the driver would lean at the balanced tilt angle for the vehicle speed and radius of turn. As it was very difficult for a driver to maintain a constant velocity as well as radius of turn, the test would not be completely steady state and the lean angle would require adjustment. The aim was to compare the perceived lateral acceleration, the steer angle, and the roll angle measurements to determine how the driver reacted to an imbalance: establish whether there would there be a minimum amount of perceived lateral acceleration after which the driver adjusts the steer angle, resulting in a change roll. Besides determining steering characteristics and driver leaning behaviour, the order of magnitude of the steady state steering torque was assessed using equation (2.18). The steering torque was expected to be small or zero, because at steady state there would not have been any major changes in the steering direction. Finally, the steady state tests were completed with various tilt axis inclination angles. The larger the inclination the greater the positive rear wheel steer angle as the vehicle leans. It was expected that the increase in rear wheel steer would result in a decrease in steer at the handle bars because of the increased side force from the rear wheels.

4.2.2 Procedure

The steady state test procedure was to drive around a constant radius circle at a speed that was as constant as possible. A circular path of approximately 22m was measured out, with a margin of 0.5m left and right. The drivers were instructed to keep a constant speed between 20kph (5.56m/s) and 25kph (6.94m/s). In order to establish the effect of the tilt axis inclination, the rear suspension strut between the front and the rear unit was replaced by a rigid link. The length of this link could be varied resulting in a tilt axis inclination angle between 10 and 16 degrees. During this procedure, driver 1 was mountain bike and motorcycle rider, driver 2 did not regularly ride a bicycle, and driver 3 was a regular bicycle rider.

4.2.3 Results

4.2.3.1 Steer Angle

Figure 4.7 shows the relationship between the lateral acceleration and the steer angle. The radius of turn was constant at 21m, so for neutral steer, the steer angle should have been constant and

corresponding to L/R ≈ 3.85 degrees. The results show that the larger the lateral acceleration, the larger the steer angle. This indicated that the vehicle understeered.

As was noted in the objectives, the driver found it difficult to maintain a constant velocity and steer angle and as a result, there were small path deviations. As can be seen in Figure 4.8, during a single turn around the track the radius of the path varied, yet the coordinates show that the overall path was still as close to a circle as could be expected from a human operator. Thus, the average radius of the path taken by the driver was constant, even though during the manoeuvre the radius varied. Consequently, the steering angle should, on average, be equal the steady state value if the vehicle is a neutral steering vehicle. Figure 4.9 shows the steer angle, total lateral acceleration and velocity of the vehicle for the path shown in Figure 4.8(a). The steer angle averages at around 8 degrees from 30 to 40 seconds, when the velocity is more or less constant. As the velocity changes during the period from 40 to 50 seconds, the steer angle is also adjusted resulting in notable changes in the total lateral acceleration. Although this manoeuvre was not completely steady state, the steer angle was significantly larger than the steer angle expected from a neutral steering vehicle, indicating that the vehicle indeed understeers.

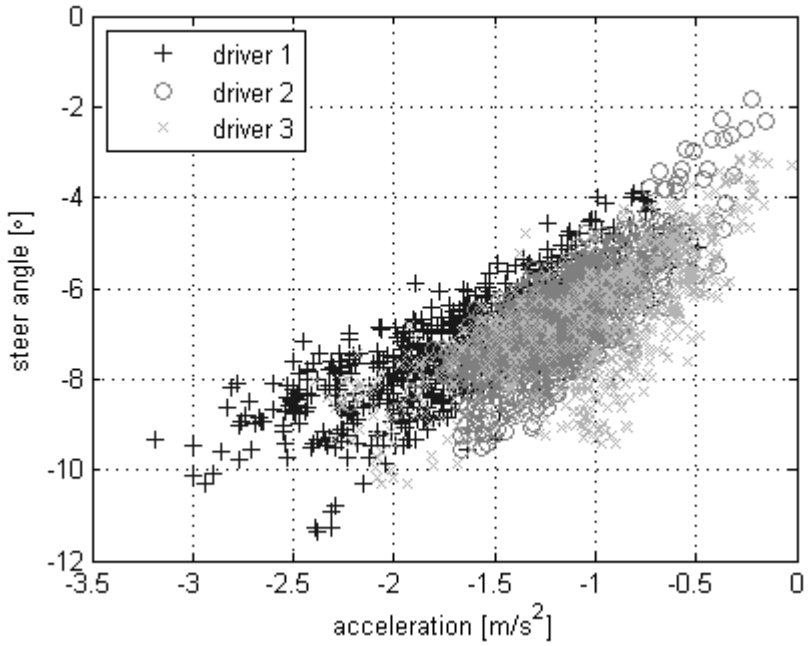

Figure 4.7 – Relationship between the total lateral acceleration and steer angle

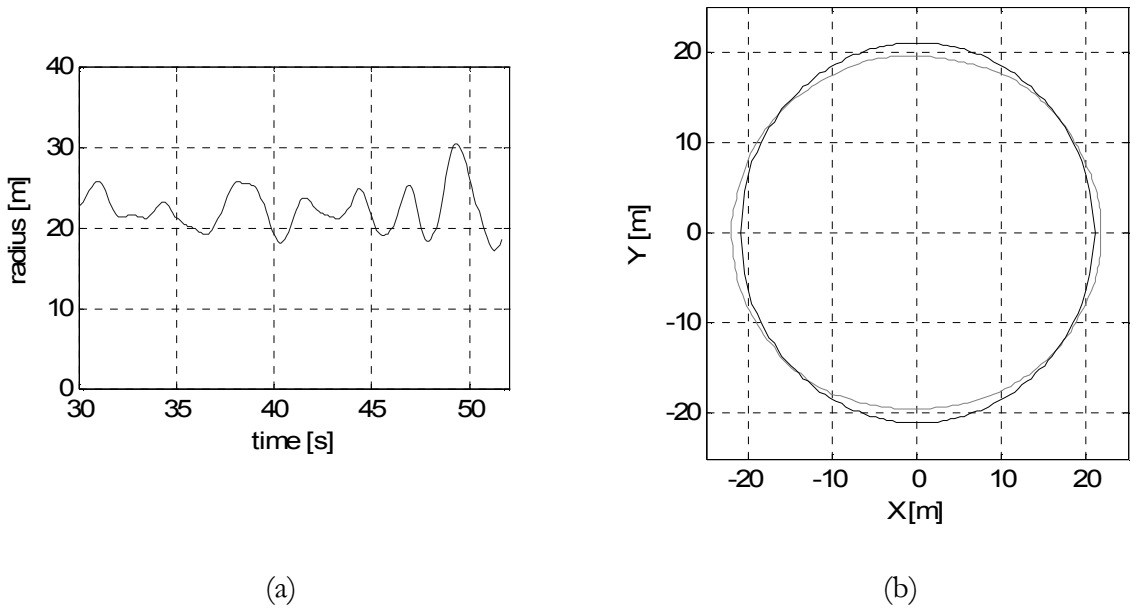

(a) (b)

Figure 4.8 – (a) Measured path radius (b) Path taken by the driver (light grey) in comparison with a 21m radius circle

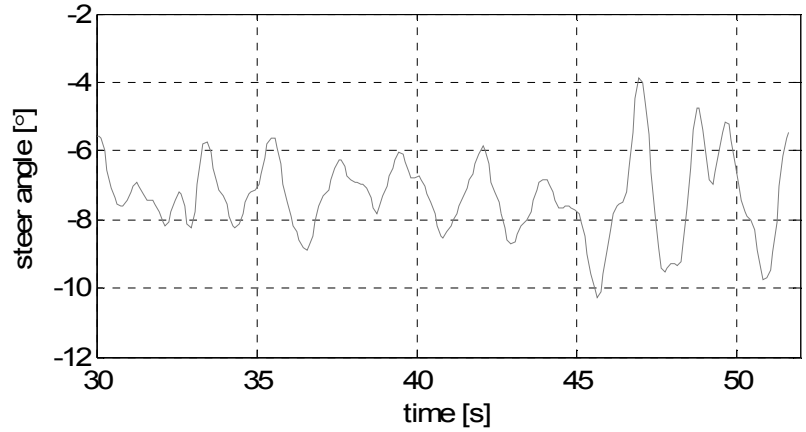

(a)

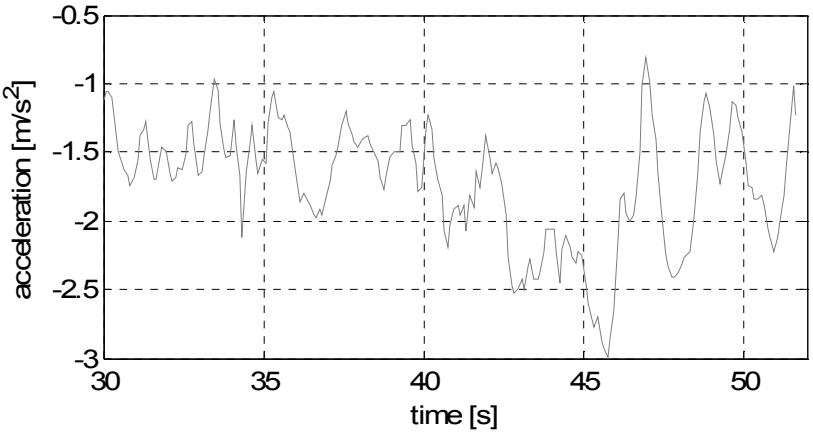

(b)

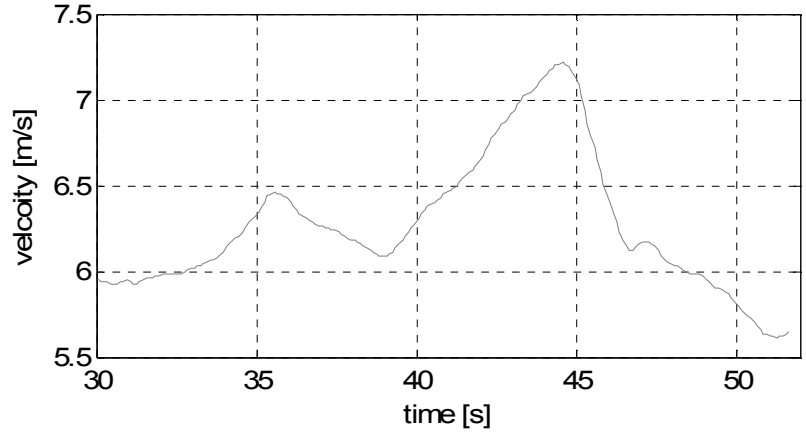

(c)

Figure 4.9 – (a) Steer angle progression with time for one single turn around the circular track (b) Total lateral acceleration (c) Forward velocity

Table 4.2 shows that the average steer angle throughout the 'steady state' manoeuvre varied between 7.2 and 9.6 degrees. On average, the driver applied a larger steer angle than would be expected from the path, again indicating understeer characteristics.

The table also shows that the average applied steer was larger when the tilt axis inclination angle was decreased. As was explained in chapter 3, when the vehicle rolls into a turn, the rear wheels also steer into the turn because of the inclination of the tilt axis. The amount of rear wheel steer for a given roll angle varies with the tilt axis inclination angle: the greater the inclination angle, the great the amount of steer. This additional steer increases the slip angle at the rear wheels and therefore the lateral tyre force at the rear wheels. The rear steer therefore increases the total lateral force and therefore lateral acceleration, but it can decrease the total yaw moment of the vehicle. The results presented in Table 4.2 indicate that the additional rear steer from an increased tilt axis inclination angle overall helps the vehicle turn under 'steady state' conditions and reduces the understeer characteristics.

Inclination angle [°]	15.9	14.8	13.6	12.4	11.2	10
driver 1	-6.61	-6.80	-7.03	-7.38	-8.36	-8.59
driver 2	-6.32	-6.59	-6.86	-7.31	-7.50	-8.11
driver 3	-6.64	-6.72	-7.19	-7.79	-7.94	-8.58

Table 4.2 – Average steer angle δ_f in degrees

It was noted that there were small differences in the average speed between the manoeuvres as shown in Table 4.3. However, when the average steer angles were adjusted to remove the effect of manoeuvre speed, see Table 4.4, the effect of the tilt axis inclination angle was still present.

Inclination angle [°]	15.9	14.8	13.6	12.4	11.2	10	mean
driver 1	7.0	6.2	6.2	6.3	7.2	7.1	6.7
driver 2	5.8	5.6	5.8	6.2	6.0	6.6	6.0
driver 3	6.5	5.8	6.5	6.8	6.5	6.9	6.5

Table 4.3 – Average forward velocity U in m/s

Inclination angle [°]	15.9	14.8	13.6	12.4	11.2	10	mean
driver 1	-5.69	-6.54	-6.78	-7.04	-6.95	-7.28	-6.71
driver 2	-6.55	-7.10	-7.15	-7.13	-7.52	-7.36	-7.13
driver 3	-6.12	-6.94	-6.68	-6.87	-7.29	-7.42	-6.89

Table 4.4 – Average steer angle δ_f in degrees normalised with speed

4.2.3.2 Tilt Angle

Theoretically, for a balanced vehicle, the tilt angle should increase with the lateral acceleration, therefore a correlation between the lateral acceleration and the steer angle should result in a correlation between the steer and the tilt angle. For small angles, this correlation will appear linear as can be seen in Figure 4.10. However, the relationship was not constant and it was dependent on the driver. Table 4.5 shows the variation in the average ratio between the steer angle and the tilt angle for various tilt axis inclination angles and drivers. The tilt axis inclination angle did not appear to affect the ratio, but it did seem to be driver dependent. This ratio between the steer and angle and the tilt angle could be interpreted as the driver gain.

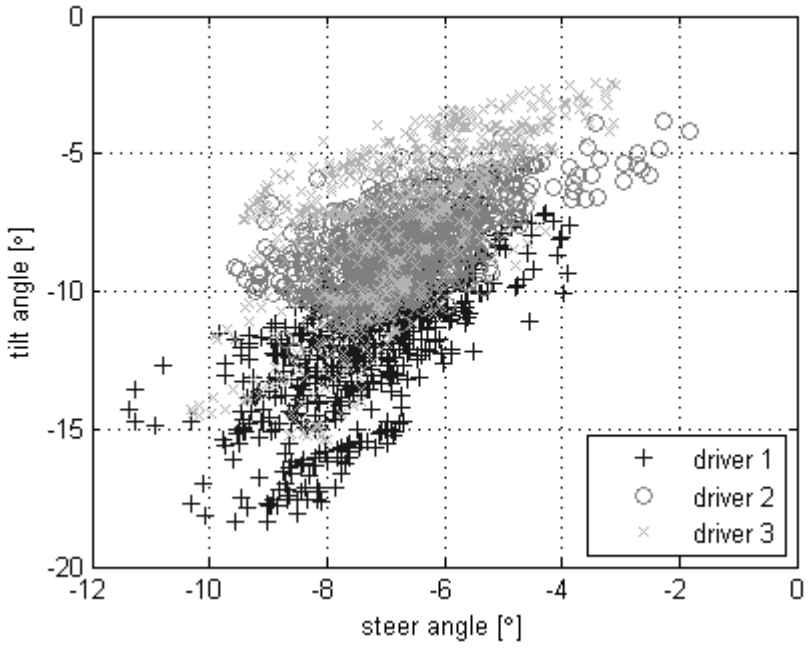

Figure 4.10 – Proportional relationship between steer angle and tilt angle

Inclination angle [°]	15.9	14.8	13.6	12.4	11.2	10	mean
driver 1	2.074	1.748	1.727	1.594	1.870	1.785	1.800
driver 2	1.420	1.748	1.559	1.627	1.484	1.642	1.580
driver 3	1.595	1.748	1.640	1.706	1.533	1.668	1.648

Table 4.5 – Calculated average ratio between δ_f and φ

It was found that the tilt angle was larger than the balanced tilt angle as seen in Figure 4.11. This implied that with respect to the total lateral acceleration, the vehicle was generally overleaning. This unexpected result could have been caused by various effects. The manoeuvre was not completely steady state: there were small variations in speed and steering. Additionally, the margins of error of both the acceleration and the tilt angle measurements would have to be

accounted for. However, these errors did not entirely explain the consistent overlean. The tilt angle measured was the effective tilt angle as shown in Figure 4.12 and quantified in equation (4.3) from Cossalter [46]. The difference between the balanced tilt angle based on the vector between the lateral acceleration and the gravitational acceleration and the effective tilt angle measured between the vertical and the motorcycle plane is illustrated in this figure. Table 4.6 shows that this difference is more than 10% for an average 75kg driver and could, together with the rear unit roll associated with the tyre compliance, account for the experimental differences.

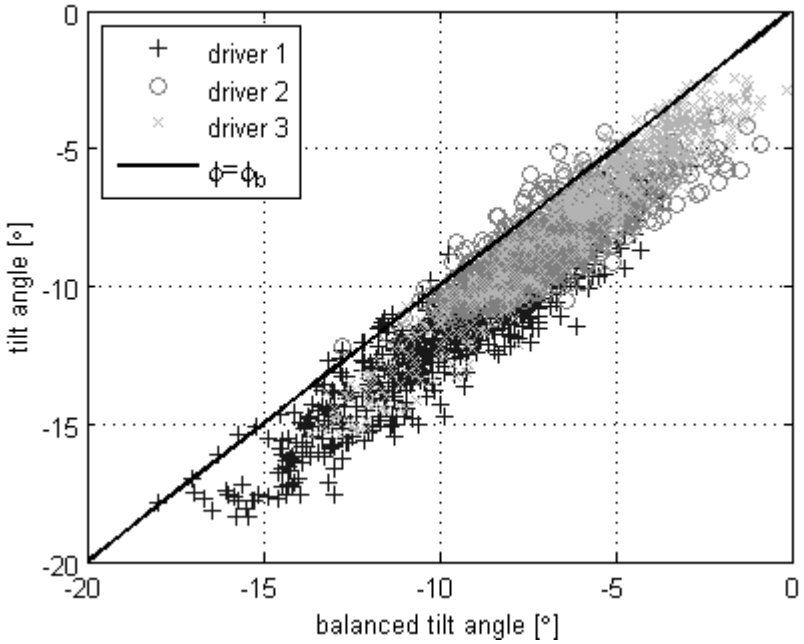

Figure 4.11 – Relationship between lateral acceleration and tilt angle

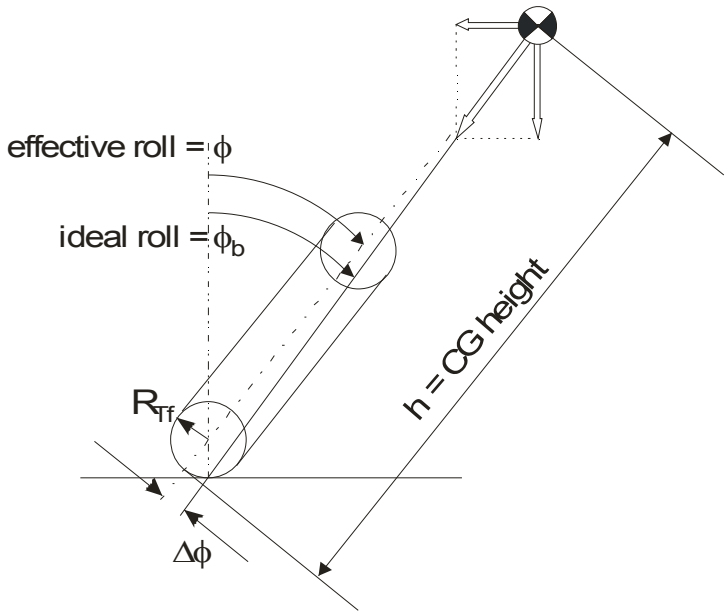

Figure 4.12 – Difference between the balanced roll angle and the effective roll angle

$$\phi = \phi_b + \Delta\phi = \tan^{-1}\left(\frac{v_x\dot{\psi}}{g}\right) + \sin^{-1}\left(\left\{\frac{R_{Tf}\sin\left[\tan^{-1}\left(\frac{v_x\dot{\psi}}{g}\right)\right]}{h - R_{Tf}}\right\}\right) \tag{4.3}$$

The effective tilt angle was derived from equation (4.3) and plotted against the measured tilt angle in Figure 4.13. The figure shows that, on average, the effective and the measured tilt angle were equal. This demonstrates that all three drivers managed to achieve 'balanced' lean during the steady state manoeuvre.

a_y [m/s2]	1.0	2.0	3.0	4.0	5.0	6.0	7.0	8.0
ϕ_b [°]	5.82	11.52	17.01	22.18	27.01	31.45	35.51	39.20
ϕ_e [°]	6.64	13.14	19.37	25.23	30.68	35.67	40.21	44.31
error [°]	0.82	1.62	2.36	3.05	3.67	4.22	4.70	5.11
error [%]	14.1	14.0	13.9	13.8	13.6	13.4	13.2	13.0

Table 4.6 – The difference between the balanced tilt angle and the effective tilt angle

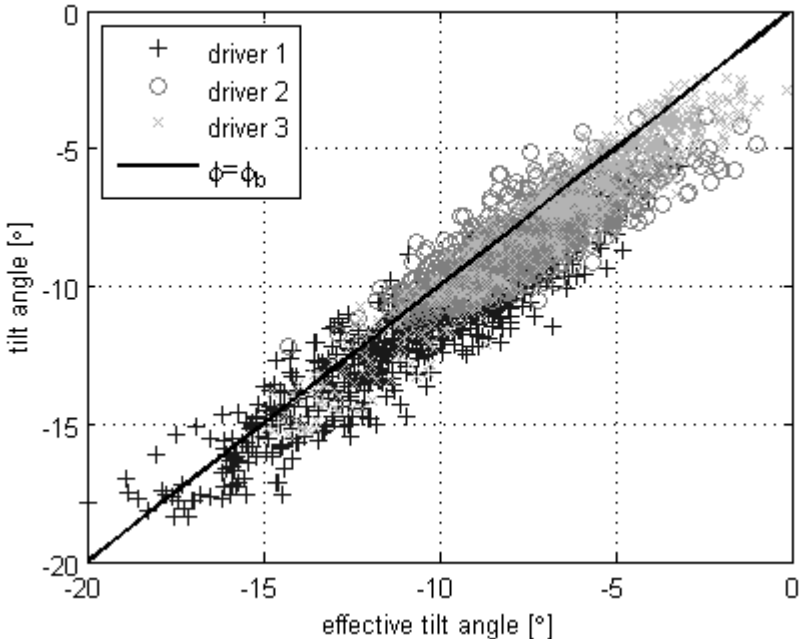

Figure 4.13 – Comparison of the effective tilt angle and the measured tilt angle

4.2.3.3 Lateral Acceleration

The total lateral acceleration of a vehicle with neutral steering characteristics under steady state conditions can be calculated from the steer angle and the velocity. This lateral acceleration estimate was compared to the measured lateral acceleration in Figure 4.14. This shows that the measured total lateral acceleration is proportional to the Ackerman steady state total lateral acceleration. However, the measured acceleration is approximately double the Ackerman estimate. This shows that the Ackerman lateral acceleration estimate does not apply to this vehicle. Nevertheless, the estimate can be used with an appropriate gain to predict the total lateral acceleration.

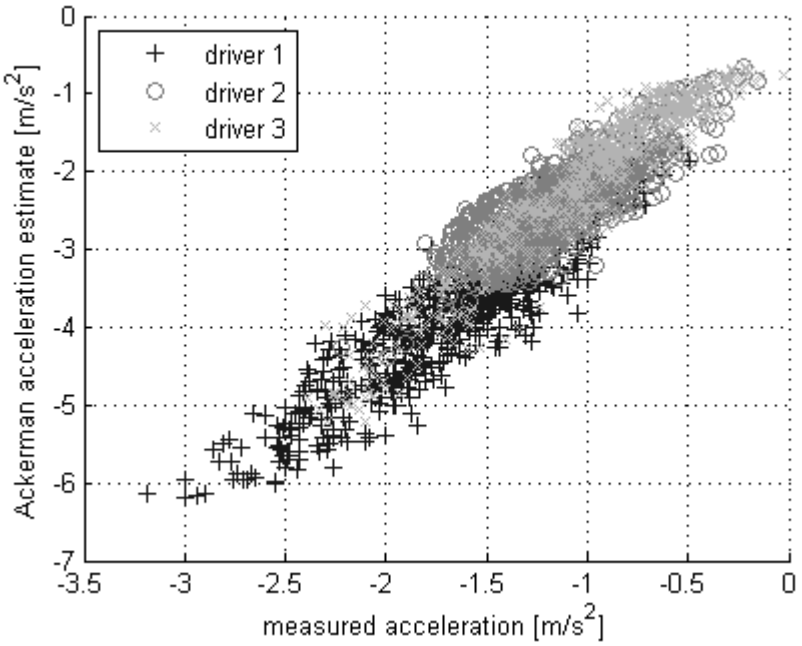

Figure 4.14 – Comparison of the measured lateral acceleration with the Ackermann acceleration $\delta_f V_x^2/L$

The total measured lateral acceleration consisted of the acceleration of the mass in the lateral plane plus the centripetal acceleration from the yaw rate. When driving around a constant radius circular track, only the centripetal component of the acceleration should be present, however Figure 4.15 illustrates that this was not the case during these experiments. In the discussion of the steer angle results, it was found that the average trajectory resulted in a circular path, but during the manoeuvre, the path radius varied. The driver completed the manoeuvre by constantly adjusting the steering to stay on the path. These adjustments resulted in variations in the side forces, thus changes in the measured lateral acceleration. This manoeuvre has shown that in practice, the driver approaches a 'steady state' manoeuvre as a succession of transient turns.

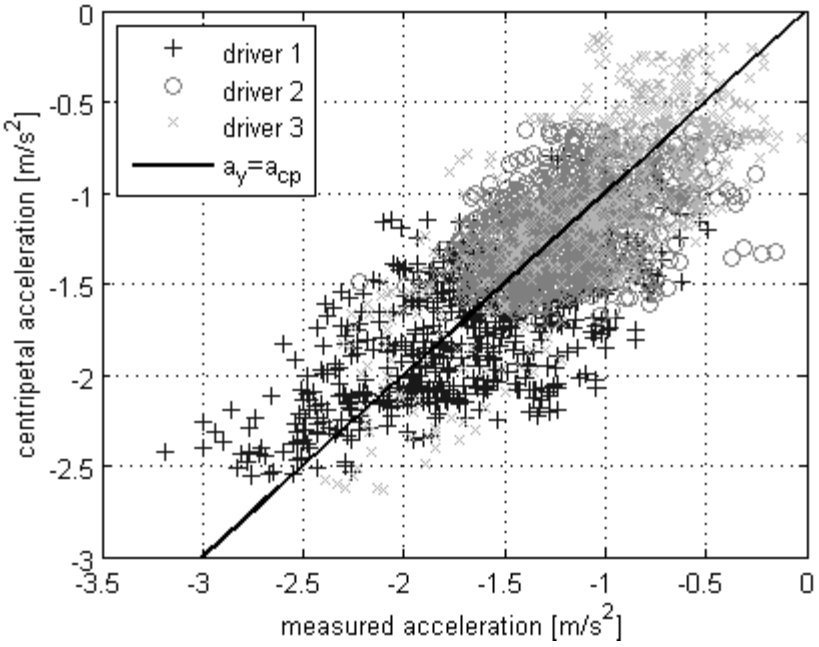

Figure 4.15 – Measured lateral acceleration compared to the centripetal acceleration

4.2.3.4 Steering Torque

Theoretically, the steering torque during a steady state manoeuvre is zero as can be derived from equation (3.16). However, the steering torque was estimated from the measured data using equation (3.18). This equation predicts that at steady state, a gyroscopic moment around the steering axis from the yaw rate and the rotating wheel remains. The moments from the normal force and the weight of the steering assembly because of the steer angle also remain at steady state. Assuming that the lateral and vertical forces on the road are balanced between the front and the rear wheels and that the roll angle is equal to the balanced roll angle, the definition of the steady state steering torque becomes equation (4.4).

$$T_s \approx t_t \frac{bmg}{L} \sin(\varepsilon)\,\delta_f - \omega_w I_{Yw} \dot{\psi} \sin(\varepsilon) + g m_f e \sin(\varepsilon)\,\delta_f \tag{4.4}$$

This nonzero steady state steering torque requires the driver to apply a small force on the handlebars to hold them in place. The dependency of the steady state steering torque on the steer angle is illustrated in Figure 4.16. This figure shows that the larger the steering angle, the greater the torque the driver needs to apply, as was predicted by the definition of the torque. The effect of the forward velocity on the steering torque is seen in Figure 4.17. The greater the velocity, the greater the gyroscopic moment from the rotating front wheel and the yaw rate.

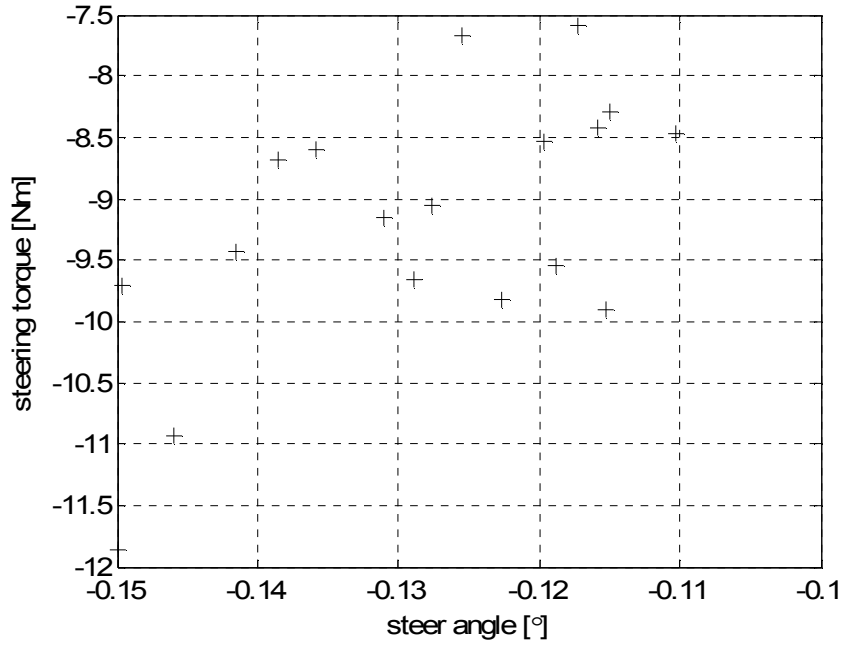

Figure 4.16 – Plot of the average steer angle and the average steering torque of all the manoeuvres

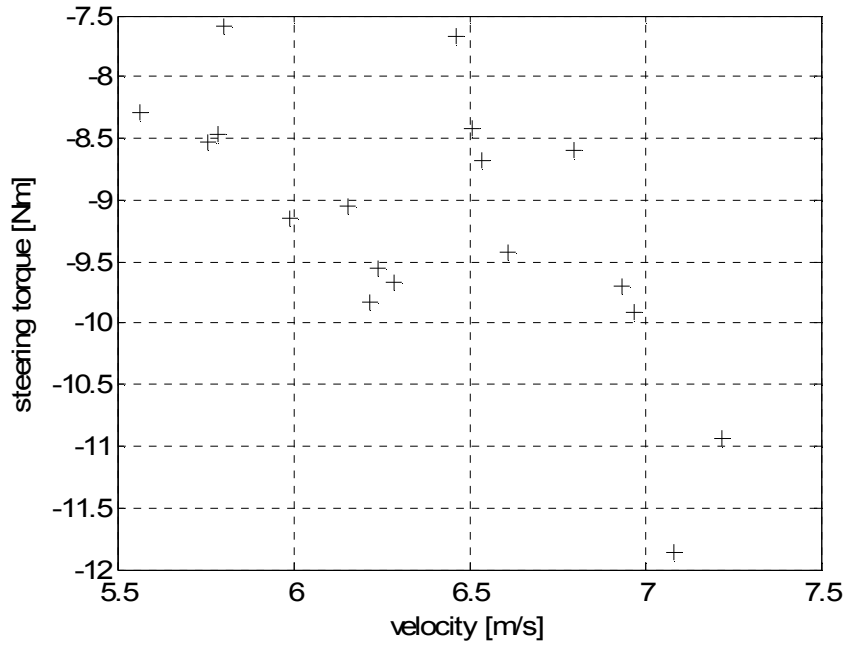

Figure 4.17 – Plot of the average velocity and the average steering torque for all the manoeuvres

Although the steering torque was expected to be zero at steady state, this was not a perfect steady state manoeuvre and there were additional dynamics. The combination of these factors resulted in the driver needing to apply some force on the handlebars to maintain a constant steering angle. A measurement of the steering torque would therefore not be a good indicator of the vehicle states that might be used in a steer tilt controller.

4.2.3.5 Perceived Lateral Acceleration

The perceived acceleration was rarely zero during the steady state manoeuvre as illustrated by Figure 4.18. The average perceived acceleration was approximately 0.25 m/s^2 and varied between 0.048 and 0.368 m/s^2 as shown in Table 4.7. The mean of the tilt acceleration was zero, so the perceived acceleration was a direct result of the tilt angle being generally larger than the balanced tilt angle for the given lateral acceleration. This unexpected result may have been partially caused by the driver shifting his upper body in order to balance and an error could have occurred in the measurement because the rear rolled out of the bend by a small amount due to tyre compliance effects. It was noted that driver 3 experienced, on average, less lateral acceleration than the other drivers. The driver possibly leant their upper body less with respect to the vehicle than the other drivers.

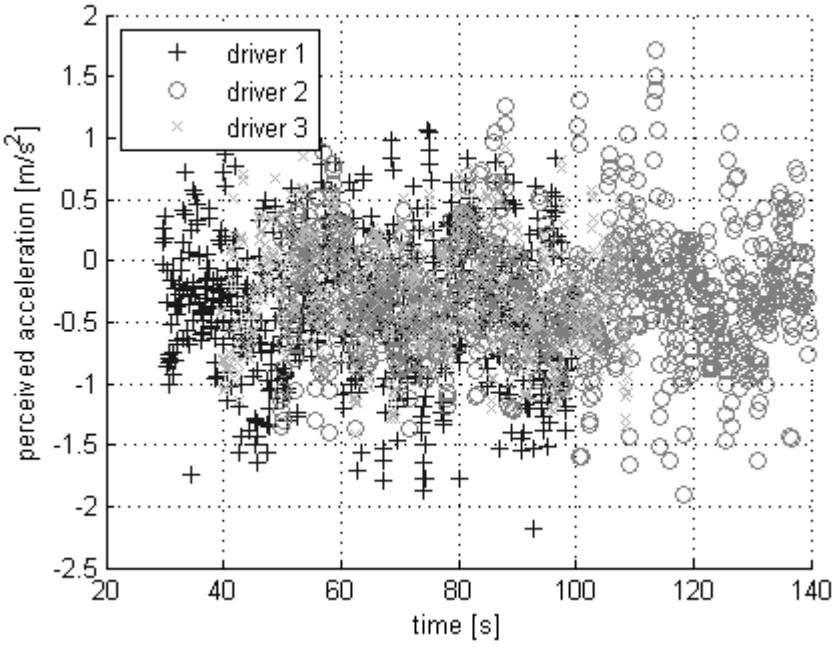

Figure 4.18 – Measured perceived lateral acceleration during the manoeuvre

Inclination angle [°]	15.9	14.8	13.6	12.4	11.2	10
driver 1	-0.234	-0.321	-0.359	-0.237	-0.351	-0.368
driver 2	-0.059	-0.308	-0.360	-0.352	-0.311	-0.331
driver 3	0.048	-0.234	-0.172	-0.232	-0.179	-0.297

Table 4.7 – Average perceived acceleration in m/s²

4.2.3.6 Effect of Tilt Axis Variations

In chapter 3 the kinematics of the tilt axis inclination were examined. On the Honda Gyro, the tilt axis inclination can be varied from 10 to 15.9 degrees. Figure 4.19 illustrates how, for a given roll angle, the predicted rear wheel steer is increased as the tilt axis inclination rises.

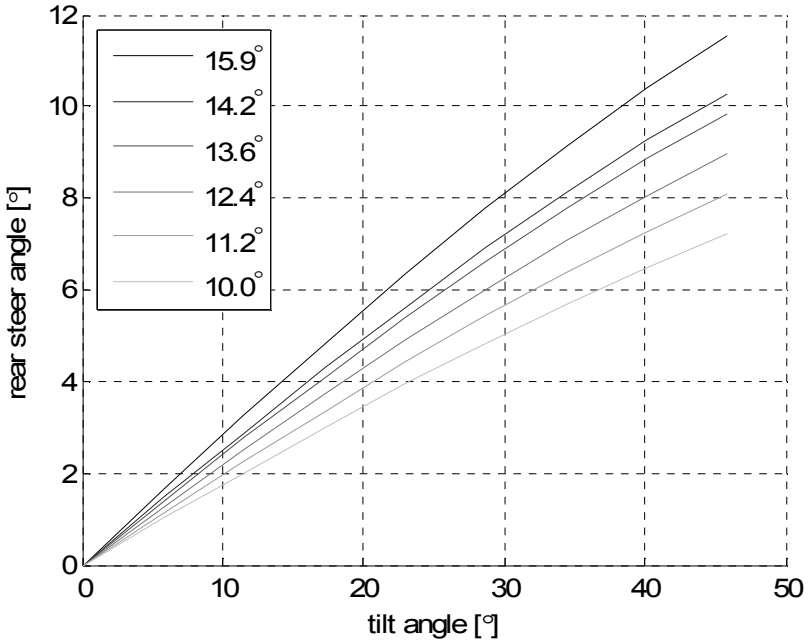

Figure 4.19 – Variation of the rear steer angle with tilt angle for a range of tilt axis inclinations

The effect this rear steer has on the vehicle in terms of its kinematics is illustrated in Figure 4.20. The slip angles are the same in the top and bottom diagram, only the rear wheels are steered into the turn in the bottom diagram. The diagram shows that the introduction of rear steer increases the kinematic turn centre radius. Therefore, in order to maintain a constant path radius with rear steer, it would be necessary to increase the front steer angle.

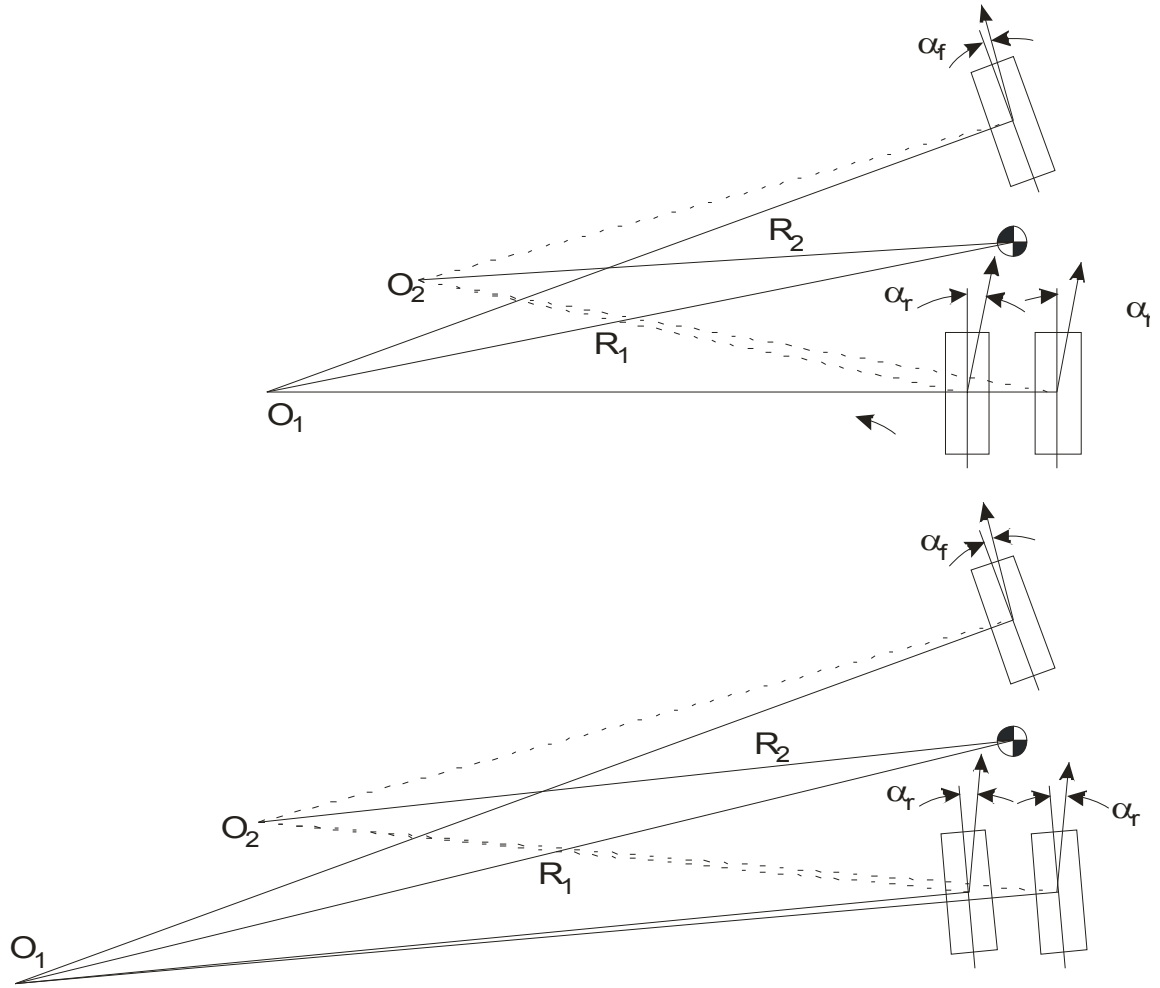

Figure 4.20 – Schematic diagram illustrating the difference in turn radius with and without rear wheel steer where O_1 is the kinematic turn centre and O_2 is the actual turn centre

Figure 4.21 shows the tilt angle plotted against the front steer angle for the range of tilt axis inclination angles and the three different drivers. These plots were expected to show that, for a given tilt angle, the driver applied a larger steer angle when the tilt axis inclination was increased. In other words, the data sets were expected to have different gradients. This is not evident from the results.

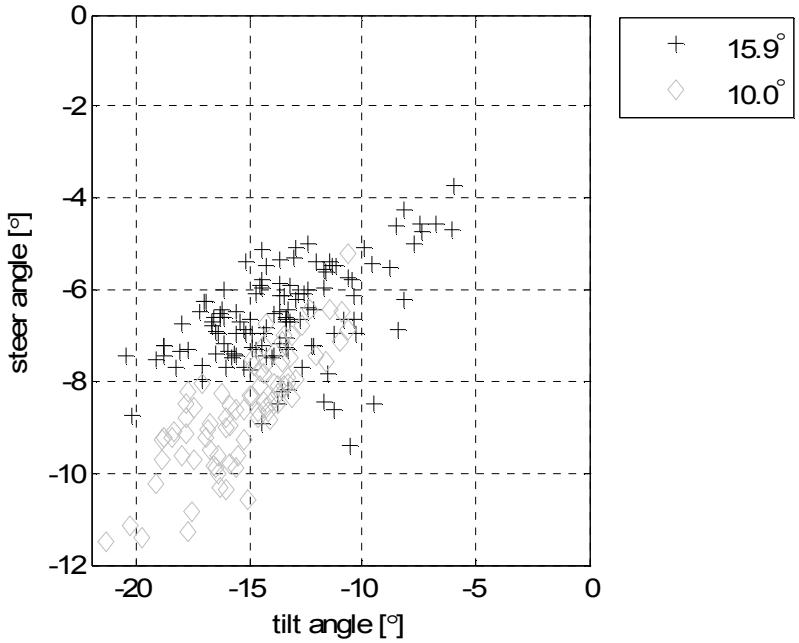
0
-2
-4
-6
-8
-10
-12
-20
-15
-10
-5
0
steer angle [°]
tilt angle [°]
15.9°
10.0°

(a)

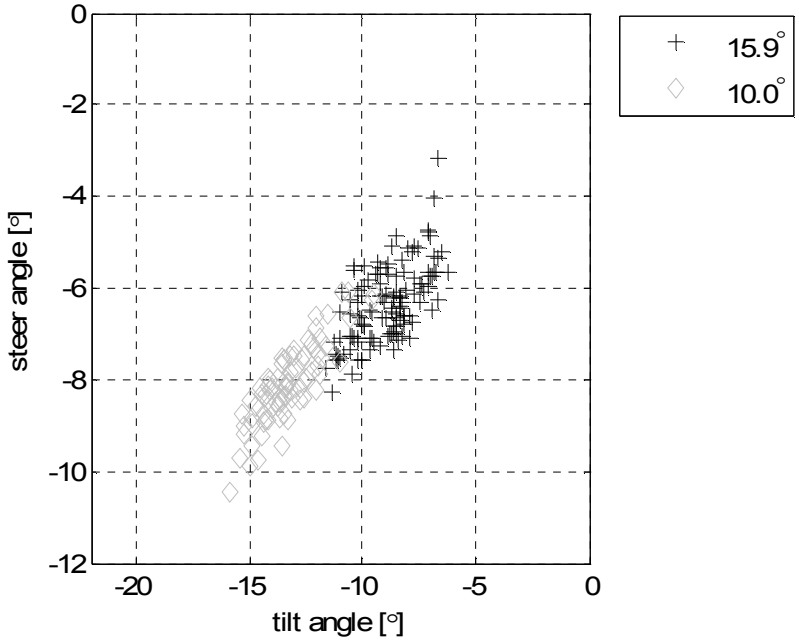
0
-2
-4
-6
-8
-10
-12
-20
-15
-10
-5
0
steer angle [°]
tilt angle [°]
15.9°
10.0°

(b)

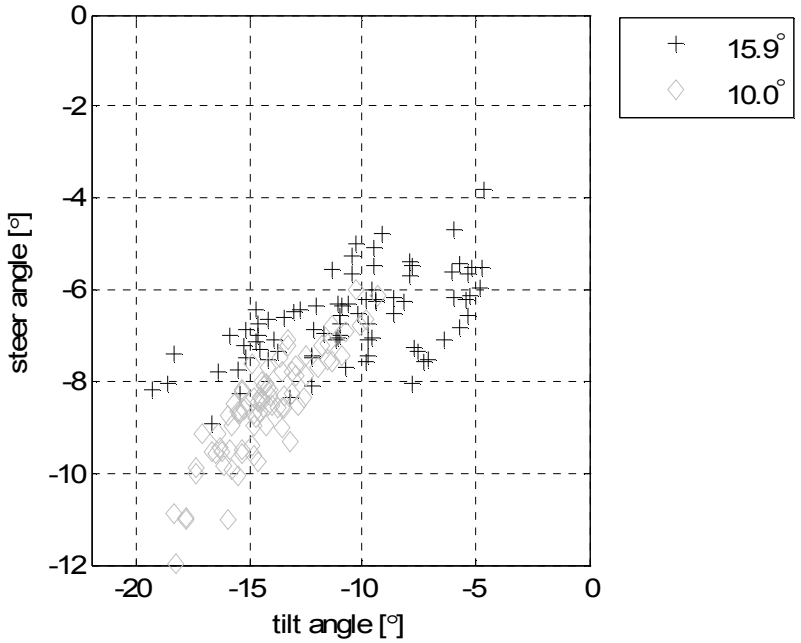

(c)

Figure 4.21 – Relationship between the tilt angle and the steer angle for the range of tilt axis inclination angles (a) driver 1 (b) driver 2 (c) driver 3

The results in Figure 4.21 were affected by differences in the manoeuvre velocity. The results were adjusted for these differences and plotted in Figure 4.22. However, there was still no noticeable difference in the gradients between the data sets for different tilt axis inclination angles. Figure 4.19 shows that for the measured tilt angles, the difference in magnitude of the rear steer between the 15.9° and 10° tilt axis inclination angles was approximately 2 degrees. The magnitude of steering compensation for this level of difference would fall within the magnitude of steering adjustments the driver would apply to follow the path regardless of the tilt axis inclination angle.

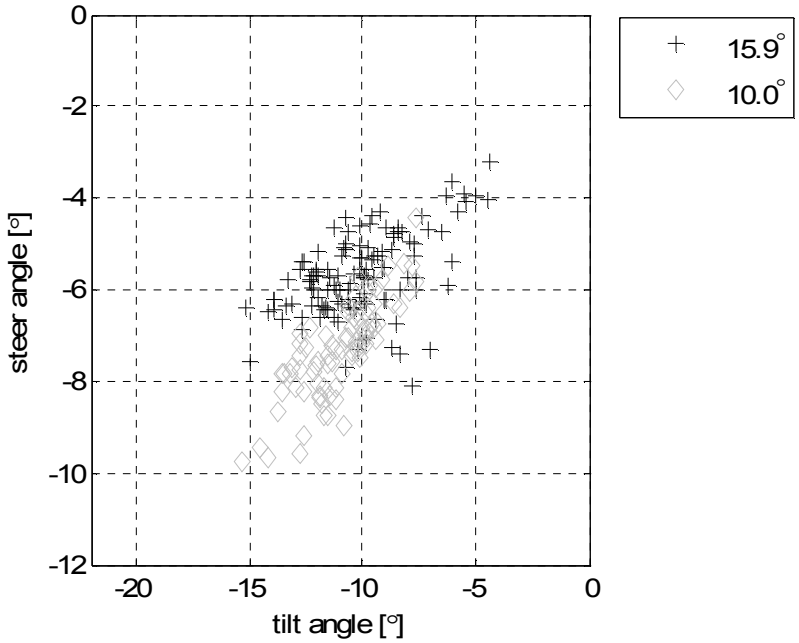
0
-2
-4
-6
-8
-10
-12
-20
-15
-10
-5
0
steer angle [°]
tilt angle [°]
15.9°
10.0°

(a)

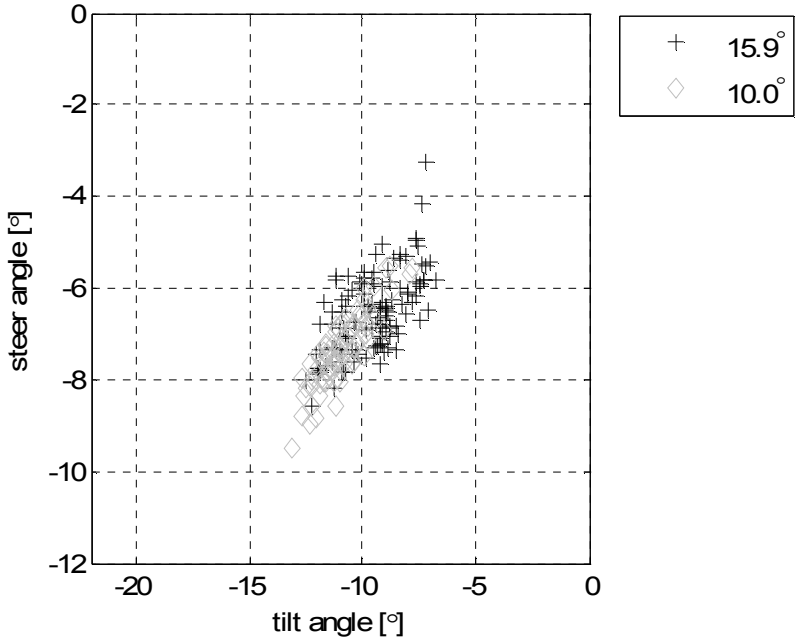
0
-2
-4
-6
-8
-10
-12
-20
-15
-10
-5
0
steer angle [°]
tilt angle [°]
15.9°
10.0°

(b)

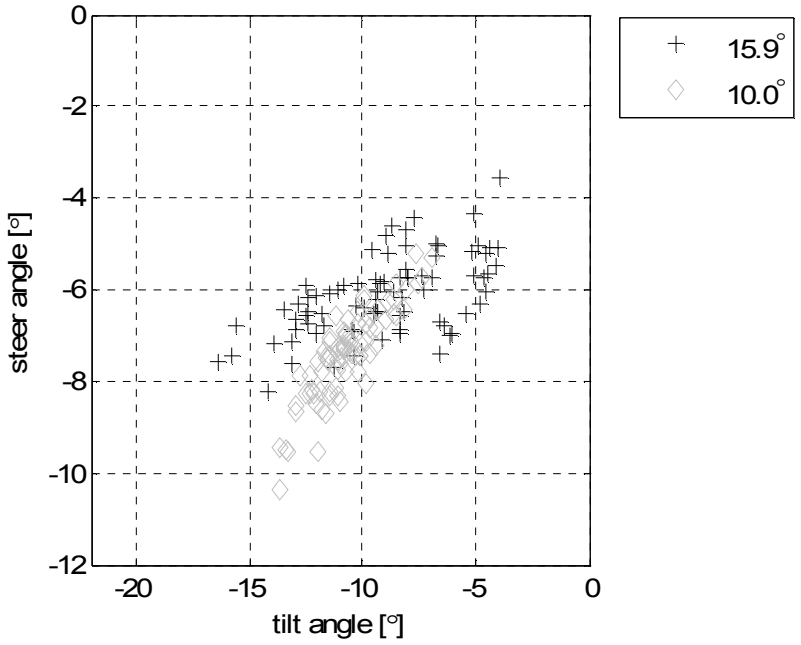

(c)

Figure 4.22 – Effect of the tilt axis inclination angle on the relationship between the tilt angle and the steer angle results adjusted for variations in velocity (a) driver 1 (b) driver 2 (c) driver 3

4.3 TRANSIENT MANOEUVRES

4.3.1 Objectives

In order to start leaning, motorcycle riders apply a small amount of countersteer before they steer into a turn. Steer is one of the control tools a motorcycle rider can use to balance the bike. In order to develop a controller that is based on applying steer to control the lean, it was thought to be important to study how a driver performed this task. The hypothesis was that there would be a correlation between manoeuvre velocity and countersteer magnitude and the period of time during which the countersteer was applied. It was also thought that for a given manoeuvre and a more or less constant velocity, the drivers would apply a similar amount of countersteer. Once the driver's mechanism for applying countersteer was understood, an algorithm could be developed for a steer tilt controller. In addition to understanding the human driver's countersteer behaviour, the experimental data were expected to be used to validate a simulation model of the vehicle and its tyres.

4.3.2 Car Park Results

4.3.2.1 Objectives

The University car park was used to obtain initial results and a preliminary overview of the transient vehicle dynamics. The path the drivers had to follow was either a single or a double loop of the car park shown in Figure 4.23, or a single corner. In the first experiment, the aim was to determine how countersteer could be determined from the results. The second experiment aimed to show the effects of the driver wearing a seatbelt. It was thought that without a seatbelt, the driver would shift his weight whilst driving, affecting the tilt angle and therefore a number of other dynamic variables.

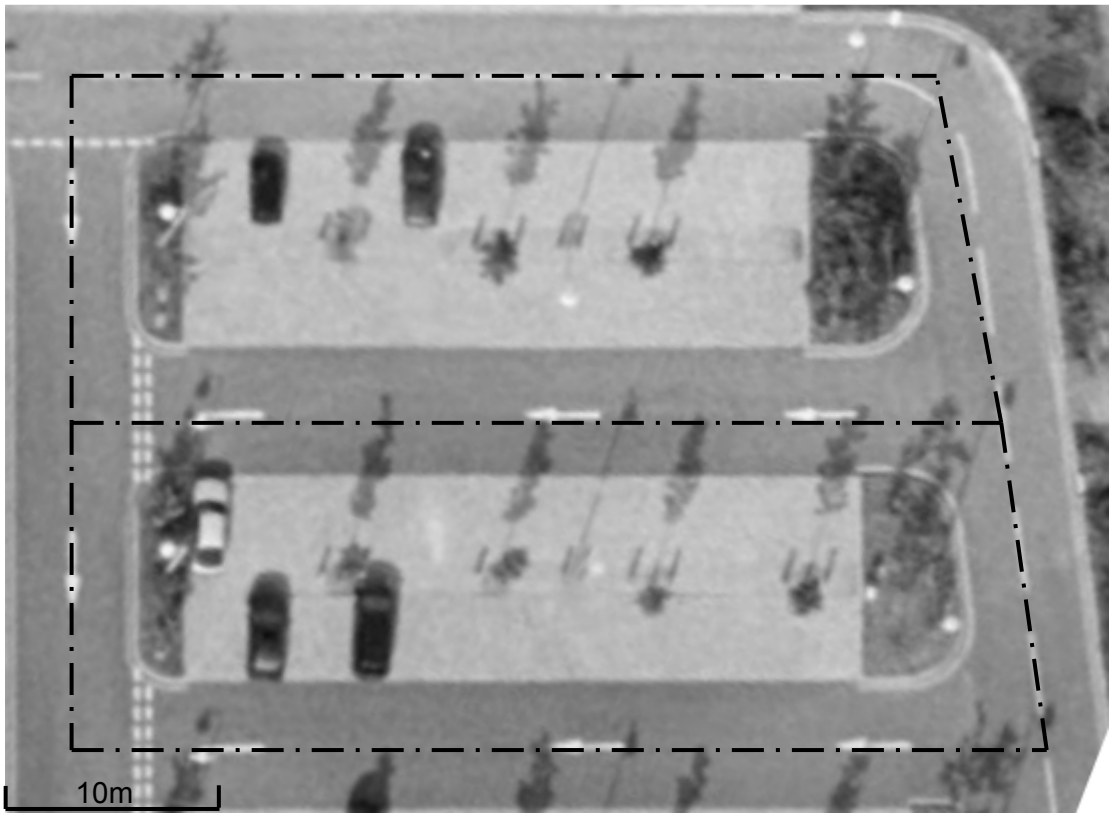

Figure 4.23 – Satellite image of the car park

4.3.2.2 Experiment 1: Determine Countersteer

Figure 4.24 shows the path the drivers followed around the car park. The path takes the drivers around the course clockwise for two whole laps. Then the drivers cross over to driver around the course anti clockwise for one and a half laps. The objective was to measure both right and left hand turns.

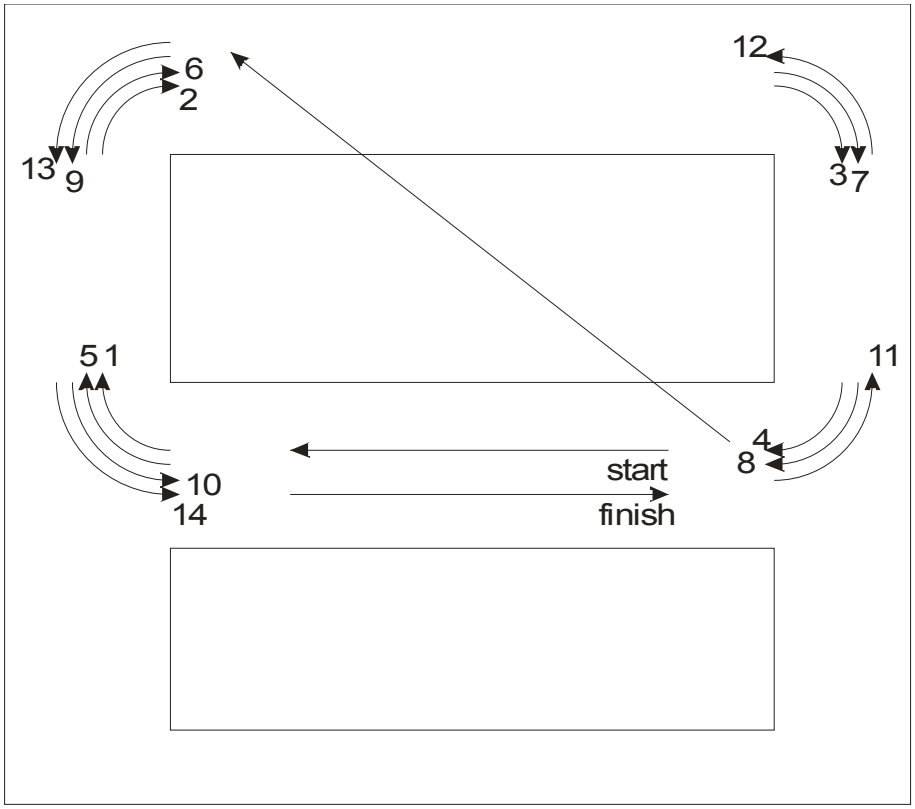

Figure 4.24 – Manoeuvre driving directions and turn numbers

It was shown that the individual drivers had different styles of driving. The drivers were numbered according to their experience in riding motorcycles and bicycles: driver 1 was the most experienced and driver 3 the least experienced. The difference in experience and confidence was evident in the speed at which they preferred to driver around the circuit: this varied between 11.6kph and 20.7kph as shown in Figure 4.25. The difference in manoeuvre speed would affect the rest of the results: lateral acceleration, steer angle and tilt angle.

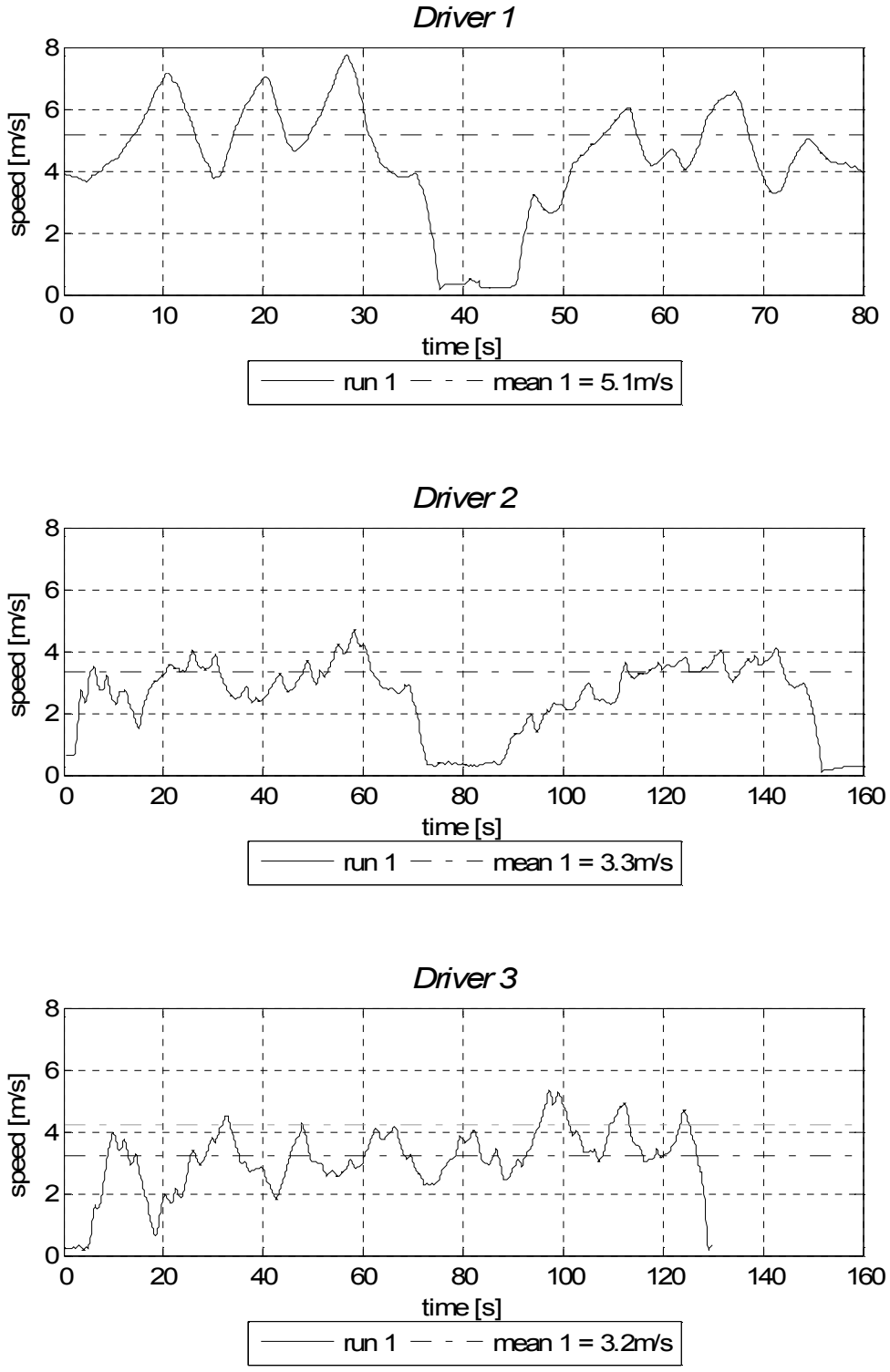

Figure 4.25 – Manoeuvre velocities of the different drivers

Driver 1 manoeuvred the fastest and therefore the lateral accelerations were the largest as shown in Figure 4.26. In normal circumstances, the continuous clockwise turns would require positive lateral acceleration throughout and vice versa for anti-clockwise turns. However, on some

occasions, e.g. after turns 10 and 12, driver 1 had to steer such that the lateral acceleration changed direction in order to straighten up after a turn. This could be considered as an example of countersteer. A change in direction of the lateral acceleration was also seen in the manoeuvres of the other drivers, but it was not as significant as the behaviour of driver 1. These results indicated that countersteer would be a measurable variable.

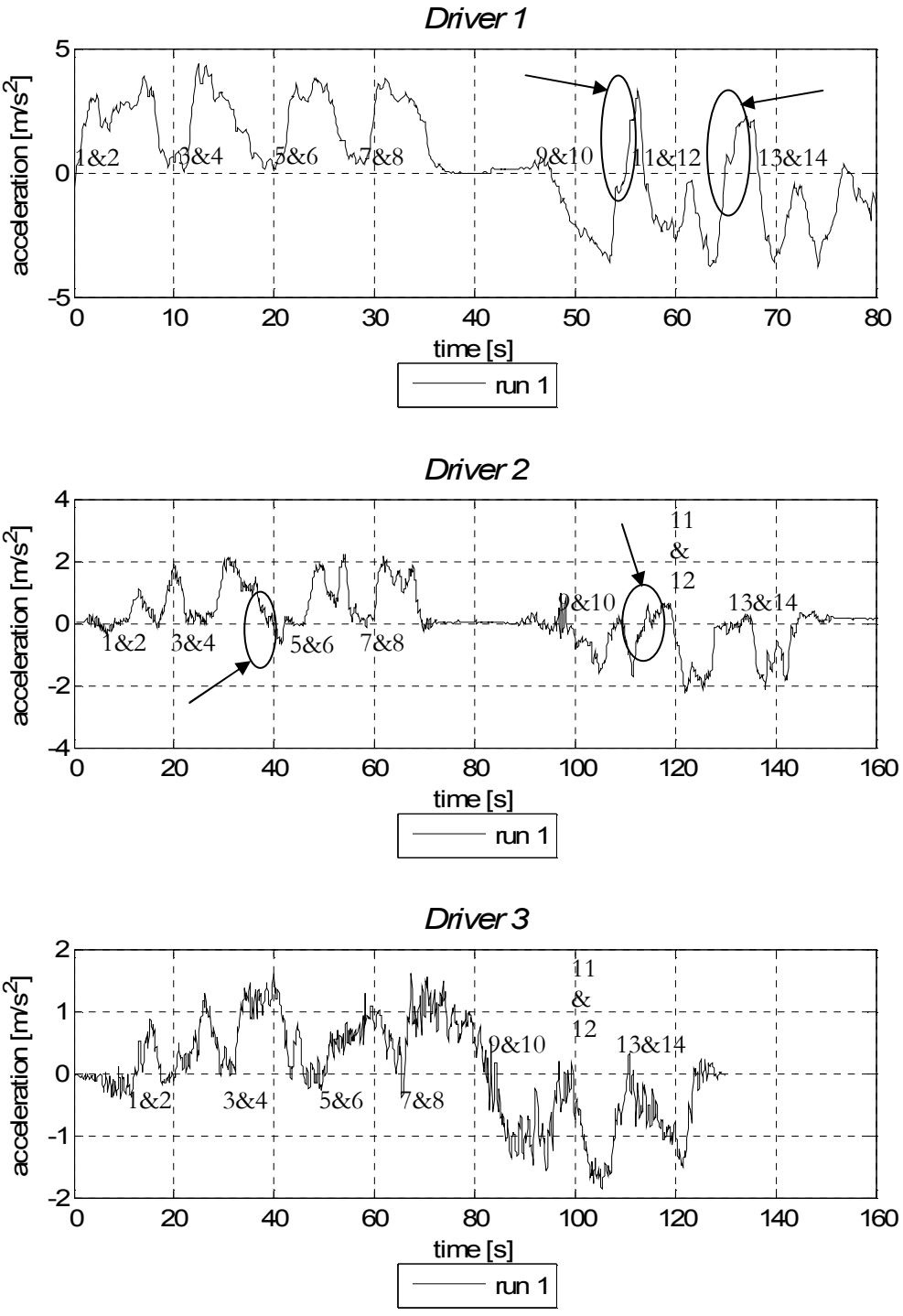

Figure 4.26 – Lateral accelerations during the manoeuvre for different drivers

Having noted the countersteer in the lateral acceleration measurements, it was thought that they should also be apparent in the steer angle measurements given in Figure 4.27. This was indeed the case. It was also noted that the maximum steer angle during the manoeuvre did not vary significantly amongst the drivers. In other words, the variation in lateral acceleration was mainly caused by the difference in manoeuvre speed and not steer. Driver 1 was the most experienced rider. It was expected that the steering results from this driver would show countersteer very clearly. However, the driver completed the trajectory so fast that he was almost constantly cornering. This meant that there was no occasion where the driver needed to change direction from going straight to going into a turn, so there was no countersteer required. Driver 2 was less experienced than the first driver. This could be deduced from the additional adjustment made in the steering. Driver 3 was not an experienced bicycle or motorcycle rider. The result was that the driver was adjusting the steering frequently. Also, the effect of countersteer was not easily deducted from the results: it was unclear whether a steer input was an adjustment or countersteer.

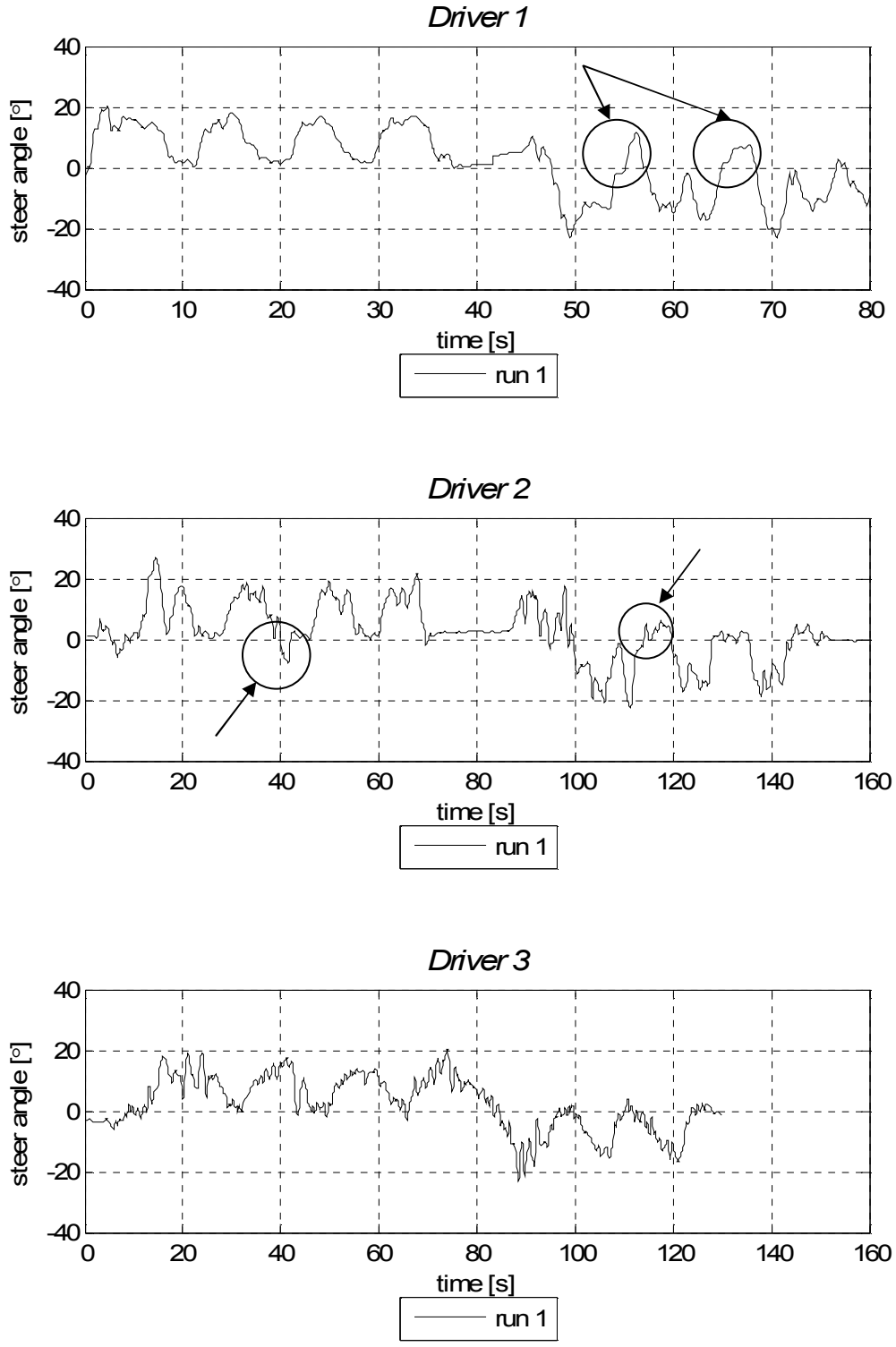

Figure 4.27 – Steer angles for different drivers during the manoeuvre

It was thought that the countersteer actions from the driver were purely to balance the vehicle and that they would not manifest themselves in the tilt angle. However, Figure 4.28 illustrates that the tilt angle was also affected. This was not entirely surprising, because the roll moment

caused by the steering actions could have resulted in the lean angle overshooting the intended position.

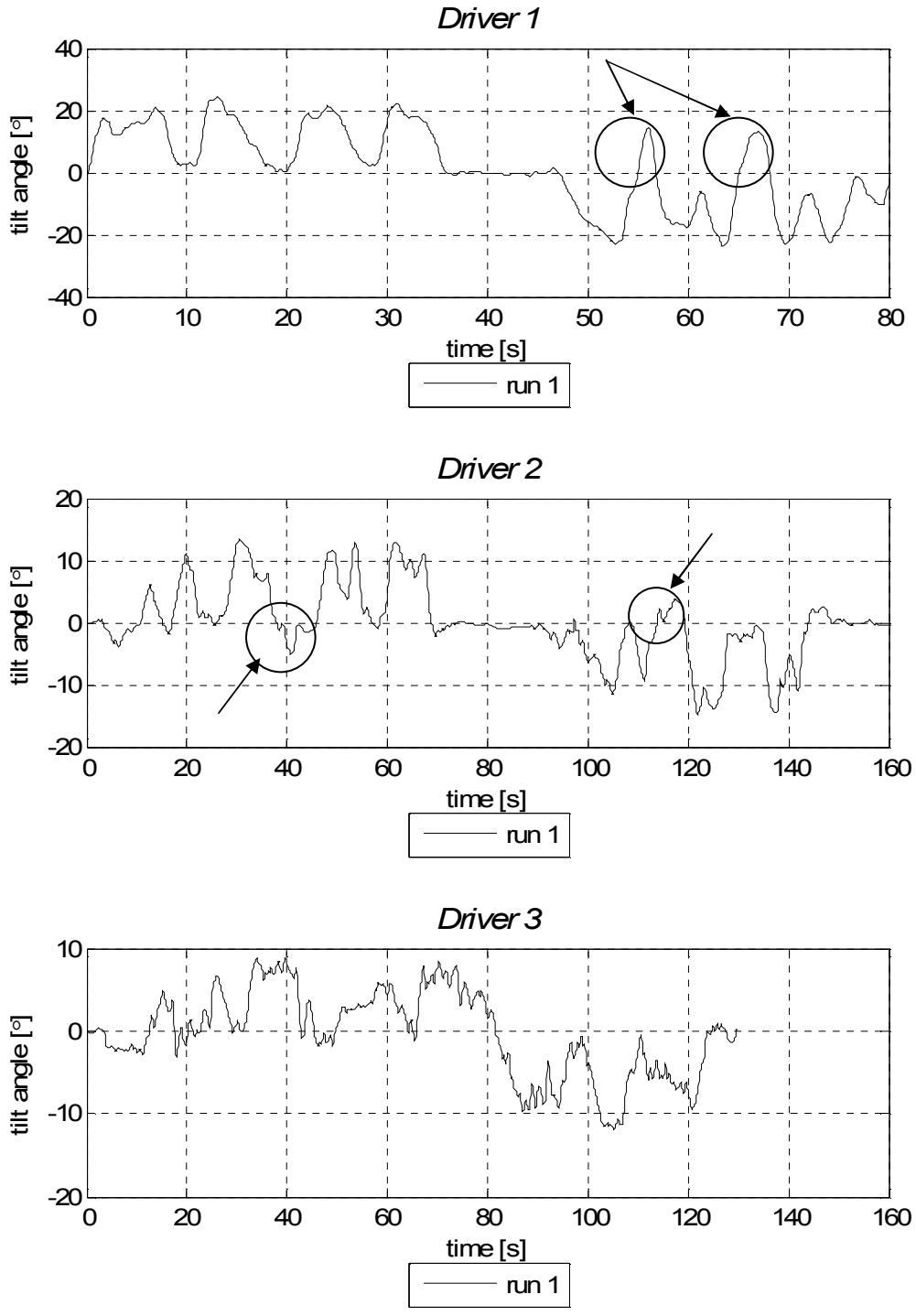

Figure 4.28 – Variation in tilt angle

Figure 4.29 shows the paths taken by the drivers. The figure illustrates that even the longer sections of the rectangular track were executed by the drivers as if they were curved sections with

a large radius. In other words, the drivers were constantly cornering as was previously noted. For better results, the track had to be extended to a double loop.

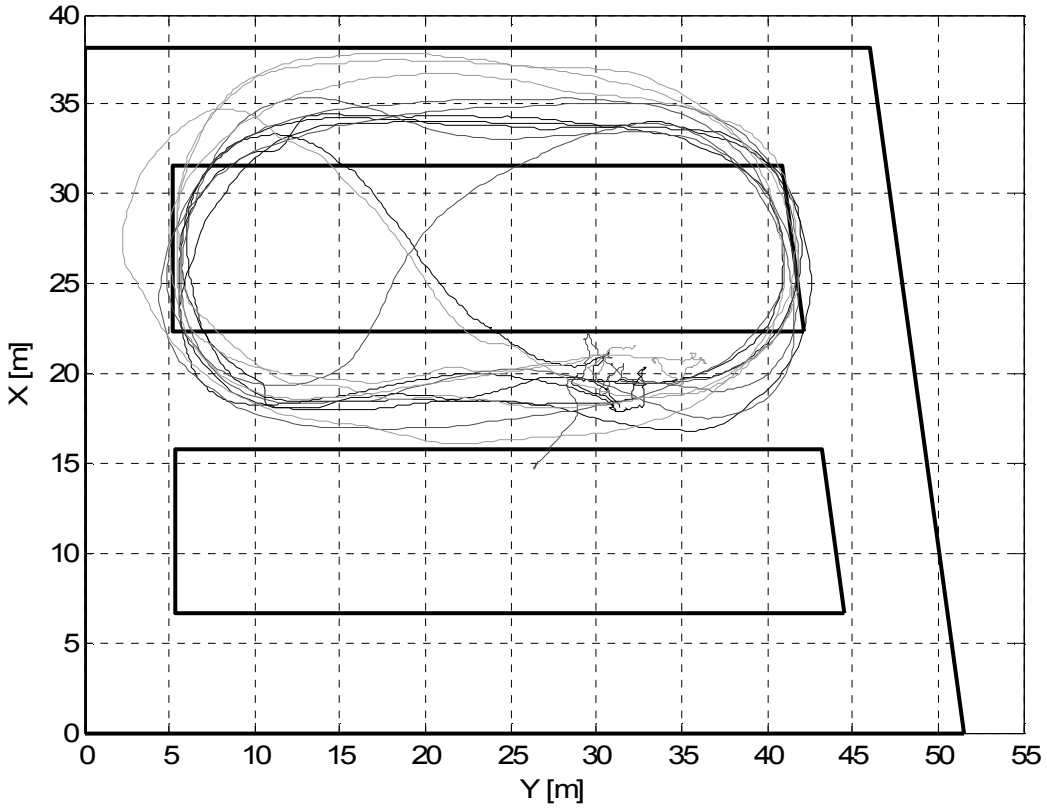

Figure 4.29 – Variation in paths taken

4.3.2.3 Experiment 2: With and Without Seatbelt

A small study was carried out to determine the effect of the driver being strapped into the seat by seatbelts. It was suspected that the driver was shifting his weight during the cornering manoeuvres, which would have affected the tilt angle results. A seatbelt would restrict the extent to which the driver could lean their upper body. In terms of steering, it was thought that the driver would adjust the steering more when supported by a seatbelt in comparison to being free to move. When not restrained, the driver could compensate for slight instabilities by moving his torso. When held in place by a seatbelt, the driver would have to compensate for these instabilities by small steering adjustments.

Figure 4.30 shows that, in terms of steering input, there was no noticeable difference in the driver steering input with or without seatbelt. In either case, the driver adjusted the steering by similar amounts at similar frequencies. This resulted in similar paths taken by the driver as shown in

Figure 4.31. It should be noted that for this single 90° turn manoeuvre, it was clear that the driver countersteered on either entry or exit of the turn.

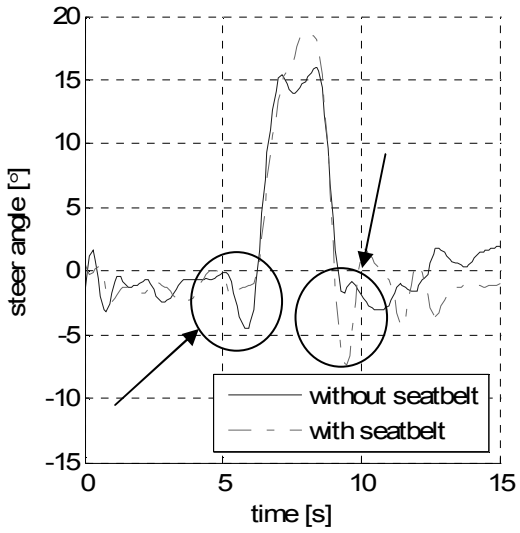

Figure 4.30 – Steering input for a 90° turn manoeuvre

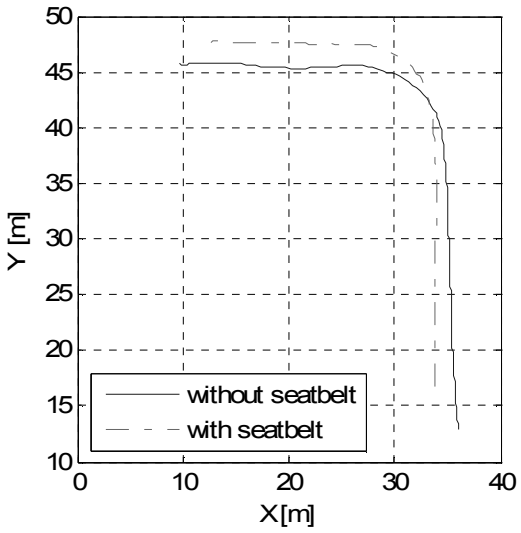

Figure 4.31 – Vehicle trajectory of a 90° turn manoeuvre

With respect to the tilt angle, the driver underleaned in both tests, see Figure 4.32. This showed that the driver did not shift his weight to compensate for overlean or underlean. The underlean could be a result of the speed of the manoeuvre: it was rapid, therefore the driver did not have the time to realise that he was not leaning enough. Also he may not have had enough time to produce a large enough roll moment. When plotting the measured tilt angle φ and the balanced tilt φ_b angle against time, as shown in Figure 4.33 and Figure 4.34, it was evident that some overlean occurred at the start of the turn. At this point, the driver would have countersteered to create a side force leaning the vehicle into the turn. The vehicle would be leaning before the driver started steering into the turn, which would result in large differences between the measured lean angle and the balanced lean angle at that point in time. When exiting the turn, the lean angle tended to be somewhat smaller than the balanced lean angle. This was expected as the driver was intending to straighten up and therefore seeking to achieve a lateral acceleration causing the vehicle to roll back up.

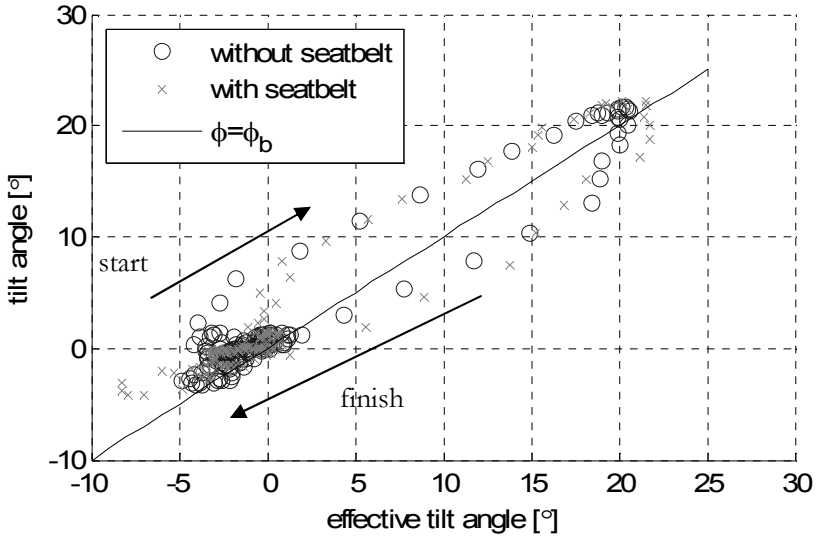

Figure 4.32 – Relationship between tilt angle and effective tilt angle for a 90° turn manoeuvre

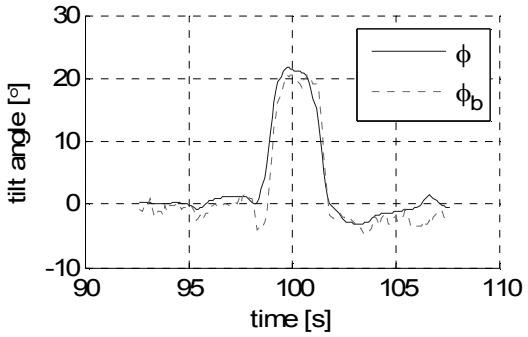

Figure 4.33 – Tilt angle for a turn manoeuvre without seatbelt

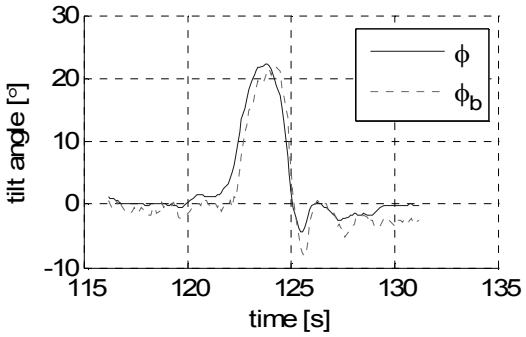

Figure 4.34 – Tilt angle for a turn manoeuvre with seatbelt

To confirm that the driver's torso movement had little effect on the control of the vehicle, the same measurements were taken whilst driving straight ahead. It was expected that the driver would make different minor adjustments whilst trying to drive in a straight line. There did not appear to be a large difference in the amount or the frequency of the steering adjustments as shown in Figure 4.35. Under both circumstances, the driver managed to follow a straight line within a 0.5m boundary as illustrated by Figure 4.36. Overall, the effect of the seatbelt was not significant.

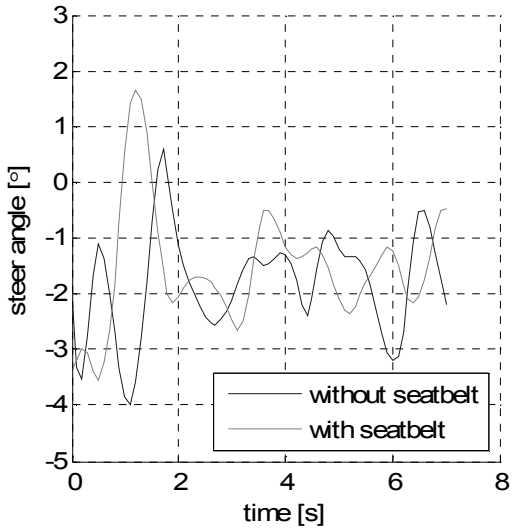

Figure 4.35 – Steer angle when driving in a straight line

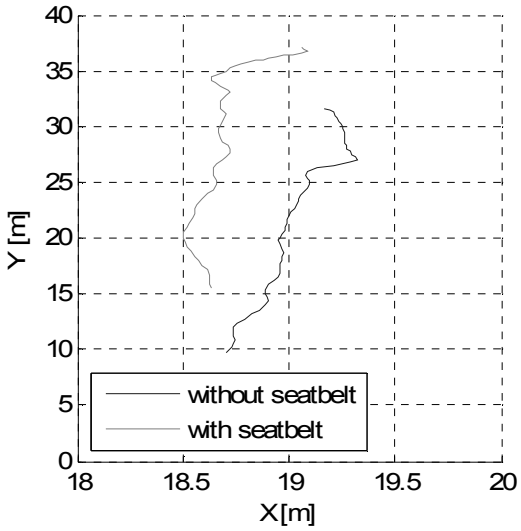

Figure 4.36 – Achieved straight line trajectory

4.3.3 Open Road Conditions - Colerne Airfield Results

4.3.3.1 Manoeuvre Description

To study the driver behaviour negotiating a 90-degree turn, a test track was set up at Colerne airfield. The trajectory consisted of a long straight section, a sharp turn and another long straight section. The first straight section was included so that there would be a clear difference between the driver applying minor steering adjustments, and the driver countersteering to take the turn. The second straight section was added so that the results would show the actions of the driver straightening up. The driver would pause at the start and at the end of every manoeuvre. The first trajectory consisted of a left turn only, the second trajectory a right turn. An aerial view of the test area can be seen in Figure 4.37 and a typical manoeuvre trajectory is shown in Figure 4.38.

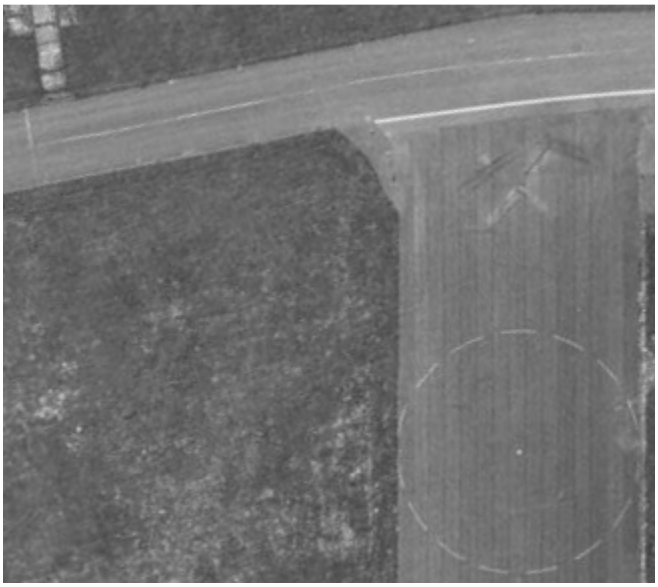

Figure 4.37 – Satellite image of the track used at Colerne

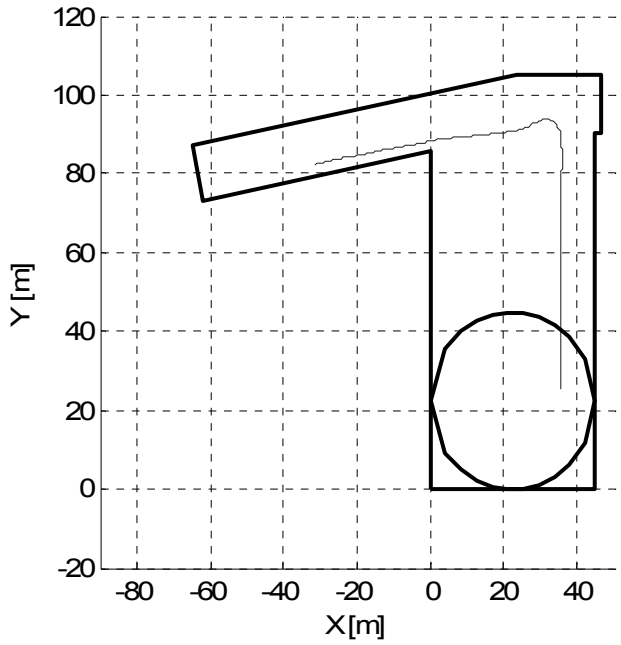

Figure 4.38 – Typical test trajectory

4.3.3.2 Steer Angle and Lateral Acceleration

The relationship between the steer angle and the lateral acceleration was proportional as shown in Figure 4.39 and Figure 4.40. Here, the left hand turn showed more consistent results than the right hand turn. The differences shown in Figure 4.40 were caused by the difference in average manoeuvre speed: Figure 4.41 shows that the average manoeuvre speed was approximately the same for all drivers during the left hand turn, but driver 1 completed the right hand turn faster

than the other two drivers as shown in Figure 4.42. In general, the data showed that the steer angle and the lateral acceleration were proportional and countersteer effects were small. Furthermore, they showed that the faster the manoeuvre the larger the steer angle for a given lateral acceleration.

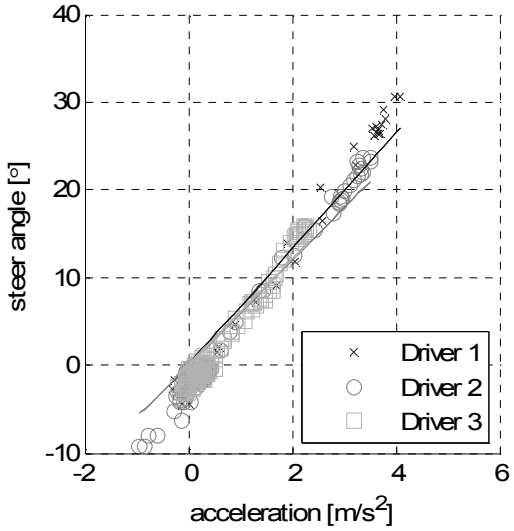

Figure 4.39 – Relationship between lateral acceleration and steer for a left hand 90^o turn

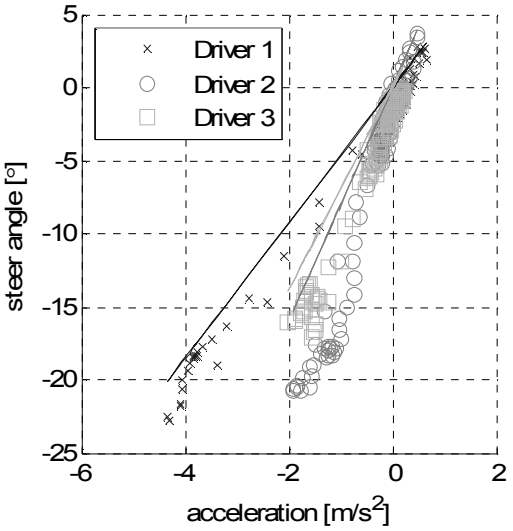

Figure 4.40 – Relationship between lateral acceleration and steer for a right hand 90^o turn

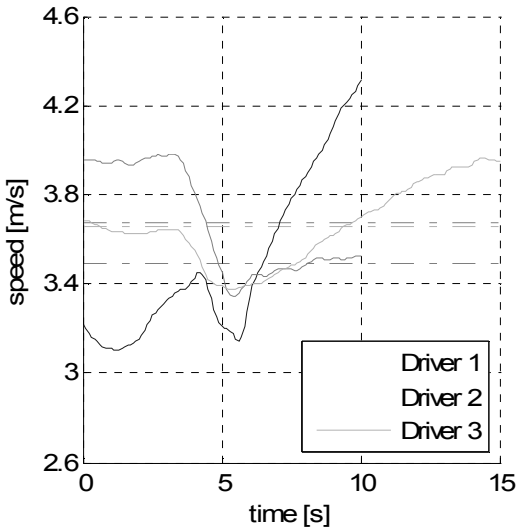

Figure 4.41 – Speed progression with time for a left hand 90^o turn. Mean velocities: 3.5, 3.68, 3.65 m/s for drivers 1, 2 and 3 respectively.

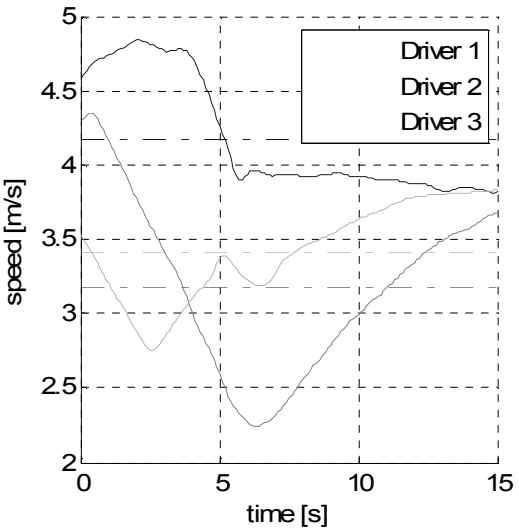

Figure 4.42 – Speed progression with time for a right hand 90^o turn. Mean velocities: 4.18, 3.17, 3.42 m/s for drivers 1, 2 and 3 respectively.

4.3.3.3 Countersteer

The steering inputs from the drivers showed clear signs of countersteer, see Figure 4.43 and Figure 4.44. This countersteer was analysed in terms of its magnitude, duration, and resultant lateral acceleration. This analysis revealed that the countersteer was not a fixed parameter: there were various courses of countersteer that achieved an appropriate roll moment and balanced roll angle.

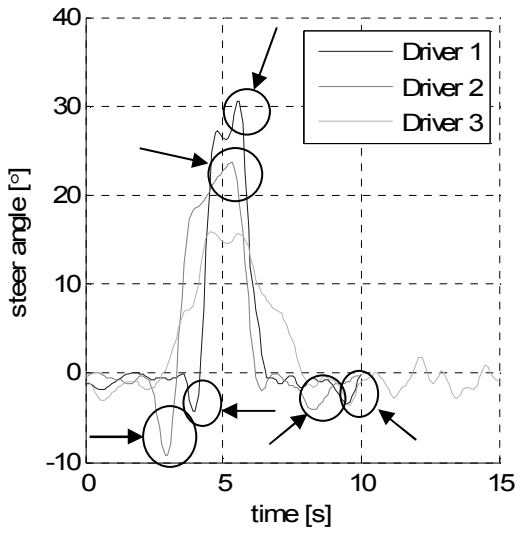

Figure 4.43 – Steer angle progression with time for a left hand 90° turn

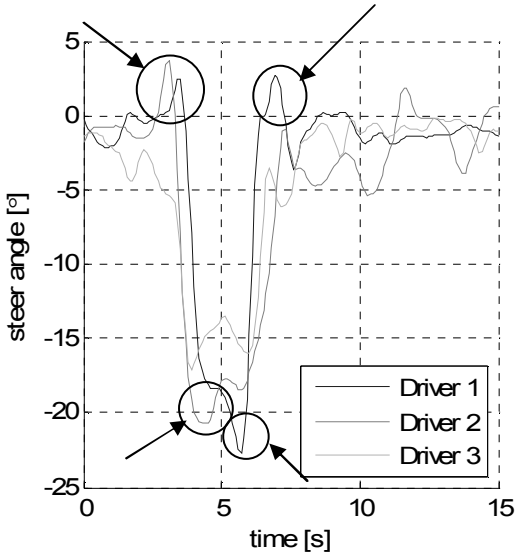

Figure 4.44 – Steer angle progression with time for a right hand 90° turn

The approach speed for the manoeuvres was between 3.5 and 4.5 m/s (12.6 to 16.2 kph) for all the drivers. In some cases, the driver would slow down more than others. This caused the variations in steer angle and lateral acceleration during the manoeuvre. Nevertheless, the magnitude of the countersteer δ_f(c.s.max) was determined from the results as shown in Figure 4.45, with a number of other measurements: the total time the driver countersteered t(c.s.), the mean velocity over this time period v_X(c.s.), the resulting maximum of the measured total lateral acceleration from the countersteer a_Y(c.s.max), the maximum roll moment caused by the countersteer T_{roll}, the roll angle when the countersteer is at its maximum 'φ at δ_f (c.s.max)', the roll angle when the driver starts steering in the direction of the turn 'φ at δ_f=0', the average velocity of the manoeuvre v_X(mean), and the maximum total measured lateral acceleration of the manoeuvre a_Y(max).

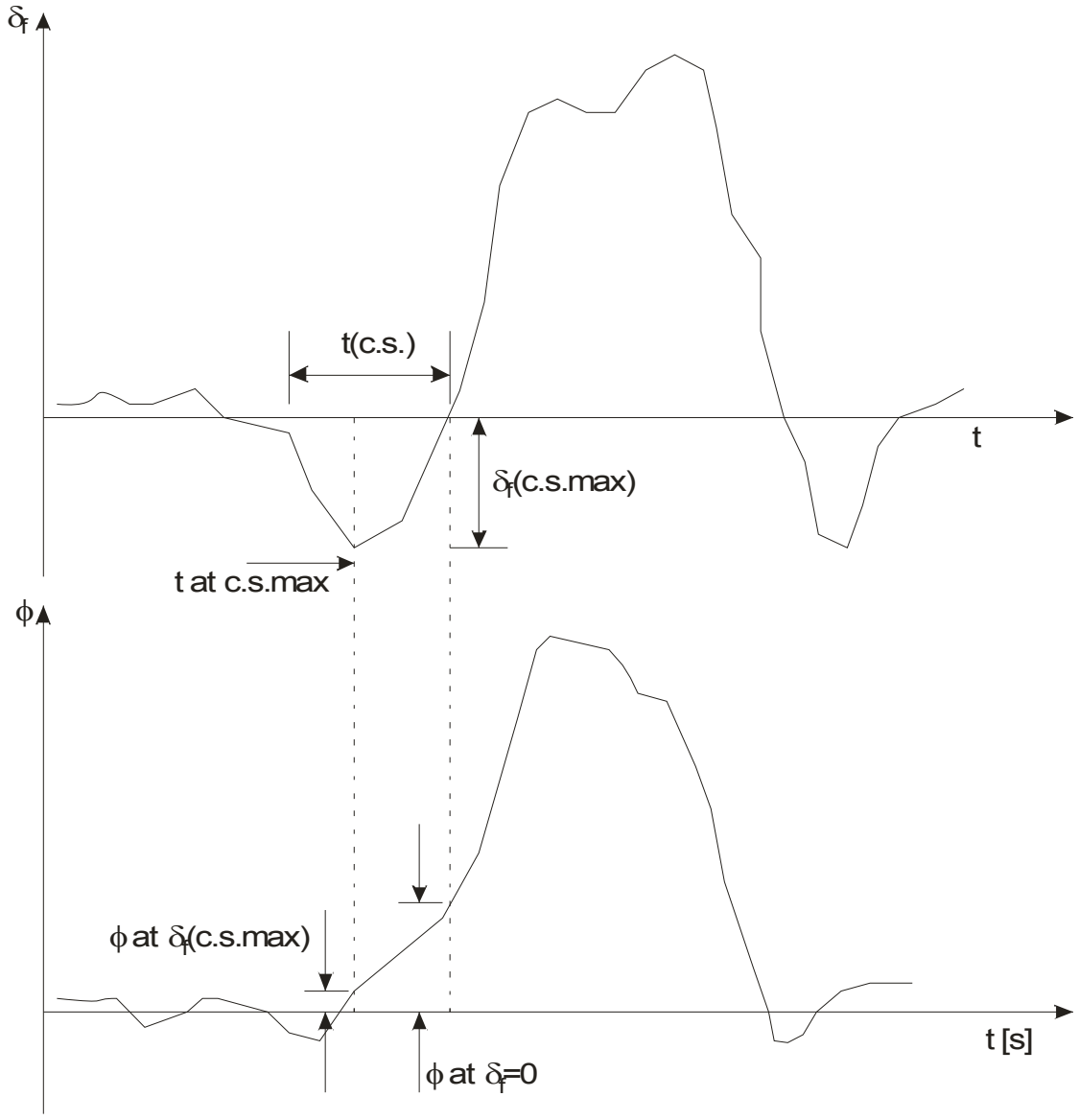

Figure 4.45 – Schematic diagram illustrating how the countersteer was measured

Table 4.8 and Table 4.9 summarize these measurements described in the previous section. The first row holds the values for the maximum countersteer from smallest to largest. From the summary tables, Table 4.8 and Table 4.9, it appeared that the maximum countersteer angle was larger with an increased approach speed. However, this increase was not consistent and varied per driver and per manoeuvre. The length of time the countersteer was applied followed a trend opposite to what was expected: the faster the approach the longer the countersteer manoeuvre. It seemed that the driver would start countersteering earlier and therefore longer when approaching faster.

maximum countersteer angle δ_f(c.s.max)	[°]	1.15	2.81	4.01	4.01	4.70	5.21
total countersteer time t(c.s.)	[s]	0.73	1.18	0.51	0.91	0.60	0.58
mean velocity during countersteer v_X(c.s.)	[m/s]	4.40	4.80	3.40	4.90	3.70	4.00
maximum measured lateral acceleration during countersteer a_Y(c.s.max)	[m/s^2]	0.14	0.35	0.32	0.67	0.76	0.92
roll moment achieved by countersteer T_{roll}	[Nm]	98	173	185	230	193	247
roll angle when the countersteer is at its maximum ϕ at δ_f(c.s.max)	[°]	0.92	4.64	3.72	4.87	2.29	3.84
roll angle when the steer angle changes direction ϕ at δ_f=0	[°]	3.50	10.37	8.94	11.57	7.62	9.68
mean velocity of the manoeuvre v_X(mean)	[m/s]	3.90	4.20	3.70	4.10	3.50	3.60
maximum measured lateral acceleration during the manoeuvre a_Y(max)	[m/s^2]	3.40	4.40	4.10	4.40	3.90	4.10

Table 4.8 – Driver 1 left hand turn countersteer behaviour

maximum countersteer angle δ_f(c.s.max)	[°]	2.18	3.78	4.47	5.50	7.79	8.48
total countersteer time t(c.s.)	[s]	1.16	0.93	0.79	0.68	0.70	1.11
mean velocity during countersteer v_X(c.s.)	[m/s]	4.10	3.90	3.40	3.70	4.60	4.00
maximum measured lateral acceleration during countersteer a_Y(c.s.max)	[m/s^2]	0.42	0.57	0.43	0.50	1.41	1.36
roll moment achieved by countersteer T_{roll}	[Nm]	85	108	89	120	196	149
roll angle when the countersteer is at its maximum ϕ at δ_f(c.s.max)	[°]	2.01	2.23	2.12	2.12	0.11	0.46
roll angle when the steer angle changes direction ϕ at δ_f=0	[°]	5.56	7.05	6.07	7.28	7.73	9.11
mean velocity of the manoeuvre v_X(mean)	[m/s]	3.80	3.50	3.20	3.70	4.20	3.70
maximum measured lateral acceleration during the manoeuvre a_Y(max)	[m/s^2]	3.80	3.20	1.90	2.30	2.90	3.50

Table 4.9 – Driver 2 left hand turn countersteer behaviour

It was expected that an increased countersteer angle would result in an increased lateral acceleration, and it was expected that the maximum roll moment would also be larger. The results

in Table 4.8 and Table 4.9 indicate that there is a correlation between the maximum countersteer angle, the lateral acceleration and the resulting roll moment.

Part of the predicted countersteer behaviour included the driver countersteering until a minimum tilt angle was achieved. The results showed that the tilt angle at the point of maximum countersteer was still very small: smaller than 5 degrees. This angle would be barely noticeable, so the tilt angle could not have been a major indicator to complete the countersteer action. The roll moment caused by the countersteer was thought to be another indicator to the driver to start steering into the turn. The results showed that there were significant variations in the maximum achieved roll moment during countersteer regardless of the approach speed and maximum lateral acceleration of the turn. The results in Table 4.8 and Table 4.9 demonstrate that there are no trends in the method of applying countersteer. The drivers appear to apply an arbitrary amount of countersteer for an arbitrary period of time in order to cause a roll moment. Once the vehicle is rolling and cornering, the driver controls the tilt by making small adjustments throughout the manoeuvre.

4.3.3.4 Steer angle and Tilt Angle

The mean velocities of the turn and the velocities at the maximum turning point lied in a similar range for each driver, see Table 4.10. However, the maximum steer angle and therefore the maximum lateral acceleration varied significantly as Table 4.11 illustrates. This variation was attributed to the small differences in the path the drivers had taken during the manoeuvre. Typical paths for a left and right hand turn are plotted in Figure 4.46 and Figure 4.47 respectively. The tighter the turn, the larger the lateral acceleration required to achieve the turn at a given velocity.

Left	driver 1				driver 2				driver 3			
v_X(mean) [m/s]	3.47	3.63	***3.50***	3.44	3.47	3.92	***3.67***	3.78	3.70	3.53	***3.66***	3.47
v_X(at turn) [m/s]	2.90	3.09	***3.22***	2.91	3.52	3.59	***3.63***	3.75	3.34	2.92	***3.40***	3.06
Right												
v_X (mean) [m/s]	3.79	3.76	4.30	***4.39***	3.62	3.25	4.16	***2.79***	3.06	3.75	3.98	***3.16***
v_X (at turn) [m/s]	3.55	3.47	4.24	***4.28***	3.56	3.20	4.27	***2.65***	3.07	3.27	3.29	***3.23***

Table 4.10 – Mean velocities and velocities at the apex of the turn, the values in bold were measured from Figure 4.46 and Figure 4.47

Left	driver 1				driver 2				driver 3			
δf(max) [rad]	0.503	0.472	***0.429***	0.490	0.287	0.338	***0.344***	0.324	0.182	0.224	***0.270***	0.270
ay(max) [m/s^2]	3.572	3.838	***3.672***	3.604	2.516	2.815	***3.137***	3.218	1.505	1.416	***2.323***	1.881
Right												
δf(max) [rad]	0.271	0.310	0.256	***0.252***	0.200	0.215	0.212	***0.273***	0.241	0.270	0.263	***0.209***
ay(max) [m/s^2]	2.778	3.342	3.800	***3.783***	1.755	1.618	2.721	***1.412***	1.506	2.033	2.062	***1.440***

Table 4.11 – Maximum steer angle and total measured lateral acceleration for the left and right hand turns, the values in bold are those presented in Figure 4.46 and Figure 4.47

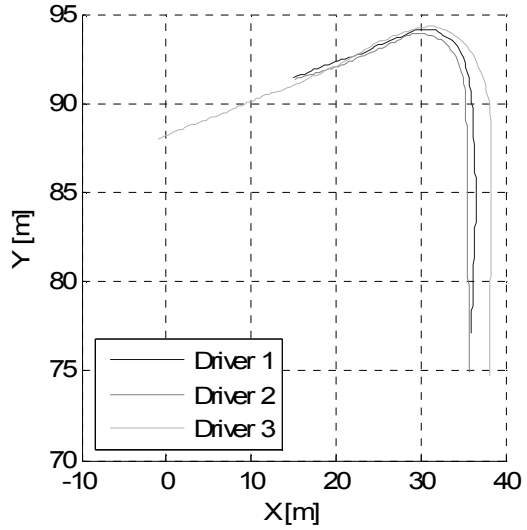

Figure 4.46 – Left hand turn path

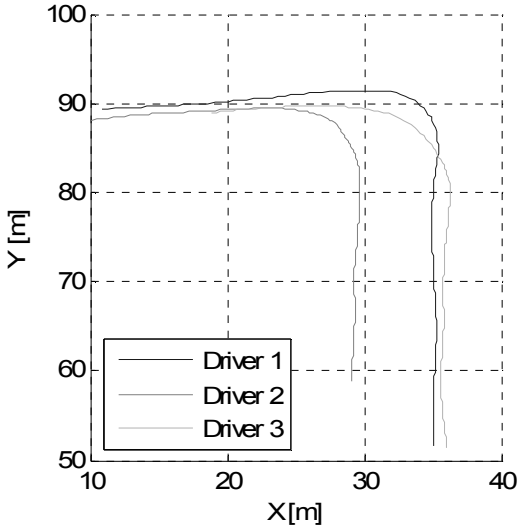

Figure 4.47 – Right hand turn path

As was noted in previous experiments, the relationship between the lateral acceleration and the tilt angle did not always follow the theoretical balanced relationship. At the start of the manoeuvre, the tilt angle was larger, because the tilt led the lateral acceleration in the process of tilting. After the apex of the turn, the tilt angle was smaller than its theoretical balanced value, because the vehicle was in the process of straightening up. From a control point of view, the theoretical balanced tilt angle would not be the value to aim for, but it would form the basis of the tilt angle demand depending on whether the vehicle were tilting or straightening.

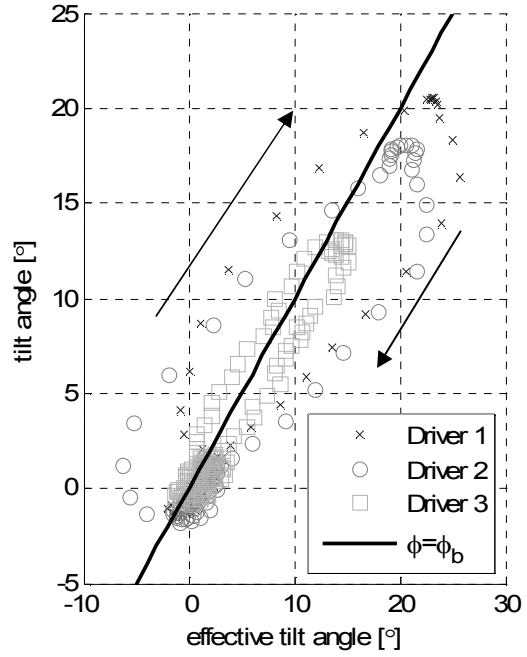

Figure 4.48 – Tilt angle variation with the lateral acceleration for a left hand 90° turn.

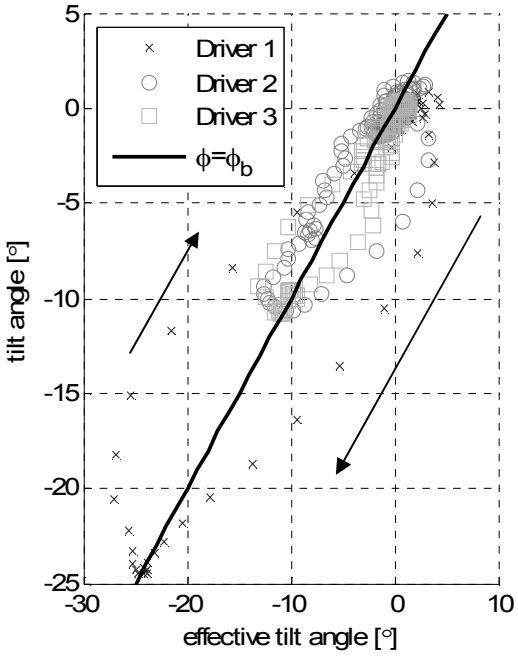

Figure 4.49 – Tilt angle variation with the lateral acceleration for a right hand 90° turn.

4.3.3.5 Steering Dynamics

The steering torque was estimated using equation (3.18). The typical trend of the steering torque during the left hand manoeuvre is shown in Figure 4.50 and Figure 4.51. These figures showed that countersteer was also manifested in the steering torque. After the 'counter-torque', the drivers rapidly applied a torque in the 'correct' direction to reach a maximum. In some cases, the applied torque then reduced by approximately 20%, to increase again to the original maximum value. This was attributed to an increase in steer in order to augment the lateral acceleration and straighten up the vehicle. Subsequently the applied torque decreased to approximately zero for straight ahead driving with the occasional adjustment.

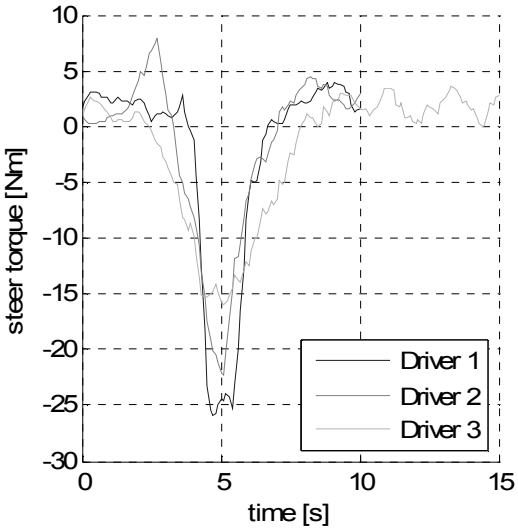

Figure 4.50 – Estimated steer torque for a left hand 90° turn.

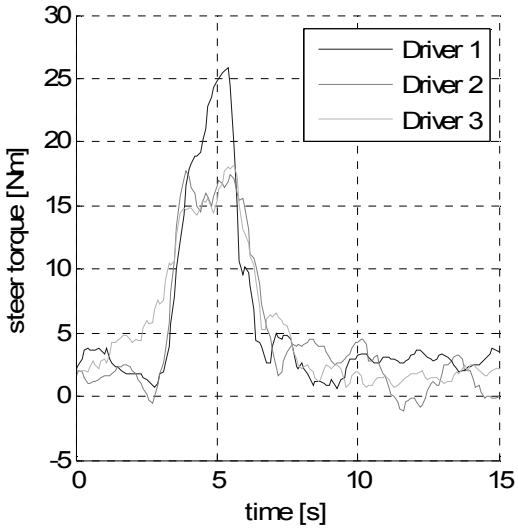

Figure 4.51 – Estimated steer torque for a right hand 90° turn.

The steering velocity was estimated by differentiating the steer angle data to improve the understanding of the drivers' steering actions. The steering velocity showed signs of countersteer: in Figure 4.52 the steering velocity at the start of the turn is negative indicating steer in the opposite direction of the turn (positive) and in Figure 4.53 the steering velocity is positive at the start of the turn, again indicating steer against the direction of the turn (negative). After countersteering, the velocity increased to reach the maximum steer angle, minor adjustments were made, and finally the steering velocity changed direction to return the handle bars to the straight ahead position. Though an estimated value, the steering velocity showed the driver behaviour well: many fast adjustments. It could be seen that driver 3 was adjusting his steering significantly more than driver 1.

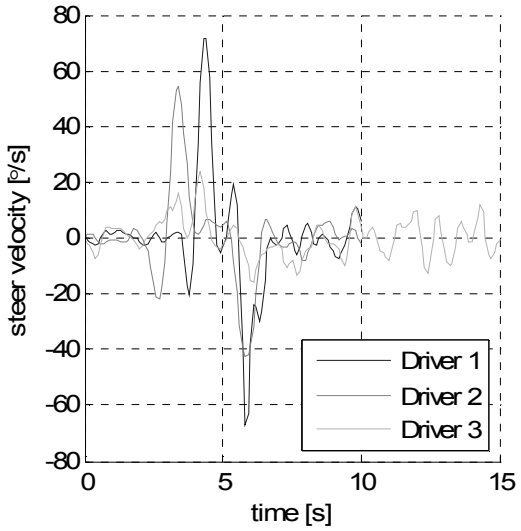

Figure 4.52 – Estimated steering velocity for a left hand turn

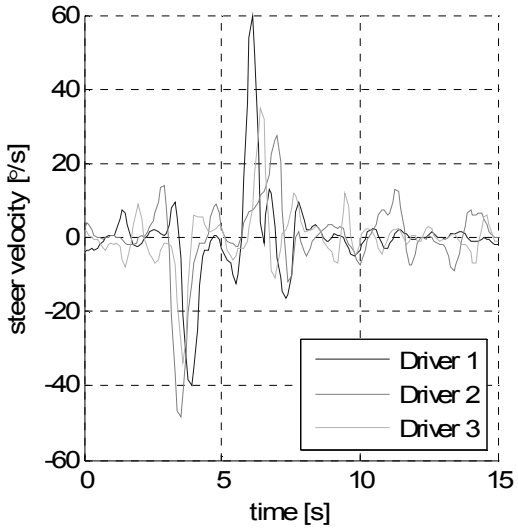

Figure 4.53 – Estimated steering velocity for a right hand turn

As was shown in equation (3.18), the steering torque was dependent on a large number of factors. Therefore, it would be difficult to determine any relationships between the torque and other variables. It was expected that the faster the manoeuvre, the larger the steering torque required to turn. Table 4.12 shows that such a relationship was not reflected in the results. In general, the steering acceleration and therefore velocity would only be a small component of the total steering torque, but Table 4.13 shows that the faster the countersteer, the larger the steering torque. This is important with regards to a steer tilt control system, which will be limited by the actuator: if the demand velocity is too great, the actuator may not be able to provide the torque. This table also shows that the approach velocity did not have an effect on the steering velocity. As would be expected, the faster the countersteer velocity, the larger the resultant maximum countersteer angle.

v_X(mean) [m/s]	3.4	3.4	3.4	3.2	3.5	3.9	3.7	3.8	3.6	3.4	3.5	3.2
v_X(at turn) [m/s]	2.9	3.1	3.2	2.9	3.5	3.6	3.6	3.7	3.3	2.9	3.4	3.1
T_s(max) [Nm]	-25.2	-29.9	-22.9	-25.5	-18.9	-18.7	-20.0	-18.1	-16.7	-15.0	-14.7	-14.6

Table 4.12 – Comparison of the maximum steer torque with the mean velocity and the velocity at the turning point.

v_X (c.s.max) [m/s]	3.65	4.00	3.40	3.90	3.95	4.05	4.35	4.85	4.75	3.70	4.60	3.40
T_s(c.s.max) [Nm]	3.82	1.29	1.61	0.85	2.55	0.60	1.42	1.37	0.97	3.16	4.01	2.90
$d\delta_f/dt$(c.s.max) [°/s]	16.62	20.05	17.19	9.74	18.33	5.16	3.44	10.31	8.02	17.19	25.21	12.03
δ_f(c.s.max) [°]	4.58	5.16	4.01	4.01	8.59	2.29	1.15	4.01	2.86	5.73	8.02	4.58

Table 4.13 – Comparison of the velocity, steer torque, steering velocity and steer angle at countersteer

4.4 CONCLUDING REMARKS

A range of manoeuvres were carried out with the instrumented Honda Gyro moped to improve the understanding of the dynamics of this vehicle and its driver. It was found that the vehicle understeered and therefore the Ackerman estimation of the total lateral acceleration would be inappropriate for the modelling of this vehicle, unless an 'understeer gain' was introduced. The inclination of the tilt axis did not have measurable effects on the dynamics of the vehicle under testing conditions. The range of the inclination axis and its effect on the vehicle under testing conditions was too small. Any additional steering adjustments from the driver caused by the changes in the vehicle dynamics would have been of a similar magnitude to any other small correcting adjustments. Carrying out a steady state test with a human driver was not possible, because the driver was unable to maintain a constant velocity or constant steering angle. Even though the steady state manoeuvre was not perfect, the estimated steering torque and measured perceived acceleration were expected to be small if not zero. It was found that, in reality, the steering torque could not be zero, due to gyroscopic effects and the steering geometry. So a zero measure of steering torque could not be used as a measure for a steer tilt controller to indicate steady state. Similarly, great care should be taken if using the perceived lateral acceleration in a steer tilt control system to determine if the vehicle is balanced. During the steady state manoeuvre, the driver tilted the vehicle to a tilt angle somewhat above or below the balanced tilt angle.

The transient manoeuvre results showed that the driver overleaned the vehicle with respect to the balanced tilt angle at the start of the turn to keep tilting. After the apex of the turn, the driver underleaned the vehicle in order to straighten it back up to the vertical. Tests where the driver wore a seatbelt demonstrated that in the case of a three-wheeled tilting vehicle in which the driver sits upright, the driver did not lean his upper body into or out of a turn. The best method to determine countersteer was by making the drivers negotiate single individual corners. The countersteer that was measured during these experiments did not exhibit any correlation with the

manoeuvre velocity, or the manoeuvre trajectory: countersteer and the period of time it was applied appeared arbitrary. The driver applied some countersteer to commence, change the direction, or stop the roll and made small steering adjustments to maintain balance. The steering velocity of the countersteer was found to affect the steering torque, an important factor when designing an active steer actuation system.

The dynamic measurement data from these experiments will be used in the following chapters to develop and validate a simulation model of a three-wheeled tilting vehicle. The characteristics of the driver behaviour that have been found will be used to develop a new STC algorithm.

CHAPTER 5. VEHICLE, TYRE AND DRIVER MODEL DEVELOPMENT

The experimental results presented in chapter 4 showed various characteristics of driver behaviour. The various dynamic measurements from the experimental testing will be used in this chapter to develop a simulation model of the vehicle. This model and the experimental results will then be used to determine the parameters of a Magic Formula model. This complete vehicle and tyre model were to be used in the development of a new roll control algorithm to demonstrate the performance of the controller when combined with the non-linear vehicle dynamics. The final section of this chapter discusses the development of a driver model. The purpose of the driver model was to include it in the vehicle model with roll controller and determine the driver's reaction to the steer controller's actions. The aim was to model a driver that simulated real driver behaviour.

5.1 VEHICLE MODELLING

5.1.1 Geometric Vehicle Model

The Ackermann vehicle model assumes that the vehicle can be modelled geometrically. Therefore, the lateral dynamics and the yaw dynamics can be calculated from the steer angle at the front wheel and the longitudinal velocity as seen in equations (2.5) and (2.6). No information is needed on the tyres.

Using the steer angle and velocity data from the experimental work presented in chapter 4, the total lateral acceleration and the yaw rate were calculated using the geometry based equations. The equations predicted a lateral acceleration and yaw rate within the same order of magnitude of the measured data as shown in Figure 5.1 and Figure 5.2. The geometric equations tended to overestimate the states. In chapter 4 the cornering characteristics of the vehicle were described as understeer, therefore the applied steer angle was larger than the geometric steady state steer angle

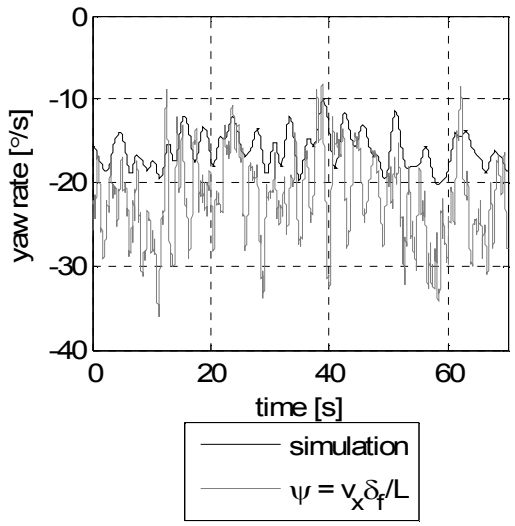

Figure 5.1 – Example of the difference between the measured yaw rate and the yaw rate estimated by the geometric model equations for a steady state manoeuvre: v_x = 6m/s and R = 22m so ψ = 15.6 °/s

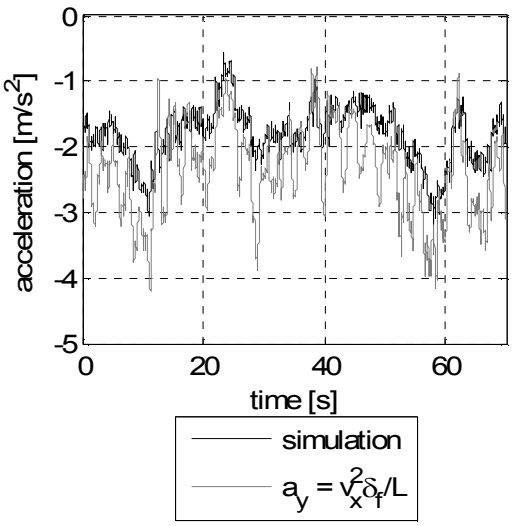

Figure 5.2 – Example of the difference between the measured lateral acceleration and the acceleration estimated by the geometric model equations for a steady state manoeuvre: v_x = 6m/s and R = 22m so $a_{centripetal}$ = 1.64 m/s²

It is clear that the measured accelerations are subject to noise, which is less evident on the accelerations predicted by the geometric model. However, there is still some inherent mismatch between the two. Therefore, this model was found to be inadequate for the development of a steer tilt controller. There were also concerns over the fact that the model did not include non-linearities and delays from the tyre or higher order dynamics.

5.1.2 Dynamic Vehicle Model

The geometric vehicle model was found to be too simple and lacking too many dynamic effects. The model presented in this section assumes that the forces causing the motion come from the tyres and the tyre forces are a result of the slip angle and camber angle. The relationships between the tyre forces and the lateral and yaw dynamics are presented in equations (5.1) and (5.3) respectively. This model is adapted from Pacejka [45]. Equation (5.1) describes the linearised lateral dynamics. The linearization assumption is that the steer angle is sufficiently small that $\sin(\delta_f)$ can be approximated by δ_f, and $\cos(\delta_f)$ is 1. It shows how the lateral tyre forces not only cause the lateral acceleration, but also components of the yaw, roll and steer acceleration because of the steering geometry where k and e are geometric variables illustrated in Figure 3.14. The aim is to determine a vehicle model which includes all the important dynamics, but which does not require many higher order terms. The experimental data from section 4.3.3 were used to determine the magnitude of each term in equation (5.1). It was found that the yaw acceleration of

the front assembly and the steer acceleration of the front assembly were significantly smaller than the other terms. In theory, for a constant velocity manoeuvre, the longitudinal force is small, so this term can generally be assumed negligible. However, when comparing the model estimates with experimental results from section 4.3.3, this term should be included, because the forward velocity is not strictly constant. The resulting lateral dynamics equation is equation (5.2).

$$\begin{aligned} F_{\mathrm{Yf}} + F_{\mathrm{Yr}} = \quad & m\left(\dot{v_{\mathrm{Y}}} + v_{\mathrm{X}}\dot{\psi}\right) + \\ & + m_{\mathrm{f}}\, k\ddot{\psi} + m_{\mathrm{c}} h_{\mathrm{c}}\ddot{\phi} + m_{\mathrm{f}}\, e\ddot{\delta}_{\mathrm{f}} - \\ & - F_{\mathrm{Xf}} \cos(\varepsilon)\, \delta_{\mathrm{f}} \end{aligned} \tag{5.1}$$

Table 5.1 – Typical peak transient force values in Newton for each term in the lateral dynamics equation when turning 90° corners

$m\left(\dot{v_{\mathrm{Y}}} + v_{\mathrm{X}}\dot{\psi}\right)$	600	600	700	725	630	600	800	750	700
$m_{\mathrm{f}}\, k\ddot{\psi}$	6.00	6.00	8.00	5.50	5.00	5.00	10.0	8.00	7.00
$m_{\mathrm{c}} h_{\mathrm{c}}\ddot{\phi}$	50.0	50.0	51.0	45.0	24.0	26.0	30.0	40.0	24.0
$m_{\mathrm{f}}\, e\ddot{\delta}_{\mathrm{f}}$	0.48	0.46	0.43	0.31	0.23	0.25	0.22	0.38	0.18
$F_{\mathrm{Xf}} \cos(\varepsilon)\, \delta_{\mathrm{f}}$	24.0	33.5	8.20	8.00	8.00	20.0	13.0	21.5	20.0

$$F_{\mathrm{Yf}} + F_{\mathrm{Yr}} = m\left(\dot{v_{\mathrm{Y}}} + v_{\mathrm{X}}\dot{\psi}\right) + m_{\mathrm{c}} h_{\mathrm{c}}\ddot{\phi} - F_{\mathrm{Xf}} \cos(\varepsilon)\, \delta_{\mathrm{f}} \tag{5.2}$$

Equation (5.3) describes the linearised yaw dynamics. The elements of this equation were also analysed to determine which terms were negligible. Firstly, the aligning moment from the tyres was not known. In comparison with the tyre forces, these were assumed to be small.

Table 5.2 shows that the lateral acceleration of the steering assembly had a more important effect on the dynamics than the yaw acceleration of this assembly had on the lateral dynamics. The steer acceleration component and the gyroscopic components were negligibly small. The drag force component was small. The longitudinal force component would be small under theoretical constant velocity conditions; however, it should be included in the model comparison. When the small terms of equation (5.3) are omitted, the yaw dynamics can be defined by equation (5.4).

$$\begin{aligned} a F_{\mathrm{Yf}} - b F_{\mathrm{Yr}} + M_{\mathrm{Zf}} + M_{\mathrm{Zr}} = \quad & m_{\mathrm{f}}\, k \left(\dot{v}_{\mathrm{Y}} + v_{\mathrm{X}} \dot{\psi} \right) + \\ & + I_{\mathrm{Z}} \ddot{\psi} + I_{\mathrm{XZc}} \ddot{\phi} + \left(m_{\mathrm{f}}\, e\, k + I_{\mathrm{Zf}} \cos(\varepsilon) \right) \ddot{\delta}_{\mathrm{f}} - \\ & - I_{\mathrm{Yw}} \dot{\phi} \omega_{\mathrm{w}} - I_{\mathrm{Yw}} \sin(\varepsilon)\, \dot{\delta}_{\mathrm{f}} \omega_{\mathrm{w}} - \\ & - F_{\mathrm{D}} h_{\mathrm{D}} \phi - F_{\mathrm{Xf}} \left(t_{\mathrm{t}} + a \cos(\varepsilon) \right) \delta_{\mathrm{f}} \end{aligned} \tag{5.3}$$

Table 5.2 – Typical peak transient moment values in Newton meters for each term in the yaw dynamics equation when turning 90° corners

$m_{\mathrm{f}}\, k \left(\dot{v}_{\mathrm{Y}} + v_{\mathrm{X}} \dot{\psi} \right)$	10.0	12.0	14.0	14.0	13.8	13.4	17.4	16.4	15.0
$I_{\mathrm{Z}} \ddot{\psi}$	55.0	58.0	70.0	50.0	41.0	42.0	90.0	60.0	58.0
$I_{\mathrm{XZc}} \ddot{\phi}$	22.0	25.0	22.0	20.0	10.0	12.0	12.8	18.0	11.0
$\left(m_{\mathrm{f}}\, e\, k + I_{\mathrm{Zf}} \cos(\varepsilon) \right) \ddot{\delta}_{\mathrm{f}}$	1.40	1.35	1.25	0.90	0.75	0.77	0.75	0.76	0.45

$I_{Yw}\sin(\varepsilon)\dot{\delta}_f\omega_w$	0.22	0.24	0.25	0.21	0.20	0.24	0.25	0.23	0.19
$I_{Yw}\dot{\phi}\omega_w$	0.34	0.42	0.34	0.30	0.24	0.30	0.44	0.41	0.35
$F_D h_D \phi$	0.60	0.60	0.80	0.66	0.60	0.70	1.00	0.85	0.90
$F_{Xf}(t_t + a\cos(\varepsilon))\delta_f$	29.0	45.5	10.4	11.1	12.0	29.0	18.0	28.0	27.5

$$aF_{Yf} - bF_{Yr} = m_f k\left(\dot{v_Y} + v_X\dot{\psi}\right) + I_Z\ddot{\psi} + I_{XZc}\ddot{\phi} - F_{Xf}(t_t + a\cos(\varepsilon))\delta_f \quad (5.4)$$

5.1.3 Roll Model

The roll models presented in the literature were two dimensional inverted pendulum equations. The roll acceleration was assumed to balance the components of the lateral acceleration and the gravitational acceleration of the tilt assembly. In a more complex vehicle context, the roll acceleration is a part of the roll equation that also includes the product of inertia of the cabin, gyroscopic effects, the steer moment and the overturning moment from the front tyre, see equation (5.5).

Table 5.3 illustrates that the steer and gyroscopic moments were small in comparison to the effect of lateral acceleration and rotational accelerations as shown in

Table 5.3. If the overturning moment and the normal force and weight component acting on the steer assembly are assumed negligible, the roll equation can be reduced to (5.6). However,

Table 5.3 shows that these moments are of a similar order of magnitude as the moment from the product inertia of the cabin, so equation (5.7) was used as the equation to determine the roll dynamics.

$$
\begin{aligned}
M_{xf} = \quad & m_c h_c \left(\dot{v_Y} + v_X \dot{\psi} \right) \cos(\phi) + \\
& + I_{XZc} \ddot{\psi} + \left(m_c h_c^2 + I_{Xc} \right) \ddot{\phi} + \left(m_f \, e \, h_f + I_{Zf} \sin(\varepsilon) \right) \ddot{\delta}_f + \\
& + I_{Yw} \dot{\psi} \omega_w + I_{Yw} \cos(\varepsilon) \dot{\delta}_f \omega_w - \\
& - \left(t_t F_{Zf} + m_f \, e \, g \right) \delta_f - m_c h_c g \sin(\phi)
\end{aligned}
\tag{5.5}
$$

$$
\begin{aligned}
0 = \quad & m_c h_c \left(\dot{v_Y} + v_X \dot{\psi} \right) \cos(\phi) + \\
& + I_{XZc} \ddot{\psi} + \left(m_c h_c^2 + I_{Xc} \right) \ddot{\phi} - \\
& - m_c h_c g \sin(\phi)
\end{aligned}
\tag{5.6}
$$

$$
\begin{aligned}
M_{xf} = \quad & m_c h_c \left(\dot{v_Y} + v_X \dot{\psi} \right) \cos(\phi) + \\
& + I_{XZc} \ddot{\psi} + \left(m_c h_c^2 + I_{Xc} \right) \ddot{\phi} - \\
& - \left(t_t F_{Zf} + m_f \, e \, g \right) \delta_f - m_c h_c g \sin(\phi)
\end{aligned}
\tag{5.7}
$$

Table 5.3 – Typical peak transient values in Nm for each term in the roll dynamics equation when turning 90º corners

$m_c h_c \left(\dot{v_Y} + v_X \dot{\psi} \right) \cos(\phi)$	200	230	250	275	220	210	270	255	240
$I_{XZc} \ddot{\psi}$	50.0	50.0	70.0	50.0	35.0	35.0	66.0	52.0	51.0
$\left(m_c h_c^2 + I_{Xc} \right) \ddot{\phi}$	50.0	45.0	52.0	45.0	21.5	22.0	30.0	33.0	20.7
$\left(m_f \, e \, h_f + I_{Zf} \sin(\varepsilon) \right) \ddot{\delta}_f$	0.80	0.75	0.70	0.50	0.42	0.43	0.41	0.42	0.25
$I_{Yw} \cos(\varepsilon) \dot{\delta}_f \omega_w$	0.40	0.40	0.43	0.36	0.36	0.41	0.43	0.40	0.33
$I_{Yw} \dot{\psi} \omega_w$	0.90	0.86	0.95	0.88	0.75	0.73	1.24	1.06	1.00
$m_c h_c g \sin(\phi)$	260	274	272	253	174	178	211	203	206
$\left(t_t F_{Zf} + m_f \, e \, g \right) \delta_f$	39.0	40.0	35.0	37.0	28.5	27.0	26.0	28.0	26.0

$M_{Xf} \approx R_{Tf} F_{Zf} \gamma_f$	23.6	24.7	23.1	21.1	17.1	17.3	18.4	19.8	17.7

5.2 TYRE MEASUREMENT AND PREDICTION

Chapter 3 discussed the merits and weaknesses of a range of tyre modelling methods. It was concluded that the Magic Formula was the best data-fitting model to be used in the vehicle simulation. The aim of this section is to determine how the experimental data from the chapter 4 can be used to estimate the side forces, sideslip and camber angles, and identify the Magic Formula parameters to match these data. Different variations of the Magic Formula model have been tested for both the front and rear wheels in order to ensure that the best possible fit was found.

5.2.1 Parameter Estimation

The Magic Formula model offers a mathematical function where the parameters can be tuned to match experimental data. These parameters can be determined using an optimisation routine. In the following section, two methods of optimisation are discussed.

5.2.1.1 Using Force and Slip Angle

Plotting the slip angle against the force data gives a starting point for the parameter estimation. As shown in Figure 2.37, the values for the slope of the tyre's linear region, the maximum force and the slip angle at which is occurs, and the vertical and horizontal shift can be approximated. This gives the starting point of the optimisation routine. The optimisation routine changes the value of one of the parameters, calculates the force for every slip angle, compares this force with the experimental force and determines the overall error. The optimisation sequence continues until a minimum error is found.

5.2.1.2 Using the Vehicle Model

If slip angle data are not available or not sufficiently accurate, determining the tyre model parameters from the experimental vehicle dynamics data may seem a challenge. However, a method was found that was shown to produce satisfactory results. The principle is that a vehicle is simulated using the same steer, roll, and velocity inputs as were measured in the experiments, and the tyre parameters are set so that the simulation tracks the measured trajectory and therefore yaw rate and lateral acceleration.

The simulation model of the Honda Gyro as discussed in section 0 was used to derive the tyre characteristics. The inputs to this model were the steer angle, roll angle and forward velocity as

were measured in the single 90° corner experiments. The model outputs were the x and y coordinates of the vehicle and the heading angle. The optimisation function was set to minimise the error between the model outputs and their experimentally measured counterparts by changing the tyre parameters. Unlike the previous method where the initial values of the tyre model parameters could be estimated from the test results, here the initial values were based on tyre parameters of known motorcycle/car tyre models from Pacejka [52] and [45] and Blundell [68]. The final tyre model could finally be verified against other experimental data obtained by the author to ensure that the tyre model was not optimised for a single type of manoeuvre.

5.2.2 Experimental Results

In this work conventional tyre testing equipment was not available, and, in any case, the procedure would be very costly. The tyre would have to be tested for a number of loading conditions, for a range of slip angles, and in the case of a scooter tyre, a range of camber angles. These extensive data files would result in a very accurate picture of the tyre characteristics. Even then, these would change with tyre wear, temperature and road surface. The following section describes how the tyre characteristics of the Honda Gyro were approximated using basic experimental data.

5.2.2.1 State Estimation from GPS

The hypothesis was that if the vehicle states were known, the forces and slip angles could be estimated. When the side forces were plotted against the slip angles and camber angles, the tyre characteristics could be derived. Bevly et al. [114] presented a method to combine GPS measurements for heading with gyroscope yaw rate measurements to estimate the vehicle states. The GPS equipment available in Bevly's tests provided the course angle, which is the vehicle sideslip plus the heading angle. The gyroscope provided the yaw rate and the bias. It was shown by Bevly et al. that the method could successfully estimate the vehicle states and that the accuracy of the GPS system was good enough to be safely used in vehicle safety systems. The GPS method was later improved by putting the measurements through a Kalman filter to estimate the vehicle sideslip, the yaw rate and the heading angle, as well as the bias of the gyroscopic sensor (Anderson and Bevly [115]). This method was tested both in simulation and experimentally. The introduction of the Kalman filter resulted in better estimates of sideslip and yaw rate than the simple, model based methods. Besides estimating the vehicle states, the Kalman filter method successfully estimated the tyre cornering stiffness. The results obtained by Anderson and Bevly confirmed that dynamic vehicle measurements could be used to derive tyre properties but highlighted the need for proper data processing to derive accurate values.

5.2.2.2 Force Estimation

The equations for the lateral and yaw dynamics are given by equation (5.2) and equation (5.4) respectively. The terms on the right hand side of the equations were either measured in the experiments, or they could be derived from the measurements: the total lateral acceleration was measured, the yaw, roll and steer angles were measured and were differentiated twice for the second order terms, and the longitudinal force of the front tyre could be estimated from the longitudinal acceleration using equation (5.8). By solving equations (5.2) and (5.4) simultaneously, the side forces can be estimated.

$$\text{if } a_x \geq 0 \;\; F_{xf} = 0$$

$$\text{if } a_x < 0 \;\; F_{xf} = \frac{F_{zf}}{mg}\left(ma_x + C_D v_x^2\right) \tag{5.8}$$

The individual cornering results (see section 5.3.3) were used to determine the lateral forces, because the largest accelerations were measured and therefore the greatest range of forces was expected from these results. Figure 5.3 shows typical force estimation for a single corner. This figure represents a left hand turn by driver 1.

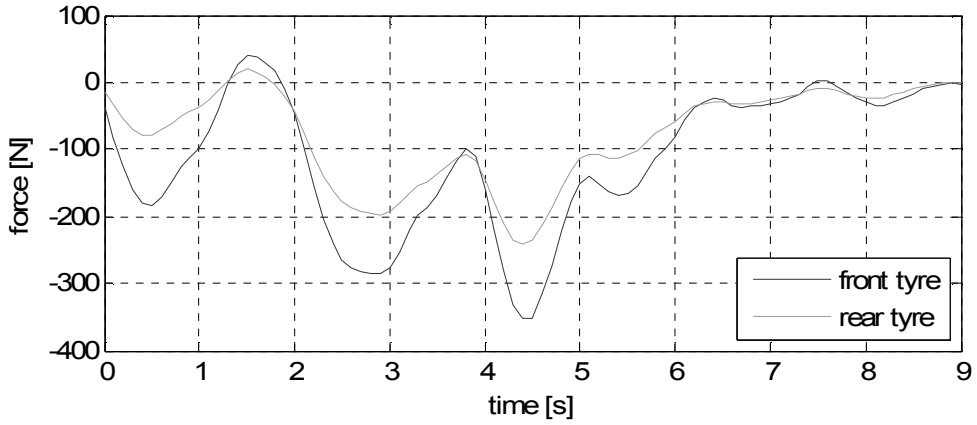

Figure 5.3 – Example of estimated lateral force at the front tyre and one of the rear tyres

5.2.2.3 Camber Angle Estimation

The camber angle was estimated from the steer and roll angle measurements using equation (3.2). Figure 5.4 shows how the camber angle changes throughout the cornering manoeuvre and how it compares to the roll angle. This camber angle corresponds to the force presented in Figure 5.3.

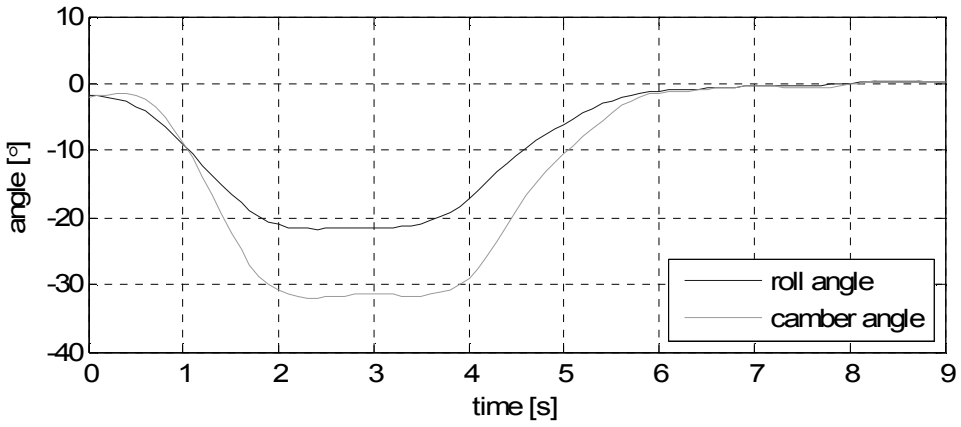

Figure 5.4 – Example of typical estimated camber angle of the front tyre in comparison to the roll angle

5.2.2.4 Slip Angle Estimation

Theoretically, the slip angles of the front and the rear wheels can be calculated using equation 2.14. In practice, the lateral acceleration measurement was found to contain too much noise to integrate; therefore, the lateral velocity measurement was not available.

Various attempts were made to estimate the lateral velocity and therefore the slip angle from the experimental results, but noise contamination prevented a successful outcome. Hence, vehicle simulations emulating the test manoeuvre were used to estimate the magnitude of the slip angles. These simulations gave a value to aim for and a starting point for the relationship between the force and the slip angle. Ultimately, the exact slip angle could not be estimated from the experimental data.

5.2.3 Front Tyre Modelling

Three Magic Formula model variations for the front tyre were selected to be optimised with the vehicle model. The first two models had been presented in the literature to characterize a motorcycle tyre. The equations for the first model were very similar to those of the original Magic Formula model as discussed in chapter 4. The second model had been adapted more substantially to represent the force generation in a motorcycle tyre. The equations of the third model were based on those of the second model, but simplified using the definitions of various components.

5.2.3.1 Model 1: Basic Magic Formula Model

The Magic Formula model variation presented in this section, equation (5.9), is based on the model presented in section 11.2.4 of Pacejka [45]. Even though the model is to represent a motorcycle tyre, it assumes that effects of the camber on the maximum force D, the slope in the

linear region K, and the horizontal and vertical shifts, are adequate to model the significant role the camber plays in the force generation of a motorcycle tyre. This equation assumes pure slip or small longitudinal slip conditions. It should be noted that this is the simplest form of the Magic Formula where the shape factor E is omitted.

$$
\begin{aligned}
Y &= D\sin\left(C\tan^{-1}\left(Bx\right)\right) + S_{\mathrm{V}} \\
x &= S_{\mathrm{H}} + \left(\alpha_{\mathrm{f}} + S_{\mathrm{H}f}\right) D/D_0 - S_{\mathrm{H}f} \\
C &= d_8 \\
D_0 &= \frac{d_4 F_{\mathrm{zf}}}{1 + d_7\gamma^2} \\
D &= \sqrt{D_0^2 + F_{\mathrm{xf}}^2} \\
C_{\mathrm{fa0}} &= d_1 F_{\mathrm{zf0}} + d_2\left(F_{\mathrm{zf}} - F_{\mathrm{zf0}}\right) \\
C_{\mathrm{fa}} &= \frac{C_{\mathrm{fa0}}}{1 + d_5\gamma^2} \\
K &= C_{\mathrm{fa}} \\
B &= \frac{K}{CD_0} \\
S_{\mathrm{H}f} &= \frac{d_3 F_{\mathrm{zf}}\gamma}{K} \\
S_{\mathrm{V}} &= d_6 F_{\mathrm{zf}}\gamma D/D_0 \\
S_{\mathrm{H}} &= S_{\mathrm{H}f} - S_{\mathrm{V}}/K
\end{aligned}
\tag{5.9}
$$

Table 5.4 contains the initial values of the parameters used for the optimisation routine. The values are based on a known motorcycle front tyre model from section 11.2.4 of Pacejka [45]. Figure 5.5 shows the resulting tyre characteristics of this tyre model for a range of slip and camber angles. This figure shows that the camber angle has a relatively small effect on the total side force produced by the tyres. However, it would be interesting to establish how this basic model performs in simulation.

	d_1	d_2	d_3	d_4	d_5	d_6	d_7	d_8
Initial Values	14.0	9.00	0.80	1.20	0.15	0.10	0.15	1.60

Table 5.4 – Magic Formula parameters for the first front tyre model

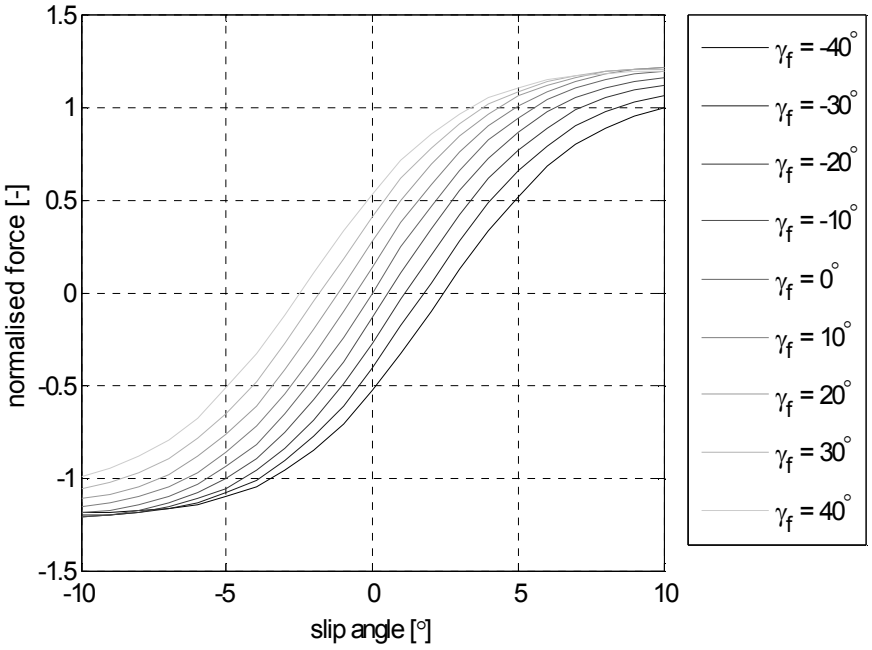

Figure 5.5 – Normalised force variation with slip angle and camber angle for the Magic Formula from equation (5.9) with parameter values from Table 5.4

5.2.3.2 Model 2: Complex Motorcycle Magic Formula Model

Equation (5.10) presents the motorcycle Magic Formula model from section 11.6.1 Pacejka [45]. This version of the model treats the force generation from slip and camber equally, resulting in an increase in the total number of parameters in comparison to the previous model. However, it is more motorcycle specific than the previous model and it is thought that it will result in a better representation of the tyre characteristics. Note that the model assumes pure slip or small longitudinal forces.

$$
\begin{aligned}
Y &= D\sin[C_\alpha \tan^{-1}\left(B_\alpha\alpha - E_\alpha\left(B_\alpha\alpha - \tan^{-1}\left(B_\alpha\alpha\right)\right)\right) + \\
&\qquad C_\gamma \tan^{-1}\left(B_\gamma\gamma - E_\gamma\left(B_\gamma\gamma - \tan^{-1}\left(B_\gamma\gamma\right)\right)\right)] \\
\alpha &= \alpha_f + |S_{H\alpha}| \\
C_\alpha &= d_1 \\
D &= \mu F_{zf} \\
\mu &= \frac{d_2 e^{(d_3 \Delta F_{zf})}}{1 + d_4\gamma^2} \\
E_\alpha &= (d_8|\gamma| + d_7)\,\mathrm{sign}\,(x) + d_6\gamma^2 + d_5 \\
K_{\alpha 0} &= d_9 F_{z0} \sin\left(d_{10}\tan^{-1}\left(\frac{F_{zf}}{F_{z0}\left(d_{11} + d_{12}\gamma^2\right)}\right)\right) \\
K_\alpha &= \frac{K_{\alpha 0}}{1 + d_{13}\gamma^2} \\
B_\alpha &= \frac{K_\alpha}{C_\alpha D} \\
S_{H\alpha} &= d_{14} \\
C_\gamma &= d_{15} \\
K_\gamma &= F_{zf}\left(d_{16} + d_{17}\Delta F_{zf}\right) \\
E_\gamma &= d_{18} \\
B_\gamma &= \frac{K_\gamma}{C_\gamma D}
\end{aligned}
\tag{5.10}
$$

Table 5.5 shows the starting values of the model parameters before the optimisation routine. The aim was to keep the parameters similar to those in Table 5.4 and estimate the rest so that the zero camber characteristics shown in Figure 5.6 matched the previous model, and the non-zero camber characteristics matched those expected from a motorcycle tyre model, Figure 5.7.

	d_1	d_2	d_3	d_4	d_5	d_6
Initial Values	1.60	1.20	0.10	0.15	0.10	0.10
	d_7	d_8	d_9	d_{10}	d_{11}	d_{12}
Initial Values	0.10	0.10	14.0	1.00	1.00	1.00
	d_{13}	d_{14}	d_{15}	d_{16}	d_{17}	d_{18}
Initial Values	0.15	0.00	1.60	14.0	1.00	-1.00

Table 5.5 – Magic Formula Parameters for the second front tyre model

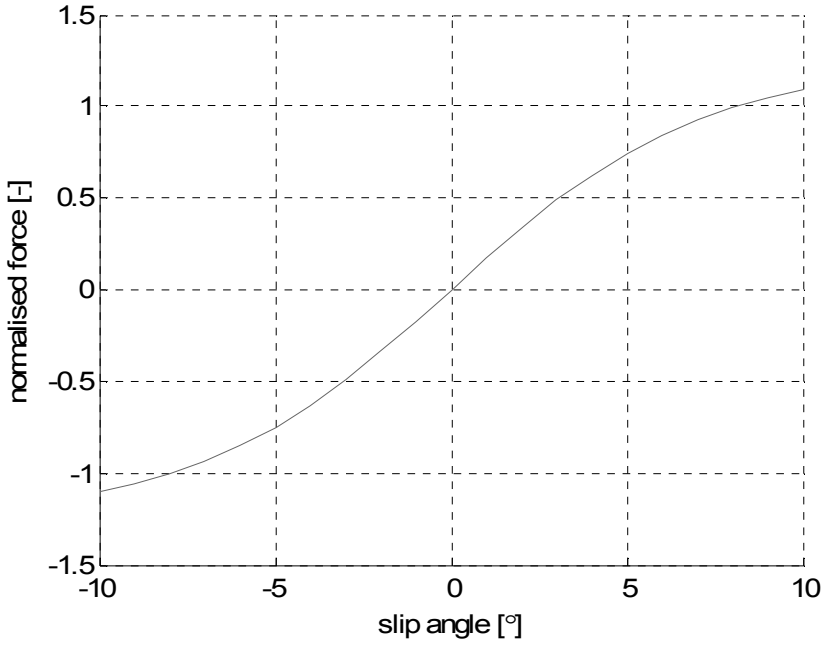

Figure 5.6 – Tyre characteristics with slip angle and zero camber of the tyre model from equation (5.10) and with parameters from Table 5.5

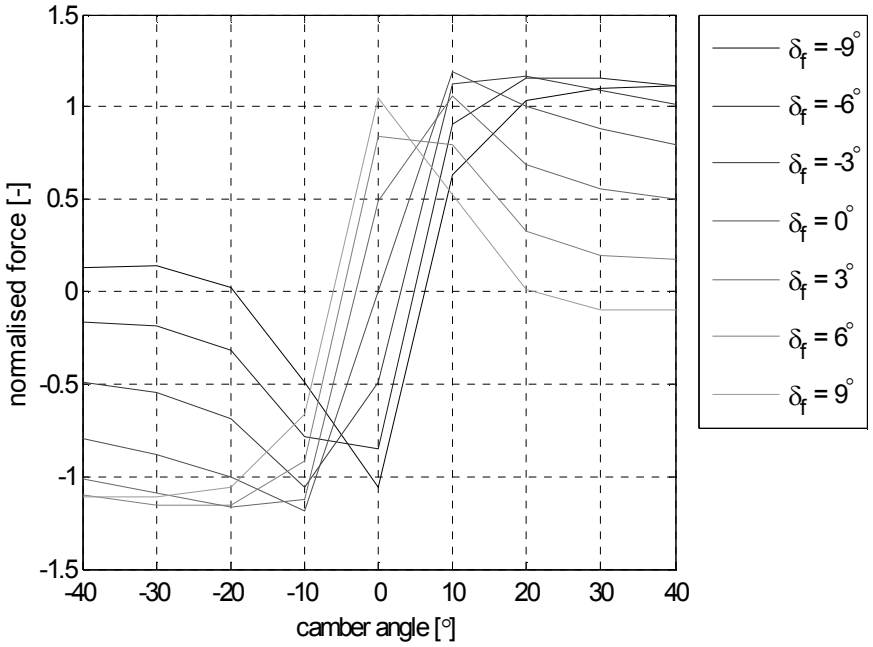

Figure 5.7 – Tyre characteristics of the tyre model from equation (5.10) and with parameters from Table 5.5 varying with camber and slip angle

5.2.3.3 Model 3: Simplified Motorcycle Model

The model presented in equation (5.11) was based on the previous model (5.10), but simplified. The reason for simplifying the model was to limit to total number of parameters that needed to be found in the optimisation process.

$$
\begin{aligned}
Y \quad &= D\sin[C_\alpha \tan^{-1}\left(B_\alpha\alpha - E_\alpha\left(B_\alpha\alpha - \tan^{-1}\left(B_\alpha\alpha\right)\right)\right) + \\
&\quad C_\gamma \tan^{-1}\left(B_\gamma\gamma - E_\gamma\left(B_\gamma\gamma - \tan^{-1}\left(B_\gamma\gamma\right)\right)\right)] \\
C_\alpha &= d_4 \\
D_0 &= \frac{d_2 F_{zf}}{1 + d_3\gamma^2} \\
D &= \sqrt{D_0^2 - F_{xf}^2} \\
E_\alpha &= \frac{B_\alpha d_6 - \tan(\pi/2C_\alpha)}{(B_\alpha d_6 - \tan^{-1}(B_\alpha d_6))} \\
K_\alpha &= d_0 F_{zf} \\
B_\alpha &= \frac{K_\alpha}{C_\alpha D_0} \\
C_\gamma &= d_5 \\
K_\gamma &= d_1 F_{zf} \\
E_\gamma &= \frac{B_\gamma d_7 - \tan(\pi/2C_\gamma)}{(B_\gamma d_7 - \tan^{-1}(B_\gamma d_7))} \\
B_\gamma &= \frac{K_\gamma}{C_\gamma D_0}
\end{aligned}
\tag{5.11}
$$

Table 5.6 shows the model parameters at the start of the optimisation process. These parameters resulted in the tyre characteristics shown in Figure 5.8 and Figure 5.9. These figures show that this model attributes a greater amount of side force to the camber angle in comparison to the first model, but not as much as the second model: Its characteristics lie in between the two models. It was expected that the tyre sideslip angle did contribute noticeably to the total force generated at the tyre contact patch, as the driver had applied large steering angles during the experiments. In a tyre model this should translate to significant changes in the lateral force as a result of the slip.

	d_0	d_1	d_2	d_3	d_4	d_5	d_6	d_7
Initial Value	14.0	0.80	1.20	0.15	1.60	1.60	0.105	0.61

Table 5.6 – Magic Formula Parameters for the third front tyre model

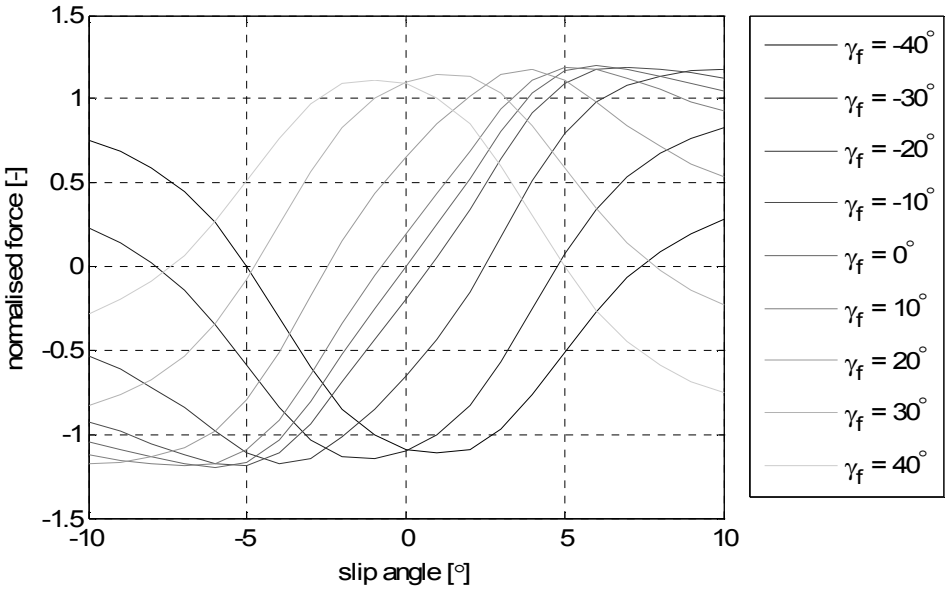

Figure 5.8 – Simplified motorcycle tyre model characteristics from equation (5.11) with the parameters from Table 5.6 showing variation with slip angle for a range of camber angles

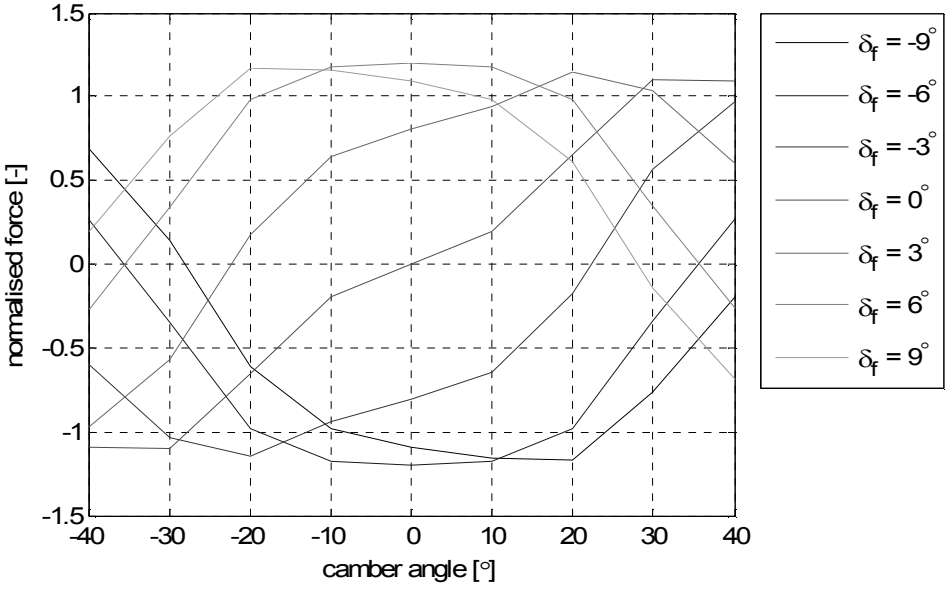

Figure 5.9 – Simplified motorcycle tyre model characteristics from equation (5.11) with the parameters from Table 5.6 showing variation with camber angle for a range of slip angles

5.2.4 Rear Tyre Modelling

The rear tyres were assumed to behave like car tyres, as the rear unit did not tilt and introduce significant camber. The rear tyre models originate from Blundell [68] and Pacejka [45] with the final model being a simplified version of the original Magic Formula model [69]. It was assumed that the camber angle at the rear tyres was negligible considering the manoeuvre velocity, the track width, and the wheel mounting.

5.2.4.1 Model 1: Basic Car tyre model

Equation (5.12) shows the Magic Formula equation as given in Blundell [68]. This equation is similar to the original model, Pacejka [69]. The curvature factor E includes the direction of the slip angle, ensuring that the tyre characteristics are approximately symmetrical in the positive and negative slip angle plane.

$$
\begin{aligned}
Y &= D\sin\left(C\tan^{-1}\left(B\alpha - E\left(B\alpha - \tan^{-1}\left(B\alpha\right)\right)\right)\right) + S_{\mathrm{V}} \\
\alpha &= \alpha_{\mathrm{r}} + S_{\mathrm{H}} \\
C &= d_0 \\
D &= \mu F_{\mathrm{zr}} \\
\mu &= d_1 F_{\mathrm{zr}} + d_2 \\
E &= \left(d_6 F_{\mathrm{zr}} + d_7\right)\left(1 - d_{17}\mathrm{sign}\left(\alpha\right)\right) \\
BCD &= d_3 \sin\left(2\tan^{-1}\left(F_{\mathrm{zr}}/d_4\right)\right) \\
B &= \frac{BCD}{CD} \\
S_{\mathrm{H}} &= d_9 + d_8 F_{\mathrm{zr}} \\
S_{\mathrm{V}} &= d_{12} + d_{11} F_{\mathrm{zr}}
\end{aligned}
\tag{5.12}
$$

Table 5.7 contains the starting values for the optimisation routine. These values were taken from the original model by Blundell. Figure 5.10 shows the characteristics of this model with sideslip angle. It can be seen that with the parameters from Table 5.7 the resulting characteristics are different depending on the slip angle direction. In practice, it would be preferable if the tyre characteristics did not vary with the direction of the slip angle.

	d_0	d_1	d_2	d_3	d_4	d_6
Initial Value	1.034	-0.2245e-5	1.322	0.6040e5	0.8777e4	0.4581e-4
	d_7	d_8	d_9	d_{11}	d_{12}	d_{17}
Initial Value	0.4682	0.3819e-6	0.5162e-2	-0.3664e-1	-0.5689e2	0.3799

Table 5.7 – Magic Formula model parameters for the first rear tyre model

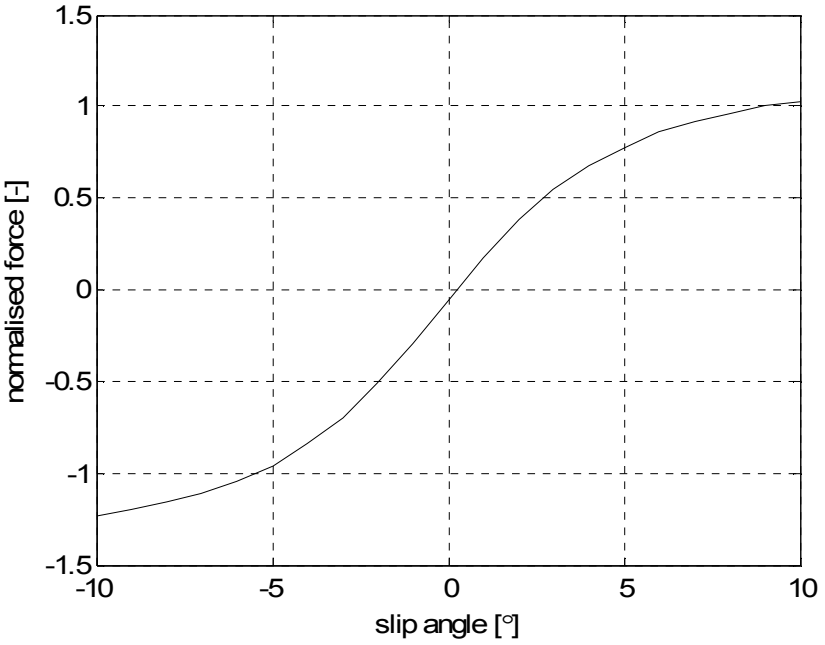

Figure 5.10 – Car tyre model characteristics from equation (5.12) with the parameters from Table 5.7 showing normalised force for a range of slip angles

5.2.4.2 Model 2: Magic Formula Model (1997)

Equation (5.13) is the Magic Formula model a presented by Pacejka and Besselink [97]. It is similar to the previous model, but it uses the vertical force F_{Zr} as well as the proportional change in load ΔF_{Zr}.

$$
\begin{aligned}
Y &= D\sin\left(C\tan^{-1}\left(B\alpha - E\left(B\alpha - \tan^{-1}\left(B\alpha\right)\right)\right)\right) + S_{\mathrm{V}} \\
\alpha &= \alpha_{\mathrm{r}} + S_{\mathrm{H}} \\
C &= d_1 \\
D &= \mu F_{\mathrm{zr}} \\
\mu &= d_3\Delta F_{\mathrm{zr}} + d_2 \\
E &= \left(d_6\Delta F_{\mathrm{zr}} + d_5\right)\left(1 - d_8\mathrm{sign}\left(\alpha\right)\right) \\
BCD &= d_{10}F_{\mathrm{zr0}}\sin\left(d_{11}\tan^{-1}\left(F_{\mathrm{zr}}/\left(d_{12}F_{\mathrm{zr0}}\right)\right)\right) \\
B &= \frac{BCD}{CD} \\
S_{\mathrm{H}} &= d_{15} + d_{16}\Delta F_{\mathrm{zr}} \\
S_{\mathrm{V}} &= \left(d_{17} + d_{18}\Delta F_{\mathrm{zr}}\right)F_{\mathrm{zr}}
\end{aligned}
\tag{5.13}
$$

The optimisation starting parameters shown in Table 5.8 have been adjusted from those in Table 5.7 to give similar tyre characteristics. These characteristics are shown in Figure 5.11, which indicates them to be more symmetrical than Figure 5.10.

	d_1	d_2	d_3	d_5	d_6	d_8	d_{10}
Initial Value	1.034	1.322	-0.2245e-5	0.4682	0.4581e-4	0.3799	0.6040e5
	d_{11}	d_{12}	d_{15}	d_{16}	d_{17}	d_{18}	
Initial Value	2.00	0.8777e4	0.5162e-2	0.3819e-6	-0.3664e-1	-0.5689e-2	

Table 5.8 – Magic Formula model parameters for the second rear tyre model

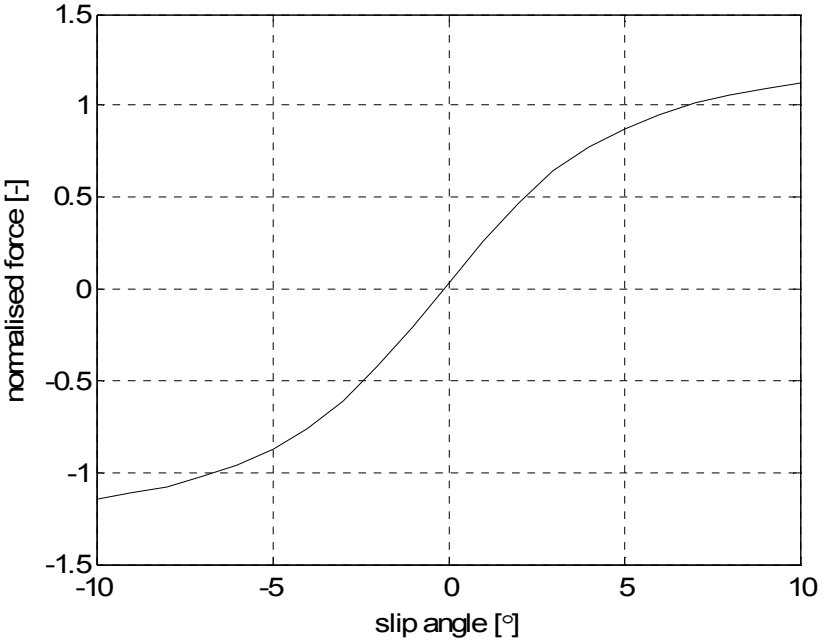

Figure 5.11 – Car tyre model characteristics from equation (5.13) with the parameters from Table 5.8 showing normalised force for a range of slip angles

5.2.4.3 Model 3: Simplified Tyre Model

The final rear tyre model was a simplified version of the original Magic Formula by Pacejka and Bakker [69] where the horizontal and vertical shifts were omitted. The equation for this model is given in equation (5.14). The advantage of this model is that only four parameters need to be estimated by the optimisation routine.

$$
\begin{aligned}
Y &= D\sin\left(C\tan^{-1}\left(B\alpha_r - E\left(B\alpha_r - \tan^{-1}\left(B\alpha_r\right)\right)\right)\right)\\
C &= d_0\\
D_0 &= d_2 F_{zr}\\
D &= \sqrt{D_0^2 - F_{xr}^2}\\
E &= \frac{d_3 B - \tan\left(\frac{\pi}{2C}\right)}{d_3 B - \tan^{-1}\left(d_3 B\right)}\\
K &= d_1 F_{zr}\\
B &= \frac{K}{CD}
\end{aligned}
\tag{5.14}
$$

The initial parameter values from the first model as given in Table 5.7 were adjusted so that the tyre characteristics of this model matched those shown Figure 5.11. The resulting initial parameters values are given in Table 5.9. The tyre characteristics as shown in Figure 5.12 are more or less symmetrical as was the case with the previous model.

	d_0	d_1	d_2	d_3
Initial Value	1.034	0.9040e1	1.322	1.45

Table 5.9 – Magic Formula model parameters for the third rear tyre model

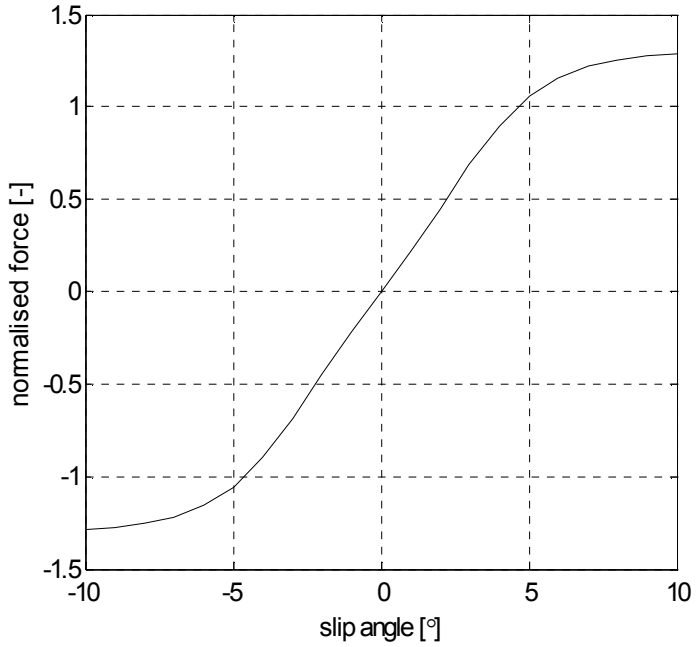

Figure 5.12 – Car tyre model characteristics from equation (5.14) with the parameters from Table 5.9 showing normalised force for a range of slip angles

5.2.5 Optimisation Results

Every front tyre model was optimised with every rear tyre model to determine the best combination of models. At the end of the optimisation routine, the vehicle model states were compared to the experimental data. The aim was to establish which combination of front and rear tyre models resulted in the best match between the simulation and experimental results. The best results were obtained with the second, complex, front tyre model from section 6.3.2 and the third, simplified, rear tyre model from section 6.4.3.

Figure 5.13 shows simulated the yaw rate in comparison with the yaw rate that was determined from the experimental data. Figure 5.14 shows the steer angle the simulation required to complete the manoeuvre in comparison to the steer angle that the driver applied during the experiment. The experimental and simulation data match well, except for a slight delay. This delay can be explained by the trajectory differences between the simulation and the experiment shown in Figure 5.15.

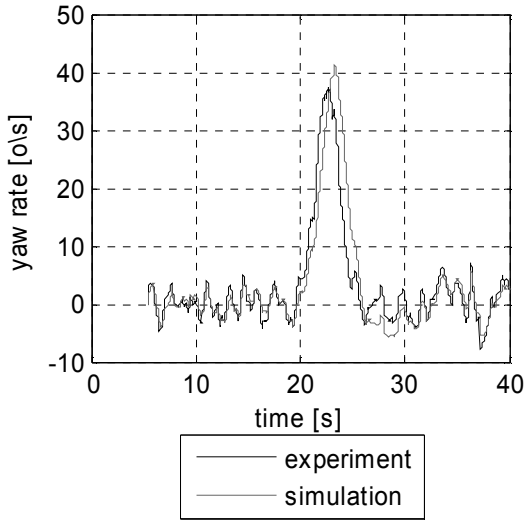

Figure 5.13 – Example of the comparison between the experimental yaw rate and the yaw rate output from the model

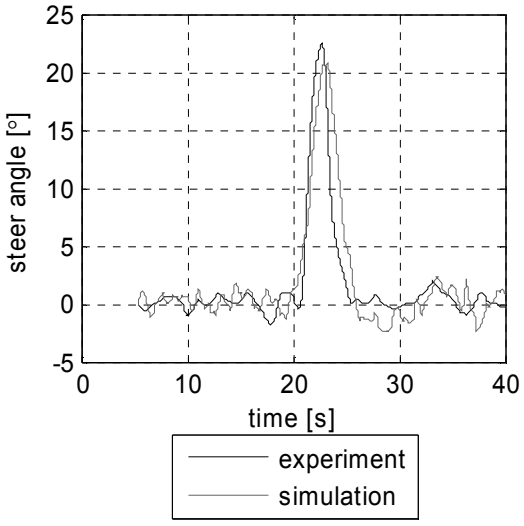

Figure 5.14 – Example of the comparison between the experimental steer angle and the steer angle used in the simulation

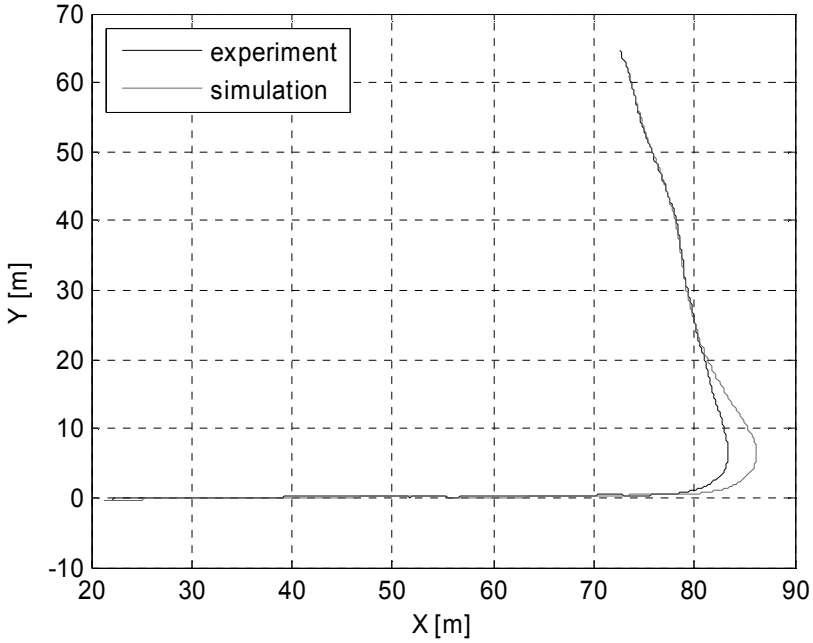

Figure 5.15 – Example of the trajectory differences between the experiment and the simulation

Table 5.10 shows the initial guesses and the optimised values of the tyre model parameters. Some parameters have changed significantly in value, whereas others have only changed by a small amount. This is due to the nature of each parameter: a small change in some can result in a large change in the overall characteristics and vice versa. The most important change in the tyre characteristics is the balance between the amount of force caused by the sideslip angle and the force generated by the camber angle: it appears that, in this vehicle, the sideslip angle causes a greater proportion of the lateral force than expected.

	d_1	d_2	d_3	d_4	d_5	d_6
Initial Values	1.60	1.20	0.10	0.15	0.10	0.10
Optimised	1.80	1.35	0.15	0.90	1.00	1.00
	d_7	d_8	d_9	d_{10}	d_{11}	d_{12}
Initial Values	0.10	0.10	14.0	1.00	1.00	1.00
Optimised	1.50	3.00	4.00	2.25	1.00	1.90
	d_{13}	d_{14}	d_{15}	d_{16}	d_{17}	d_{18}
Initial Values	0.15	0.00	1.60	14.0	1.00	-1.00
Optimised	1.50	0.00	1.15	0.10	0.10	-2.50

Table 5.10 – Optimised tyre model parameters for the complex motorcycle magic formula model

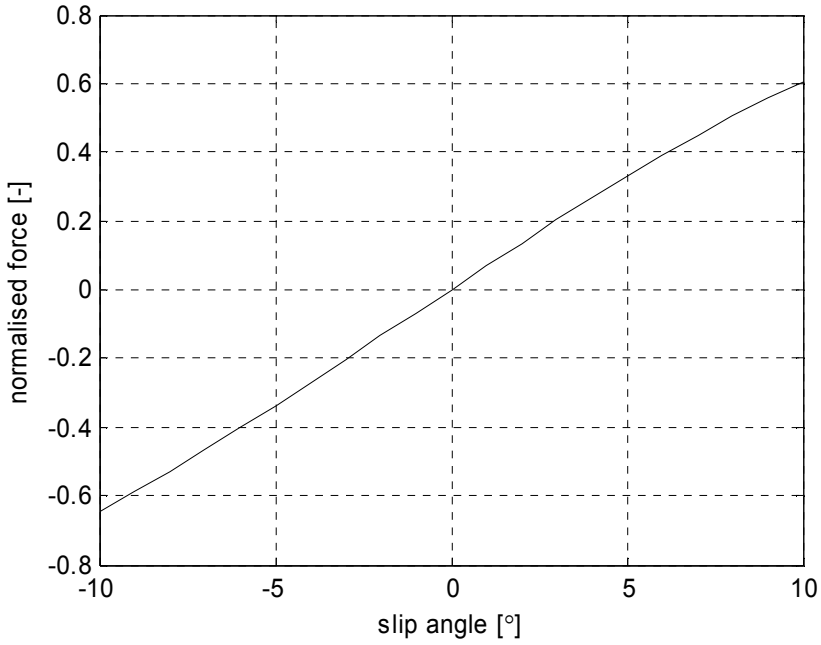

Figure 5.16 – Optimised front tyre model characteristics with slip angle

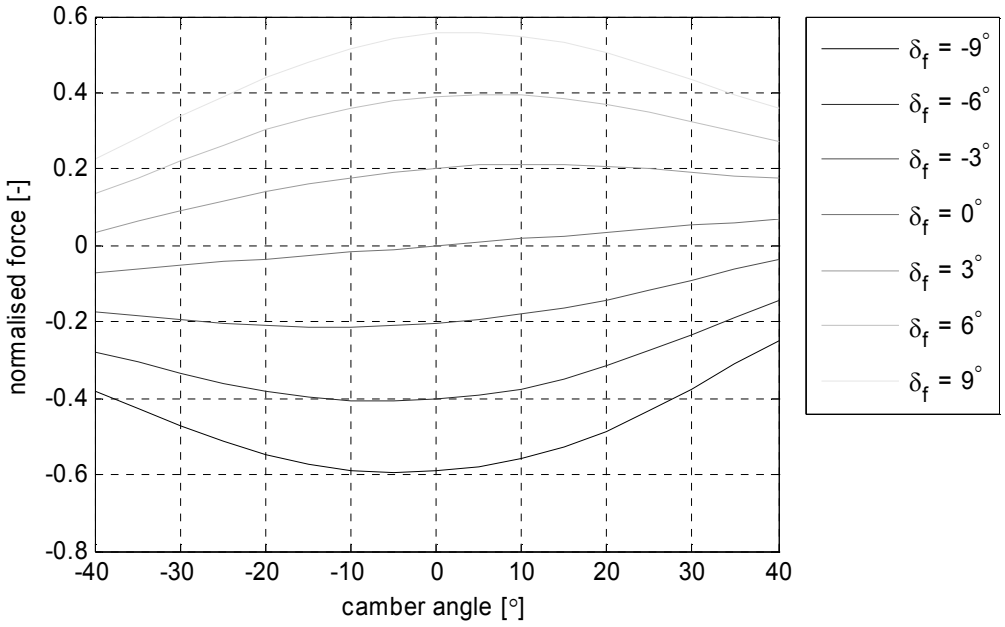

Figure 5.17 – Optimised front tyre model characteristics for a range of camber angles and sideslip angles

Table 5.11 shows the initial and optimised values of the rear tyre model parameters. The scooter rear tyre was found to be less stiff in comparison to a car tyre, hence the significant change in the d_1 parameter. As a result, the characteristics as seen in Figure 5.18 are different to those shown in Figure 5.12, which represent a typical car tyre.

	d_0	d_1	d_2	d_3
Initial Value	1.034	0.9040e1	1.322	1.45
Optimised	1.85	2.50	1.50	0.46

Table 5.11 – Optimised tyre parameters for the simplified rear tyre model

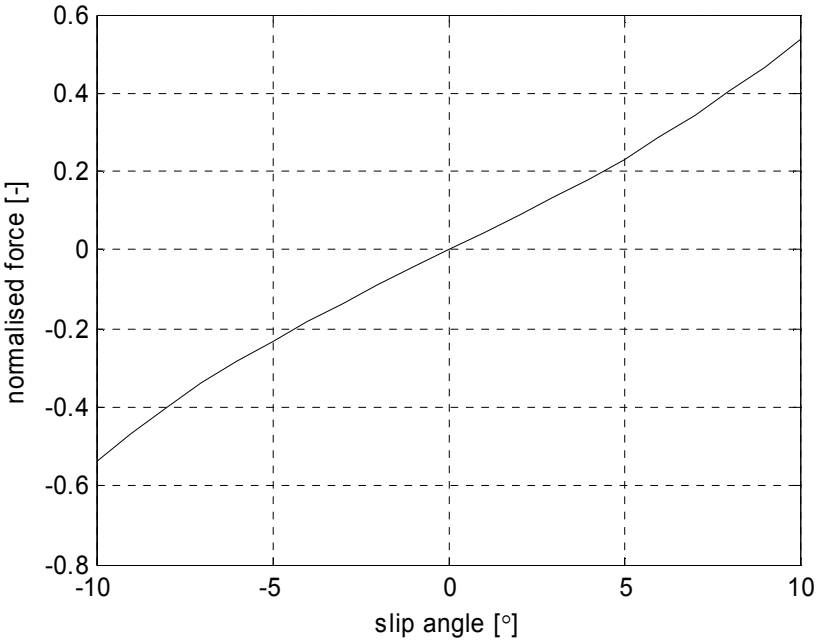

Figure 5.18 – Optimised rear tyre model characteristics over a range of slip angles

5.2.6 Limitations

The front and rear tyre models that were developed here did not take into account the longitudinal slip of the tyre, since this slip angle could not be determined from the experimental data. Neither do these models include the self-aligning moment. Again, the experimental data were too limited to estimate this moment accurately. The tyre models that were defined here did not include what is called tyre relaxation. To determine this effect accurately, more experimental data were required. However, this effect could be included in the vehicle model by assuming a speed related time delay in the slip angle generation. It was noted that these tyre models developed for the Honda Gyro from the experimental data exhibited different cornering stiffnesses in comparison to tyre models found in literature. However, many factors influence the tyre characteristics: inflation pressure (higher pressure, increased stiffness), rolling road surface, the temperature (hot tyres are less stiff), loading (trail and castor angle), and load (higher loads result in less stiff tyres). Furthermore, the slip angles and the forces that were estimated from the experimental data appeared reasonable for the types of manoeuvre from which they were derived.

5.3 DRIVER

A roll control system that applies adjustments to the input steer in order to control the moments about the roll axis, will deviate from the driver's intended path. In the following section, driver models from the literature will be tested and a final driver model will be selected for the simulation model. The aim is to examine how a driver would react to the deviation from the path and how the subsequent adjustments to the steering affect the roll control.

5.3.1 Driver model

The literature survey in chapter 2 already highlighted that there are various methods for modelling the driver. The driver controls a number of dynamic variables: heading angle and lateral position through steer, and forward velocity through acceleration and braking,. A driver model can cover all of these actions or be limited to the steer action with a given velocity profile.

The path tracking by the driver can be modelled with a control algorithm acting on a number or errors. Additionally, the driver's physical dynamics and non-linearities can be added. This section investigates which errors the driver model control algorithm should act on for the best path tracking result. Once a suitable algorithm has been established, driver dynamics and discontinuities are added.

In section 2.6, various algorithms from the literature have been discussed. Common error signals the driver model acted upon were the heading error, the lateral position error, the future heading error, and the future lateral error because of the current heading error. In the following sections, various combinations of these error signals will be discussed and tested in simulation.

The vehicle model used to test the various algorithms was the geometric model at first and once the algorithm was found successful, it was applied with the more complex final non-linear model as discussed in section 5.1.2 with a tyre relaxation coefficient of 0.03s. It is assumed that the roll angle is the equivalent roll angle to balance the roll and the lateral acceleration.

5.3.1.1 Driver as a lead term

This driver model intends to mimic the driver's actions as he interprets the trajectory ahead of the vehicle. A lead is applied to a given path consisting of x and y coordinates and a heading angle. The output of the lead block is a prediction of the future path. This future path information is used to determine a predictive driver action in terms of steer and velocity. This driver action is applied to a vehicle model and the model path output and the path demand are compared. The difficulties in this method lie in translating the future path information into an appropriate steering action. At first, the future path information was differentiated to return a yaw rate and then, assuming Ackermann dynamics, a steering angle was extracted from this yaw rate. This method was unsuccessful because of the inadequate translation of future path information to a steer angle.

5.3.1.2 Position preview control

Miyagishi et al. [66] presented a trajectory tracking method where the demand is a lateral displacement in the global reference frame for a set preview time ahead. A block diagram of this system is given in Figure 2.33. In terms of tracking, this control method tracks the lateral displacement demand well and satisfactorily rejects disturbances to the steering angle. The problem with this method is the demand signal: in practical terms, a driver will follow a road and adjust his path depending on the position of the vehicle with respect to the centre of the lane. The overall global lateral displacement as a demand does not model the driver's behaviour.

5.3.1.3 Position preview and heading angle control

Sharp et al. [116] also presented a trajectory-tracking controller that was based on comparing the predicted vehicle position with the demand vehicle position at a fixed preview time. This model acted on the position error, the longitudinal and lateral position in the global reference frame compared to the demand trajectory, at the current time and for multiple preview times ahead. To optimize the trajectory tracking, the heading angle error at the current time was also used as a control signal. This driver model tracked the demand path well. It was found that regardless of the gains and preview times, the control action had the tendency to demand high frequency, low magnitude adjustments that a human driver would never achieve.

5.3.1.4 Position and heading angle control

Kidane et al. [38] combined lateral position control with heading angle control like Sharp et al. [116] as shown in Figure 2.22 and equations (2.36) and (2.37). However, the definition of the position error was different and the trajectory tracking did not make use of any look-ahead information. The demand trajectory definition assumed steady state conditions, so the total lateral

acceleration was composed of the centripetal acceleration alone. This trajectory control method was executed in Matlab/Simulink with the full vehicle model to test its performance. The results showed that at the end of the manoeuvre, the error signals were zero. However, a comparison of the vehicle trajectory with the demand trajectory showed that the vehicle ended parallel to the demand path, but not on the path. Therefore, the total lateral displacement of the vehicle throughout the manoeuvre was equal to the demand.

5.3.1.5 Driver model algorithm development

This section discusses the driver model that has been developed for this research. In reality, a driver will be looking ahead and anticipate steering adjustments depending on the path he intends to follow. Therefore, preview control action is included in the development of the driver model.

Using the lateral displacement error as a control variable is important for the path tracking. However, the definition of the lateral error is important with respect to the control performance. In sections 5.3.1.2 and 5.3.1.3, the displacement error was defined as the total displacement of the vehicle in the global reference frame. This was deemed too dissimilar to the actions of a human driver. It was also shown that the lateral error could not be defined as the total lateral displacement of the vehicle. It is suggested here that the lateral error should be defined as the error vector between the demand path and the vehicle trajectory. Figure 5.19 illustrates how this definition of the lateral error is different.

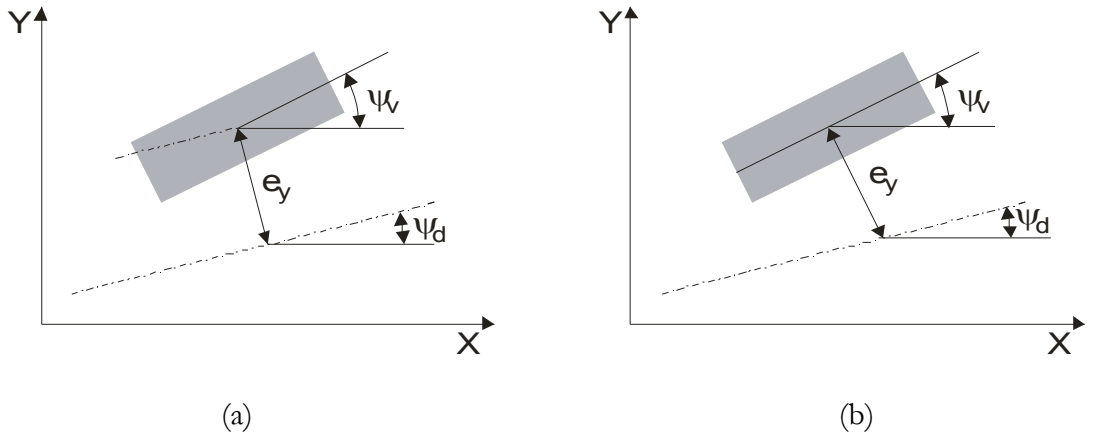

Figure 5.19 – Schematic diagram illustrating the lateral error definition (a) the lateral error is define in the demand path coordinate system (b) the lateral error is defined in the vehicle coordinate system

Overall, four error signals were identified for testing their effectiveness in trajectory tracking. The following list discusses the effect of each error when applied on its own to track the demand trajectory.

1 Current heading angle error

The controller requires multiple adjustments for a 90° turn in the demand. It was noted that the greater the controller gain, the greater the quantity of these adjustments and the greater the amplitude of the adjustments. There was a limit to the proportional gain magnitude: if the gain were too great, the vehicle became unstable. Although the controller successfully steered the vehicle to achieve the demand heading angle, this was no guarantee that the demand vehicle position was achieved: at the end of the manoeuvre, there was a significant error in the lateral position of the vehicle in comparison to the demand trajectory.

2 Future heading angle error

This trajectory tracking method was slow in comparison to the previous method. Similar to the previous method, the magnitude of the proportional gain was limited to a maximum value. Due to the slowness of this control method, it continued to act for a longer time in comparison to the previous method. It was also shown that acting on the future heading angle error resulted in the correct tracking of the heading angle, but with a significant lateral error at the end of the manoeuvre.

3 The lateral error between the current position and the demand position

Using this method to control the trajectory, the demand heading angle was never reached: the system reached an equilibrium state where the longitudinal and lateral error components of the error vector were equal and opposite. As the gain increased, the quantity and the magnitude of the steering adjustments also increased. As was seen before, the control gain was limited to a maximum after which the vehicle became unstable.

4 Lateral error between the predicted future position and the future demand position

This method resulted in a similar control response to the previous control method; that is that the demand heading angle was never achieved.

A combination of the heading angle error and the lateral error as the control signal was expected to give the better tracking results than each error individually. All possible combinations of these methods were tested. It was found that the best tracking was achieved when the controller acted on the current heading angle error and the current lateral displacement error: the preview signals tended to steer the vehicle away from the current demand trajectory. For example, if the demand were a 90° turn with a constant large radius, the preview control would try to cut the corner. Whilst the position of the vehicle at the end of the manoeuvre may be correct, this control behaviour was unwanted.

It was noted that the control actions from the heading angle error and the lateral position error could act against one another in some cases: if the heading angle were approaching its desired value, but there remained a lateral error, the heading angle error would have to increase in order to reduce the lateral error.

A number of attempts were made to reduce the effect of the two control actions opposing one another that included switches and relays. The final adjustment to the driver model was adding the demand yaw rate with a small gain to the control output. The experimental results had shown that the yaw rate and the steer angle were approximately proportional: adding a proportion of the demand yaw rate to the controller output was in essence adding a feedforward signal to the overall control. This signal could be interpreted as the anticipatory control by the driver: the driver looks ahead and will apply steer accordingly. This leaves the other control signals for small tracking adjustments.

The driver's physical dynamics were modelled using a low-pass filter. This filter removed high frequency adjustments a human driver could never physically achieve. This filter limited the bandwidth of the driver model to the bandwidth of a human driver. The block diagram of the final driver model is shown in Figure 5.20 and the model's parameters are shown in Table 5.12.

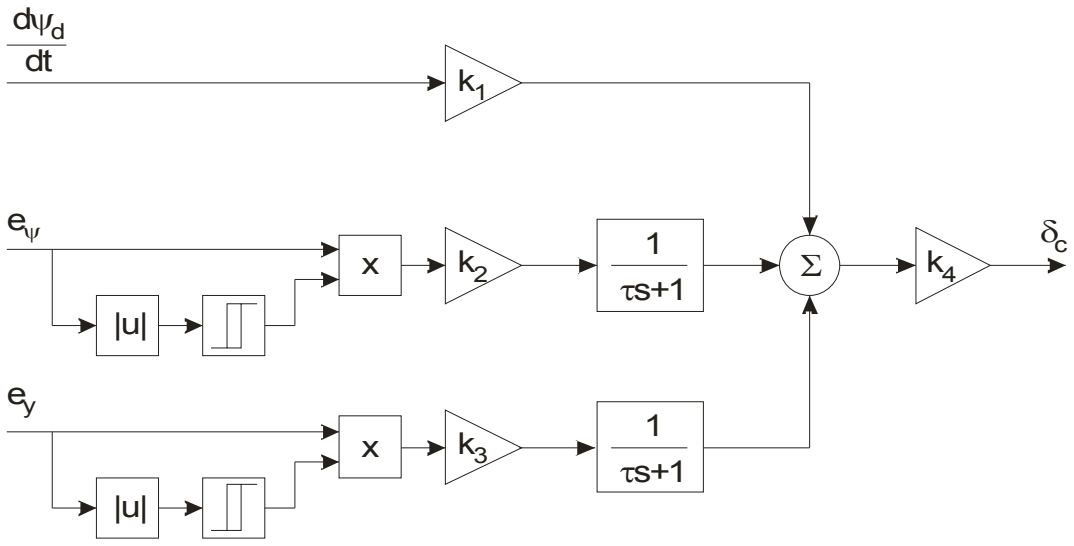

Figure 5.20 – Block diagram of the final driver model algorithm

k_1	k_2	k_3	k_4	τ	e_ψ relay lower limit	e_ψ relay upper limit	e_y relay lower limit	e_y relay upper limit
120	96.0	12.0	0.005	0.05	0.00	0.0125	0.00	0.10

Table 5.12 – Table containing the driver model algorithm gains, the driver dynamics' filter coefficients and the relay thresholds

Figure 5.21 shows the demand trajectory in comparison with the vehicle trajectory. This figure illustrates that the driver model tracks the demand trajectory well when roll control is taken out of the loop. The next section will discuss the simulation results when the driver model is combined with a steer tilt controller.

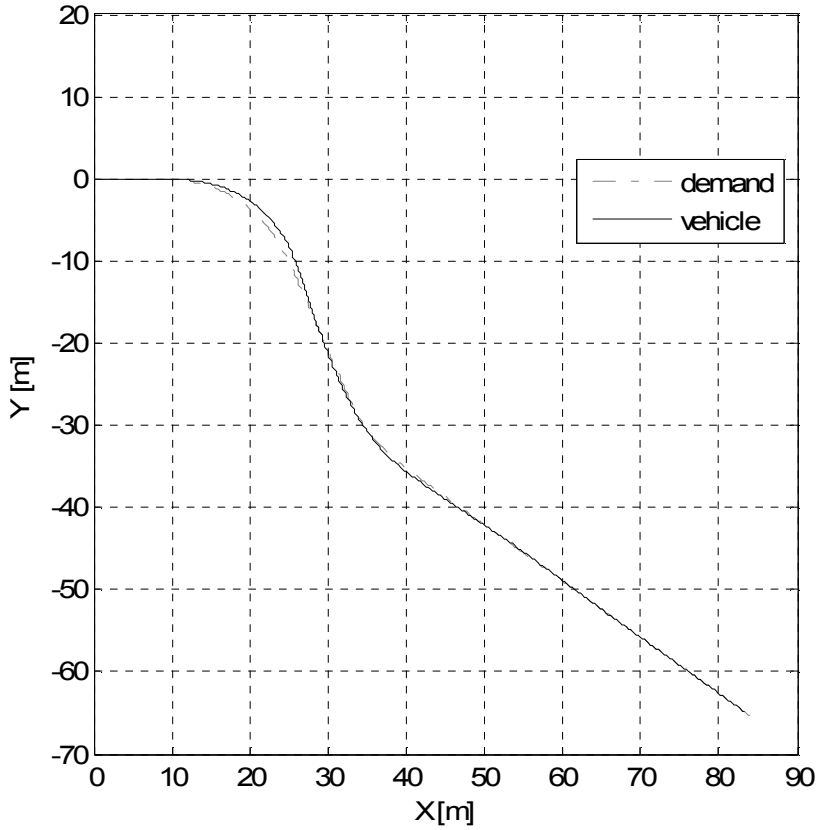

Figure 5.21 – The demand trajectory in comparison with the vehicle trajectory

5.4 CONCLUDING REMARKS

A vehicle model was developed with the aid of the dynamics data from the experiments. Each term from the model equation was calculated using experimental data to determine its order of magnitude and this illustrated which dynamics were more important than others. This enabled a numerically efficient vehicle model to be developed which included all the important non-linear dynamic elements.

A method to derive the model parameters from experimental data for a Magic Formula based tyre model was presented. The aim of the method was to provide a reasonably accurate tyre model requiring as little experimental data as possible. The vehicle model combined with the experimental data and an optimisation routine to determine the tyre model parameters. The inputs to the simulation model were the velocity, roll angle, heading angle, and the vehicle coordinates from the experiments. The optimisation routine was set to adjust the tyre model parameters so that the error between the simulated vehicle trajectory and the measured vehicle trajectory was minimised. The optimisation results were verified by comparing the yaw rate and steer angle from the simulation with those from the experiments. This method was used to find the parameters of three different tyre models for both the front and the rear tyre. The optimisation routine was applied to every combination of front and rear tyre model and a combination of a motorcycle front tyre model and simplified rear tyre model produced the best results.

The third section of this chapter discussed the development of a driver model. A range of driver models based on those presented in the literature were simulated and tested on their performance. Using the simulation results, a novel driver model was defined. This new model acted on the yaw rate demand to realise anticipatory control and it acted on both the heading angle error and the lateral error to make adjustments to the path tracking. This combination of control performed the trajectory tracking task well.

CHAPTER 6. MODEL VALIDATION AND SIMULATION OF THE COMPLETE VEHICLE SYSTEM

This chapter combines vehicle and tyre models that were presented in chapter 5 and validates the combination model with the experimental data that were presented in chapter 4. The validated model is then used to analyse PID based STC. Next, the driver model that was also developed in chapter 5 was added to the simulation to study the response of the driver to countersteer. In addition to the driver in the loop, the effect of a number of disturbances and other uncertainties that were modelled in chapter 3 were investigated. These were the effect of side wind, driving up and downhill, and road camber.

6.1 MODEL VALIDATION

The tyre was represented by the simplified model based on Pacejka's Magic Formula as discussed in chapter 5. The vehicle model was developed in Simulink and was based on equations (5.2), (5.4) and (5.7). The inputs to the system were the measured steer angle, velocity and tilt angle. The outputs were the lateral acceleration of the vehicle and the yaw rate. These outputs were compared to the measured values.

Figure 6.1 shows two examples of the differences between the experimental measurements and the simulation model output. The model tended to underestimate the total lateral acceleration. This error could originate from measurement errors and signal processing and some inaccuracies in the tyre modelling. Overall, the model estimated the lateral acceleration within the same order of magnitude as the measured value. The differences were small enough to conclude that the model was appropriate.

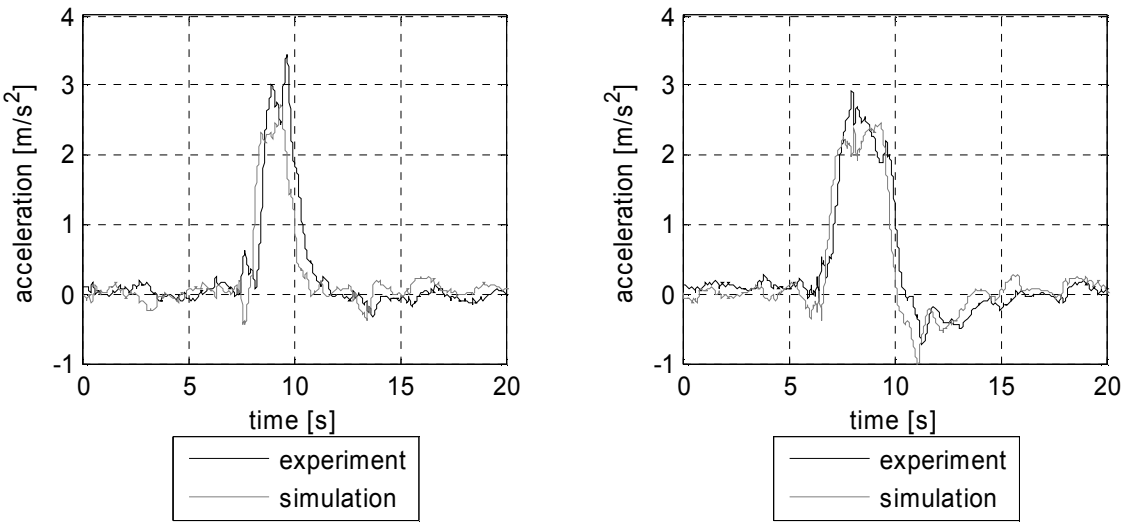

(a) (b)

Figure 6.1 – Comparison of the total lateral acceleration from the experiments with the simulation model output for a 90° left turn from (a) driver 1 (b) driver 2

Figure 6.2 illustrates the differences between the yaw rate output from the simulation and the yaw rate derived from the experimental results. As with the lateral acceleration, there are small differences that can be attributed to measurement errors and signal processing. The simulation model appeared to match the results from driver 2 better than driver 1. The reason for this could be the manoeuvre velocity: driver 1 drove faster than driver 2, therefore there were fewer data points available, and hence the results were less accurate.

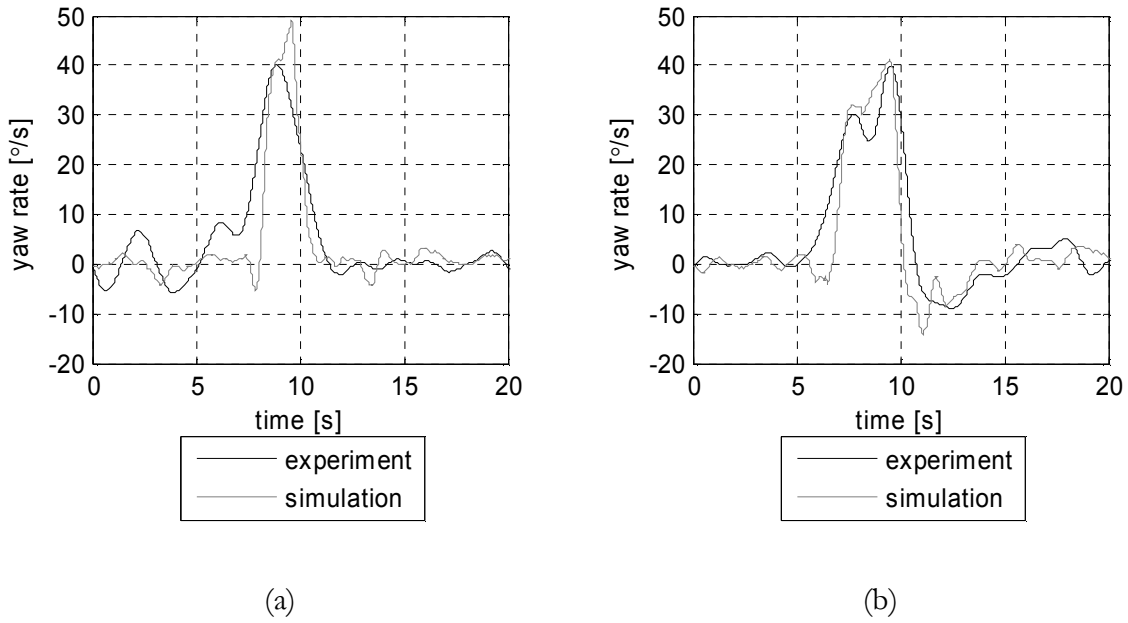

Figure 6.2 – Comparison of the yaw rate from the experiments with the simulation model output for a 90° left turn from (a) driver 1 (b) driver 2

To verify the roll model, the roll acceleration derived from the experimental data was compared to the roll acceleration estimated by the roll model with experimental data as its inputs. The basic mechanism that causes the roll moment is the balance between the moment from the lateral acceleration and the moment resulting from the tilting mass centre of gravity displacement. These moments are shown in Figure 6.3. This shows that the moment from the total lateral acceleration lags behind the roll moment from the displacement from the centre of gravity resulting in the error signal shown in Figure 6.4.

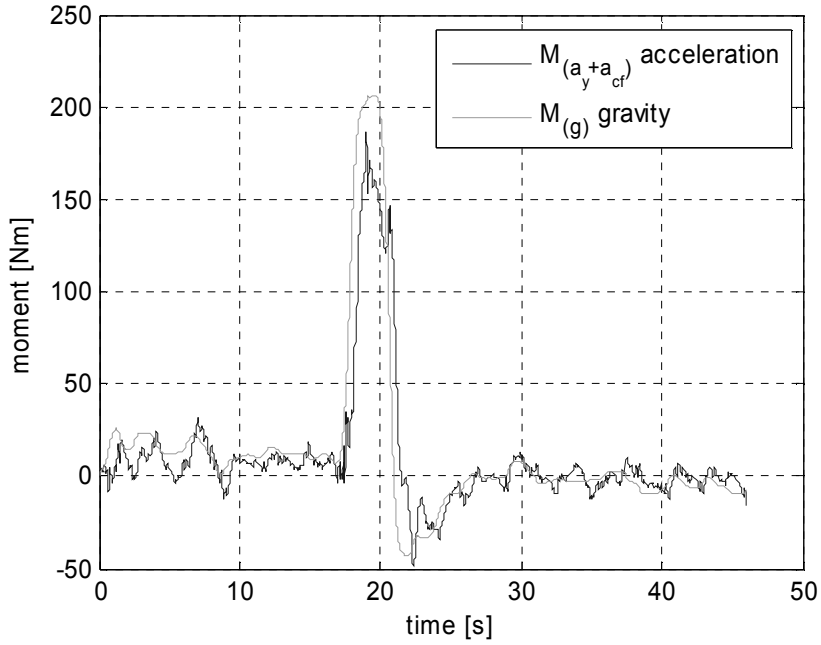

Figure 6.3 – Comparison of the roll moment from the total lateral acceleration and the roll moment of the displacement of the centre of gravity

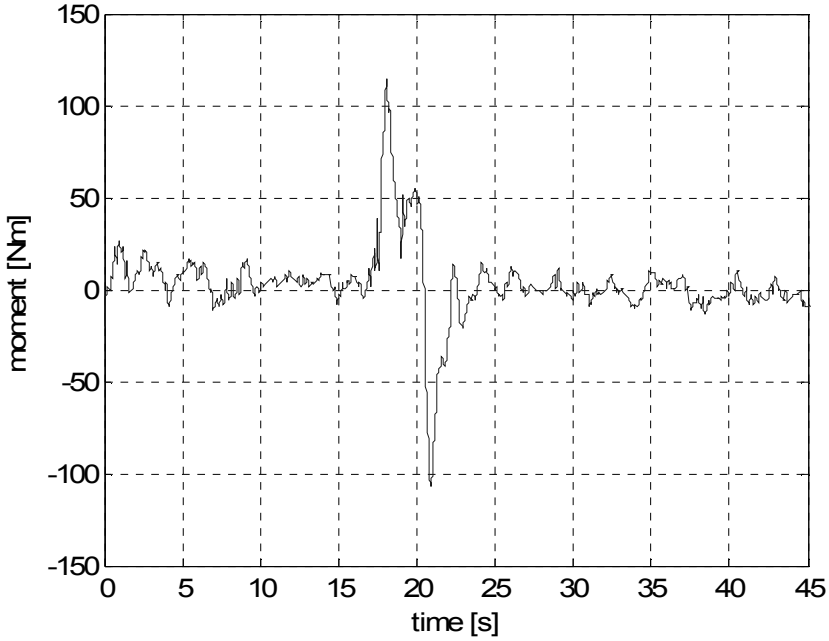

Figure 6.4 – Error between roll moment from the total lateral acceleration and the roll moment of the displacement of the centre of gravity shown in Figure 6.3

Figure 6.5 and Figure 6.6 illustrate the magnitudes of the additional components adding to the total roll moment: normal load, tyre camber and the yaw acceleration. These moments are relatively small in comparison to those shown in Figure 6.3. The result is shown in Figure 6.7: the

calculated roll moment is approximately equal to the difference between the moment from the total lateral acceleration and the roll moment from the displaced centre of gravity.

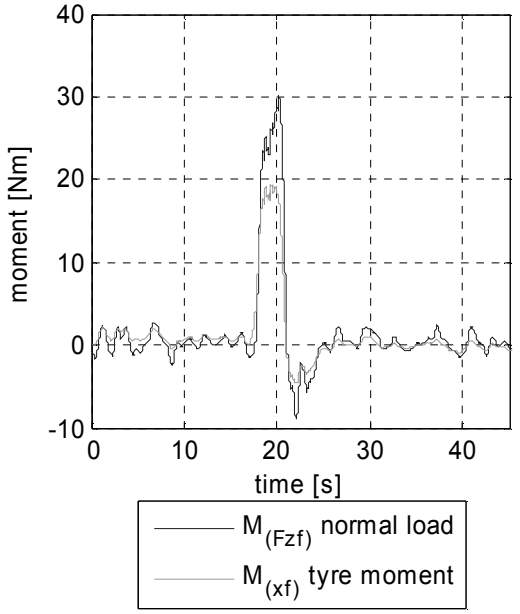

Figure 6.5 – Comparison of the roll moment from the normal load on the front tyre and the roll moment from the camber

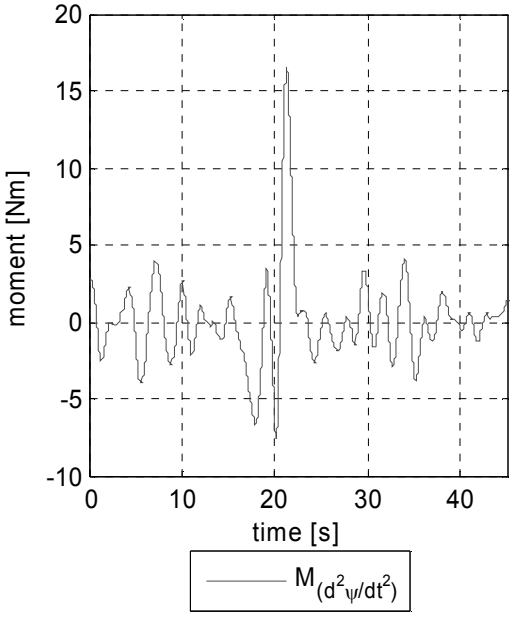

Figure 6.6 – Example of the roll moment from the yaw acceleration as a result of the longitudinal distance between the tilting mass centre of gravity location and the vehicle yaw axis location

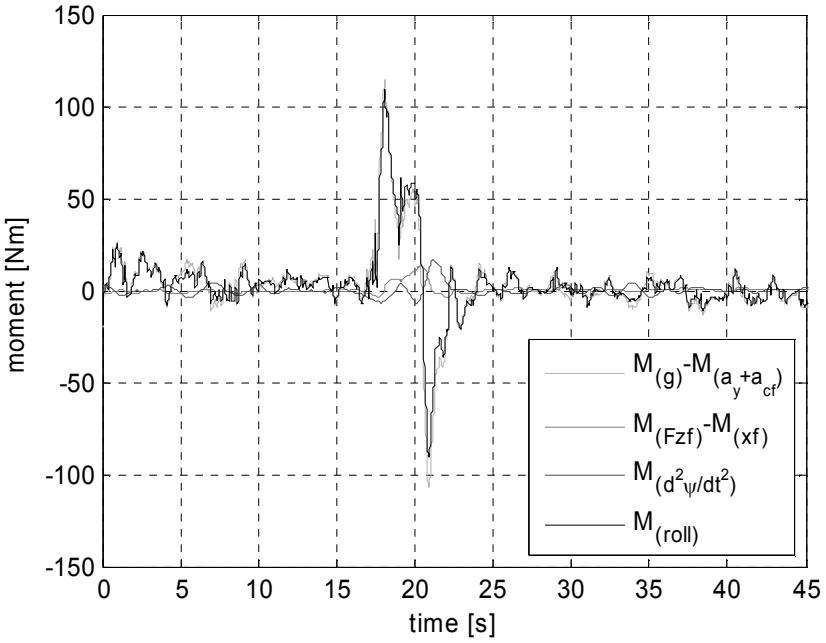

Figure 6.7 – Total roll moment in comparison to the components

The experimental roll data could not be matched by the roll model, this model was found to include the most important dynamics. The errors between the experimental data and the model output were attributed to errors in the measurements and magnitude and phase shifting from the signal processing.

6.2 STEER TILT CONTROL ANALYSIS

6.2.1 Controller Function

The controller input and output signals were studied in the context of the geometric vehicle model presented in equations (2.5)-(2.7) with the roll dynamics modelled by equation (2.8). The aim was to increase the understanding of the controller requirements. The manoeuvre illustrated here is a typical 90° turn at a constant velocity. The input steer angle of the manoeuvre is shown in Figure 6.8.

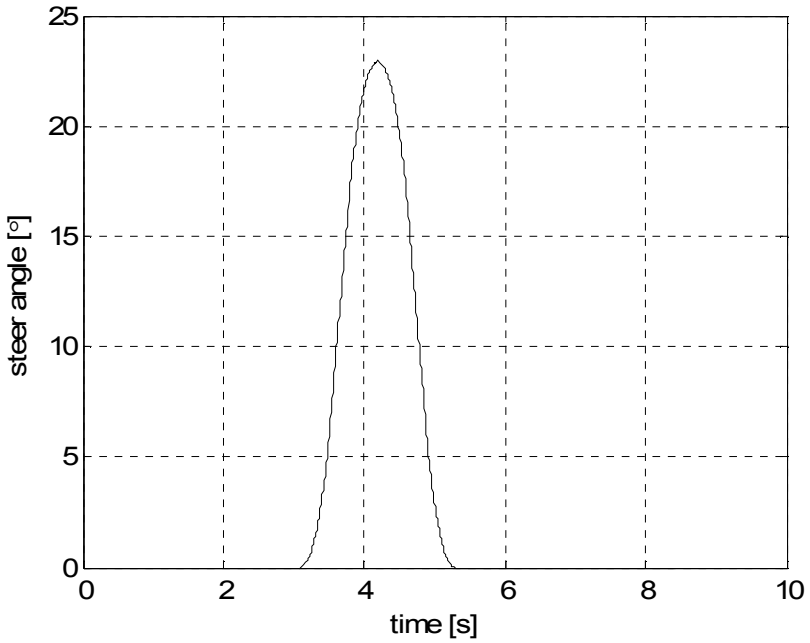

Figure 6.8 – Input steer angle for the example 90° turn manoeuvre at v_X = 5.56 m/s

The tilt error signal and its effect on the control action from the individual controller components were investigated and are shown in various plots. The error signal, Figure 6.9, to the controller was analysed first. The error was a result of the effects illustrated in Figure 6.10. At the start, the desired tilt angle was larger than the actual tilt angle, because the control system has not had a significant effect yet. The tilt angle then became slightly larger than the desired value, this error reached a maximum, decreased, and when the desired tilt angle was at its peak, so was the actual tilt angle and the error was zero. When straightening up, the opposite occurred: the tilt

angle was slightly smaller than the desired value. At the end of the manoeuvre, the tilt angle overshot zero, came back and overall required nearly a second to fully return to a non-tilting condition. The effect this had on the individual controller elements is set out in the following section.

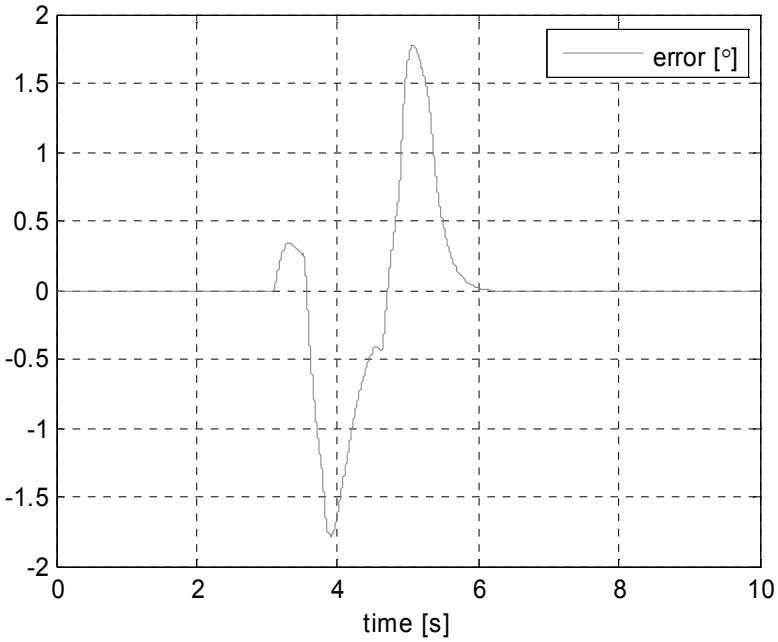

Figure 6.9 – Error between the demand roll angle and the output roll angle: error = φ_d - φ

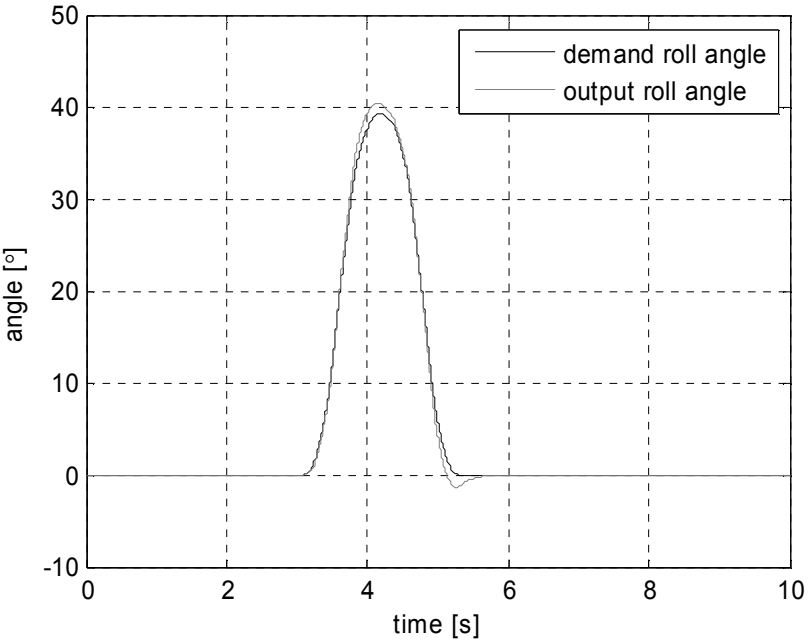
demand roll angle
output roll angle
angle [°]
time [s]
50
40
30
20
10
0
-10
0
2
4
6
8
10

(a)

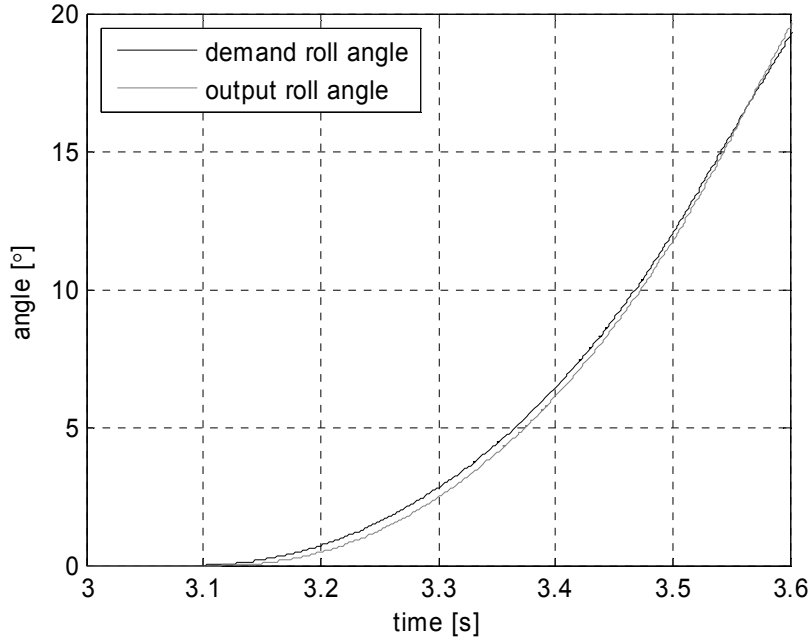
demand roll angle
output roll angle
angle [°]
time [s]
20
15
10
5
0
3
3.1
3.2
3.3
3.4
3.5
3.6

(b)

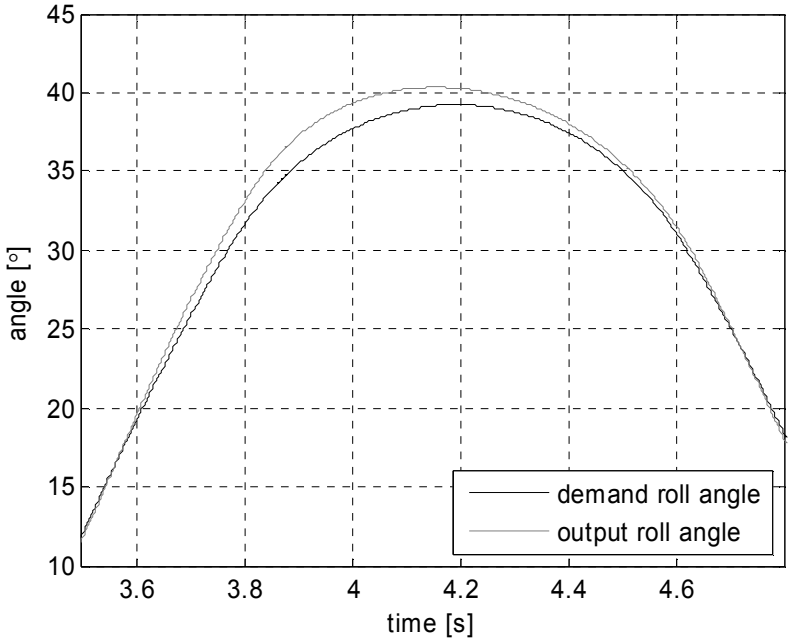

(c)

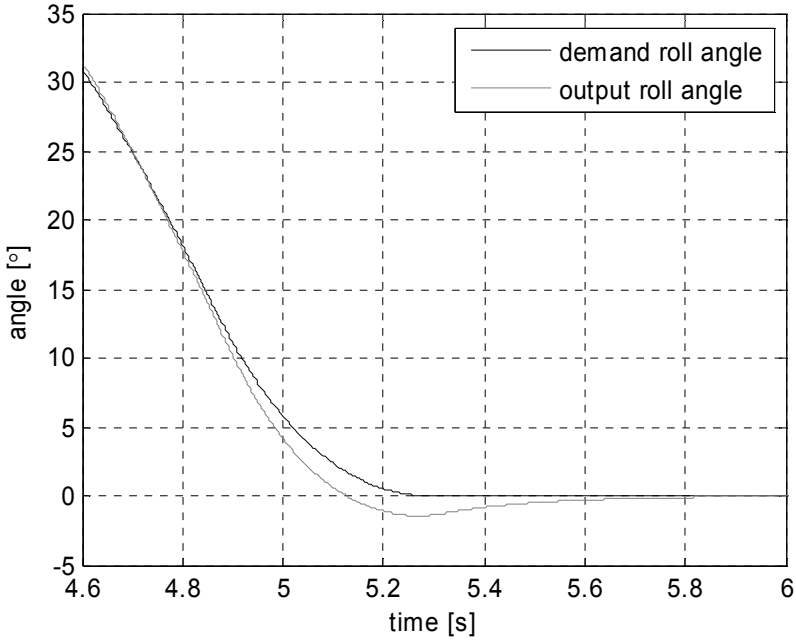

(d)

Figure 6.10 – Comparison of the demand roll angle and the roll angle achieved by the controller and the vehicle (a) whole signal (b) enlargement of the start of the manoeuvre (c) enlargement of the peak section of the manoeuvre (d) enlargement of the end of the manoeuvre

Figure 6.11 shows the contribution to the steer angle from each control component: proportional, integral, and derivative. The integral controller output was similar to the driver steer

input and showed a small amount of countersteer at the start (1). Its maximum value was marginally larger than the driver input (2). It appeared to lag behind the driver input, but this was compensated by the other control elements. The magnitude of the proportional control signal was not as large as the integral control signal, but it was essential. It accounted for approximately 60% of the countersteer at the start of the manoeuvre. After the countersteer, the proportional controller added enough steer to the lagged integral control signal that the combination of the two was similar to the driver steer angle (3). It also reacted to changes in steering velocity and at these points added small adjustments to control signal (4). The magnitude of the derivative controller was the smallest and it was mainly noted when the steering velocity was increasing or decreasing (5)-(8). At these moments, it complemented the proportional controller with small adjustments.

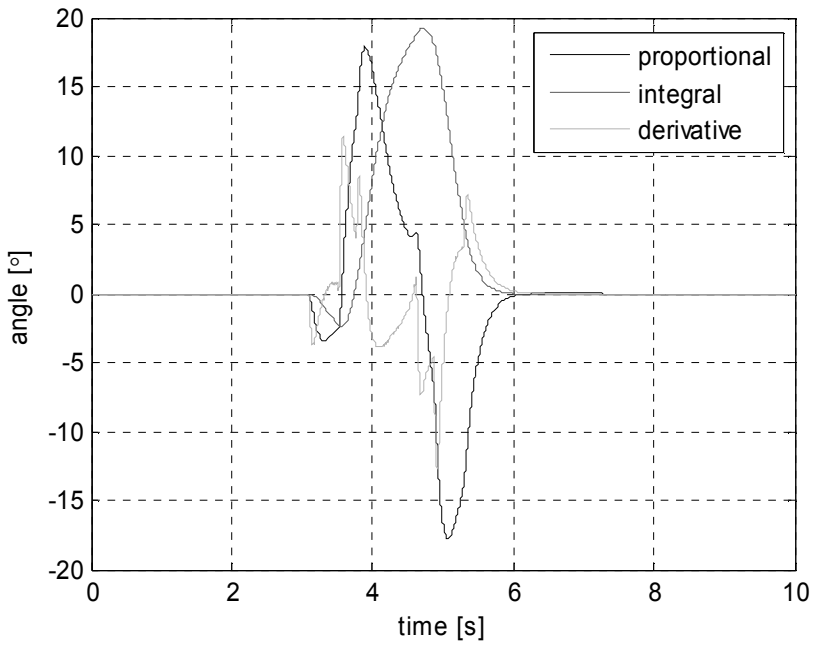

Figure 6.11 – Illustration of the control action of the individual controller elements, i.e. proportional, integral and derivative, in comparison to the driver input

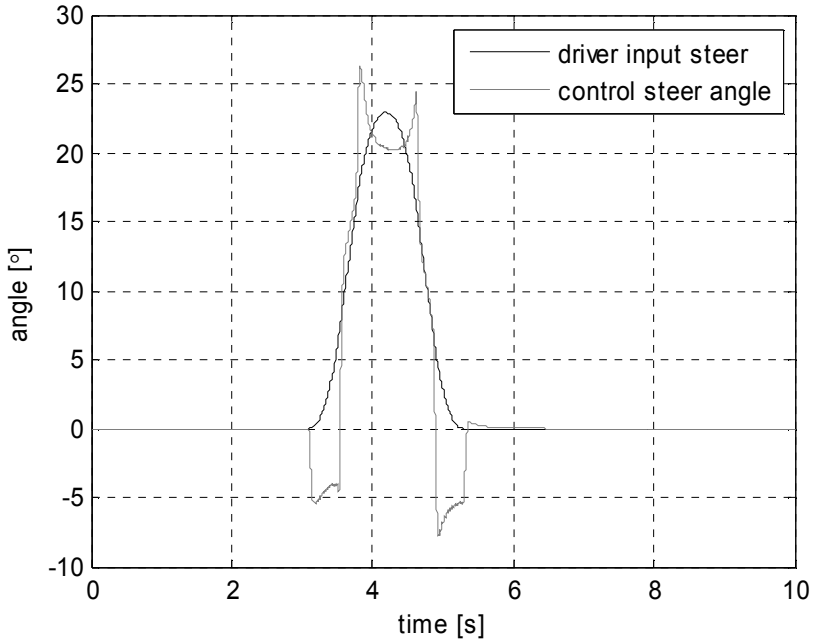

Figure 6.12 – Illustration of the controller steer angle output in comparison to the driver input

In essence, after countersteering, the controller understeered in comparison to the driver, so that the vehicle would continue to tilt. As the driver steering slowed down and changed direction, the control steer angle was larger than the driver steer so that the lateral acceleration increased resulting in a change in the tilt direction. as the driver steering velocity slowed down and the steering angle approached zero, the controller applied less steer than the driver; this reduced the lateral acceleration and the tilting was slowed down. Towards the end of the manoeuvre, the 'understeer' from the controller was in the opposite direction to the driver steer. In other words, the controller also applied countersteer to straighten up.

From these results, the following controller characteristics were derived:

- The driver steer can be used as a reference signal to which the control adjustments are added or subtracted.
- Countersteer or oversteer is required when the steering velocity is changing.
- When the steer angle and the steering velocity are of the same sign, countersteer should be applied and subsequently the steer should be limited in relation to the driver input.
- When the steer angle is increasing, but the steering velocity is decreasing, it is a sign that the driver is likely to change the steering direction. Therefore, additional steer, a steer angle larger than the driver input, is required to slow the tilting down.

- After the tilting has been slowed down, the tilting direction has to change and the vehicle should start straightening up. In this case, additional steer is also required.
- When the steer angle is decreasing and the steering velocity is decreasing, it is a sign that the driver is going to change direction or stop steering altogether. Here countersteer is required to slow the tilting down.

The characteristics of the control action for one manoeuvre had been determined. Now the effect of the steering velocity and the forward velocity on these characteristics was investigated. To determine the effect of the steering velocity, the maximum steer angle was kept constant, but it was reached in a shorter time as shown in Figure 6.13. The adjustments from the controller in comparison to the driver input would increase with the steering velocity as shown in Figure 6.14. From the latter figure it can be seen that the faster the driver input, the larger the magnitude of the adjustments. This is a result of the error building up quickly and the derivative component of the controller acting on this error.

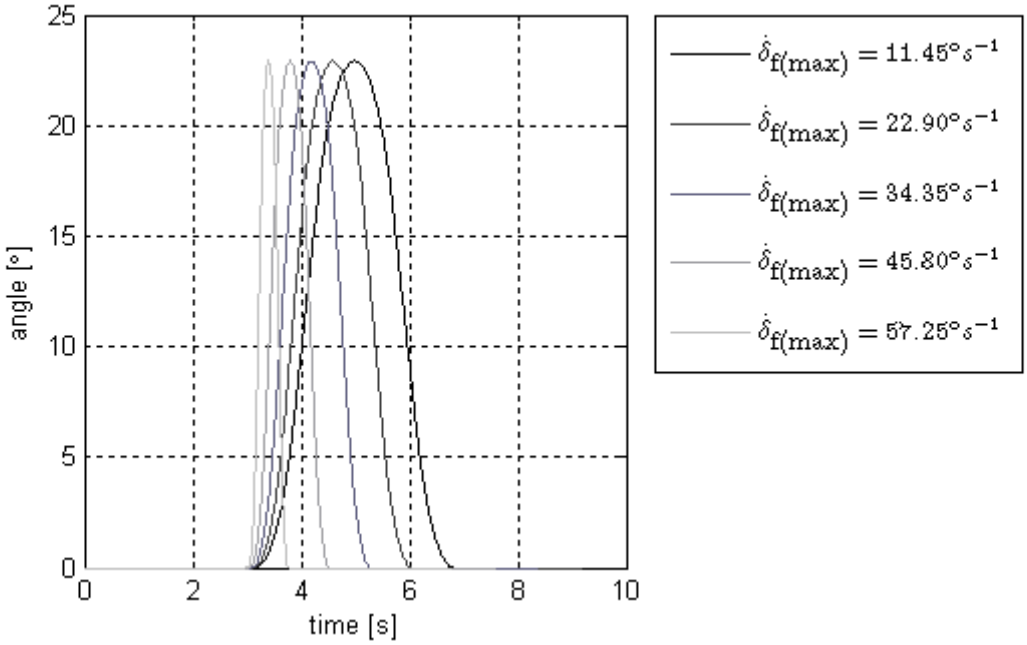

Figure 6.13 – Range of applied steer angles to reach a variety of maximum steering velocities: the maximum input steer angle was kept constant and the manoeuvre time was reduced to achieve the range of maximum velocities

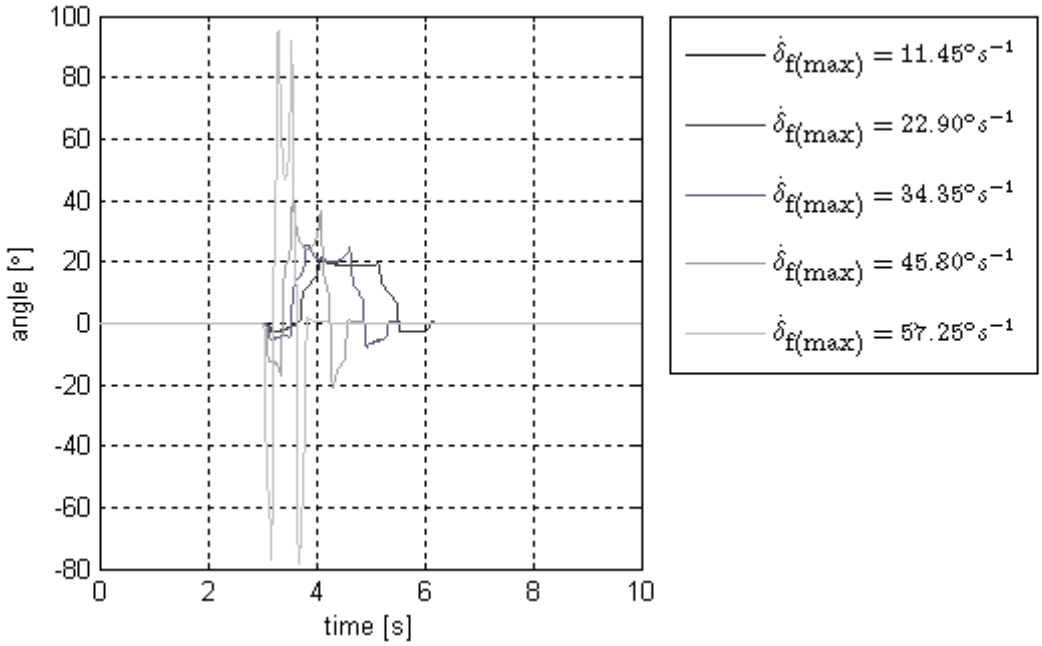

Figure 6.14 – Controller output for a range of maximum steering velocities from 11.45 degrees/s (=0.2 rad/s) to 57.25 degrees/s (=1.0 rad/s)

The same manoeuvre was also simulated with a range of constant forward velocities. The roll angle demand was kept constant at 39 degrees. As the forward velocity increased, the input steer angle was decreased accordingly. Figure 6.15 shows that the greater the velocity, the smaller the steer angle required to track the demand roll angle. This was expected, since the vehicle model dictates that if the velocity were halved, the steer angle would have to be increased fourfold to achieve the same lateral acceleration.

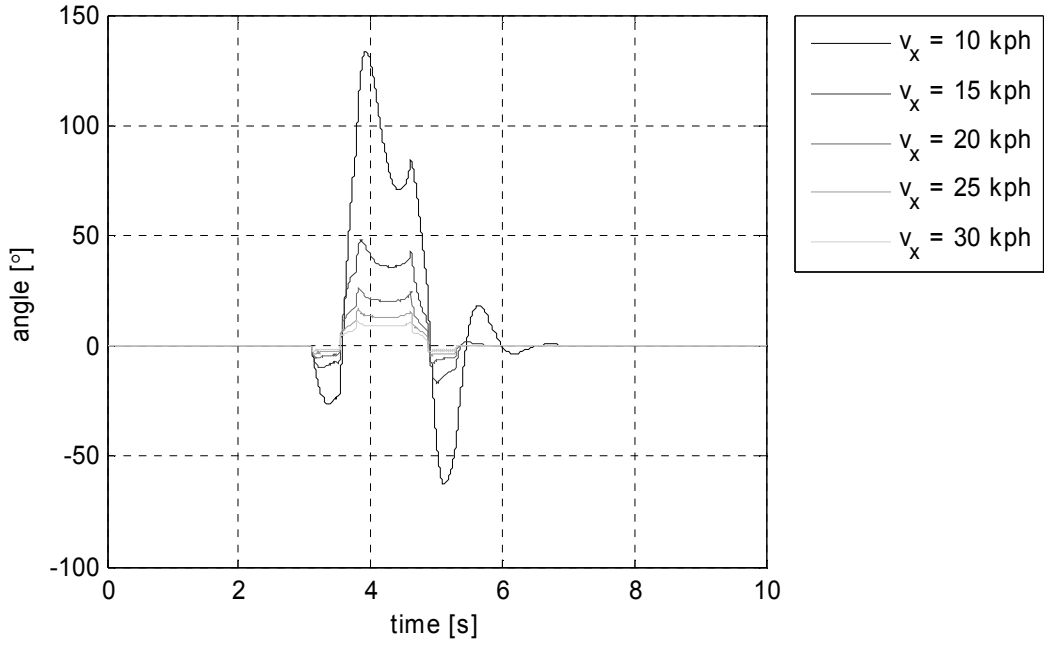

Figure 6.15 – Controller output for a range of constant forward velocities

6.2.2 Controller Performance: Non-Linear Vehicle Model

In the previous section, it was shown that PID stabilised the vehicle roll when modelling the vehicle as a very simple system where a change in steer angle instantly causes a change in lateral acceleration and the tilt dynamics only consists of the balance between the lateral acceleration and the gravity acting on the centre of mass. In this section, the performance of a PID based roll controller with the vehicle model from section 5.1.2 and the roll model from section 0 is investigated. In addition to a non-linear vehicle mode, the steer and roll kinematics that were discussed in sections 3.1.3 to 3.1.5 were included, a DC motor for steer actuation was added, variations in overall vehicle inertia derived in section 3.2.3 were incorporated, and the tyre force generation was simulated by the model discussed in chapter 6.

The velocity was set to a constant 5.6 m/s and the roll angle demand peaked at 24.4 degrees, which was approximately the largest roll angle measured during experimentation. The system was tested with a variety of tilt angle demand signals as shown in the block diagram of Figure 6.16.

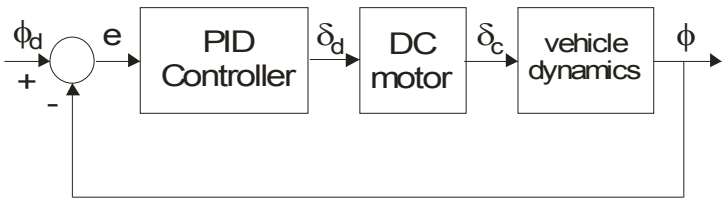

Figure 6.16 – Block Diagram of the STC with the non-linear vehicle modelled by equations (5.2), (5.4) and (5.7) and a DC motor for the steer actuation

First, the system was tested with a roll demand input similar to the steering input shown in Figure 6.8. The maximum magnitude of this demand signal was varied as well as the total length of time over which it was applied. The maximum roll demand was limited to 15 degrees. In addition, the roll demand could only be very smooth, that is, the roll demand velocity was also limited. This has shown that a PID steer tilt controller is restricted in its operational range when applied to a vehicle model that includes a range of non-linearities that are applicable to a real vehicle system.

6.2.2.1 Trajectory

The vehicle trajectory was investigated using the final vehicle model without the tyre relaxation length. The input steer angle and demand roll angle were set so that the vehicle model would take a 90° turn. In the process of determining the best combination of steer and roll angle, the balance between the gravity moment about the roll axis and the lateral acceleration moment was assured. Figure 6.17 shows how the demand trajectory and the output trajectory compare. At the start of the manoeuvre, the error in the trajectory is small: this error would not cause a driver to adjust the steering. At the end of manoeuvre, the controller has caused the vehicle to yaw less than the demand. Without any adjustment, the vehicle will continue along a trajectory that takes it further away from the path as time goes on. The cause of the error is the controller action that results in the lateral acceleration shown in Figure 6.18. This figure compares the demand lateral acceleration with the output lateral acceleration. The controller causes the vehicle to accelerate less than the demand at the start of the manoeuvre to create a roll moment. At the apex of the manoeuvre, the controller makes the vehicle accelerate more than the demand in order to change the direction of the moment and start straightening up. Finally, at the end of the manoeuvre the controller needs to slow down the roll and causes the vehicle to accelerate less than the demand. Figure 6.18 shows that this decreased and increased acceleration is not balanced, hence the vehicle does not follow the path.

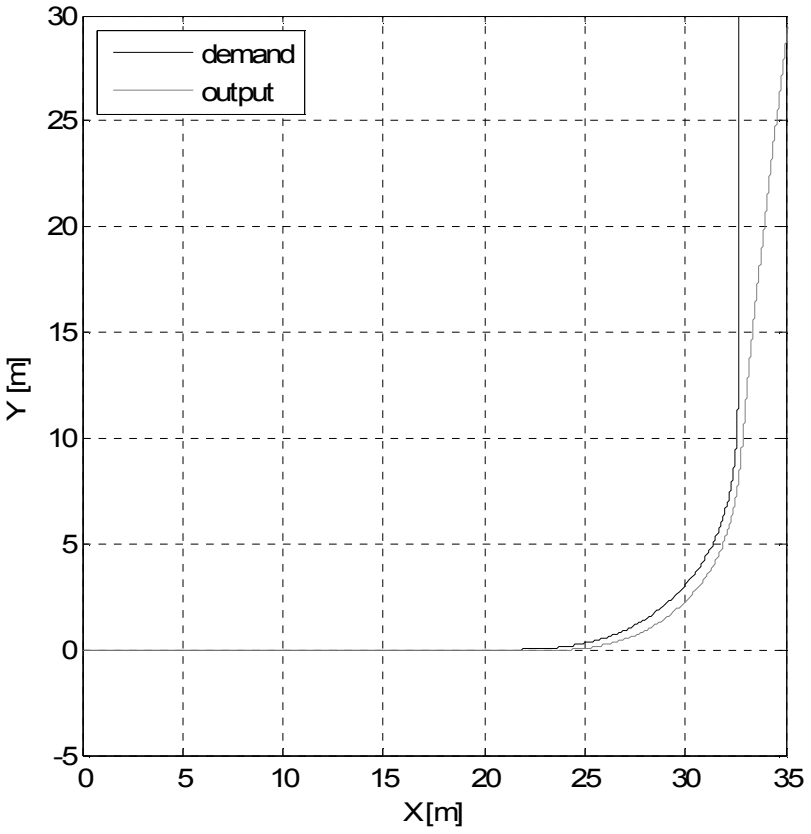

Figure 6.17 – Comparison of the demand trajectory based on the roll demand and an appropriate steer angle, and the output trajectory based on the roll output and the controller output steer angle δ_c

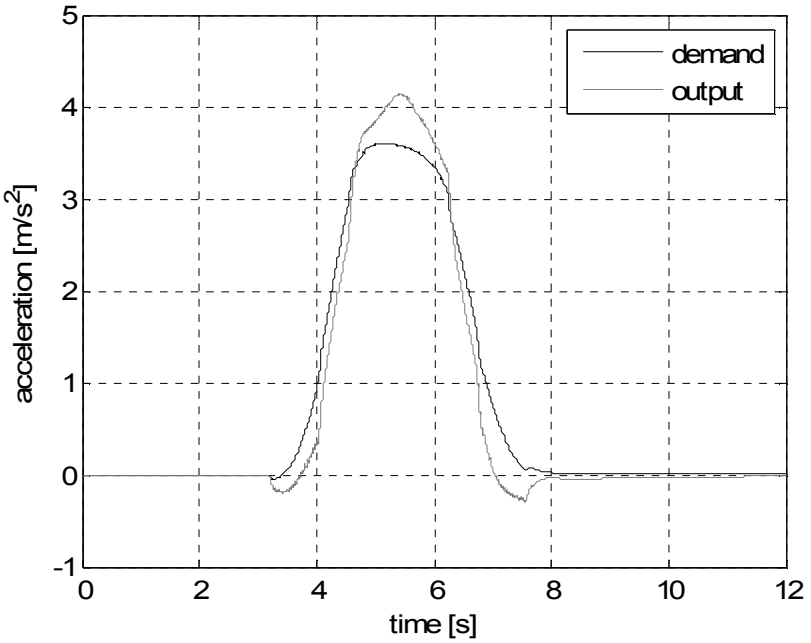

Figure 6.18 – Comparison of the demand lateral acceleration based on the roll demand and an appropriate steer angle, and the resulting vehicle lateral acceleration based on the output roll angle and the controller output steer angle δ_c

6.2.2.2 Roll Demand

In the previous sections, the inputs to the vehicle model were a demand roll angle and a forward velocity. In practice, the demand should be derived from the steer input and the forward velocity. The demand trajectory was achieved by setting the roll angle proportional to the steering angle. The gain between the steer and the roll angles will vary with the forward velocity. The algorithm used to determine the roll angle demand from the velocity and steer inputs is important for the vehicle stability as well as the error in the demand trajectory at the end of a manoeuvre.

In the examples presented in this chapter, the demand has been a smooth input: slowly increasing at the start, and then gradually decreasing at the apex, and so on. When this smooth input was replaced by a step, even a low-pass filtered step, the controller was unable to act on the demand satisfactorily. The controller was able to apply countersteer to start the roll, but as it attempted to apply extra steer to slow the roll, it applied too much causing the vehicle system to become unstable. Overall, it was found that the controller's ability to act on a demand was dependent on a combination of the roll demand magnitude as well as the roll demand velocity. In other words, the PID steer controller was limited in its ability to deal with a range of inputs.

6.2.2.3 Perceived Acceleration

In addition to verifying the tracking of the roll angle and the resulting dynamics, the perceived lateral acceleration was determined. Figure 6.19 demonstrates that the perceived acceleration for a 90° turn manoeuvre is largely composed of the roll acceleration. The lateral acceleration and the gravity components were almost equal and opposite. At the start and at the end of the manoeuvre, the lateral acceleration component was smaller than the gravity component, and at the peak of the manoeuvre, the lateral acceleration component was larger than the gravity component. This has shown that in terms of control strategy, it cannot be expected that the perceived acceleration is zero during a transient manoeuvre although the controller may not be any worse than a passive vehicle 'balanced' by the rider.

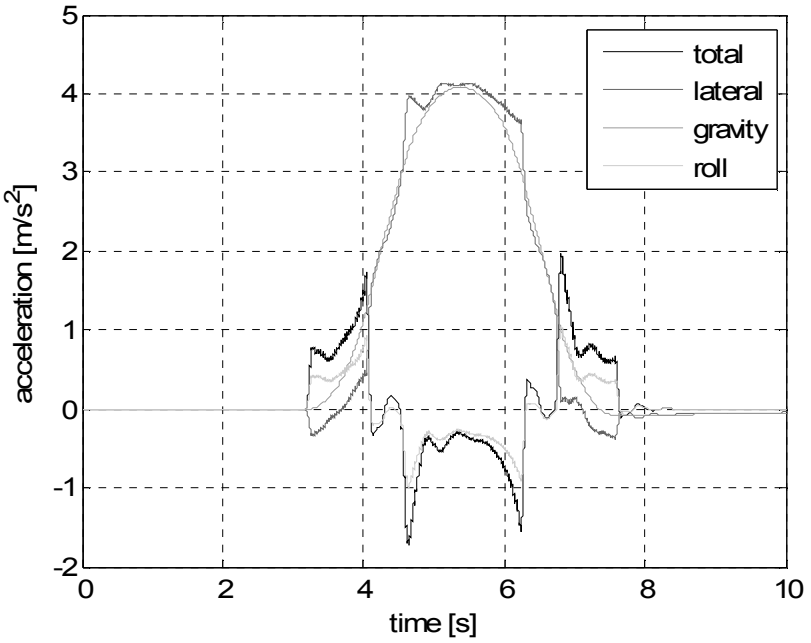

Figure 6.19 – Comparison of the components adding to the perceived acceleration: lateral acceleration, gravity, and roll acceleration

6.2.3 STC combined with a Driver Model

It has been established that a steer tilt control system will deviate from a driver's intended path in order the balance the vehicle. If the deviation is small, the driver will not react to the deviation because either it is below the adjustment threshold, or the driver has not registered the deviation. However, if the driver does act on the deviation, the steer tilt controller could potentially become unstable. The following section discusses the simulation results where the driver model is combined with a PID based steer tilt controller.

First, a heading angle control driver model was combined with a steer tilt control system to get an impression of how the driver would react. The result was a completely unstable system, because the driver control would almost instantly make an adjustment to oppose the countersteer from the steer tilt controller. In reality, the driver would allow a small deviation from his intended path before adjusting the steering angle.

The driver model that was presented in the previous section was developed to allow for small path deviations before coming into action. For the driver model to work with the steer tilt control, the driver model gains and relay values had to be modified as shown in Table 6.1. It was essential that the relay lower limits were non-zero: this allowed the roll control to apply countersteer without the driver algorithm interfering.

	k_1	k_2	k_3	k_4	τ	e_ψ relay lower limit	e_ψ relay upper limit	e_y relay lower limit	e_y relay upper limit
before	120	96.0	12.0	0.005	0.05	0.000	0.0125	0.000	0.100
after	50.0	24.0	6.00	0.005	0.05	0.025	0.0750	0.100	0.300

Table 6.1 – Driver model parameters before and after integration with the roll model

Figure 6.20 shows how the driver model and the roll control were integrated with the vehicle model: the driver acts on the errors between the demand and the vehicle feedback, the driver's output is converted to a demand roll angle for the roll control which steers the vehicle.

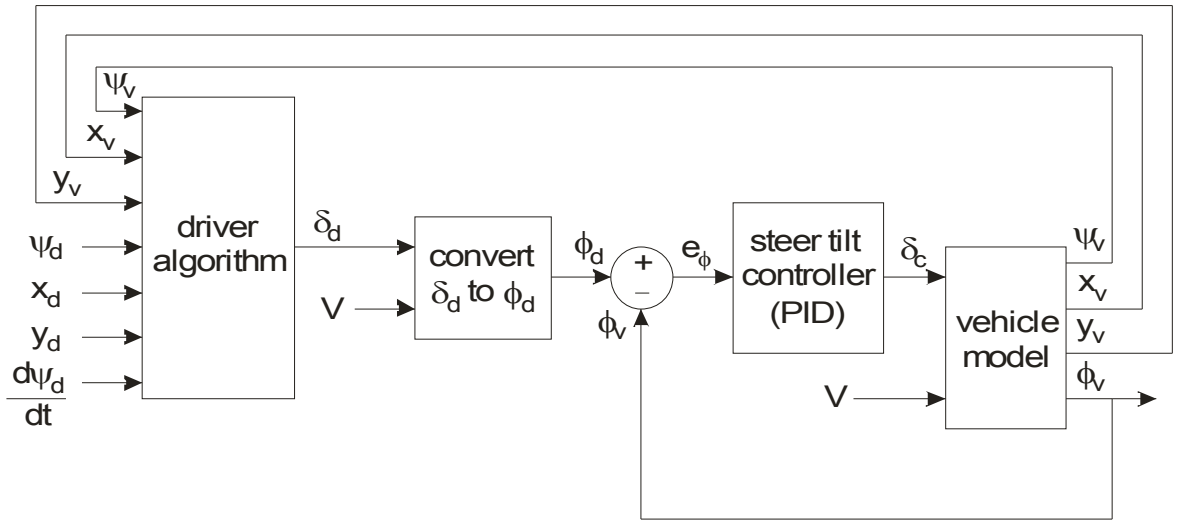

Figure 6.20 – Block diagram showing the integration of the driver model with the roll control and the vehicle

In section 6.2.2, it was noted that the vehicle model with PID steer tilt control was limited by the magnitude and velocity of the roll demand. Additionally, the conversion of the driver input steer angle into a demand roll angle was found to be a crucial element to the success of the control. The experimental results had shown that the ratio between the steering angle and the resulting roll angle was not constant and not only related to the manoeuvre velocity, but also to the type of manoeuvre.

The demand yaw rate and input velocity were taken from the experimental measurements. The conversion factor between the steering angle and the demand roll angle was based on the ratio between the steering angle and the roll angle measurements and was adjusted to ensure system stability. Figure 6.21 shows the demand trajectory that was measured in the experiment as well as the trajectory of the vehicle from the simulation output. At the start of the manoeuvre, the driver and the roll control appear to work well together, but at the end of the manoeuvre, the vehicle veers off course. The cause of this deviation can be seen in both the steering angle and the roll angle results shown in Figure 6.22 and Figure 6.23 respectively. After the apex of the turn, the driver should straighten the vehicle up and continue along a straight line, the simulation straightens up so fast that the vehicle starts rolling in the opposite direction. At the point where the vehicle trajectory and demand trajectory are approximately equal, the vehicle is still rolled; therefore, additional steering adjustments are necessary resulting in a significant deviation from the demand path. This simulation result was typically seen when the driver model and PID steer tilt control were combined.

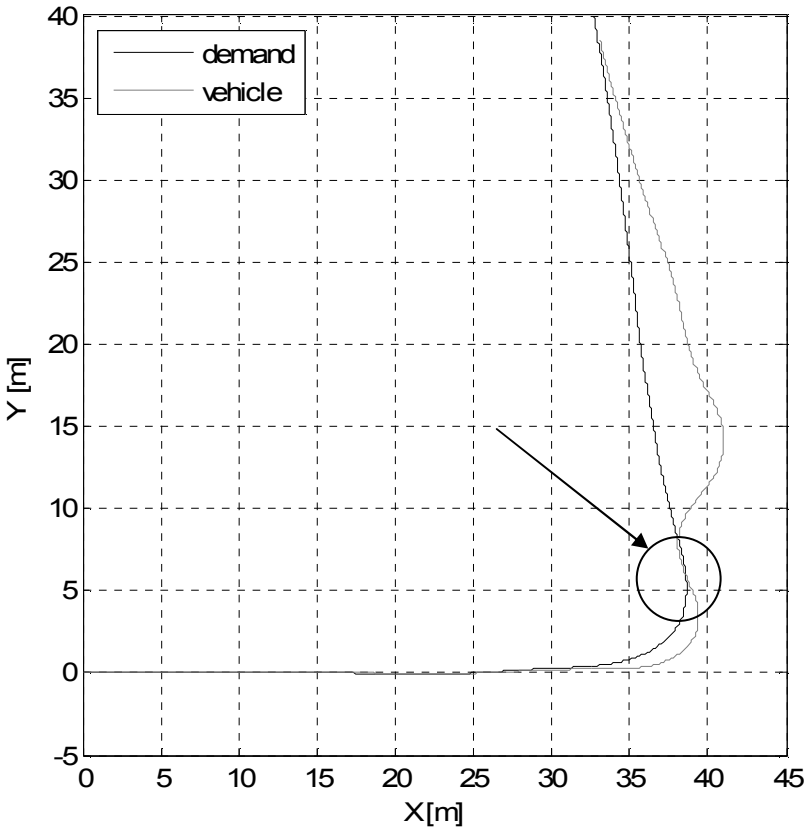

Figure 6.21 – Comparison of the demand trajectory with the vehicle output trajectory

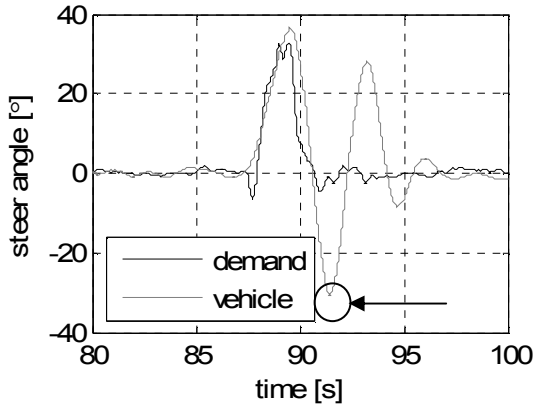

Figure 6.22 – Comparison of the measured steer angle and the roll control steer angle

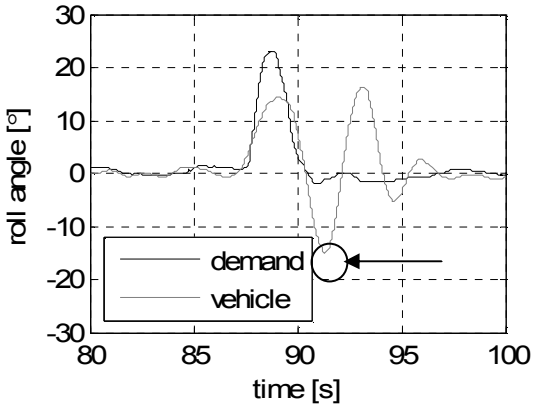

Figure 6.23 – Comparison of the measured roll angle and the simulation model output roll angle

The simulations have shown that if a real driver drove a vehicle with PID steer tilt control, the driver and the STC would act against one another. This conflict could be limited if the driver allowed for path deviations and if the PID gains of the STC could be adjusted during the manoeuvre.

6.3 DISTURBANCES

A good controller will be able to perform its tasks even when there are disturbances present. These can be internal disturbances such as signal noise, as well as external forces. Three external disturbances were selected: road camber, hill driving and crosswind. The effects of these three disturbances have been discussed in chapter 3. The following sections discuss the controller performance and the overall vehicle response when these disturbances are added to the simulation.

6.3.1 Road Camber

In chapter 3, the difficulties of driving a tilting three-wheeled vehicle along a cambered road have been discussed. In this section, a selection of simulation results of a tilting vehicle driving along a cambered road is presented. In the first simulation, the roll angle feedback to the roll equation was reduced by a fixed amount. This fixed amount was related to the road camber. The set up ensured that even though the front section of the vehicle was rolled in relation to the rear, the roll dynamics recognised that the front section of the vehicle was upright. After each increase in relative roll, the driver model adjusts the steering and settles at a steady state value. Whilst the steering is adjusted, the vehicle yaws and translates in the lateral plane. As the vehicle settles into a steady state, the front tyre slip angle and camber angle cause equal and opposite side forces. The direction of the velocity vector at the rear tyres is equal to the rear steer angle, so there is no slip at the rear tyres. It is assumed that the friction between the rear tyres and the road is large enough to prevent the rear unit from sliding down the camber. The only non-zero terms of the roll equation are a small moment from the roll angle error, a roll moment from the camber and the tyre width and a small moment from the normal force. Table 6.2 shows the steady state steer angle the driver would have to apply to continue in a straight line. The table also shows the equivalent roll angle as it would be measured in the global reference frame. These data show a linear increase in the corrective steer angle as the road camber angle increases.

camber θ [o]	0.00	5.00	10.0	15.0	20.0	25.0	30.0	35.0	40.0	45.0
corrective steer angle δ_f [o]	0.00	1.01	2.02	3.03	4.04	5.05	6.06	7.07	8.08	9.09
roll angle ϕ [o]	0.00	4.49	8.99	13.48	17.98	22.47	26.96	31.46	35.95	40.45

Table 6.2 – Extrapolated steady state corrective steer and the roll angle for various road camber gradients assuming steady state conditions at 16.2 kph

The data shown in Table 6.28 were generated under ideal simulation conditions where the forward velocity and the road camber angle were constant and there were no additional disturbances. The simulation model had shown that a change in road camber required the driver to adjust the steering significantly. The simulation also illustrated that the driver would have difficulty following the path: the steady state stability was achieved by a constant lateral trajectory error resulting in a constant driver adjustment and therefore roll angle demand. This roll angle demand ensures that the vehicle rolls to the appropriate angle for the road camber. In reality, the driver will continue to increase the steering angle when the lateral error does not decrease.

In other words, road camber can cause the vehicle system to become unstable because the driver and the roll control will act against one another. The driver will only react to small deviations from the path, so the driver's steering input will, initially, not balance with the road camber. The driver may eventually adapt to apply the correct amount of steer to balance with the road camber; however, this driver behaviour cannot be achieved with the available driver model but may be 'learnt' by a real driver.

6.3.2 Hill Driving

In chapter 3, potential problems with driving up or down hills whilst controlling the roll angle of the vehicle have been discussed. To test the effect of driving up or down hills, the vehicle simulation model with driver model and roll control has been made to drive around a corner either up or down hill. First, velocity and yaw rate inputs from the experiments were used for the simulation. The simulation was run for the vehicle going uphill and downhill for a range of hill gradients. Next, the effect of the road gradient on various dynamic variables was established by setting the velocity and the demand yaw rate to a constant value and running the simulation for a range of gradients.

The simulation results for the first test where inputs from the experimental manoeuvre were used showed very little difference in the vehicle's dynamics between a flat road and a downhill trajectory. However, the vehicle would become unstable going up a hill with a gradient greater than 14%. This could be explained by the differences in load distribution: when going downhill. The load on the front wheel increases which allows a greater side force to be generated for a given slip and camber angle. However, when travelling uphill the static load on the front wheel is reduced and the vehicle is accelerating to counteract the gravity component, which causes load to be transferred to the rear wheels. This overall reduction of the normal load on the front tyre reduces the amount of force that can be generated at the tyre contact patch, thus reducing the

ability of a steer controller to generate large enough forces to balance the vehicle. This is not dissimilar to a situation where the tyre slip stiffness changes because of tyre wear or road conditions and may present a significant control problem.

The simulations where the velocity and demand yaw rate were fixed to a constant value resulted in the following observations: When travelling uphill, the driver has to increase the steering by a fraction of a degree to maintain the same trajectory as when travelling along a flat road. As a result, the front slip angle is slightly larger and the rear slip angle is slightly smaller. When travelling downhill, the driver has to reduce the steering angle by a fraction of a degree with a slightly decreased front slip angle and a slightly increased rear slip angle as a result.

6.3.3 Side Wind

A crosswind was recognised as a possible disturbance to the vehicle roll. A crosswind could cause the vehicle to veer off the trajectory if going in a straight line and a gust of wind could hamper the vehicle stability when cornering. To test the effect of a crosswind on a tilting vehicle the following cases were isolated, namely: A gust of wind whilst driving in a straight line, a constant crosswind whilst driving in a straight line, and a gust of wind whilst cornering. The magnitude of the wind force was based on the Beaufort wind force scale as shown in Table 6.3. This table shows the Beaufort wind force scale, the average wind velocity, and the resulting force on the Honda Gyro.

Beaufort Wind Force	1	2	3	4	5	6	7	8
Wind Velocity [m/s]	0.8	2.4	4.3	6.7	9.3	12.3	15.5	18.9
Force on Gyro [N]	0.326	2.935	9.420	22.87	44.06	77.08	122.4	182.0

Table 6.3 – Wind force on the Honda Gyro assuming the wind direction is perpendicular to the direction of travel

A sudden gust of wind on the Honda Gyro travelling along a straight road was found to roll the vehicle and cause a trajectory error. First, the roll error caused the roll controller to steer the vehicle to ensure the vehicle was balanced. Once the lateral error had passed the threshold, the driver started to make small adjustments to the steering to return to the path. In general, the roll controller could control the roll caused by the gust of wind. However, the path deviation for heavy gusts of wind was greater than the width of a driving lane, which would be very dangerous. A rolling vehicle is more susceptible to path deviations as a result of a crosswind, because the vehicle roll will generate a lateral tyre force from the camber. The simulation showed that if the roll joint were locked so that the vehicle could not roll, the path deviation was more or less halved.

If the wind was blowing with a more or less constant velocity, the vehicle response was found to be similar to that of a vehicle driving along a cambered road. The roll control would tilt the vehicle such that the roll moment due to gravity and the centre of mass location would be equal and opposite to the moment caused by the wind. In order to maintain a rectilinear trajectory, the driver had to apply a small steer angle. The constant roll angle demand from the driver was caused by a constant lateral error as was discussed in the Road Camber section. In reality, a real driver would not allow for a constant lateral error and would steer more in order to return to the trajectory. Eventually, a driver will learn that he has to apply a fixed steering angle to remain on the trajectory. However, a constant crosswind acting on the vehicle could cause the vehicle to become unstable if the interaction between the driver and the steer tilt controller becomes such that the roll control can no longer deal with the driver's demands in combination with the roll moment caused by the wind. A simulation where the driver increases the steering angle if the lateral error becomes more or less constant showed that, with a constant crosswind, the roll controller applies a saw tooth pattern steering angle. The roll angle corresponded with a similar characteristic and the vehicle zigzagged about a rectilinear trajectory parallel to the demand trajectory.

The final case where a gust of wind blows perpendicular to the vehicle when it is turning produced varying results depending on the wind direction and the direction of the turn. When the gust of wind blew such that it increased the roll, the controller had difficulties increasing the steering angle fast enough to generate a lateral force to prevent the vehicle from falling over. However, when the gust of wind blew in the other direction, that is decreasing the roll angle, the vehicle remained stable even when the wind force surpassed 125N, or a wind velocity of 15.66m/s. In the former case, the roll controller had to increase the steering angle to ensure the vehicle would not roll over. In the latter case, the roll controller only needed to decrease the steering angle by a small amount, which did not cause any stability problems.

6.4 CONCLUDING REMARKS

Steer Tilt Control based on a PID algorithm was analysed to determine what is required of a steer controller and where its limitations lie. The effect of a linearised roll model was illustrated: the steering adjustments from the controller vary depending on whether the roll model is linear or non-linear; hence, the resulting vehicle trajectory differs. Another factor that could cause problems with the control was the steer control actuation system. Initially this was modelled as a lag. This lag actuation model filtered high frequency low amplitude adjustments from the control demand, but as the time constant increased, introduced low frequency high amplitude

adjustments. Finally, the PID based STC was combined with a complex non-linear vehicle model, a DC motor model for steer actuation and a tyre model with tyre relaxation. The simulation demonstrated the limitations of PID based steer tilt control: it can demand extreme steering angles from the steering actuator for certain combinations of steering velocity, steer angle and vehicle speed. In addition, it was found that whenever the vehicle model parameters were changed, the PID controller gains had to be adjusted to ensure stability.

One of the aims of the driver model development was to combine it with the steer tilt controller to determine how a driver would react to the unexpected changes in the steer. It was shown that it was possible have the controllers act concurrently. However, the PID and the driver gains had to be modified depending on the manoeuvre.

The final section of the chapter discussed the effect a selection of external disturbances would have on the vehicle-controller system. These disturbances were road camber, road inclination and side wind. Each of these external factors was shown to cause major problems in terms of the vehicle roll stability and the path following. If these disturbances were to be included in a control algorithm, additional logic routines and instrumentation would be required.

CHAPTER 7. CONTROLLER DEVELOPMENT

In the previous chapters experimental results illustrating driver behaviour have been presented, a vehicle and tyre model have been developed and validated by the experimental results, the properties of a Steer Tilt Controller have been analysed, and the effect of a driver in the loop has been demonstrated. This chapter combines what has been learnt to develop a new algorithm for a Steer Tilt Controller and test it in simulation.

7.1 STEER TILT CONTROLLER DEVELOPMENT

PID Steer Tilt Control as is found in literature is incomplete: it controls the tilt angle without taking into account the path the driver intends to follow. Controlling both the path and the tilt angle are conflicting control demands. Besides, classic steer tilt control is often based around balancing the tilt angle around zero and is less effective under transient conditions.

7.1.1 Inverted Pendulum on a Cart

The inverted pendulum problem is one of the most discussed control problems in literature. It is an example used in every textbook, and many novel control methods have been tested on the inverted pendulum problem. In essence, the tilt control problem is an inverted pendulum problem where the cabin is the pendulum and the rear unit is the cart on which the pendulum is mounted. The control problem is to balance the pendulum and control the lateral motion of the cart.

Section 2.2 discussed the equations for an inverted pendulum system (equations 2.3 to 2.9). In order to develop an improved steer tilt control system for the tilting vehicle, it was thought that a study into the numerous methods of controlling an inverted pendulum would provide a good starting point.

7.1.1.1 PID Control of an Inverted Pendulum on a Cart

The pendulum and cart were modelled using equations (2.8) and (2.9). These linearised equations were transformed into the transfer functions in equations (7.1) to (7.3). The pendulum controller

was a Proportional-Integral-Derivative controller set with appropriate gains for the systems characteristics: the geometry and mass data of the system were set to simulate the Honda Gyro as shown in Table 7.1. Figure 7.1 shows the block diagram of the controller.

$$\frac{\Phi(s)}{\mathrm{F}(s)} = \frac{-mh\mathrm{s}^2}{[(I_\mathrm{x} + mh^2)(M+m) + m^2h^2]\mathrm{s}^4 - mgh(M+m)\mathrm{s}^2} \tag{7.1}$$

$$\frac{\mathrm{Y}(s)}{\mathrm{F}(s)} = \frac{(I_\mathrm{x} + mh^2)\mathrm{s}^2 - mgh}{[(I_\mathrm{x} + mh^2)(M+m) + m^2h^2]\mathrm{s}^4 - mgh(M+m)\mathrm{s}^2} \tag{7.2}$$

$$\frac{\Phi(s)}{\mathrm{Y}(s)} = \frac{-mh\mathrm{s}^2}{(I_\mathrm{x} + mh^2)\mathrm{s}^2 - mgh} \tag{7.3}$$

M [kg]	**m [kg]**	**I_x [kg m^2]**	**h [m]**
40	160	25.2	0.711

Table 7.1 – Honda Gyro equivalent parameter values

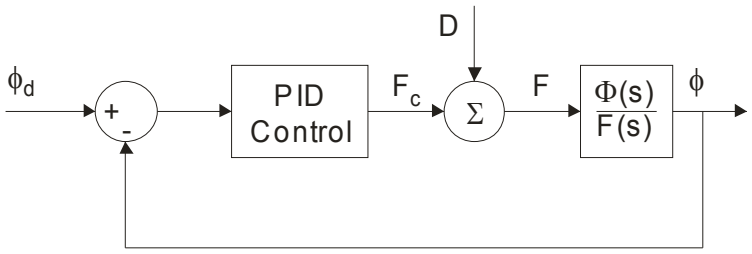

Figure 7.1 – Block diagram of the inverted pendulum on a cart system

To start, the disturbance to the system was a pulse force and the controller's goal was to balance the tilt angle about zero. The controller output was equal and opposite to the disturbance D. The total force applied to cart was a small positive pulse at the start of the disturbance and a small negative pulse at the end of the disturbance. The effect of the applied force was a small, a fraction of a degree sway of the pendulum from left to right. At the start of the disturbance, the cart started to move sideways and stopped at the end of the disturbance. When the disturbance force was changed to a step disturbance whilst the roll angle demand remained zero, the following was found. The roll angle displayed a small disturbance as the step was applied, but quickly returned to zero. The roll and lateral acceleration signals also demonstrated small disturbances at the step time, but returned to zero promptly. The lateral velocity however,

showed a step change so that the cart continued to move sideways. So if there were a constant disturbance, the cart would have to keep moving to balance the pendulum.

The next step was to remove the disturbance force and set the roll angle demand to a non-zero value. A step change in the roll demand resulted in a constant lateral acceleration. This lateral acceleration was equal to the lateral acceleration needed to balance the demand roll angle according to equation (2.24). This response demonstrated that the system would be stable when going around a constant radius circular path. Under these steady state conditions, external disturbance forces were easily rejected by the controller. When the roll angle demand was set to a pulse, which imitated a lane change or a cornering manoeuvre, the resultant lateral velocity would remain non-zero after the demand had returned to zero. This was similar to the system response when the roll angle demand was zero and there was a constant disturbance force.

The examples in this section have illustrated that an inverted pendulum on a cart controlled by a PID controller is not an appropriate analogy of a tilting vehicle. The PID roll control allows the cart to translate laterally which causes a vehicle to deviate from its intended trajectory. There are control strategies that make use of observers and Linear Quadratic Controllers that control both the pendulum roll angle and the cart position. However, these control methods were found to be impractical for a vehicle since the inverted pendulum on a cart control problem was too far removed from the case of a vehicle with a driver: the cart's dynamics are too simple in comparison with the dynamics of a vehicle.

7.1.2 Driver Behaviour and Controller Properties

The experimental results presented in chapter 5 showed that the human driver applied countersteer to balance the vehicle, but the amount of countersteer was related to the driving style and less related to the speed of the manoeuvre, the radius of the turn, or any other variable. In other words, there is no single unique solution to the amount of countersteer required for one specific turn.

In addition to the driver applying an arbitrary amount of countersteer, it was found that, under transient conditions, the driver did not follow the theoretical balanced roll angle, but either overleaned or underleaned; the driver overleaned at the start of a turn and underleaned at the end of a turn. For these reasons, it was decided to develop a control method that applied some countersteer to start the tilting process. This amount would have to be related to the driver's inputs: speed, steering angle and direction, and steering velocity and direction. A strategy was required to determine when to stop the countersteer. It was suggested that the controller apply a

countersteer until a set 'minimum' roll angle was reached. Once the roll angle feedback indicated that that the vehicle had reached this minimum, the roll would be controlled by balancing the lateral acceleration of the vehicle with the gravity component acting on the rolling assembly. This balancing control would also depend on the driver inputs: whether the driver displayed the desire to continue tilting, remain at a constant roll angle or straighten up.

The 'minimum' roll angle can be achieved in numerous ways: even a small amount of lateral acceleration will start the vehicle rolling. If the countersteer caused a brief and low magnitude lateral acceleration, the resulting roll moment would be small and the roll angle would slowly reach the 'minimum'. If the countersteer caused a significant lateral acceleration and it were applied for a notable period of time, the minimum roll angle would be reached very quickly and the magnitude of the roll acceleration at the end of the countersteer application would be significant. It is not desirable for the roll acceleration at the end of the countersteer manoeuvre to be large, because it will subsequently require a lot of effort to slow the roll down to maintain a constant roll angle or to straighten up. The aim is to determine the best way to define the countersteer.

The experimental results had demonstrated that the steering angle, lateral acceleration and the roll angle exhibited similar features as shown in Figure 7.2 to Figure 7.4. Figure 7.2 illustrates a more or less proportional relationship between the steering angle and the total lateral acceleration albeit with a lag. These dynamic variables are related, because the steering angle causes part of the lateral forces that result in the acceleration. Similarly, Figure 7.3 shows a more or less proportional relationship between the roll angle and the total lateral acceleration where the acceleration lags behind the roll angle. The lateral acceleration and gravitational roll moments are the principal moments that are balanced in the roll equation. These two moments are expected to be of equal magnitude to balance the vehicle and only cause small roll accelerations. Figure 7.4 combines the fact that both the steering angle and the roll angle are proportional to the total lateral acceleration; hence, these two variables have to be proportional. Assuming the steering angle and roll angle are proportional, their respective velocities must also be proportional. This is important, since if the controller applies countersteer to reach a minimum tilt angle, the countersteer should be applied in such a way that the tilting velocity is approximately proportional to the driver's steering velocity.

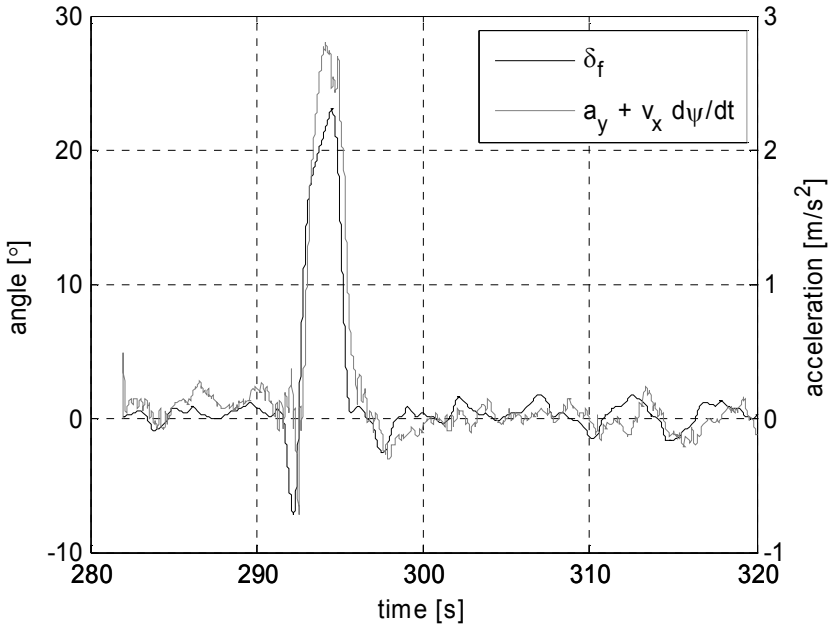

Figure 7.2 – Comparison of the typical features of the steering angle and the total lateral acceleration signals when cornering from section 4.3.3

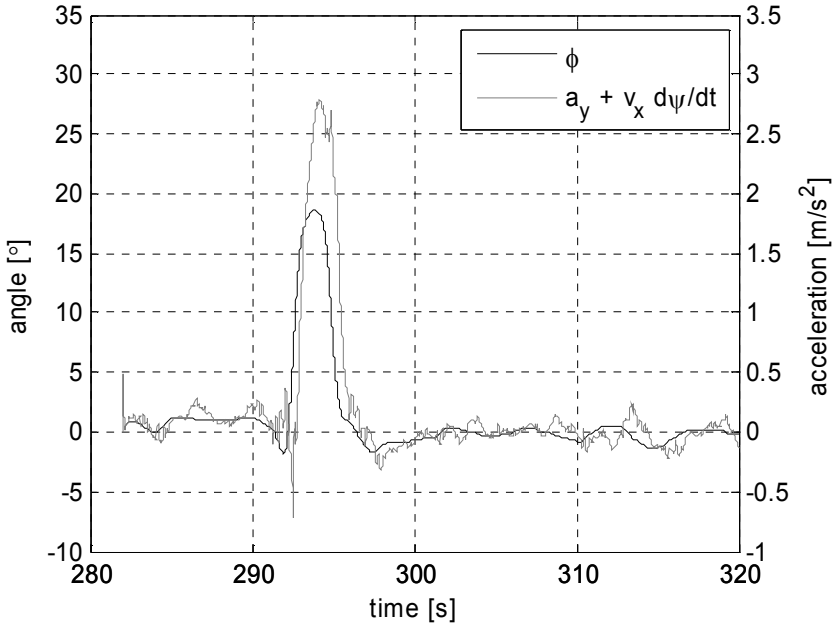

Figure 7.3 – Comparison of the typical features of the roll angle and the total lateral acceleration signals when cornering from section 4.3.3

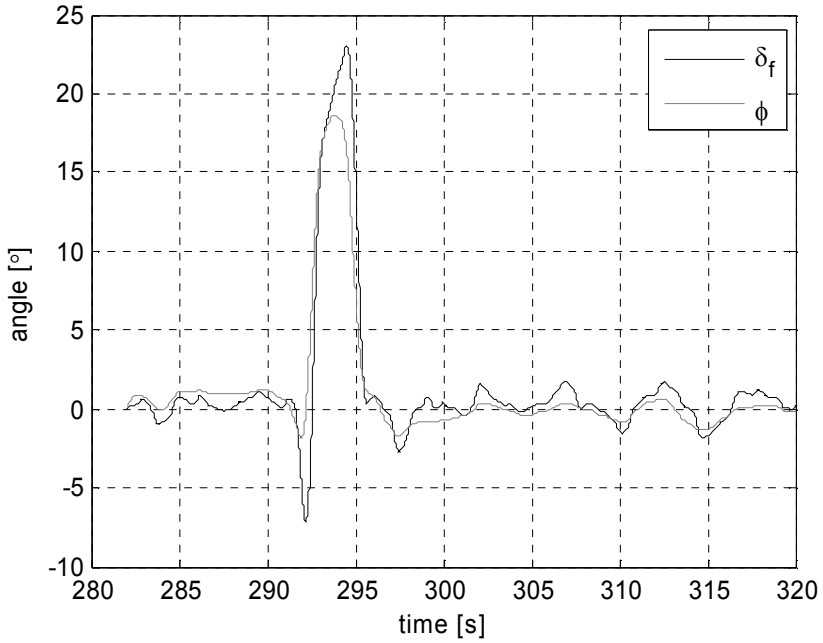

Figure 7.4 – Comparison of the typical features of the steering angle and the roll angle when cornering from section 4.3.3

7.1.2.1 Countersteer to Minimum Roll Angle

The previous section described the concept of applying countersteer to roll the vehicle to a minimum angle and subsequently managing the steer and therefore lateral acceleration depending on the driver's input. The block diagram shown in Figure 7.5 shows the basic system: the switch block checks if the roll angle has passed the minimum value. If the roll angle is less than the minimum value, a lateral acceleration proportional to the error is applied. If the roll angle is equal to or greater than the minimum value of 5 degrees, a lateral acceleration proportional to the moment due to gravity is applied.

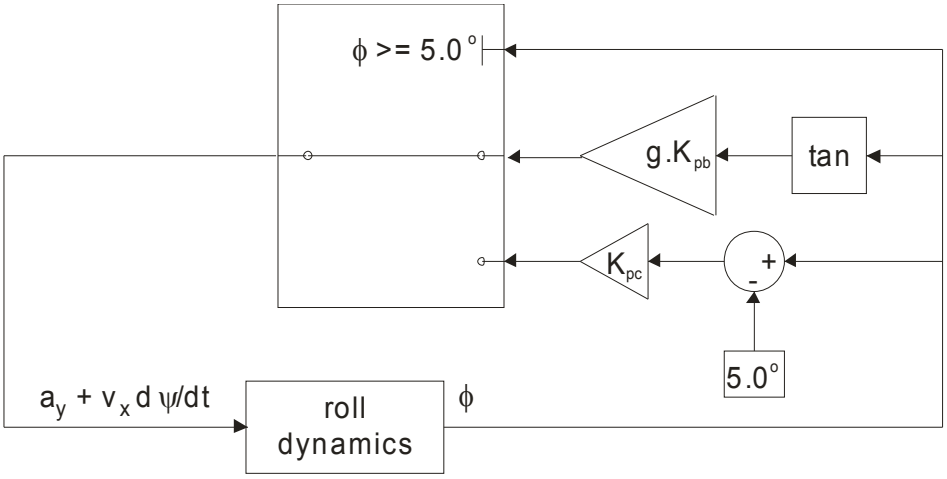

Figure 7.5 – Block diagram of the basic system to apply an opposing lateral acceleration to achieve a minimum roll angle and subsequently apply a small lateral acceleration to slow the roll velocity

This system successfully caused the vehicle to lean. The tilt velocity depended on the gains that were set for both the countersteer, K_{pc}, and the limiting lateral acceleration, K_{pb}. The countersteer gain K_{pc} determined how fast the vehicle reached the minimum tilt angle: the larger the gain the quicker. The limiting acceleration gain K_{pb} determined how fast the vehicle continued the tilting motion: the larger the gain, the slower the tilting velocity.

Figure 7.6 illustrates the effect of K_{pb}: the magnitude of this gain affects the roll of the vehicle after the minimum roll angle has been achieved. If this gain is too small, it allows the vehicle to continue rolling after the initial countersteer. When this gain is equal to or greater than 1, the roll moment from the acceleration becomes greater than the roll moment due to the displacement of the centre of mass and the vehicle starts to roll in the opposite direction. The greater the magnitude of K_{pb}, the faster the roll velocity decreases and the sooner the roll slows down and changes direction.

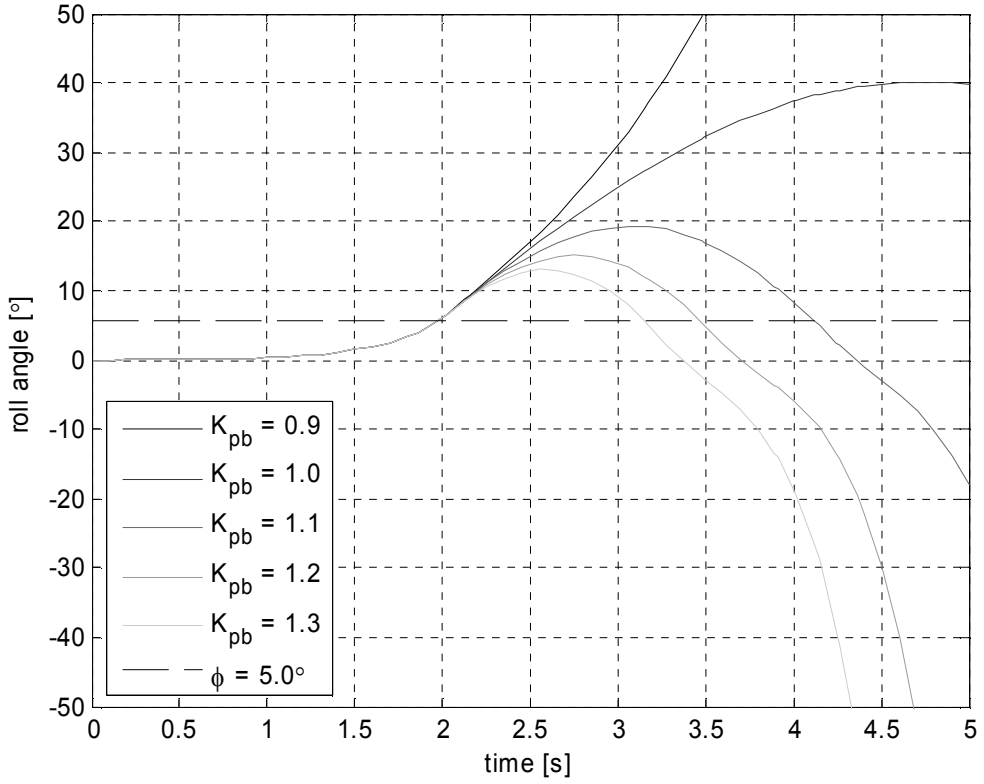

Figure 7.6 – Effect of the limiting acceleration gain K_{pb} on the roll angle when the countersteer gain K_{pc} = 0.10

Figure 7.7 shows the effect of the countersteer gain K_{pc} on the roll angle progression. As would be expected, the greater this gain, the faster the roll angle reaches the minimum set value of 5 degrees.

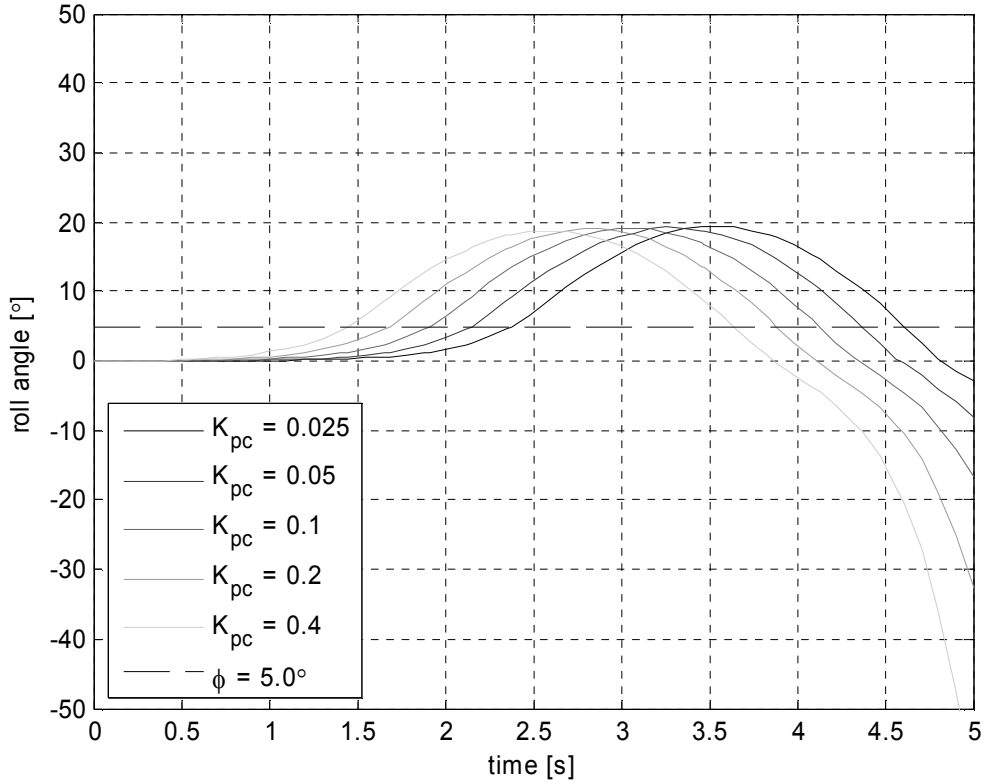

Figure 7.7 – Effect of the countersteer gain K_{pc} on the roll angle when the limiting acceleration gain K_{pb} = 1.10

Figure 7.8 shows that the roll velocity barely varies with the gain: the gain appears to affect how soon the vehicle reaches the minimum steer angle, but the roll dynamics are fixed. This behaviour can be explained by the balance between the roll moments: the moment from the lateral acceleration is small and is only necessary to start the roll process and once the roll has started, it is governed by the gravitational acceleration.

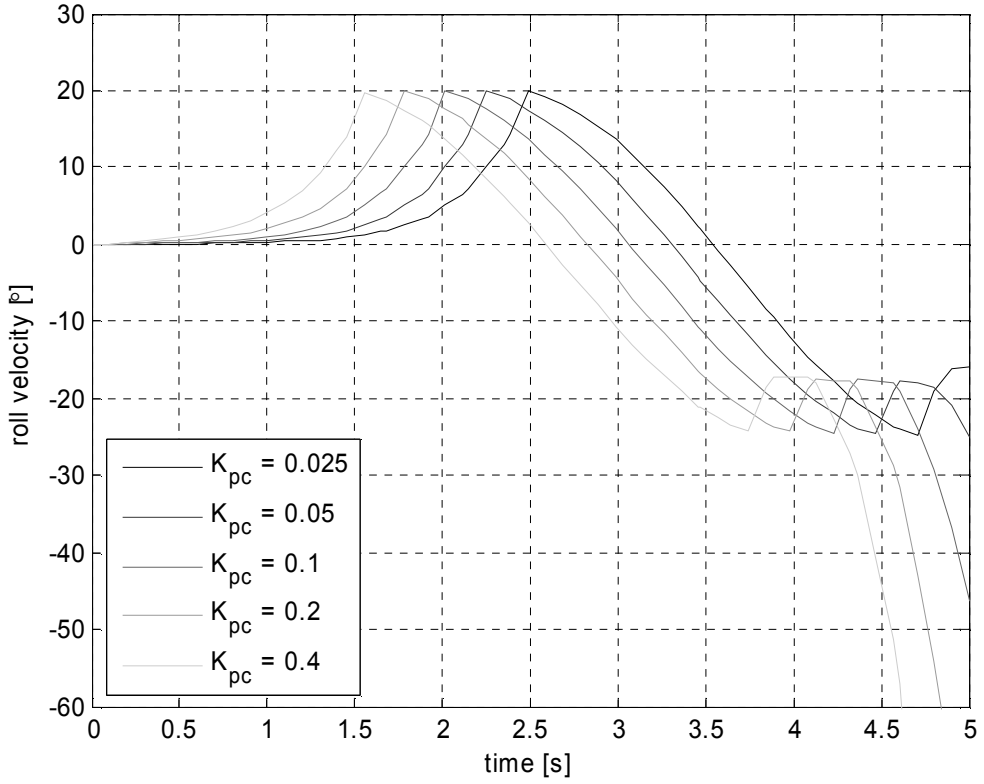

Figure 7.8 – Effect of the countersteer gain K_{pc} on the roll velocity when the limiting acceleration gain K_{pb} = 1.10

7.1.2.2 Countersteer to Reach a Minimum Roll Angle, Tilt to a Maximum Roll Angle and Straighten Up

In the first step, the lateral acceleration was controlled to ensure the vehicle rolled to a minimum angle and subsequently controlled either to lean the vehicle more, or to slow the leaning to start straightening up. This section discusses a method to lean the vehicle to a set maximum roll angle and then straighten up by controlling the lateral acceleration.

Figure 7.9 shows the block diagram of the control system where the control switches between tilting the vehicle to a minimum roll angle, applying a lateral acceleration so that the vehicle continues to tilt, or applying a lateral acceleration to straighten the vehicle back up. The switching depends on the current roll angle. If the roll angle is less than the minimum, a negative, countersteer equivalent, acceleration is applied. If it is greater than the minimum but less than the maximum, an acceleration that allows the vehicle to continue tilting is applied. In all other cases an acceleration that causes the vehicle to straighten up again is applied.

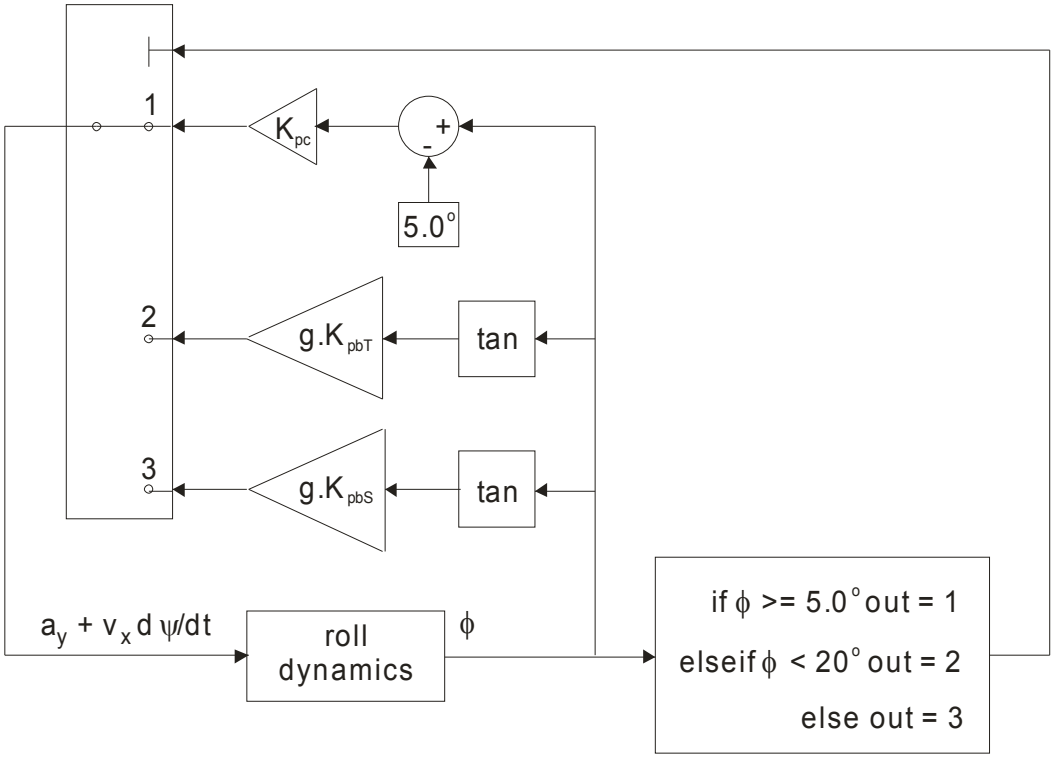

Figure 7.9 – Block diagram of the acceleration controller switching between countersteer, tilting and straightening up

The effect of the countersteer and tilting gains, K_{pc} and K_{pbT} respectively, is the same as shown in Figure 7.6 and Figure 7.7. This modified system did also allow the straightening up of the vehicle to be controlled as shown in Figure 7.10. This figure demonstrates that the greater the gain, the quicker the vehicle straightens up. In all the cases shown in Figure 7.10, the vehicle continues to tilt at least another 5 degrees after it has passed the maximum roll threshold. This indicates that there may be a need to apply an increased lateral acceleration to commence the straightening up before limiting the lateral acceleration, similar to applying a countersteer equivalent lateral acceleration.

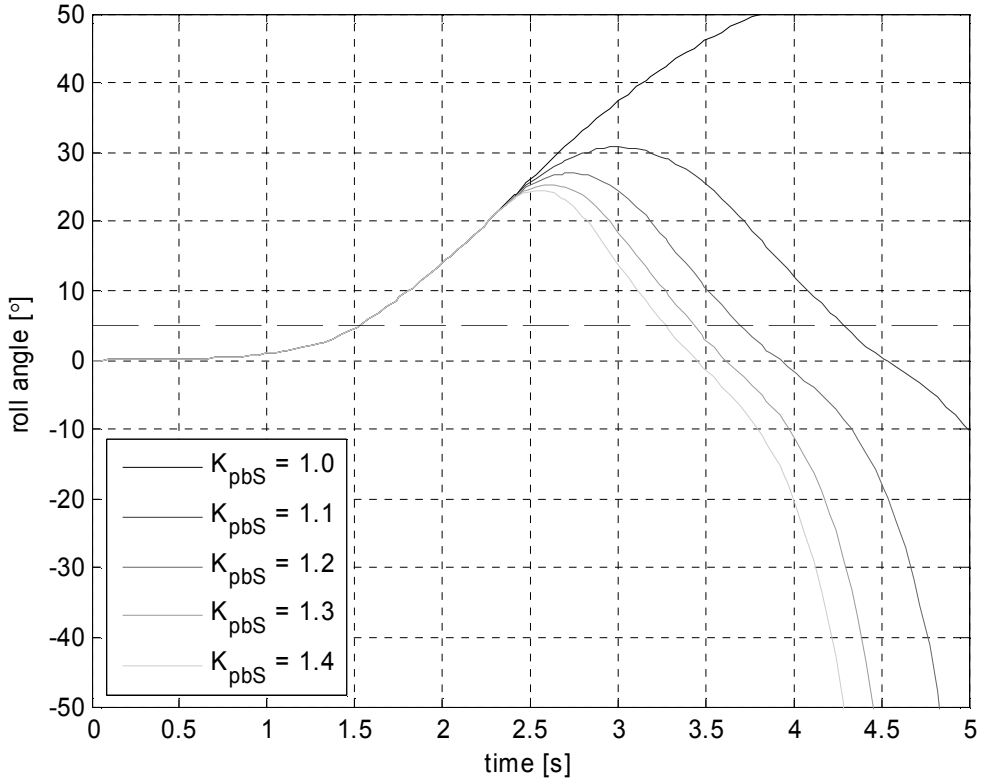

Figure 7.10 – Effect of the straightening up gain K_{pbS} when $K_{pbT} = 0.9$ and $K_{pc} = 0.2$

The control stratagems presented so far have assumed that the controller detected the need to roll the vehicle and straighten up again. These methods did not include a strategy for the end of the manoeuvre where the roll angle has to return to zero. In the case of a real vehicle, the driver's steering input will indicate what the roll controller is required to do: roll, straighten up, or return to zero. The next section will discuss how the driver's input is incorporated.

7.1.2.3 Incorporating the Driver's Input in the Controller's Actions

The previous section discussed a roll control method that set a minimum and maximum tilt angle. This section discusses the use of the driver's steering input to indicate what action is required from the controller. For example, if the steering angle is zero, the roll needs to be zero, but if the steering angle changes from zero to non-zero, a countersteer action is needed to commence the rolling. As long as the steering angle and steering velocity are of the same sign, the vehicle needs to continue to roll. When the steering angle and the steering velocity are of opposite signs, the vehicle needs to straighten up: see the comparison of the steering angle and its velocity shown in Figure 7.11.

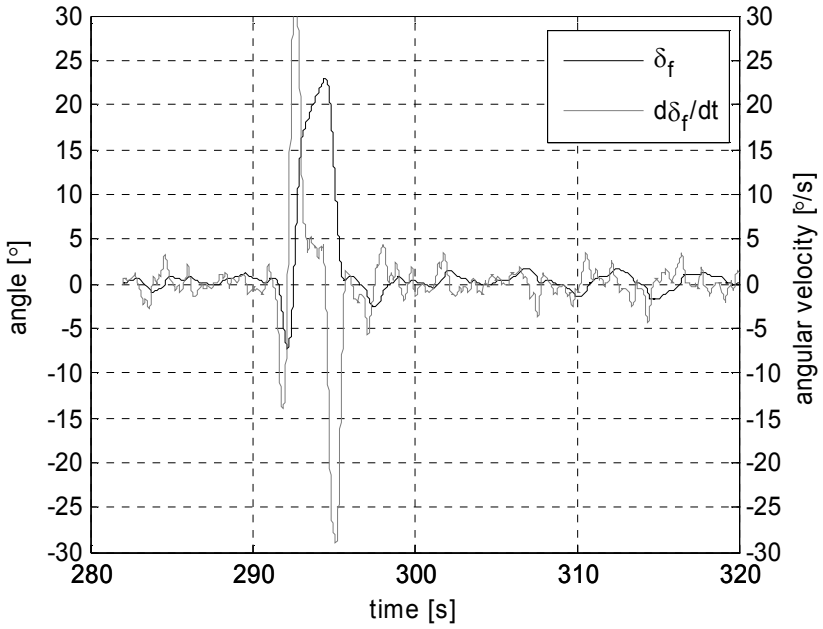

Figure 7.11 – Typical time progression of the steering angle and the steering velocity for a 90o turn at 13.3 kph taken from the experimental results discussion in section 4.3.3

The maximum roll angle condition was replaced by setting the condition for changing the controller gain from tilting to straightening up to be dependent on the direction of the steering angle and velocity: if the steering angle and velocity have the same sign, the vehicle should continue to lean and if they have opposing signs, the vehicle should straighten up. Figure 7.12 shows a flow chart of this controller algorithm as well as the definition of the minimum roll angle: the minimum roll angle was set to zero when the steering angle was zero. To improve the performance of the algorithm, the gains K_{pc}, K_{pbT} and K_{pbS} were adjusted during the manoeuvre depending on the error between the roll angle and a proportion of the steering angle. However, the starting values of K_{pc}, K_{pbT} and K_{pbS} were largely dependent on the maximum steering angle magnitude of the manoeuvre and therefore the steering velocity. Hence, this method was not ideal, because a controller cannot predict what the driver will do next.

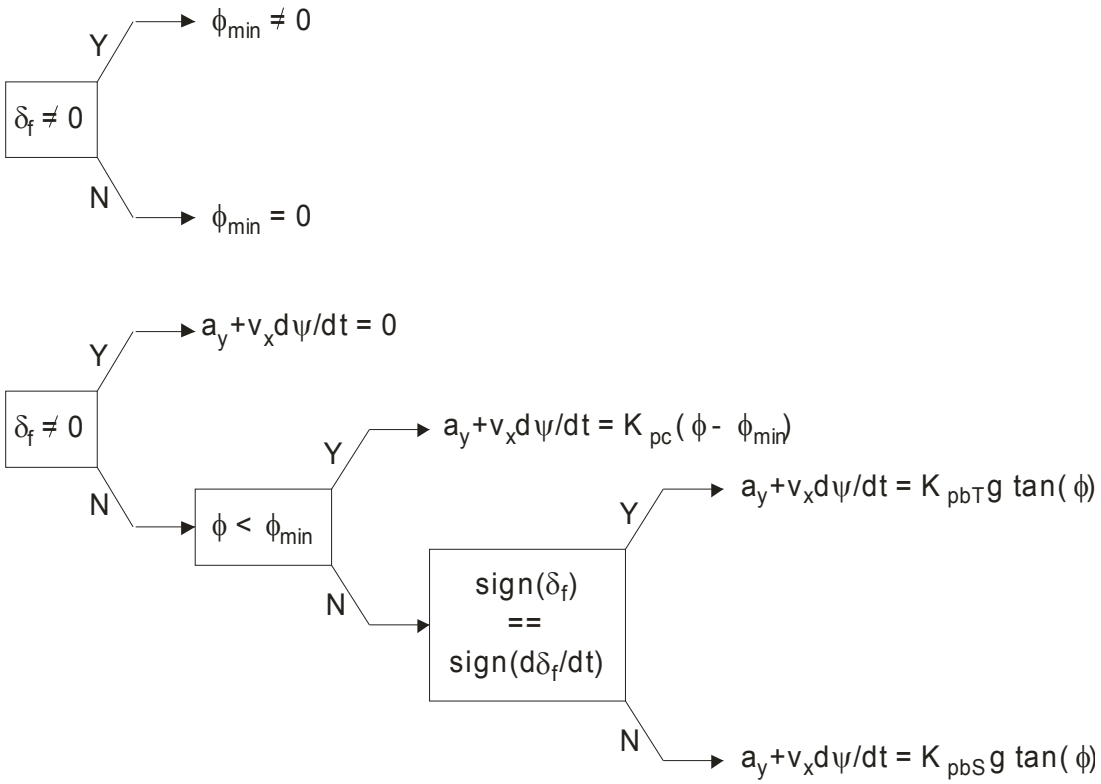

Figure 7.12 – Flow diagram of the controller algorithm taking into account the driver's steering input

7.1.2.4 Countersteer to Minimum Roll, Limit Accelerations and Apply Balance Control

Even with an algorithm that successfully adjusts the K_{pbT} and K_{pbS} gains, the current method does not include the small steering adjustments necessary to balance the vehicle about a zero roll angle. The balancing control of the PID roll controller was thought to guarantee the best results when the roll angle demand was set to zero. This section discusses the integration of the two methods.

When the driver's steering input is small, the goal is to stabilise the roll angle about the vertical; that is, the roll should be zero. Only when the driver's steering angle and velocity pass a certain threshold should the roll control come into action, otherwise the PID should ensure that the vehicle remains upright.

Although this method showed that it could control the roll angle, there was a multitude of drawbacks. First the transition between tilting and balancing: once the PID controller switched off, the roll angle already lagged behind the roll angle required for the driver's manoeuvre. As a result, the roll velocity rapidly increased to reach the required roll and subsequently overshot the necessary roll angle. Hence the roll velocity whilst straightening up was also increased and the roll

angle overshot the vertical. In order to return to the vertical, the PID had to apply a significant steering adjustment.

7.1.3 Control Algorithm

The controller algorithms that have been discussed so far could not be tuned to perform at acceptable standards: balance the vehicle roll angle with minimum adjustment of the driver's steering input and minimum levels of perceived acceleration by the driver. Thus, an entirely different approach was taken. The roll dynamics are such that the steering adjustments that cause the roll angle are small in comparison to the steering adjustments to negotiate the turn. Hence, the roll controller should only need to add or subtract small amounts of steer from the driver's input. These small amounts of steer can be called **countersteer** and **oversteer**. It was also recognised that generally the controller adjustments should occur whenever the driver's steering velocity changed direction or slowed down as marked in Figure 7.13.

The goal was to develop a controller that could be easily implemented in practice. What this meant was that the programming of the controller had to be relatively simple and the inputs to the controller needed to be measurable and reliable vehicle states.

It was identified that steer tilt control could cause the vehicle to leave the path the driver had intended to follow. Therefore, the basis of the applied steering angle had to be the driver's input with the controller adding or subtracting small amounts of steer. This was thought to minimise the interference of the roll control on the driver's intended path.

7.1.3.1 Controller Logic

At state 1 in Figure 7.13, the controller detects that the driver wants to turn and therefore wants to roll the vehicle, so the controller needs to apply countersteer. At state 2, the steering velocity is slowing down indicating that the driver has either reached the apex of the turn or steady state. This tells the controller that the roll has to slow down and the controller has to apply oversteer. State 3 on Figure 7.13 indicates to the controller that the driver has indeed reached the apex of the turn and the vehicle has to straighten up. More oversteer has to be added to the driver's steer to start rolling in the other direction. As the driver's steer slows down again, at state 4, it tells the controller that the roll velocity has to slow down to zero. Thus, the controller has to apply countersteer to slow the roll.

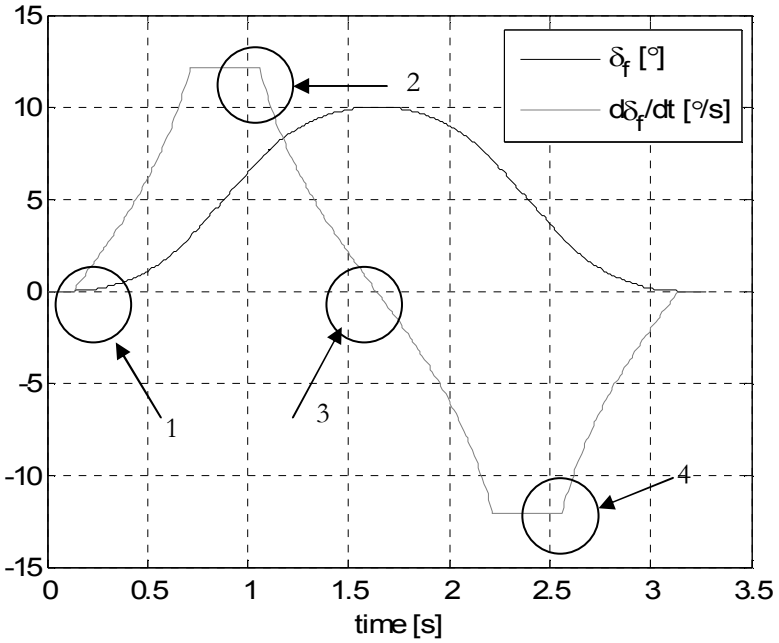

Figure 7.13 – Typical driver steer angle and steering velocity input

The controller logic was set up as shown in the flow diagram in Figure 7.14. This part of the controller logic only deals with whether or not the controller needs to apply countersteer or oversteer. This logic is executed from the start at every time step: once a decision has been reached, the logic resets and starts again.

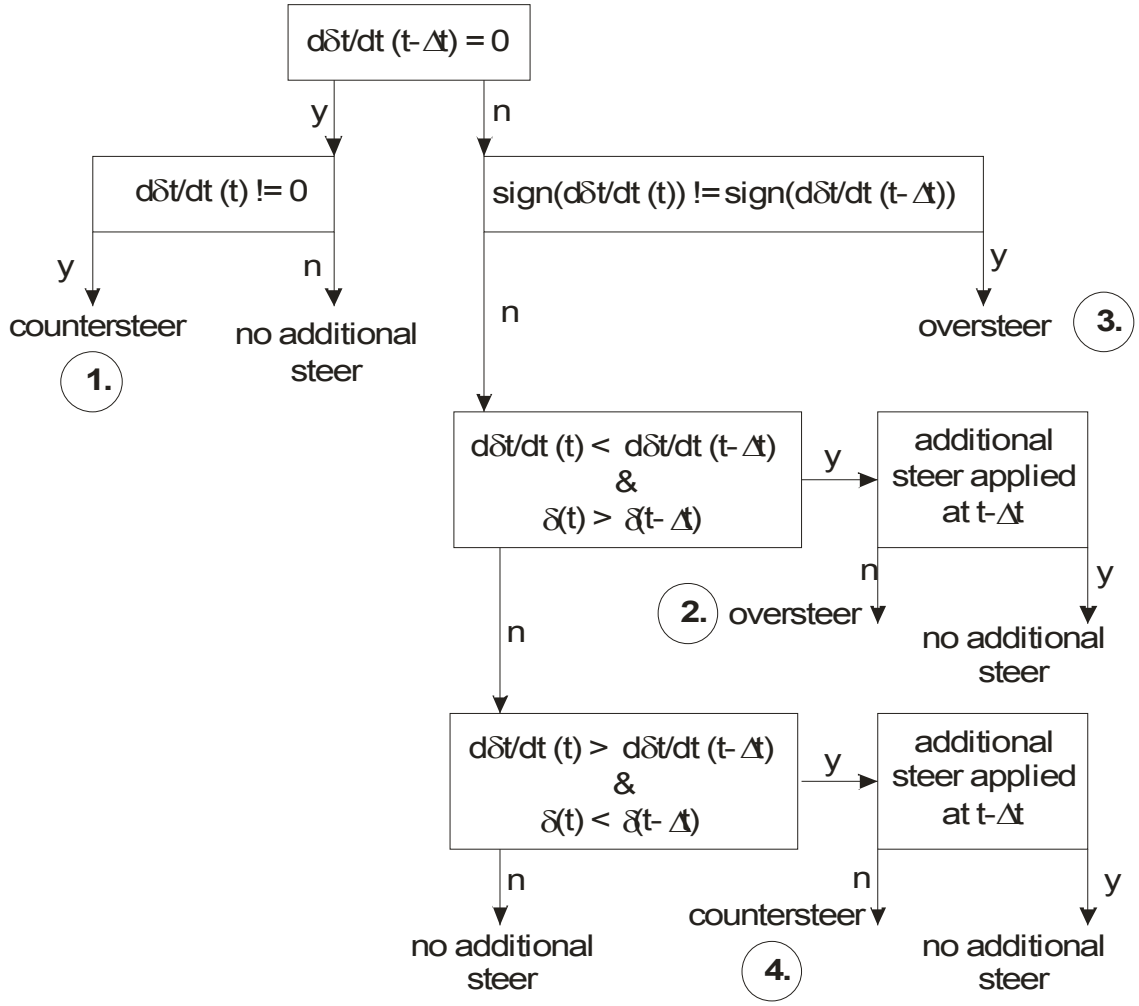

Figure 7.14 – Logic Flow diagram of the controller executed from the start at every time step

The simulation model was set up in such a way that when the controller decided on countersteer, it would output a negative pulse, and when the controller decided on oversteer, it output a positive pulse. This pulse was subsequently passed through a second order filter to generate a smooth steering angle that was added to the driver's input. An example of one of these filtered pulses is shown in Figure 7.15.

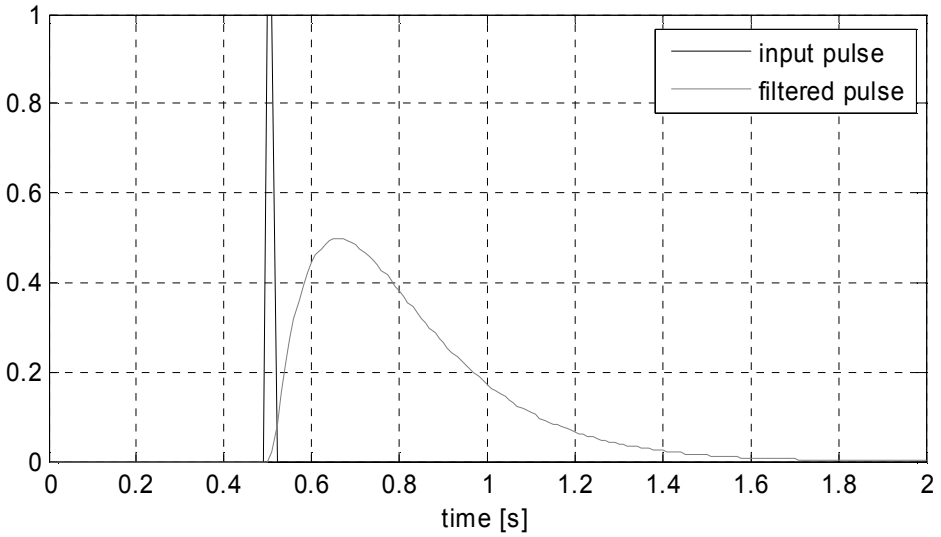

Figure 7.15 – Comparison of the impulse signal and the filtered impulse signal

7.1.3.2 Controller Gains

It was found that for the four different cases where the controller added countersteer or oversteer to the driver's input, the magnitudes of the adjustments had to be different. The magnitude of the countersteer at the start of the manoeuvre was found to affect the magnitudes of the steering adjustments during the rest of the manoeuvre.

The first pulse of countersteer can be interpreted as a nudge to start the vehicle rolling. The effect of this nudge depends on the type of manoeuvre and the manoeuvre velocity. If the nudge is relatively small, the resulting roll moment may not be sufficient as shown in Figure 7.16a and Figure 7.17a. This means that as the moment from the lateral acceleration increases due to the driver applying more steer, the moment from the vehicle's centre of mass displacement does not increase with it. Hence, the moment from the lateral acceleration become larger than the moment from the centre of mass displacement and straighten the vehicle back up and it starts leaning/falling in the opposite direction as is illustrated by Figure 7.17a. If the countersteer is relatively large, the resulting roll moment could be so great, that the lateral acceleration moment caused by the driver's steering input cannot catch up as shown in Figure 7.16b. In this case, the vehicle will have fallen over into the direction of the turn, see Figure 7.17b, before the driver can react.

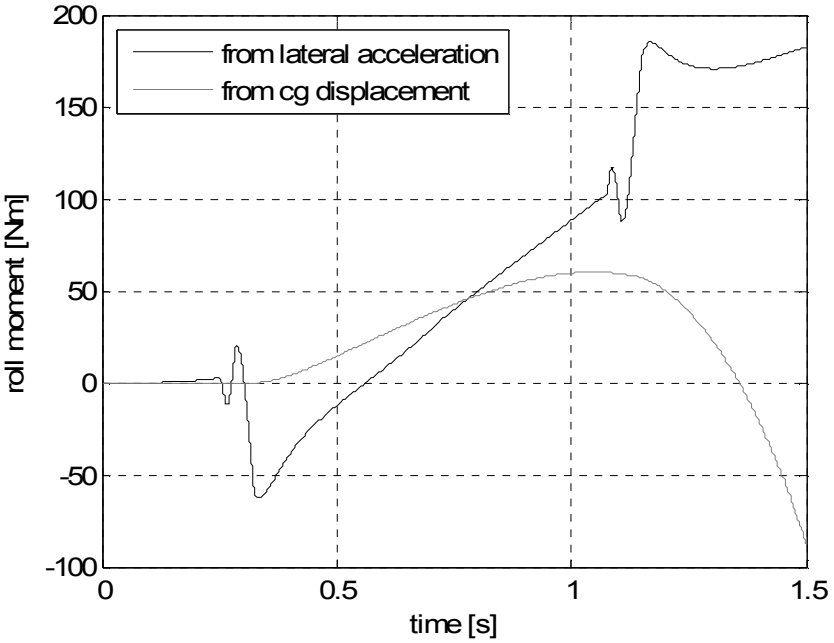

(a)

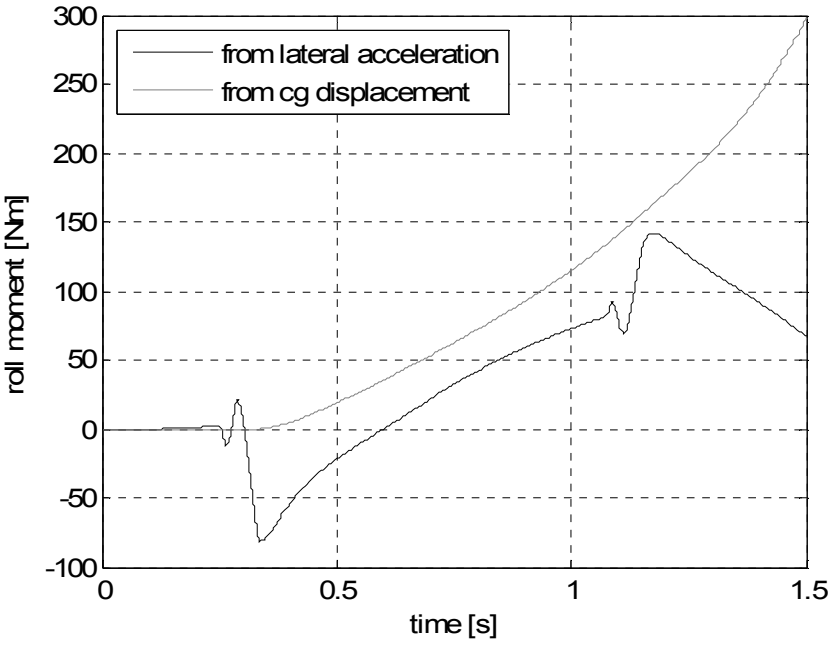

(b)

Figure 7.16 – Roll moments from the lateral acceleration and the displacement of the centre of gravity (a) when the initial countersteer was too small (b) when the initial countersteer was too large

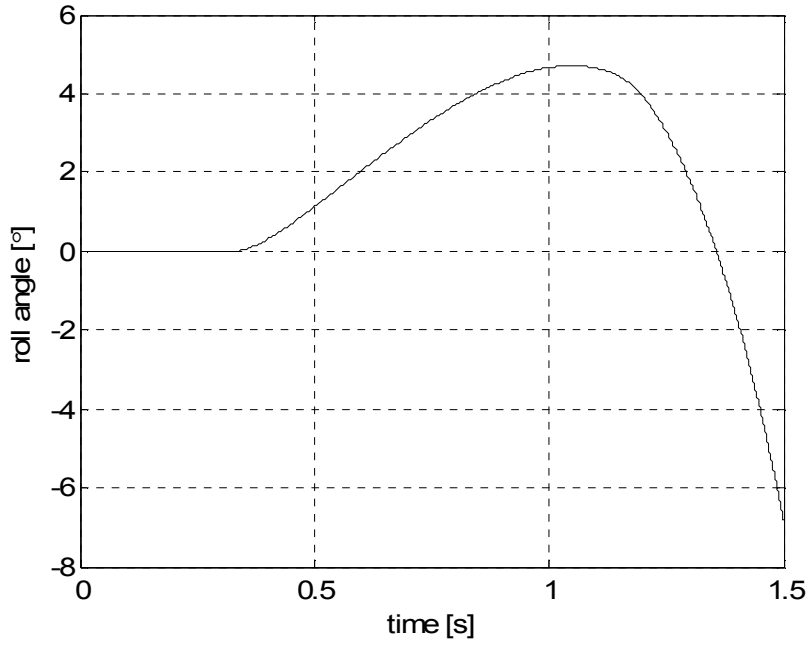

(a)

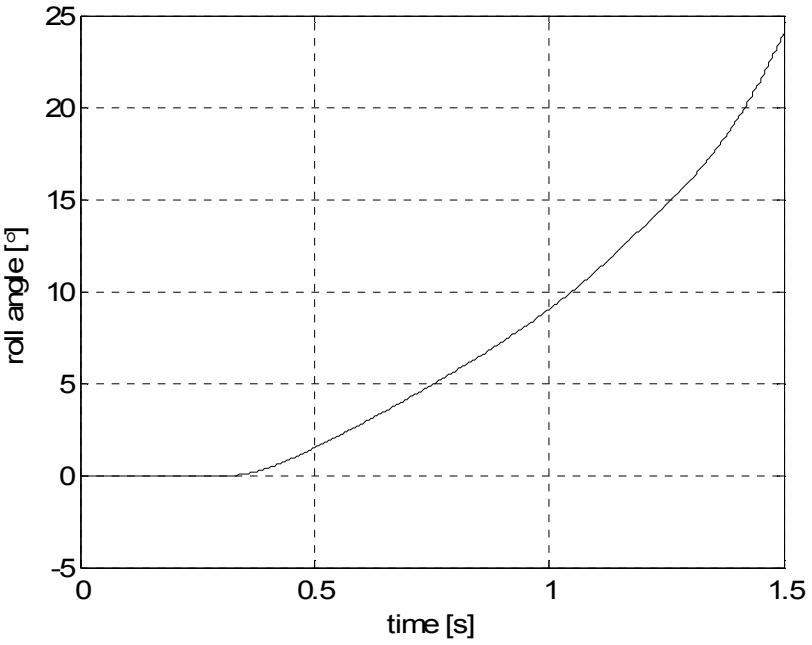

(b)

Figure 7.17 – Resulting roll angle from the roll moments shown in Figure 7.16 (a) when the initial countersteer was too small (b) when the initial countersteer was too large

Ideally, the countersteer magnitude is such that the resulting moment from the displacement of the centre of gravity keeps pace with the moment from the lateral acceleration. Thus after the countersteer, the roll acceleration and therefore the perceived acceleration are small. The gain for

the first countersteer has to be determined at the start of manoeuvre. Simulation results showed that the gain depends on the following manoeuvre characteristics: the vehicle speed, the manoeuvre magnitude (the maximum steering angle from the driver) and the manoeuvre length (the time during which the driver applies the steering angle). The vehicle speed can easily be monitored, but the manoeuvre type and length are unknown at the start. The steering velocity at the start of the manoeuvre gives an indication as to whether the manoeuvre type, but this is not conclusive. Nevertheless, the steering velocity should be used to determine an initial countersteer gain, but subsequently, it is essential that the roll is monitored so that additional steer can be added or subtracted if necessary.

As was mentioned before, the first countersteer affects the magnitude necessary for the second steering adjustment. If the first countersteer were small, the oversteer necessary to slow down the roll can also be small. Similarly, if the first countersteer is large, the oversteer also needs to be large. The magnitude of this oversteer can be determined from the perceived acceleration measurement. If the perceived acceleration is very small when it is time for the oversteer, then the oversteer magnitude only needs to be marginally smaller (90%) than the gain of the countersteer. If the perceived acceleration is in the opposite direction to the roll angle shown in Figure 7.18, when it is time for the oversteer, then the oversteer gain has to be small as the roll is already slowing down.

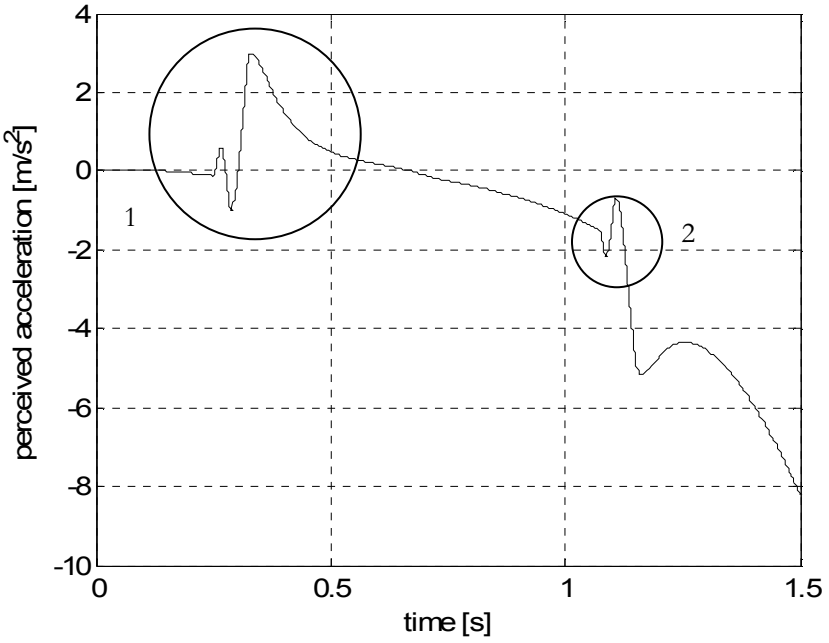

Figure 7.18 – Example where the perceived acceleration is in the opposite direction to the roll angle when the oversteer needs to be applied

The magnitude of the second oversteer, which has to straighten the vehicle up, was dependent on the magnitude of the first oversteer. Figure 7.19 shows that when the second oversteer is applied, the roll velocity is close to zero. Therefore, the magnitude of this second oversteer could be of a similar magnitude to the first oversteer albeit marginally smaller (85%). If the roll velocity is significantly greater than zero, the magnitude of the second oversteer would have to be significantly greater than the first oversteer. Similarly, if the roll velocity was significantly smaller than zero, the magnitude of the second countersteer would only need to be very small.

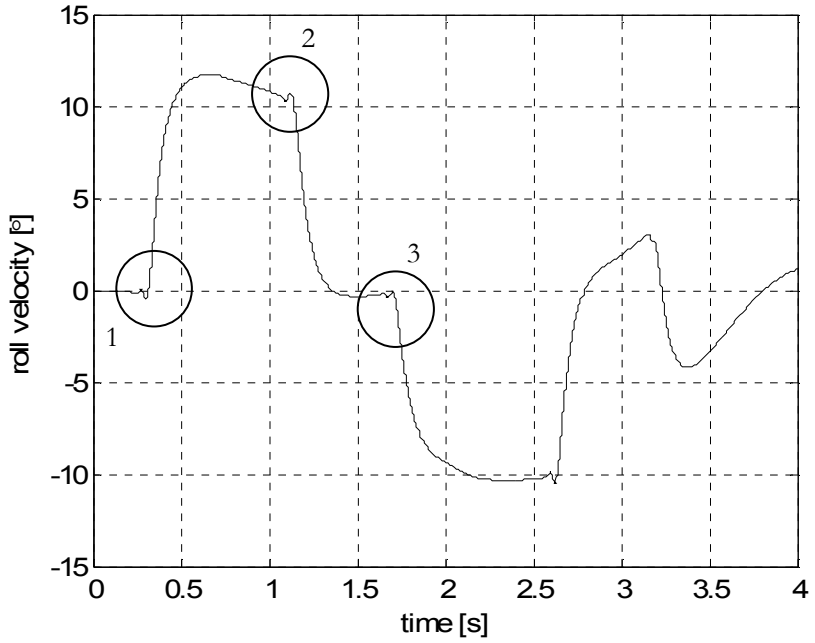

Figure 7.19 – Example of the roll velocity during the manoeuvres when the gains were set so that the vehicle was balanced throughout the manoeuvre

Once the second countersteer has been applied, the perceived acceleration, the roll angle and its velocity need to be monitored to ensure the vehicle does not straighten up too quickly as shown in Figure 7.20. Here, the roll velocity to straighten up has become so large, that the final countersteer cannot slow the roll down.

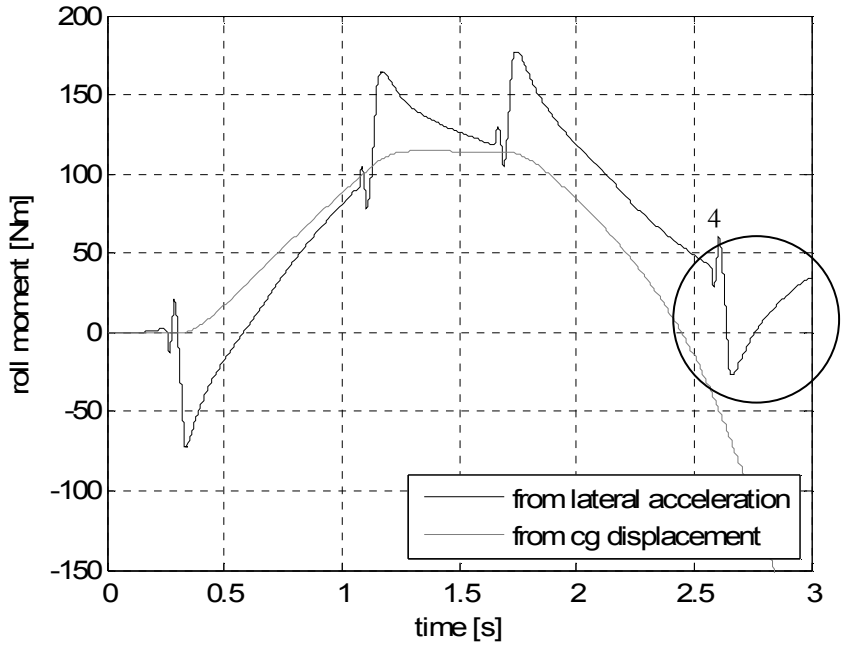

Figure 7.20 – Example of the roll moments where the second oversteer adjustment was too great

The magnitude of the final countersteer was found to depend on the roll angle and the roll velocity at the time where the final adjustment was to be made. The previous steering adjustments should have ensured that the vehicle straightened up at a similar rate to the reduction in lateral acceleration. If the vehicle straightened up very quickly, the magnitude of the final countersteer would have to be large to slow the roll down and vice versa if the vehicle straightened up slowly. In general, the magnitude of the final countersteer adjustment was found to be similar to the magnitude of the oversteer adjustment that had caused the vehicle to straighten up (number 3).

7.1.3.3 Improved Stability

The controller presented so far does not balance the vehicle about a zero roll angle when the driver wants to follow a rectilinear path. In addition, the final countersteer does not always ensure that the roll is zero at the end of the manoeuvre. For these two reasons, a PID roll controller was added to the overall system to guarantee the vehicle's stability when following a rectilinear path. The demand angle for the PID steer controller will be zero in most circumstances and it will only be employed when the driver's steering input is close to zero.

7.1.3.4 Feedback Signals

In section 7.1.3.2 it was mentioned that the roll angle, the roll angle velocity and the perceived acceleration have to be fed back to the controller in order to adjust the gains. The roll angle was

measured on the vehicle so this measurement would not be a problem. The steering velocity was derived from the steering angle measurement, so a similar derivation could be applied to the roll angle, since the controller mainly needs to know whether the roll velocity is close to zero or not. The perceived acceleration signal would be more difficult to use, as it is expected to be a noisy signal. Similar to the roll velocity measure, the controller needs to know the direction of the perceived acceleration and whether it is close to zero: the precise magnitude of the signal is not imperative. Hence, this signal can be filtered before reaching the controller without the small amount of the data loss from the filtering inhibiting the controller.

7.1.3.5 Calculation Examples

The control system was tested for a range of vehicle speeds, inputs steering angles and manoeuvre lengths similar to those measured in the experiments. For each test, the controller gains that would result in a stable manoeuvre were determined. The aim was to establish a correlation between the input and feedback signals and the magnitudes of the steering adjustments: no concrete correlation could be determined. However, with the correct gains, the controller performed well in terms of the roll control and the limited deviation from the driver's intended path as shown in Figure 7.21.

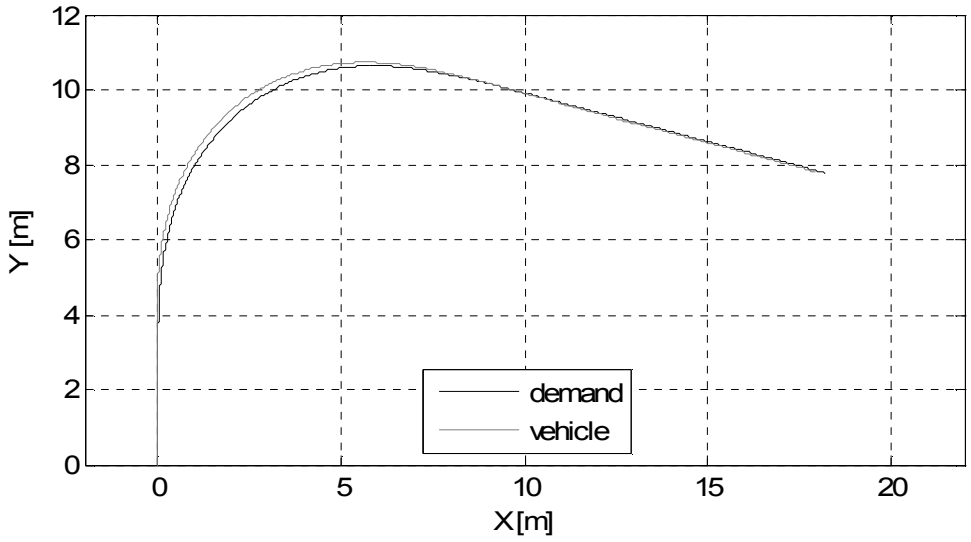

Figure 7.21 – Example of the vehicle's trajectory with the controller

The steering angle that was applied to the vehicle using the DC motor actuator is shown in Figure 7.22. This figure illustrates that the controller only needs to apply small amounts of steer to change to overall roll moment.

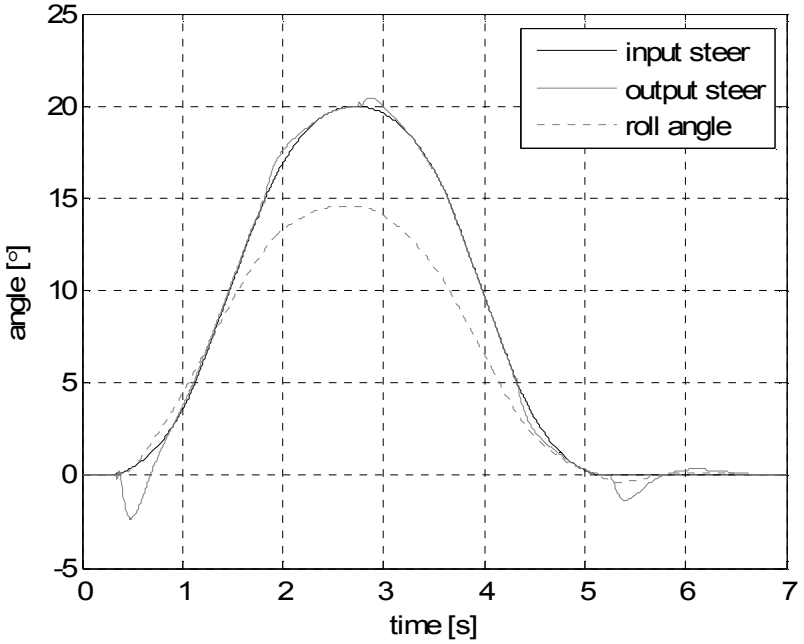

Figure 7.22 – Comparison of the driver's demand steer angle and the controller output steer angle as well as the resulting vehicle roll angle

Figure 7.23 shows the effect of the additional steering angle on the vehicle's lateral acceleration compared to the lateral acceleration the driver would expect from his steering input. The countersteer has had a clear effect on the lateral acceleration and has caused a large enough roll moment to balance the vehicle.

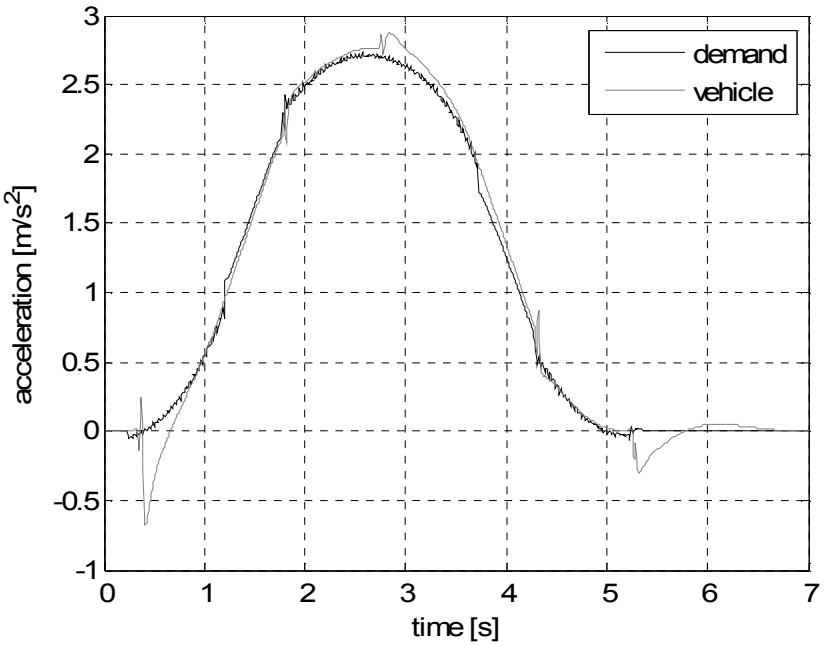

Figure 7.23 – Comparison of the lateral acceleration expected from the driver's input steer angle and the vehicle's lateral acceleration when controlled

This calculation example was a transient manoeuvre, therefore a large portion of the perceived acceleration consisted of the roll acceleration, see Figure 7.24. When the controller applies a steering adjustment, it causes a roll moment and acceleration, as can be seen in the figure.

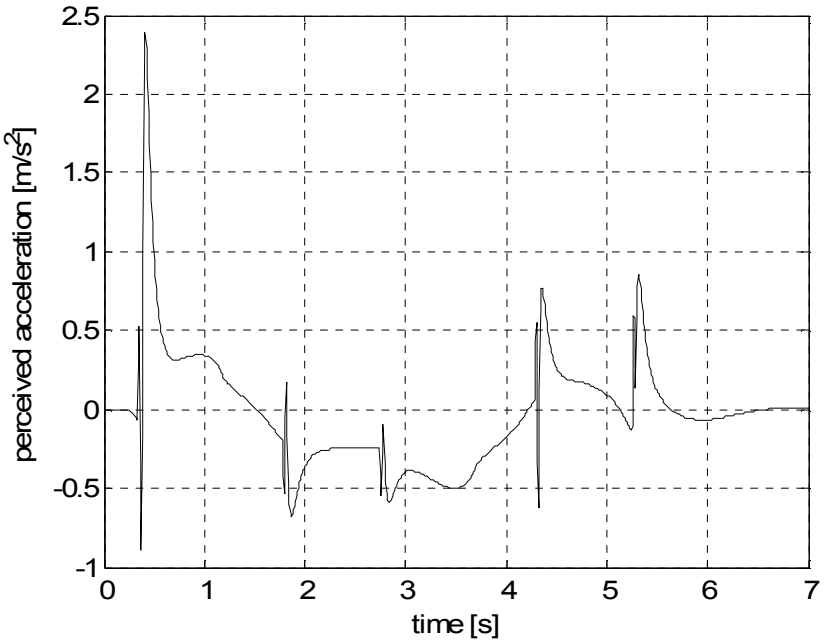

Figure 7.24 – Perceived acceleration as measured at the driver's head height during the manoeuvre

7.2 CONCLUDING REMARKS

The development process of a novel steer tilt controller has been presented in this chapter. The aim was to design a controller that would be simple enough to be realized with a microprocessor and that would have a minimal effect on the driver's intended path.

The experimental results presented in chapter 5 had shown that a human driver did not roll the vehicle to the theoretical balanced roll angle under transient conditions. Instead, the driver overleaned at the start of the turn and underleaned after the apex of the turn. Hence, the new controller was designed such that the vehicle started to roll when the driver's steering input indicated the start of a turn, and straightened the vehicle back up once the driver's inputs implied that the apex of the turn had been reached.

The proposed concept was a controller that would add small amounts of countersteer and oversteer to the driver's steering input. The controller algorithm consisted of a set of logic questions that derived the driver's intentions from the steering inputs. The magnitudes of the controller's steering adjustments were to be regulated using the feedback signals of the perceived acceleration and the roll velocity. So far, no successful regulation method could be developed that ensured the vehicle's stability for the majority of driving conditions. The gains had to be manually adjusted for every calculation example although satisfactory performance was achieved with this approach.

The overall stability of the system was improved by the addition of a PID steer controller that ensured the vehicle was balanced when the driver's steering inputs were zero and at the end of a manoeuvre.

CHAPTER 8. CONCLUSIONS AND FUTURE WORK

8.1 CONCLUSIONS

The main objective of this work was to develop a vehicle and driver model for a three-wheeled tilting vehicle and to design a novel roll control system that could be tested with the complete vehicle system simulation.

It was demonstrated that the vehicle dynamics experimental results and the subsequent vehicle model would be subject to a number of non-linearities, uncertainties and environmental factors. First, the unique kinematics of a three-wheeled tilting vehicle with a tilting and a non-tilting subassemblies were evaluated and new equations were presented. The most important kinematic effect was the relative yaw between the tilting and non-tilting assemblies causing a small steer angle at the rear wheels. It was shown that the mass and the inertias of the vehicle varied significantly with different sized drivers and with the roll angle. The kinematics study led to a review of the definition of the perceived acceleration and it was shown that the equation required additional dynamic terms. The definition of the steering torque was also investigated and a calculation example illustrated that to determine the steering torque a large number of vehicle states needed to be known.

The findings from this investigation into the uncertainties were applied in the data processing of the experimental results to study the handling of a three-wheeled tilting vehicle and the driver's control behaviour was presented. The steady state results showed that the vehicle roll was approximately equal to the theoretical balanced roll angle. Transient test results however showed different roll behaviour from the driver: the driver overleaned the vehicle at the start of a turn in order to continue to roll and underleaned at the end of the turn in order to straighten the vehicle back up. The driver employed various countersteering strategies of which the two main approaches were: a small amount of countersteer applied for a longer period of time or a larger amount of countersteer applied briefly. Both approaches could be applied successfully for an identical manoeuvre and vehicle speed. The test results showed that the most experienced driver

made fewer steering adjustments than the less experienced driver. The differences between the vehicle speeds were not great enough to justify the differences in steering adjustments. From the experimental results that were presented in this thesis it appeared that the drivers applied arbitrary amounts of countersteer and relied on their ability to make small adjustments to the steering to control the roll.

A dynamic non-linear vehicle model was developed based on vehicle models from the literature. The model was validated using experimental data and shown to provide a good prediction of the yaw rate and the lateral acceleration. The validation of the roll dynamics was limited by the model's sensitivity to measurement errors and small changes in signal phase and magnitude after data processing. A new method to estimate the model parameters of a Magic Formula tyre mode was presented. This method consisted of a vehicle model with experimental data as its inputs that optimised the tyre model parameters so that the model outputs matched the experimental results. The complete vehicle model was used to test a steer tilt controller based on PID control. This method of STC was only successful in a very limited number of driving scenarios.

A new driver model algorithm with satisfactory trajectory performance with characteristics similar to that of a real driver was developed. When the driver model was combined with the PID based STC, the driver model gains and the PID gains had to be adjusted to allow the two to work in synchronisation. The result was a vehicle that meandered about the demand trajectory with lateral errors of sufficient magnitude to place the vehicle on the wrong side of the road.

The vehicle model was also used to establish the precise effect of three external disturbances that were identified and modelled: side winds, road gradient, and road camber profile. The side wind and the road camber profile were shown to be external factors that would confuse a roll controller. Additional state feedback and control loops would be necessary to ensure vehicle stability. The road gradient was shown to cause changes in the vehicle handling which could result in unexpectedly large steering angles being required when driving up a steep road.

A novel control strategy was developed aiming to minimise the deviation from the driver's intended path. The objective was to keep the control algorithm simple enough so that it could be programmed onto a microcontroller. The principle of the new controller was to add or subtract small amounts of steer to or from the driver's input. These small amounts of countersteer and oversteer would result in small lateral forces that in turn would cause small moments about the roll axis. The magnitudes of the adjustments depended on the cornering radius and the vehicle speed. With the right gain settings, these small adjustments ensured that the roll dynamics were

stable whilst the vehicle's deviation from the intended path was very small. It was shown that the countersteer and oversteer magnitudes would have to be regulated during the manoeuvre using the roll angle and its derivative and the perceived acceleration feedback signals.

8.2 FUTURE WORK

A significantly broader test programme may illustrate greater variations in countersteer. This programme should at least include a variety of cornering radii and for each radius a range of vehicle speeds and a range of points from which the driver is allowed to start steering. The latter variable may shed light on the countersteer behaviour relative to the driver's preview distance.

A prototype steer tilt controlled tilting three-wheeled vehicle could be developed on the basis of this work. In order to do this, a method to adjust the control system gains would need to be established based on the input signals and the feedback measurements.

The Honda Gyro has the potential to be modified so that the driver steers the vehicle via a steering wheel and controls the brake and the throttle via two pedals. This configuration should give the driver the impression that he is driving a car rather than a moped. If this system were to be developed as a steer-by-wire controller, it would be important to give the driver some feedback in terms of steering feel. The feedback could initially be as simple as a torsional spring that returns the steering wheel to the neutral position. The steering actuation could be realized with a rotary motor parallel to the steering axis and a belt drive between the two. With this type of steer-by-wire system, the controller calculates the steering adjustments for the roll control and adds them to the measured steering angle. This sum is then passed from the controller to the motor position controller as the position demand. This type of system will be appropriate to prove the controller is a viable alternative to PID control. An experimental prototype would enable the human driver interaction in a narrow track STC vehicle to be determined. This is a critical factor in the potential success of this type of vehicle since the driver must feel safe and in control of the vehicle trajectory at all times.

If implemented on a broader scale, a semi-steer-by-wire system could be developed instead, since it would only be necessary to perturb the front wheel steering angle with the new controller. This can be realized with an actuator in series with the direct steering link from the steering wheel. Either a hydraulic or a linear electrical actuator could push or pull the front wheel to effect the small steering adjustments. From a safety point of view, the small perturbations provided by the active steer system should not present any significant danger. Alternatively, a planetary gearbox

might provide a more acceptable fail safe characteristic due to the direct link between the steering wheel and front wheel.

REFERENCES

1. Anon, *Der elektrisch betriebene Dreiradwagen (The electrically driven three-wheel automobile)*, in *Wirtschafts-Motor -- Nutz-Motor*1920. p. pp. 11-12.
2. Wesnigk, E., *Motordreiraeder*, in *VDI Zeitschrift*1933. p. pp. 96-97.
3. Rishavy, E.A., *Special purpose care for commuting*, 1969, Society of Automotive Engineers.
4. www.maxmatic.com/ttw_moto.htm.
5. Chang, C.-N. and D.-H. Ding, *Theoretical stability analyses of the cornering behaviour of three-and four-wheel vehicles.* International Journal of Vehicle Design, 1994. **15**(3-5): p. pp. 301-317.
6. www.statistics.gov.uk/.
7. www.uk.smart.com.
8. www.toyota.co.uk.
9. www.monotracer.com/.
10. www.bath.ac.uk/mech-eng/zedis/.
11. Drew, B., et al., *Experimental evaluation of a hydraulically actuated tilt system for a narrow track three-wheeled vehicle*, in *ASME International Mechanical Engineering Congress and Exposition*2006: Chicago, Illinoins, USA.
12. Drew, B., et al., *System development for hydraulic tilt actuation of a tilting narrow vehicle*, in *The 9th Scandinavian International Conference on Fluid Power*2005: Linkoeping, Sweden.
13. www.clever-project.net/.
14. Bertoluzzo, M., et al. *Electric tilting 3-wheel vehicle for a sustainable urban mobility*. in *10th International Workshop on Advanced Motion Control, AMC'08, March 26, 2008 - March 28, 2008*. 2008. Trento, Italy: Institute of Electrical and Electronics Engineers Inc.
15. Cossalter, V., et al., *Development of a novel three-wheeled vehicle*, in *3. internationalen motorradkonferenz*2000.
16. Pohl, M. and A. Conrads, *A research threewheeler vehicle with processor controlled tilting and steering mechanism*, in *Research and Education in Mechatronics*2006: Stockholm, Sweden.
17. Solero, L., et al., *Nonconventional three-wheel electric vehicle for urban mobility.* IEEE Transactions on Vehicular Technology, 2001. **50**: p. 1085-1091.
18. Cossalter, V., N. Ruffo, and P. Agostinetti, *Experimental analysis of handling of a three wheeled vehicle*, in *9th International Conference High -tech Cars and Engines*2003: Modena, Italy.
19. Huston, J.C., B.J. Graves, and D.B. Johnson, *Three wheeled vehicle dynamics*, 1982, Society of Automotive Engineers. p. pp. 45-58.
20. Karnopp, D. and R. Hibbard, *Optimum roll angle behaviour for tilting ground vehicles.* ASME Dynamic Systems and Control Division (DSC), 1992. **44**: p. pp. 29-37.
21. Karnopp, D. and C. Fang, *A simple model of steering-controlled banking vehicles.* ASME Dynamic Systems and Control Division (DSC), 1992. **44**: p. pp. 15-28.
22. Hibbard, R. and D. Karnopp, *The dynamics of small, relatively tall and narrow tilting ground vehicles.* ASME Dynamic Systems and Control Division (DSC), 1993. **52**: p. pp. 397-416.
23. So, S.-G. and D. Karnopp, *Active dual mode tilt control for narrow ground vehicles.* Vehicle System Dynamics, 1997. **27**(1): p. pp. 19-36.
24. So, S.-G. and D. Karnopp, *Switching strategies for narrow ground vehicles with dual mode automatic tilt control.* International Journal of Vehicle Design, 1997. **18**(5): p. pp. 518-532.
25. Snell, A.S., *An active roll moment control strategy for narrow tilting commuter vehicles.* Vehicle System Dynamics, 1998. **29**(5): p. pp. 277-307.
26. Hess, R.A. and S.A. Snell, *Flight control system design with rate saturating actuators.* Journal of Guidance, Control, and Dynamics, 1997. **20**: p. 90-96.
27. Siwakosit, W., S.A. Snell, and R.A. Hess, *Robust flight control design with handling qualities constraints using scheduled linear dynamic inversion and loop-shaping.* IEEE Transactions on Control Systems Technology, 2000. **8**: p. 483-494.

28. Snell, S.A., D.F. Enns, and W.L. Garrard Jr, *Nonlinear inversion flight control for a supermaneuverable aircraft*. Journal of Guidance, Control, and Dynamics, 1992. **15**: p. 976-984.
29. Snell, S.A. and R.A. Hess, *Robust, decoupled, flight control design with rate-saturating actuators*. Journal of Guidance, Control, and Dynamics, 1998. **21**: p. 361-367.
30. Snell, S.A. and P.W. Stout. *Full envelope longitudinal flight control law using a nonlinear controller combined with quantitative feedback theory*. in *Proceedings of the 1995 ASME International Mechanical Engineering Congress and Exposition, November 12, 1995 - November 17, 1995*. 1995. San Francisco, CA, USA: ASME.
31. Chiou, J.C., et al. *Tilting motion control in narrow tilting vehicle using double-loop PID controller*. in *2009 7th Asian Control Conference, ASCC 2009, August 27, 2009 - August 29, 2009*. 2009. Hong Kong, China: IEEE Computer Society.
32. Chiou, J.-C. and C.-L. Chen, *Modeling and verification of a diamond-shape narrow-tilting vehicle*. IEEE/ASME Transactions on Mechatronics, 2008. **13**: p. 678-691.
33. Pauwelussen, J.P., *The dynamic behaviour of man-wide vehicles with an automatic active tilting mechanism*, in *7th International Congress European Automobile Engineers Cooperation*1999. p. pp. 193-197.
34. Pauwelussen, J.P., *The dynamic performance of narrow actively tilting vehicles*, in *5th International Symposium on Advanced Vehicle Control*2000: Ann Arbor, Michigan. p. paper 69.
35. www.carver-worldwide.com/.
36. Gohl, J., et al., *The development of tilt-controlled narrow ground vehicles*, in *American Control Conference*2002: Anchorage, Alaska. p. pp. 2540-2545.
37. Gohl, J., et al., *Active roll mode control implementation on a narrow tilting vehicle*. Vehicle System Dynamics, 2004. **42**(5): p. pp. 347-372.
38. Kidane, S., et al., *A fundamental investigation of tilt control system for narrow commuter vehicles*. Vehicle System Dynamics, 2008. **46**(4): p. pp. 295-322.
39. Kidane, S., et al. *Experimental investigation of a narrow leaning vehicle tilt stability control system*. in *2007 American Control Conference, ACC, July 9, 2007 - July 13, 2007*. 2007. New York, NY, United states: Institute of Electrical and Electronics Engineers Inc.
40. Kidane, S., et al., *Development and experimental evaluation of a tilt stability control system for narrow commuter vehicles*. IEEE Transactions on Control Systems Technology, 2010. **18**: p. 1266-1279.
41. Committee, V.D.S., *Vehicle Dynamics Terminology*, 2008, Society of Automotive Engineers.
42. Dorf, R.C. and R.H. Bishop, *Modern Control Systems*. 7th ed1995, London: Pearson.
43. Milliken, W.F. and D.L. Milliken, *Race car vehicle dynamics*1995, Warrendale: SAE International.
44. Allen, R.W., et al., *Steady state and transient analysis of ground vehicle handling*, 1987, Society of Automotive Engineers.
45. Pacejka, H.B., *Tyre and vehicle dynamics*. 2nd edition ed2006, Oxford: Butterworth-Heinemann Publications.
46. Cossalter, V., *Motorcycle Dynamics*. 2nd ed2006, United States: LULU (self publishing).
47. Berote, J., van Poelgeest, A., Darling, J., Edge, K., Plummer, A., *The dynamics of a three-wheeled narrow-track tilting vehicle*, in *Fisita World Automotive Congress*2008: Muenchen.
48. Fajans, J., *Steering in bicycles and motorcycles*. American Journal of Physics, 2000. **68**(7): p. pp. 654-659.
49. Whitt, F.R. and D.G. Wilson, *Bicycling Science*. 2nd ed1982, London: The MIT Press.
50. Getz, N. and J.E. Marsden, *Control for an autonomous bicycle*, in *IEEE International Conference on Robotics and Automation*1995. p. pp. 1397-1402.
51. Getz, N.H., *Internal equilibrium control of a bicycle*, in *IEEE Conference on Decision and Control*1995. p. pp. 4285-4287.
52. Lee, S. and W. Ham, *Self stabilizing strategy in tracking control of unmanned electric bicycle with mass balance*, in *IEEE International Conference on Intelligent Robots and Systems*2002. p. pp. 2200-2205.
53. Tanaka, Y. and T. Murakami, *Self sustaining bicycle robot with steering controller*, in *International Workshop on Advanced Motion Control*2004. p. pp. 193-197.
54. Weir, D.H. and J.W. Zellner, *Lateral-directional motorcycle dynamics and rider control*, 1978, Society of Automotive Engineers.
55. Rice, R.S., *Rider skill influences on motorcycle maneuvering*, 1978, Society of Automotive Engineers.
56. Katayama, T., A. Aoki, and T. Nishimi, *Control behaviour of motorcycle riders*. Vehicle System Dynamics, 1988. **17**(4): p. pp. 211-229.
57. Chi, C.-T. *Improvement of bike stability control based on the self-adjusting biker posture approach*. in *2005 International Symposium on Intelligent Signal Processing and Communication Systems, ISPACS 2005,*

December 13, 2005 - December 16, 2005. 2005. Hong Kong, China: Inst. of Elec. and Elec. Eng. Computer Society.
58. Yokomori, M., T. Oya, and A. Katayama, *Rider control behavior to maintain stable upright position at low speed.* JSAE Review, 2000. **21**: p. pp. 61-65.
59. Marumo, Y. and M. Nagai, *Steering control of motorcycles using steer-by-wire system.* Vehicle System Dynamics, 2007. **45**(5): p. pp. 445-458.
60. Iuchi, K. and T. Murakami. *An approach to fusion control of stabilization control and human input in electric bicycle.* in *IECON 2006 - 32nd Annual Conference on IEEE Industrial Electronics, November 6, 2006 - November 10, 2006*. 2006. Paris, France: Inst. of Elec. and Elec. Eng. Computer Society.
61. Plochl, M. and P. Lugner, *3-Level driver model and its application to driving simulations.* Vehicle System Dynamics, 2000. **33**(suppl): p. pp. 71-82.
62. McRuer, D.T., et al., *Measurement of driver-vehicle multiloop response properties with a single disturbance input.* IEEE Transactions on Systems, Man and Cybernetics, 1975. **SMC-5**: p. 490-497.
63. Plochl, M. and J. Edelmann, *Driver models in automobile dynamics application.* Vehicle System Dynamics, 2007. **45**: p. 699-741.
64. Frezza, R., A. Beghi, and S. A., *Model predictive for path following with motorcycles: Application to the development of the pilot model for virtual prototyping*, in *IEEE Conference on Decision and Control*2004. p. pp. 767-772.
65. Frezza, R. and A. Beghi, *A virtual motorcycle drover for closed-loop simulation*, in *Control Systems Magazine*2006. p. pp. 62-77.
66. Miyagishi, S., et al., *Study on construction of a rider robot for two-wheeled vehicle.* JSAE Review, 2003. **24**(3): p. pp. 321-326.
67. Yuhara, N. and J. Tajima, *Advanced steering system adaptable to lateral control task and driver's intention.* Vehicle System Dynamics, 2001. **36**(2-3): p. pp. 119-158.
68. Blundell, M., *Multibody systems approach to vehicle dynamics.* Butterworth-Heinemann publications. Vol. Oxford. 2004.
69. Pacejka, H.B. and E. Bakker, *Magic formula tyre model.* Vehicle System Dynamics, 1992. **21**(suppl): p. pp.1-18.
70. Bernard, J.E., L. Segel, and R.E. Wild, *Tire shear force generation during combined steering and braking maneuvers*, 1977, Society of Automotive Engineers.
71. Loeb, J.S., et al., *Lateral stiffness, cornering stiffness and relaxation length of the pneumatic tyre*, 1990, Society of Automotive Engineers.
72. Maurice, J.P. and H.B. Pacejka, *Relaxation length behaviour of tyres.* Vehicle System Dynamics, 1997. **27**(suppl): p. pp. 339-342.
73. Radt, H.S., *Processing of tire force/moment data*, 1995, Society of Automotive Engineers.
74. Lugner, P., H. Pacejka, and M. Plochl, *Recent advances in tyre models and testing procedures.* Vehicle System Dynamics, 2005. **43**: p. 413-436.
75. Sakai, H., O. Kanaya, and H. Iijima, *Effect of main factors on dynamics properties of motorcycle tires*, 1979, Society of Automotive Engineers.
76. Cossalter, V., et al., *Dynamic properties of motorcycle and scooter tyres: Measurement and comparison.* Vehicle System Dynamics, 2003. **39**(5): p. pp. 329-352.
77. Captain, K.M., A.B. Boghani, and D.N. Wormley, *Analytical tire models for dynamic vehicle simulation.* Vehicle System Dynamics, 1979. **8**(1): p. pp. 1-32.
78. Zegelaar, P.W.A. and H.B. Pacejka, *In-plane dynamics of tyres on uneven roads.* Vehicle System Dynamics, 1996. **25**: p. 714-730.
79. Pacejka, H.B. and R.S. Sharp, *Shear force development by pneumatic tyres in steady state conditions a review of modelling aspects.* Vehicle System Dynamics, 1991. **20**(3): p. pp. 121-175.
80. Fujioka, T. and K. Goda, *Discrete brush tire model for calculating tire forces with large camber angle.* Vehicle System Dynamics, 1996. **25**(suppl.): p. pp. 200-216.
81. Hewson, P., *Method for estimating tyre cornering stiffness from basic tyre information.* IMechE Journal of Automobile Engineering, 2005. **219**: p. pp. 1407-1412.
82. Li, L., F.-Y. Wang, and Q. Zhou, *Integrated longitudinal and lateral tire/road friction modeling and monitoring for vehicle motion control.* IEEE Transactions on Intelligent Transportation Systems, 2006. **7**(Compendex): p. 1-19.
83. Meijaard, J.P. and A.A. Popov, *Tyre modelling for motorcyle dynamics.* Vehicle System Dynamics, 2005. **43**(suppl): p. pp. 187-198.

84. Miyashita, N. and K. Kazuyuki, *A study of the cornering force by use of analytical tyre model.* Vehicle System Dynamics, 2005. **43**(suppl): p. pp. 123-134.
85. Fiala, E., *Seitenkrafte am rollenden Luftreifen*, in *VDI Zeitschrift*1954.
86. Gafvert, M. and J. Svendenius, *A novel semi-empirical tyre model for combined slips.* Vehicle System Dynamics, 2005. **43**: p. 351-384.
87. Lot, R., *A motorcycle tire model for dynamic simulations: Theoretical and experimental aspects.* Meccanica, 2004. **39**: p. 207-220.
88. Lugner, P. and P. Mittermayr, *A measurement based tyre characteristics approximation.* Vehicle System Dynamics, 1992. **21**(suppl): p. pp. 127-144.
89. Svendenius, J. and M. Gafvert, *A semi-empirical tyre model for combined slips including the effects of cambering.* Vehicle System Dynamics, 2005. **43**: p. 317-328.
90. Bakker, E., L. Nyborg, and H.B. Pacejka, *Tyre modelling for use in vehicle dynamics studies*, 1986, Society of Automotive Engineers.
91. Bakker, E., H.B. Pacejka, and L. Lidner, *A new tyre model with application in vehicle dynamics studies*, 1989, Society of Automotive Engineers.
92. Lee, J.-H., *Analysis of tire effect on the simulation of vehicle straight line motion.* Vehicle System Dynamics, 2000. **33**: p. pp. 373-390.
93. van Oosten, J.J.M. and E. Bakker, *Determination of magic tyre model parameters.* Vehicle System Dynamics, 1992. **21**(suppl): p. pp. 19-29.
94. Vries, E.J.H., de and H.B. Pacejka, *Motorcycle tyre measurements and models.* Vehicle System Dynamics, 1998. **29**(suppl): p. pp. 280-298.
95. Lidner, L., *Experience with the magic formula tyre model.* Vehicle System Dynamics, 1992. **21**(suppl): p. pp. 30-46.
96. Lu, C.-Y. and M.-C. Shih, *Application of the pacejka magic formula tyre model on a study of a hydraulic anti-lock braking system for a light motorcycle.* Vehicle System Dynamics, 2004. **41**: p. 431-448.
97. Pacejka, H.B. and I.J.M. Besselink, *Magic formula tyre model with transient properties.* Vehicle System Dynamics, 1997. **27**(suppl): p. pp. 234-249.
98. Sharp, R.S. and M. Bettalla, *Shear force and moment descriptions by normalisation of parameters and the Magic Formula.* Vehicle System Dynamics, 2003. **39**(1): p. pp. 27-56.
99. Barker, M., et al., *Steady-state steering of a tilting three-wheeled vehicle.* Vehicle System Dynamics, 2010. **48**: p. 815-830.
100. Clauser, C.E., J.T. McConville, and J.W. Young, *Weight, volume, and center of mass of segments of the human body*, 1969, AMRL Technical Report.
101. Williams, R.A., *Automotive active suspensions part 1: basic principles.* Proceedings of the Institution of Mechanical Engineers Part D: Journal of Automobile Engineering, 1997. **211**(6): p. pp. 415-426.
102. Robinson, J., *Motorcycle tuning: chassis.* 2nd edition ed1994, Oxford: Newnes.
103. Sharp, R.S., *The stability and control of motorcycles.* Journal Mechanical Engineering Science, 1971. **13**(5): p. pp. 316-329.
104. Fuchs, A., *Trim of aerodynamically faired single-track vehicles in crosswinds*, in *3rd European Seminar of Velomobiles*1998: Roskilde, Denmark.
105. Quinn, A.D., C.J. Baker, and N.G. Wright, *Wind and vehicle induced forces on flat plates-Part 2: Vehicle induced force.* Journal of Wind Engineering and Industrial Aerodynamics, 2001. **89**: p. 831-847.
106. Quinn, A.D., C.J. Baker, and N.G. Wright, *Wind and vechicle induced forces on flat plates-Part 1: Wind induced force.* Journal of Wind Engineering and Industrial Aerodynamics, 2001. **89**: p. 817-829.
107. Iniguez-de-la-Torre, I. and J. Iniguez, *Cycling and wind: does sidewind brake?* European Journal of Physics, 2006. **27**(1): p. pp. 71-74.
108. Iniguez-De-La-Torre, I. and J. Iniguez, *Cycling and wind: Does sidewind brake?* European Journal of Physics, 2006. **27**: p. 71-74.
109. Evangelou, S., M.D.J.N. Limebeer, and M.T. Rodriguez, *Influence of road camber on motorcycle stability.* Journal of Applied Mechanics, Transactions ASME, 2008. **75**: p. 0610201-06102012.
110. Kidane, S., et al. *Road bank angle considerations in modeling and tilt stability controller design for narrow commuter vehicles.* in *2006 American Control Conference, June 14, 2006 - June 16, 2006*. 2006. Minneapolis, MN, United states: Institute of Electrical and Electronics Engineers Inc.
111. Deur, J., et al., *Analysis of lateral tyre friction dynamics.* Vehicle System Dynamics, 2009. **47**: p. 831-850.

112. Kuijpers, A. and G. Van Blokland, *Tyre/road noise models in the last two decades: a critical evaluation*, in *International Congress and Exhibition on Noise Control Engineering*2001: The Hague, The Netherlands.
113. Winder, S., *Analog and digital filter design*. 2nd edition ed2002, Oxford: Newnes.
114. Bevly, D.M., C.J. Gerdes, and C. Wilson, *The use of GPS based velocity measurements for measurement of sideslip and wheel slip*. Vehicle System Dynamics, 2003. **38**(2): p. pp. 127-147.
115. Anderson, R. and D.M. Bevly, *Estimation of tire cornering stiffness using GPS to improve model based estimation of vehicle states*, in *Proceedings of the IEEE Intelligent Vehicles Symposium*2005: Las Vegas, Nevada, USA. p. pp. 801-806.
116. Sharp, R.S., D. Casanova, and P. Symonds, *A Mathematical Model for Driver Steering Control, with Design, Tuning and Performance Results*. Vehicle System Dynamics: International Journal of Vehicle Mechanics and Mobility, 2000. **33**(5): p. 289 - 326.